On algebraic and geometric aspects of fluid dynamics: New perspectives based on Nambu mechanics and its applications to atmospheric dynamics

Dissertation
zur Erlangung des akademischen Grades eines Doktors der Naturwissenschaften (Dr. rer. nat.)

am Fachbereich Geowissenschaften
der Freien Universität Berlin

vorgelegt von
Annette Müller

Berlin, 20. März 2018

1. Gutachter	**PD Dr. Peter Névir** Freie Universität Berlin Fachbereich Geowissenschaften Institut für Meteorologie Carl-Heinrich-Becker-Weg 6-10 12165 Berlin, Deutschland
2. Gutachter	**Prof. Dr. Henning Rust** Freie Universität Berlin Fachbereich Geowissenschaften Institut für Meteorologie Carl-Heinrich-Becker-Weg 6-10 12165 Berlin, Deutschland
3. Gutachter	**Prof. Dr. Rupert Klein** Freie Universität Berlin Fachbereich Mathematik and Informatik Institut für Mathematik Arnimallee 2-6 14195 Berlin, Deutschland
Tag der Disputation	26. Juni 2018

Abstract

Vortices play a crucial role in atmospheric dynamics across all scales. Anticyclonic and cyclonic rotating vortices, also known as high-and low pressure systems, determine our weather on the larger, synoptic scale. Such larger-scale vortices have horizontal radii of about 1000 km and their vertical extend is much smaller. Therefore, their motion can be described by quasi-two-dimensional fluid dynamics. Rotating supercells are examples of vortices on smaller scale that occur and influence our weather more locally. The radius of a supercell is about 10 km. Therefore, the horizontal and vertical length scales have about the same order of magnitude and three-dimensional fluid dynamical models are used to describe vortex motions on the smaller, convective scale.

In order to gain a comprised description of vortices on different scales, this thesis concerns the Nambu representation for two- and three-dimensional vortex dynamics. Nambu mechanics can be seen as a generalization of Hamilton's formulation. The equations of motion are represented in terms of two constitutive conserved quantity: the energy and a vortex-related conserved quantity. In the first part of this thesis, we will show how this concept allows for a novel, geometric classification of planar point vortex motions. Furthermore, we will use the idealized point vortex model to explain atmospheric blockings.

Regarding further conserved quantities, the Nambu representation of the Helmholtz vorticity equation provides an algebraic structure for incompressible, inviscid fluids. We will explore this algebraic approach in the second part of this thesis. First, we will introduce a novel matrix representations for the Lie algebra for two- and three-dimensional vortex dynamics. From these Lie algebra representations we will derive novel Lie group representations for two- and three-dimensional vortex flows. This approach can be seen as a structural integration of the vorticity equation, because the vortex group is directly derived from the Helmholtz vorticity equation. Now, we can regard incompressible, inviscid vortex dynamics from a different perspective leading to a better understanding of various problems.

As an example for the applicability of the here derived algebraic approach, we will show how splitting storms can be explained by analyzing helicity density fields with respect to their sign structure. Moreover, the explanation of splitting storms and the associated breakup of vortices might lead to a better understanding of turbulent structures. Finally, we

will show how the vortex algebra allows for the investigation of shortest paths of point vortices. Such vortex geodesics can be compared to special point vortex constellations that we will have discussed in the first part of the thesis. We will also outline a concept for the derivation of 3D vortex geodesics.

In summary, this thesis will concern algebraic and geometric studies of fluid dynamics combining the different disciplines of mathematics, physics and meteorology. In this way, based on Nambu mechanics, we will investigate new perspectives on fluid dynamics and show several applications to atmospheric dynamics.

Zusammenfassung

Auf allen Skalen in unserer Atmosphäre haben Wirbel einen Einfluss auf unser Wettersystem. Auf den größeren Skalen bestimmen die Antizyklonen und Zyklonen, welche auch unter dem Namen Hoch- und Tiefdruckgebiet bekannt sind, unser Wetter in den mittleren Breiten. Sie entscheiden, ob es stürmisch, sonnig oder regnerisch ist. Weil die horizontalen Radii solch großskaliger, synoptischer Wirbel ca. 1000 km misst, kann deren Dynamik mathematisch mit dem Gleichungssystem der quasi-zweidimensionalen Hydrodynamik ausgedrückt werden. Superzellen hingegen sind Beispiele von Wirbeln auf kleinerer Skala, die unser Wetter lokal beeinflussen. Die horizontale Ausdehnung einer Superzelle beträgt ca. 10 km. Somit haben die horizontalen und vertikalen Skalen solcher kleiner skaligen Wirbel die gleiche Größenordnung und es müssen dreidimensionale Modelle verwendet werden, um die Dynamik von Wirbeln auf der kleineren, konvektiven Skala bestmöglichst zu erfassen.

Um Wirbel auf den verschiedenen Skalen zu beschreiben, werden wir in dieser Arbeit die Nambu-Darstellungen der zwei-und dreidimensionalen Wirbeldynamik betrachten. Nambu-Mechanik kann als Verallgemeinerung der Hamilton'schen Sichtweise aufgefasst werden, wobei als konstituierende Größen neben der Energie auch Wirbelerhaltungsgrößen fungieren. Im ersten Teil der Arbeit werden wir zeigen, wie die zusätzliche Wirbelerhaltunsgröße in der diskreten Nambu-Darstellung eine neue, geometrische Klassifikation von Punktwirbelbewegungen ermöglicht. Zudem werden wir das idealisierte Konzept der Punktwirbel auf Hoch-und Tiefdruckgebiete übertragen und blockierende Wetterlagen erklären.

Im zweiten Teil dieser Arbeit werden wir die kontinuierliche Nambu-Mechanik und die daraus abgeleitete algebraische Struktur der Wirbeldynamik erörtern und auf sich teilende Superzellen anwenden. Aus der Helmholtz'schen Wirbelgleichung kann eine Nambu-Klammer abgeleitet werden, die eine Lie algebra erzeugt. Wir werden eine Matrixdarstellung der Lie Algebra einführen und daraus verschiedene Gruppendarstellungen für zwei- und dreidimensionale Wirbelbewegungen ableiten. Dies ermöglicht eine neue, algebraische Sichtweise, mit der die Mechanismen verschiedener atmosphärische Prozesse neu verstanden werden können. Als Beispiel werden wir den Zerfall von Superzellen mithilfe der neuen Gruppe für inkompressible, dreidimensionale Wirbeldynamik erklären. Hierbei werden wir Helizitätsfelder hinsichtlich deren Vorzeichenstrukturen analysieren und

aus den verschiedenen Vorzeichen der Helizität Rückschlüsse auf den Zerfallsmechanismus von Wirbeln ziehen. Damit könnte der algebraische Ansatz auch für ein besseres Verständnis in Bereichen der Turbulenztheorie herangezogen werden.

Im letzten Kapitel erläutern wir, wie die im Rahmen dieser Arbeit hergeleitete Gruppe angewendet werden kann, um Wirbelgeodedäten abzuleiten. Dabei werden wir zeigen, dass in zwei Dimensionen die Geodäten mit ausgezeichneten Punktwirbelsystemen verbunden sind, die wir bereits im ersten Teil dieser Arbeit diskutiert haben werden.

Zusammengefasst betrachten wir in dieser Arbeit sowohl algebraische als auch geometrische Aspekte der Wirbeldynamik, die durch Anwendung der Nambu-Mechanik sichtbar werden. Dabei versuchen wir mithilfe mathematischer Konzepte physikalische Mechanismen atmosphärischer Phänomene zu erklären.

Contents

Chapter 1

INTRODUCTION

Vortices play a crucial role in atmospheric dynamics across all scales. Larger-scale anticyclonic and cyclonic rotating vortices, also known as high- and low pressure systems, determine our weather in the midlatitudes – if it is stormy, sunny or rainy. Sometimes these vortices are arranged such that they form persistent blocked weather situations causing droughts or floods that last for several days or even for weeks. On this larger, so-called synoptic scale the typical horizontal length scale of vortices is about 500-1000 kilometers, whereas the vertical extend only yields a few kilometers. For synoptic processes, the horizontal wind speed is much larger than vertically such that for larger scale weather simulations the equations of motions are mainly determined by horizontal dynamics.

Rotating supercells are examples of vortices on smaller scale that occur and influence our weather locally in the midlatitudes. Here, the vertical height of the vortices has about the same length scale as their horizontal extension, and the vertical motion plays a crucial role for 3D vortex dynamics. Therefore, for smaller scales, three-dimensional models are usually considered to describe small-scale vortex motions. Thus, two-dimensional as well as three-dimensional vortex dynamics are essential to describe and simulate the different processes in our atmosphere (see, e.g., Kuo, 1949; Gage, 1979; Boer and Shepherd, 1983; Pedlosky, 2013; Müller et al., 2018). The aspect of different equations of motions on different scales plays an important role in recent research. Klein (2010) introduced a multiscale asymptotic approach for a transition between the equations of motions for different scales.

In this thesis we will consider Nambu mechanics to discuss atmospheric vortex motions across the different scales. Nambu (1973) introduced a for-

mulation for the Euler equation for a rigid rotator for classical mechannics. Roughly speaking, the equations of motions are expressed by the constitutive quantities. In his example, Nambu (1973) formulated the equations of motion with respect to the energy and the squared angular momentum. Névir and Blender (1993) adapted this concept to introduce a Nambu representation for vortex motions in terms of the fluid dynamical constitutive quantities. The Nambu formulation for fluids was also regarded by e.g. Takhtajan (1994), Guha (2001), Guha (2004), Bihlo (2008), Salazar and Kurgansky (2010), Sommer et al. (2011), Blender and Lucarini (2013), or Blender and Badin (2015).

What are the advantages of formulating the fluid dynamical equations in terms of the Nambu representation? To give one answer, we will regard the different perspectives of the descriptions. We can describe fluids from the Lagrangian as well as from the Eulerian perspective. The first analysis of fluid dynamics were based on the Lagrangian representation providing a canonical Hamilton structure similar to classical mass point dynamics. The first approach to represent fluids from the field perspective is based on the Clebsch representation in the Eulerian reference frame (Clebsch, 1859; Bateman, 1929). This leads to a representation of the Eulerian field equations, where the Lagrangian conservation of the particles are shifted to the constrains. The Clebsch representation is endowed with a canonical Hamiltonian structure. A formulation of vortex dynamics that is based on the Lie-Poisson bracket and the corresponding non-canonical structure was introduced by Arnold (1966) and further studied by e.g. Salmon (1982), Marsden and Weinstein (1983), Arnold and Khesin (1992), Holm et al. (1998), or Shepherd (1990); The non-canonical Hamilton structure provides a Lagrangian formulation for the Euler equation of incompressible fluids. Some authors also consider the Helmholtz vorticity equation, where the vorticity (and not the energy) acts as a dynamical variable. But so far, all representations for fluid flows are endowed with an Hamiltonian structure.

Névir and Blender (1993) showed that the Helmholtz vorticity equation can also be formulated in terms of Nambu mechanics, which can be seen as a generalization of Hamiltonian dynamics. They introduced a Nambu-field-representation for vortex dynamics that – compared to the Hamiltonian view – is based on more than one conserved quantities: The energy *and* a vortex related quantity! Five years later, Névir (1998) showed how the primitive equations can be represented in terms of the Nambu formu-

lation and the corresponding conserved quantities. The Lagrangian as well as the Eulerian reference frame provide advantages. The Lagrangian view is useful for theoretical investigations, because it has a more simple, canonical structure. However, the Eulerian perspective allows for better practical investigation, since it requires less computer efforts.

In this thesis, we will regard the Nambu formulation for vortex dynamics introduced by Névir and Blender (1993). Compared to the Hamiltonian formulation, the Nambu representation is directly based on the vorticity equation and expressed in terms of vortex-related conserved quantities. Therefore, we think that the Nambu formulation allows for a more direct analysis of vortex motions compared to the classical description of fluids that are based on Hamiltonian structures.

We will explore atmospheric phenomena regarding the discrete as well as the continuous Nambu formulation for hydrodynamical systems. Both descriptions of atmospheric dynamics exhibit benefits compared to the direct analysis of the classical equations of motion. The discrete Nambu formulation allows for a geometric view on vortex dynamics such as the classification of planar point vortex motions. Continuous Nambu mechanics allows for algebraic studies of hydrodynamical systems such that a Lie group and a Lie algebra for 2D and 3D vortex dynamics can be found. Using this algebraic approach, we will search for an explanation of vortex splits and derive vortex geodesics, i.e. shortest paths of vortex motions. To investigate both formulations and their atmospheric applications this thesis is structured into two parts as sketched in fig. 1.1.

First, we will examine discrete Nambu mechanics and the idealized point vortex model; in the second part we will use continuous Nambu mechanics to analyze vortex dynamics from an algebraic point of view. Nambu mechanics can be seen as a generalization of Hamilton's description. But in contrast to Hamilton mechanics, Nambu's formulation is based on more than one conserved quantity. This allows for an illustrative geometric study: each three-dimensional phase space trajectory can be represented as intersection of two surfaces, where the two surfaces are given by two conserved quantities. After an introduction to discrete Nambu mechanics in chapter 2, in chapter 3 we will apply discrete Nambu mechanics in a three-dimensional state space to two dimensional vortex dynamics. We will follow Müller and Névir (2014) and show how the application of Nambu mechanics leads to a geometric approach to classify the motions

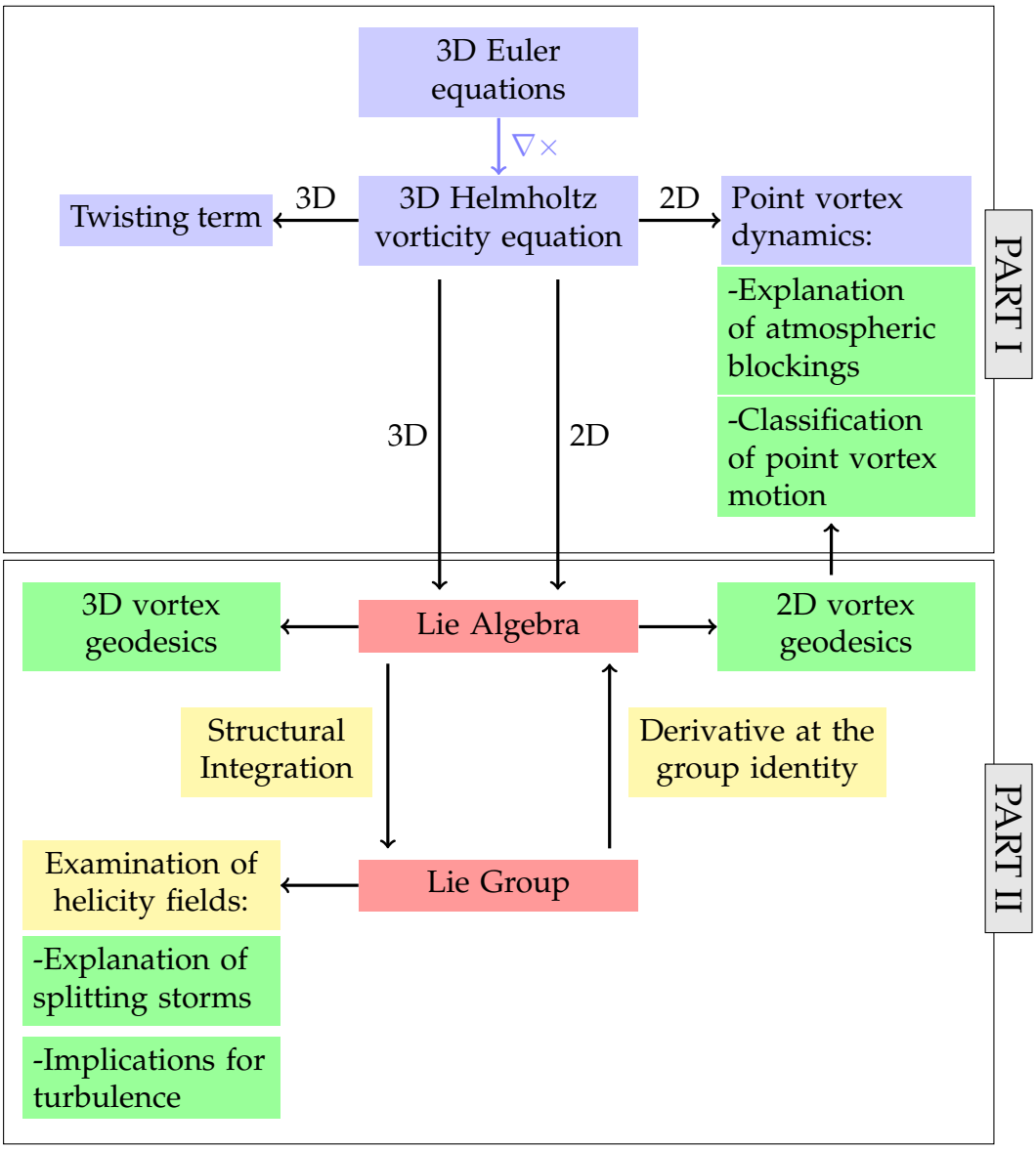

Figure 1.1: Thesis structure: In the first part of this thesis we will consider discrete vortex dynamics and in the second part we will explore vortex dynamics from an algebraic point of view.

of three point vortex systems. A geometric approach was introduced by Synge (1949), and further analyzed by e.g. Blackmore et al. (2007) or Aref (2009) considering a different phase space. Point vortices are an idealized, discrete model for planar vortex motions, where the equations of motion only depend on the local coordinates and the circulations. The latter quantity is a global measure of the strength of vortex rotations.

In chapter 4 we will see that the order of magnitudes of the circulations and the relative distances of the theoretical, idealized point vortex model coincide with our calculations of the circulations and distances of atmo-

spheric vortices on synoptic scale. This motivates us to apply point vortex theory to high- and low pressure areas. We will show, how point vortex theory can be used to explain atmospheric blockings. This concept is published in Müller et al. (2015). Usually, persistent weather situations are explained by continuous Rossby waves. Therefore, point vortex theory can be seen as a complementary discrete approach to explain atmospheric blockings. Thereby, we will apply our concept to two case studies, where we compare the wind velocity from reanalysis data sets with the theoretical point vortex velocity. These case studies are currently statistically corroborated by Hirt et al. (2018), where we analyzed more than 300 blockings.

While in part I we will consider a discrete model of atmospheric dynamics, in part II, we will regard continuous Nambu mechanics and explore vortex dynamics from an algebraic point of view. The steps are sketched in fig. 1.1. In part II, we will start with a short summary of the basic definitions and properties of Lie groups and the corresponding Lie algebras in chapter 6. In chapter 7 we will give an overview on the continuous Nambu representation for 2D and 2D incompressible vortex flows. The Nambu formulation for the Helmholtz vorticity equation was introduced by Névir and Blender (1993). The key difference to the Hamiltonian representation are the constitutive conserved quantities that determine the dynamics. Regarding Nambu mechanics vortex dynamics is determined by the energy *and* vortex-related constitutive quantities. Previous works on algebraic fluid dynamics explored Hamiltonian structures that are mainly based on the kinetic energy. The Nambu formulation for two-dimensional inviscid, incompressible fluids is based on the kinetic energy and the enstrophy. And in three dimensions, the constitutive conserved quantities that determine the dynamics of vortex flows are the kinetic energy and the helicity.

The Nambu bracket for hydrodynamic systems generates a Lie algebra for vortex dynamics. In chapter 8 we will introduce matrix representations for the vortex Lie algebra for two- as well as for three-dimensional vortex flows. Moreover, starting from this matrix representation we will derive different group representations for two- and three-dimensional vortex dynamics. The Vortex-Heisenberg group operation itself was communicated with Névir in private communication with Schober in 2010. In this thesis, we will derive the Vortex-Heisenberg group and introduce a novel matrix representation of the group and the algebraic structure for two- and three-

dimensional vortex flows. A group is a set of elements, and these elements can be combined by a corresponding group operation. We will regard atmospheric states as group elements and interpret the mathematical group operation as their interaction. We will further apply group theory to investigate splitting storms in chapter 9. In this way, we will show how the algebraic formulation of incompressible, inviscid fluid dynamics leads to the conditions of the onset of splitting storms. Thereby, we will define vortex splits with respect to the plus-minus structure of helicity density fields, because splitted vortices rotate in opposite directions which is reflected by different signs in the helicity field. Furthermore, we will show how an extension of the vortex group can be introduced by including more physical information. Then, this extended vortex group can be used to show the existence of further vortex breakups to smaller scales. We will shortly discuss, why the algebraic approach based on Nambu mechanics for fluid dynamics might lead to a better understanding of turbulent vortex flow structures.

A further field of vortex dynamics concerns the search for variational principles. In chapter 10 we will search for geodesics of vortices, i.e. we will tackle the question: What is the shortest path of a vortex in a constrained system? In which space can we find vortex geodesics? So far, the Hamiltonian view and Riemannian geometry has been applied to find geodesics for hydrodynamic systems. A special property of the Vortex-Heisenberg Lie algebra provides the applicability of sub-Riemannian geometry to find geodesics for incompressible, inviscid 2D and 3D vortex dynamics as we will discuss in chapter 10. Compared to Riemannian geometry sub-Riemannian geometry can be applied to search for geodesics of constrained systems such as vortex flows, where the vortex motion is restricted by vortex-related conservation laws. We will show how the derived 2D vortex geodesics correspond to point vortex equilibria, which we will have discussed in the first part of the thesis.

The discrete as well as the continuous Nambu representation for hydrodynamical systems is directly based on the Helmholtz vorticity equation. The dynamics is not only formulated by energy, it is also based on further conserved quantities that are expressed with respect to the vorticity. Classical algebraic representations of the vortex equations are based on Hamiltoniann structures and the Euler equations, some authors also derived Hamilton structures for the vorticity equation. But Hamiltonian structures are always related to the energy and not to a quantity that takes vortex rota-

tions into account. Therefore, we think that Nambu mechanics seems to be a suitable choice for the investigation of vortex dynamics.

Because of the approach to unify interdisciplinary concepts of mathematics, physics and meteorology in this doctoral research study (point vortices, blocked weather situations, Nambu mechanics, Lie groups, Lie algebras, splitting storms, turbulence, differential geometry) we will give an introduction to each topic in the beginning of each chapter and a short summary at the end of each chapter.

Part I

Geometric aspects of discrete fluid dynamics

Chapter 2

Introduction to discrete Nambu mechanics and its application to atmospheric dynamics

In 1973 Nambu introduced a generalization of canonical Hamiltonian mechanics of discrete systems. He generalized the bilinear, antisymmetric Poisson bracket to a trilinear, twice antisymmetric bracket – today called Nambu bracket. Regarding Nambu's formulation the dynamics of a system of N degrees of freedom is described by $N-1$ conserved quantities such that the dynamics in a phase space is described in terms of more than one conserved quantity. This is in contrast to Hamilton's formulation who only regarded the energy. Therefore, more physical information can be captured using Nambu's formalism. Moreover, in contrast to classical Hamiltonian dynamics, Nambu mechanics can be used to describe conservative systems with odd or even degrees of freedom.

Nambu (1973) discusses his bracket for the Euler-equation for a rigid rotator. He showed that Liouville's Theorem is satisfied such that the state space can be regarded as an incompressible fluid. Twenty years later, Névir and Blender (1993) adapted Nambu's trilinear asymmetrical bracket to continuous fluid mechanical models. As in Hamiltonian dynamics, the kinetic energy is needed to describe the time evolution of the physical systems. To apply Nambu's concept more than one conserved quantity needs to be regarded. And – considering vortex dynamics – the importance of the two conserved vortex quantities, the enstrophy (in even dimensions) and the helicity (in odd dimensions), becomes apparent, they even obtain an equal status likewise to the energy.

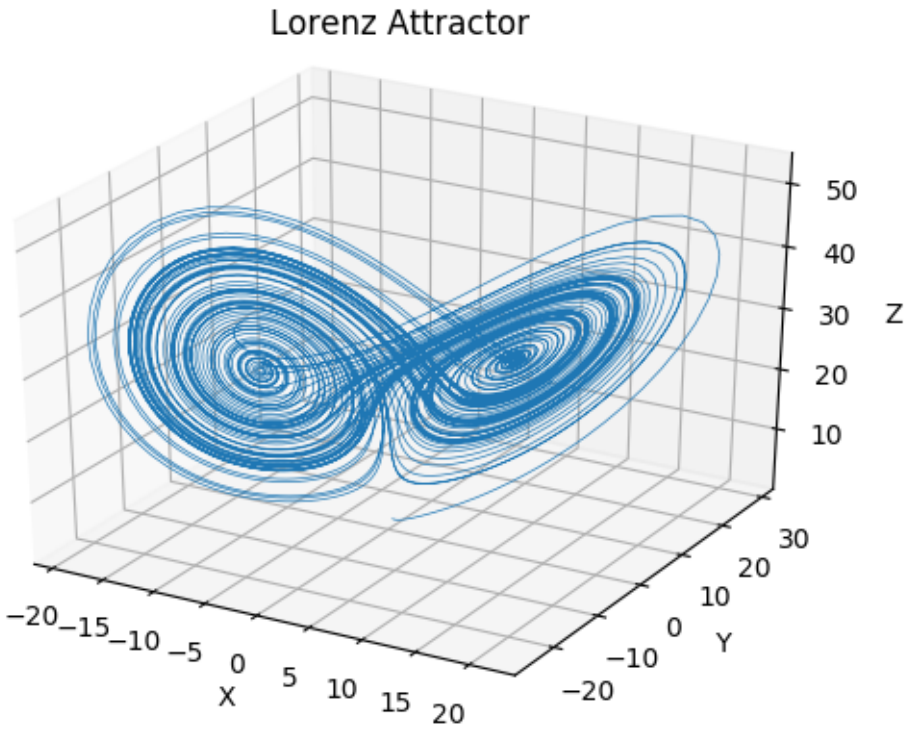

Figure 2.1: The solution of the Lorenz equations (2.2) with $r = 28$, $\sigma = 10$ and $b = \frac{8}{3}$ are shown. The trajectory is often called 'Butterfly wings'.

For an general introduction to Nambu mechanics see Nambu (1973) or Takhtajan (1994). The authors Névir and Blender (1993), Guha (2001), Guha (2004), Bihlo (2008), Salazar and Kurgansky (2010) or Blender and Lucarini (2013) applied Nambu mechanics to different hydrodynamic systems. In order to demonstrate the advantage of Nambu's formulation, we will apply Nambu-mechanics to the well known fluid dynamical set of equations introduced by Lorenz (1963). Their solution trajectory forms the well-discussed 'butterfly wings' shown in fig 2.1 indicating the unpredictability of weather systems.

2.1 Nambu mechanics in atmospheric dynamics: the non-dissipative Lorenz equations

Lorenz (1963) discovered that there are systems that behave unpredictably, such as the weather. He found an idealized model for dissipative flows. The phase space trajectories move around a fix point and are often called 'butterfly' wings. These butterfly wings are shown in fig. 2.1. Lorenz recognized that the 'jump' from one wing to the other wing is not predictable.

We will follow Névir and Blender (1994) and show how the Lorenz equations can be formulated from the Hamiltonian point of view and also show the benefits, representing equations regarding Nambu's formalism. The dissipative Lorenz equations provide an idealized model of thermal convection. They are given by the following set of equations:

$$\begin{aligned} \frac{dX}{dt} &= \sigma Y - \sigma m X \\ \frac{dY}{dt} &= rX - XZ - mY \\ \frac{dZ}{dt} &= XY - mbZ, \end{aligned} \tag{2.1}$$

where X and Y are proportional to the velocity and the temperature and Z is proportional to the difference in vertical temperature profile from linearity, where the fluid is heated from below; r, σ and b denote the three dimensionless numbers, r the Rayleigh number, σ the Prandtl number and b the ratio of the vertical and horizontal length. The parameter m is introduced by Névir and Blender (1994) and controls the magnitude of the dissipative terms. For $m = 1$ the classical set of Lorenz equations is obtained. Névir and Blender (1993) discussed the case of vanishing dissipation, i.e. $m = 0$. This leads to an integrable set of equations which can be formulated with two conserved quantities, H and C. These conserved quantities where introduced by Tabor (1989) and applied to the Lorenz system by Névir and Blender (1994). Considering a conservative system, the non-dissipative Lorenz equations for $m = 0$ are given by:

$$\frac{dX}{dt} = \sigma Y, \quad \frac{dY}{dt} = rX - XZ, \quad \frac{dZ}{dt} = XY. \tag{2.2}$$

From these equations Névir and Blender (1994) show that the conserved quantities H and C with respect to the phase space coordinates X, Y, Z can

be derived by integrating $\frac{dy/dt}{dz/dt}$ and $\frac{dz/dt}{dx/dt}$:

$$\begin{aligned} H(Y,Z) &= \frac{1}{2}Y^2 + \frac{1}{2}Z^2 - rZ = const. \\ C(X,Z) &= \frac{1}{2}X^2 - \sigma Z = const. \end{aligned} \tag{2.3}$$

where the solutions can be obtained using elliptic integrals:

$$\frac{dX}{Y(X)} = \sigma dt, \quad Y(X) = \left[2H - \left(\frac{X^2}{2\sigma} - \frac{C}{\sigma} \right)^2 + \frac{rX}{\sigma} \right]^{\frac{1}{2}}. \tag{2.4}$$

See Tabor (1989) for detailed calculations.

2.1.1 A Hamilton view on the Lorenz equations

The non-dissipative Lorenz equations (2.2) can be formulated with respect to the conserved quantity H as Hamilton function leading to a non-canonical Hamilton representation (Shepherd, 1990; Névir and Blender, 1993, 1994):

$$\begin{pmatrix} \dot{X} \\ \dot{Y} \\ \dot{Z} \end{pmatrix} = \begin{pmatrix} 0 & \sigma & 0 \\ -\sigma & 0 & -X \\ 0 & X & 0 \end{pmatrix} \cdot \begin{pmatrix} \frac{\partial H}{\partial X} \\ \frac{\partial H}{\partial Y} \\ \frac{\partial H}{\partial Z} \end{pmatrix}. \tag{2.5}$$

Denoting a state vector $\mathbf{X} = (X, Y, Z)$, we can formulate the last expression as follows:

$$\dot{\mathbf{X}} = \underline{\mathbf{P}}(\mathbf{X}) \cdot \frac{\partial H}{\partial \mathbf{X}} \tag{2.6}$$

with the anti-symmetric Poisson-Tensor $\underline{\mathbf{P}}(\mathbf{X})$. We notice that $\underline{\mathbf{P}}(\mathbf{X})$ is singular, i.e. $\det(\underline{\mathbf{P}}(\mathbf{X})) = 0$. Therefore, a Casimir function $\widehat{C}$ exists, because Casimir functions are the solution of $\underline{\mathbf{P}}(\mathbf{X}) \cdot \nabla \widehat{C} = 0$. Moreover, Casimir functions are conserved. Here, it turns out that the Casimir is given by the conserved quantity C. See Névir (1998) for further readings on the role of Casimir functions, in particular related to Nambu mechanics.

The dynamics (2.5) in the phase space (X, Y, Z) can be represented geometrically, if we consider a surface that depicts C and the transformations

$$(X, Y, Z) \rightarrow (p, q, C) \tag{2.7}$$

with $q = X$and $p = \sigma y$. The Casimir function allows for a transformation of a singular system to a canonical Hamilton representation and a canonical

representation for the non-dissipative Lorenz equations is derived:

$$\dot{q} = \frac{\partial H^*}{\partial p}, \quad \dot{p} = -\frac{\partial H^*}{\partial q}, \tag{2.8}$$

where H^* denotes the conserved quantity H scaled by σ:

$$H^* = \sigma H = E_{\text{kin}}(p) + E_{\text{pot}}(q) + c^*. \tag{2.9}$$

where the kinetic and potential energy depend on the momentum p and the local coordinate q. The energies and the constant c^* are defined by:

$$\begin{aligned} E_{\text{kin}}(p) &= \frac{1}{2}p^2 \\ E_{\text{pot}}(q) &= -\frac{1}{2}(\sigma r + C)q^2 + \frac{1}{8}q^4 \\ c^* &= r\sigma C + \frac{1}{2}C^2. \end{aligned} \tag{2.10}$$

Here, the non-dissipative Lorenz equations were formulated in terms of the Hamiltonian view with respect to one conserved quantity, the energy. Next, we will discuss the Nambu formulation of the Lorenz equations that is based on the energy and an additional conserved quantity. Considering two conserved quantities provides a geometric representation of the solution of the Lorenz equations.

2.1.2 Nambu formulation of the Lorenz equations

As we will discuss in section 2.2, regarding Nambu mechanics, we can represent the dynamics in a three dimensional phase space in terms of two conserved quantities. Here, we will consider a three dimensional phase space using the above notation of the Lorenz equations (2.2) and denoting the state space vector $\mathbf{X} = (X, Y, Z)$. We will summarize the results of (Névir and Blender, 1994) who formulated the Lorenz model with respect to Nambu mechanics. Ten years later, Blender and Lucarini (2013) extended this idea for a larger state space to demonstrate the impact of viscous heating on energies in a truncated model of convection. As an example for the atmospheric applicability of Nambu-mechanics, the Lorenz equations for non-dissipative systems (2.2) can be written in Nambu formulation in terms of the two quantities that are conserved with respect to the non-dissipative

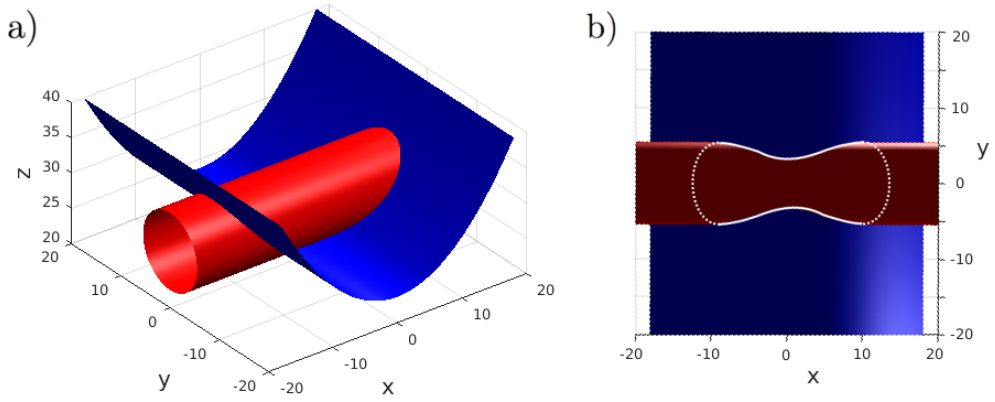

Figure 2.2: a)The surfaces of the conserved quantities H (red) and C (blue) (2.12) are shown. The intersection of the two surfaces is the phase space trajectory and depicts the set of system states of the Lorenz equations (2.2). In b) the surfaces are shown from the bottom, and the trajectory is marked by a white line. The parameters $r = 28$, $\sigma = 10$ and $H = -377$, $C = -237$ are chosen.

Lorenz system: the energy H, and the Casimir C (see (2.3)):

$$\frac{d\mathbf{X}}{dt} = \nabla C \times \nabla H. \tag{2.11}$$

The two conserved quantities (2.12) can be discussed geometrically:

$$\begin{aligned} H &= \frac{1}{2}Y^2 + \frac{1}{2}Z^2 - rZ \quad \text{Tube in X-direction} \\ C &= \frac{1}{2}X^2 - \sigma Z \qquad\qquad \text{Gutter.} \end{aligned} \tag{2.12}$$

The energy- and the C-surface are illustrated in fig. 2.2.

From (2.11) it follows that the phase space trajectory is given by the intersection of surfaces with constant H and C. There are two cases of the position of the surfaces:

Case 1: $\min(H) < \min(C)$. The slowest motion is in the lower part of the curve because the angles between the two surfaces are smaller there compared with the upper part; which is mathematically expressed by the cross product of the gradients of C and H in (2.11). The intersection und thus the trajectory has the shape of a dog bone, as shown in fig. 2.2 b).

Case 2: $\min(H) > \min(C)$. If the red tube in fig. 2.2 is shifted upwards the z-axis, the intersection of the surfaces become two separated, nearly elliptic, closed curves. These two curves indicate the two 'butterfly wings'

of the Lorenz attractor for the dissipative Lorenz equations in fig. 2.1 The trajectories represent the motion around the steady state. For further discussions of the dissipative Lorenz equations see Névir and Blender (1994) or Névir (1998).

We have seen that Nambu mechanics provides a geometric illustration of trajectories. It can be used to find geometrically trajectories that reflect the set of system states attained by the solution in the course of time of dynamical non-linear systems. In the next section we will give a brief summary of discrete Nambu mechanics in order to find geometrically solutions of three point vortex systems. The transition to continuous Nambu-mechanics will be discussed in the beginning of the second part of this thesis.

2.2 Discrete Nambu mechanics

Here, we follow Müller and Névir (2014). For a more detailed description of discrete Nambu mechanics the reader is also directed towards Nambu (1973), Névir and Blender (1993), or Blender and Lucarini (2013).

We consider a classical mechanical system with n degrees of freedom

$$\mathbf{x}(t) = (x_1, \ldots, x_n) \tag{2.13}$$

and denote $\mathbb{S}$ the phase space of the system with $n-1$ conserved quantities $H_1(\mathbf{x}), H_2(\mathbf{x}), \ldots, H_{n-1}(\mathbf{x})$, $H_j : \mathbb{S} \longrightarrow \mathbb{R},\ j = 1, \ldots, n-1$. Then, the equation of motion can be written in terms of Nambu's formalism:

$$\frac{\mathrm{d}x_i}{\mathrm{d}t} = \frac{\partial(x_i, H_1, \ldots, H_{n-1})}{\partial(x_1, \ldots, x_n)},\ i = 1, \ldots, n. \tag{2.14}$$

with respect to the Jacobi determinant. We recall that the Jacobi determinant is the determinant of the Jacobi matrix. Inserting the time derivative of an arbitrary time dependent function $F(x_1, \ldots, x_n),\ F : \mathbb{S} \longrightarrow \mathbb{R}$ in (2.14) we obtain:

$$\frac{\mathrm{d}F}{\mathrm{d}t} = \frac{\partial F}{\partial x_1}\frac{\partial x_1}{\partial t} + \frac{\partial F}{\partial x_2}\frac{\partial x_2}{\partial t} + \cdots + \frac{\partial F}{\partial x_n}\frac{\partial x_n}{\partial t} \tag{2.15}$$

We can now define the Nambu bracket that describes the time evolution of the function F:

$$\boxed{\{F, H_1, H_2, \ldots, H_{n-1}\} := \frac{\mathrm{d}F}{\mathrm{d}t} = \frac{\partial(F, H_1, H_2, \ldots, H_{n-1})}{\partial(x_1, \ldots x_n)},} \tag{2.16}$$

which was introduced by Nambu (1973). Thus, the time derivative of the functions $H_j, j = 1 \ldots n-1$ vanishes, because the Jacobi-determinant of two identical arguments becomes zero:

$$\frac{\mathrm{d}H_i}{\mathrm{d}t} = \{H_i, H_1, H_2, \ldots, H_{n-1}\} = 0. \tag{2.17}$$

Therefore, they are indeed conserved quantities. The Nambu bracket is multilinear, antisymmetric in all arguments. and the so-called Takhtajan identity that can be seen as generalization of the Jacobi-identity holds. For the proofs see (Névir and Blender, 1993; Takhtajan, 1994; Névir, 1998).

2.2.1 Nambu mechanics for $n = 2$ degrees of freedom: Transition to canonical Hamiltonian dynamics

For two degrees of freedom, Nambu's representation coincides with classical Hamiltonian dynamics. Take a system with $n = 2$ degrees of freedom and one conserved quantity given by the total energy $H = H(\mathbf{x})$. If we apply (2.14)

$$\frac{\mathrm{d}x_i}{\mathrm{d}t} = \frac{\partial(x_i, H)}{\partial(x_1, x_2)}. \tag{2.18}$$

and identify x_1 and x_2 with the local coordinate q and the momentum p, i.e. $x_1 = q$ and $x_2 = p$, we obtain the well known formula of the canonical conjugated Hamiltonian differential equations:

$$\dot{q} = \frac{\partial H}{\partial p}, \quad \dot{p} = -\frac{\partial H}{\partial q}, \tag{2.19}$$

These Hamiltonian equations can also be expressed by an antisymmetric, second-order Poisson tensor $\underline{\mathbf{P}}$:

$$\frac{\mathrm{d}x_i}{\mathrm{d}t} = P_{ij} \cdot \frac{\partial H}{\partial x_i}, \quad \underline{\mathbf{P}} = \begin{pmatrix} 0 & 1 \\ -1 & 0 \end{pmatrix}. \tag{2.20}$$

The characteristic properties of this canonical Poisson tensor are its independence from the phase space coordinates and its non degeneracy ($\det(\underline{\mathbf{P}}) \neq 0$).

2.2.2 Nambu mechanics for $n = 3$ degrees of freedom

In his first physical application Nambu discussed the Euler equation for a rigid rotator (Nambu, 1973) for $n = 3$ degrees of freedom. Névir and Blender (1993) used the Nambu representation to analyze the non-dissipative Lorenz equations, considering $n = 3$ degrees of freedom, too. In the following, we will shortly summarize the main equations for the three dimensional phase space, i.e. $n = 3$, to apply this concept in the next section, where we will show that Nambu mechanics provides a geometric approach for the classification of three point vortex motion.

Consider a system with $n = 3$ degrees of freedom, state space coordinates $\mathbf{x} = (x_1, x_2, x_3)$ and let $H_1(\mathbf{x})$ and $H_2(\mathbf{x})$ denote two conserved quantities, $H_i : \mathbb{S} :\longrightarrow \mathbb{R},\ i = 1, 2$. Now, we can apply formula (2.14) leading to the following three equations:

$$\begin{aligned}
\frac{\mathrm{d}x_1}{\mathrm{d}t} &= \frac{\partial(H_1, H_2)}{\partial(x_2, x_3)} = \frac{\partial H_1}{\partial x_2}\frac{\partial H_2}{\partial x_3} - \frac{\partial H_1}{\partial x_3}\frac{\partial H_2}{\partial x_2} \\
\frac{\mathrm{d}x_2}{\mathrm{d}t} &= \frac{\partial(H_1, H_2)}{\partial(x_3, x_1)} = \frac{\partial H_1}{\partial x_3}\frac{\partial H_2}{\partial x_1} - \frac{\partial H_1}{\partial x_1}\frac{\partial H_2}{\partial x_3} \\
\frac{\mathrm{d}x_3}{\mathrm{d}t} &= \frac{\partial(H_1, H_2)}{\partial(x_1, x_2)} = \frac{\partial H_1}{\partial x_1}\frac{\partial H_2}{\partial x_2} - \frac{\partial H_1}{\partial x_2}\frac{\partial H_2}{\partial x_1}
\end{aligned} \tag{2.21}$$

which can be summarized as follows:

$$\frac{\mathrm{d}x_i}{\mathrm{d}t} = \frac{\partial(x_i, H_1, H_2)}{\partial(x_1, x_2, x_3)} \tag{2.22}$$

with $i = 1, 2, 3$. The coordinates x are state space coordinates and therefore, the three-dimensional gradient in the state space $\mathbb{S}$ is given by:

$$\nabla = \left(\frac{\partial}{\partial x_1}, \frac{\partial}{\partial x_2}, \frac{\partial}{\partial x_3}\right)^T. \tag{2.23}$$

Considering a three dimensional phase space the canonical Nambu representation of the time evolution can be written in terms of the cross product of the state space gradients of the two conserved quantities H_1 and H_2:

$$\boxed{\frac{\mathrm{d}\mathbf{x}}{\mathrm{d}t} = \nabla H_1 \times \nabla H_2.} \tag{2.24}$$

As for n-dimensions (2.15), this definition can be extended to describe the dynamics of an arbitrary function $F : \mathbb{S} \longrightarrow \mathbb{R}$ leading to the triple

product:

$$\boxed{\frac{\mathrm{d}F}{\mathrm{d}t} = \{F, H_1, H_2\} := \nabla F \cdot (\nabla H_1 \times \nabla H_2).} \tag{2.25}$$

We notice that a triple product is equivalent to the determinant of a 3×3-matrix having three vectors either as its rows or its columns. Because of the triple product, we immediately see that the Nambu bracket is antisymmetric and also triliniear. Moreover, the divergence of (2.24) generates Liouville's theorem of Nambu mechanics:

$$\nabla \cdot \dot{\mathbf{x}} = \nabla \cdot (\nabla H_1 \times \nabla H_2) = 0 \tag{2.26}$$

Therefore, the state space has the properties of an incompressible fluid.

The central property of Nambu mechanics is that more than one conserved quantity have equal status, whereas in Hamiltonian mechanics only one conserved quantity (the energy) determines the equations — a second, or more conserved quantities, does not appear explicitly. But the singularity of the Poisson tensor, i.e. the vanishing determinant, leads to the second conserved quantity, which is called distinguished, or Casimir-, function in terms of Hamiltonian dynamics. Considering three degrees of freedom, the main advantage of the equality of two conserved quantities in Nambu formulation is the representation of the phase space trajectory as intersection line of two surfaces based on the conserved quantities. Therefore, this geometric application illustrates the kind of motion without explicitly solving the equations of motion.

Non-canonical Nambu mechanics for $n = 3$

In contrast to Hamiltonian dynamics that is characterized by the general antisymmetric second-order Poisson tensor (2.20), Nambu's formulation is based on an antisymmetric, third-order tensor (Névir, 1998). This tensor is called Nambu tensor and denoted by $N_{ijk},\ i, j, k = 1, 2, 3$. Additional conserved quantities determining the dynamics increase the order of the tensor by one dimension.

Let $F(x_i), G(x_i)$ and $H(x_i)$ now denote three arbitrary functions, mapping from the phase space to $\mathbb{R}$. Then, the canonical Nambu bracket is defined by:

$$\{F, G, H\} = \epsilon_{ijk} \frac{\partial F}{\partial x_i} \frac{\partial G}{\partial x_j} \frac{\partial H}{\partial x_k}, \quad i, j, k \in \{1, 2, 3\}, \tag{2.27}$$

where the Einstein summation convention is used and ϵ_{ijk} is the Levi-Cevita Tensor defined by:

$$\epsilon_{ijk} = \begin{cases} +1 & \text{if } (i,j,k) \text{ is } (1,2,3),(2,3,1), \text{ or } (3,1,2), \\ -1 & \text{if } (i,j,k) \text{ is } (3,2,1),(1,3,2), \text{ or } (2,1,3), \\ 0 & \text{if } i=j, \text{ or } j=k, \text{ or } k=i \end{cases} \tag{2.28}$$

meaning that ϵ_{ijk} is 1 if (i,j,k) is an even permutation of $(1,2,3)$, and $\epsilon_{ijk} = -1$ if it is an odd permutation, and $\epsilon_{ijk} = 0$ if any index is repeated. But for general Nambu systems, the total antisymmetric tensor of third order can depend on the phase space coordinates leading to a non-canonical formulation. Therefore, we will introduce the non-canonical tensor $N_{ijk},\ i,j,k \in \{1,2,3\}$, which we published in Müller and Névir (2014). This idea goes back to Névir (1998), where a hierarchy of general antisymmetric dynamics is outlined comparing the classical Poisson-tensors with the Nambu tensors. Let now Λ be the regular transition matrix transforming the tensor N_{abc} to the tensor N_{ijk} applying the well known transformation law $N_{ijk} = \Lambda^i_a \Lambda^j_b \Lambda^k_c N_{abc}$ with $\Lambda^i_a \Lambda^a_j = \delta^i_j$ and $\Lambda^a_i \Lambda^i_b = \delta^a_b$. Here, δ^i_j denotes the Kronecker-Delta symbol which is one if $i = j$ and zero if $i \neq j$. Since every antisymmetric tensor with three indices in a three- dimensional vector space is proportional to the Levi-Civita-symbol we set $N_{ijk} = c\epsilon_{ijk}$ and calculate c such that we can write the non-canonical form in terms of the Levi-Cevita symbol and compare it to the canonical form.

$$N_{ijk} = c\epsilon_{ijk} = \Lambda^i_a \Lambda^j_b \Lambda^k_c \epsilon_{abc} = \det(\Lambda^a_i)\epsilon_{ijk} \Longrightarrow c = \det(\Lambda^i_a). \tag{2.29}$$

Substituting ϵ_{ijkl} by N_{ijk} in (2.27) we obtain the canonical Nambu bracket for $\det(\Lambda^a_i) = 1$ and $\det(\Lambda^a_i) \neq 1$ leads to the non-canonical Nambu bracket which we denote with the subscript c:

$$\{F,G,H\}_c = N_{ijk} \frac{\partial F}{\partial x_i} \frac{\partial G}{\partial x_j} \frac{\partial H}{\partial x_k} = c\epsilon_{ijk} \frac{\partial F}{\partial x_i} \frac{\partial G}{\partial x_j} \frac{\partial H}{\partial x_k}. \tag{2.30}$$

The dependency on the phase space variables of the Nambu tensor is a generalization of the mechanics introduced by Nambu (1973). This generalization is relevant for the motion of three point vortices.

If $H(x_i)$ and $C(x_i)$ denote two conserved quantities, then the above generalized Nambu bracket describes the dynamics w.r.t. the function F. i.e.

$\frac{\mathrm{d}F}{\mathrm{d}t} = \{F, G, H\}$. Then,

$$\boxed{\frac{\mathrm{d}x_i(t)}{\mathrm{d}t} = \{x_i, C, H\} = N_{ijk}(x_i)\frac{\partial H}{\partial x_j}\frac{\partial C}{\partial x_k}} \tag{2.31}$$

provides the equations of motion for the phase space coordinates x_i.

Summary

In this chapter we gave an introduction to discrete Nambu mechanics, the canonical form as well as the non-canonical representation. In the next chapter we will show how this representation can be applied to illustrate the kind of motion of three point vortices without explicitly solving the equations of motion.

Chapter 3

Nambu mechanics of point vortex theory

Point vortices are an idealized concept to understand basic vortex motion that has been applied to many disciplines and different spatio-temporal scales: DNA-strings, magnetic flows, atmospheric dynamics. The set of equations for point vortex motions provides a solution of the barotropic, inviscid, incompressible Navier-Stokes equation. This set of equation for perfect fluids is called Euler equations. First, we will summarize the main definitions and equations for point vortex theory as we have published in Müller and Névir (2014) and Müller et al. (2015). Second, we will apply discrete Nambu mechanics to introduce a novel approach to classify point vortex motion without explicitly solving the differential equations of point vortex motion. Similar to the previously discussed Lorenz equations, where we have discussed that Nambu's formulation allows for a geometric view on the equations of motion in the state space, we will apply discrete Nambu mechanics for a geometric view on point vortex dynamics. We have introduced this concept in Müller and Névir (2014). Third, based on Müller et al. (2015), we will show, how the idealized concept of point vortices can be applied to atmospheric motion on the synoptic scale. More precisely, we will use point vortex theory to explain blocked weather situations.

3.1 Introduction to point vortex dynamics

The first investigations on the dynamics of point vortices in the plane can be ascribed to Helmholtz (1858). Twenty years later, Kirchhoff (1876) introduced the general Hamiltonian structure of N point vortices and Gröbli

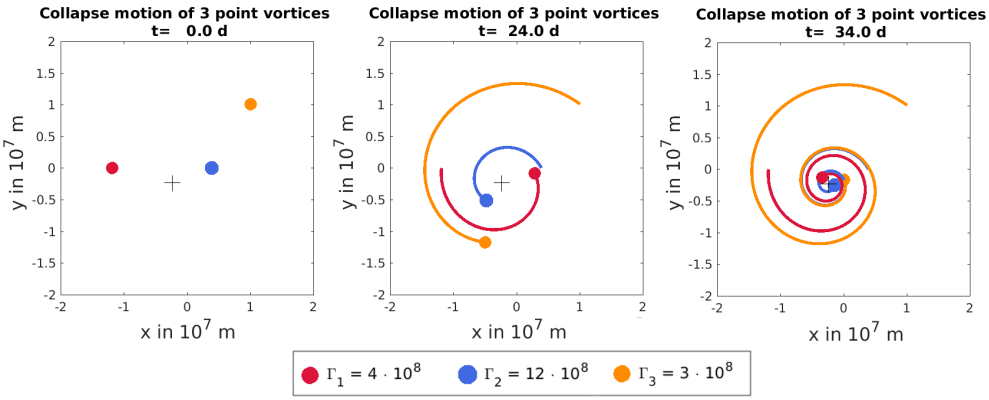

Figure 3.1: An example of the time evolution of collapse motion is shown.

(1877) analysed in detail the motion of three point vortices. He introduced the equations of motions in terms of the intervortical distances, i.e. the relative distances between the vortices. In his pioneering work he studied i.a. the self-similar contraction of triangles spanned by three point vortices. Today, this self-similar contraction is known as collapsed motion, as shown in fig. 3.1.

Since then, numerous papers have been published on the motion of three point vortices considering different aspects of point vortices, see for example the works of Novikov (1975), Newton (2001) or Aref (2007). Three point vortices forms integrable systems. The motion can be classified as periodic motion, as shown in fig. 3.2, collapsed or expanding systems, see fig. 3.1, or they form an equilibrium vortex system, that either rotates or translates depending on the initial conditions. See fig. 3.3 and fig. 3.4.

In this classical analysis of three point vortex motion, the relevant conservation laws are not considered as equitable quantities. In 1949 Synge introduced trilinear coordinates based on the three relative distances to describe the motion of three point vortices in terms of Hamiltonian dynamics (Synge, 1949; Aref, 1979; Blackmore et al., 2007; Newton, 2001; Obukhov et al., 1984). Also Aref used these trilinear coordinates to describe trajectories in a phase space (Aref, 2010). Thereby, the phase space coordinates represent the distances from the three sides of the triangle. Synge and Aref show that the physical regions of the vortex motions in this trilinear coordinate plane are bounded by conic sections (ellipse, parabola or hyperbola) (Aref, 1979; Synge, 1949).

In chapter 2, we have introduced discrete Nambu mechanics, which, in 1998, Névir and Makhaldiani simultaneously applied to three point vor-

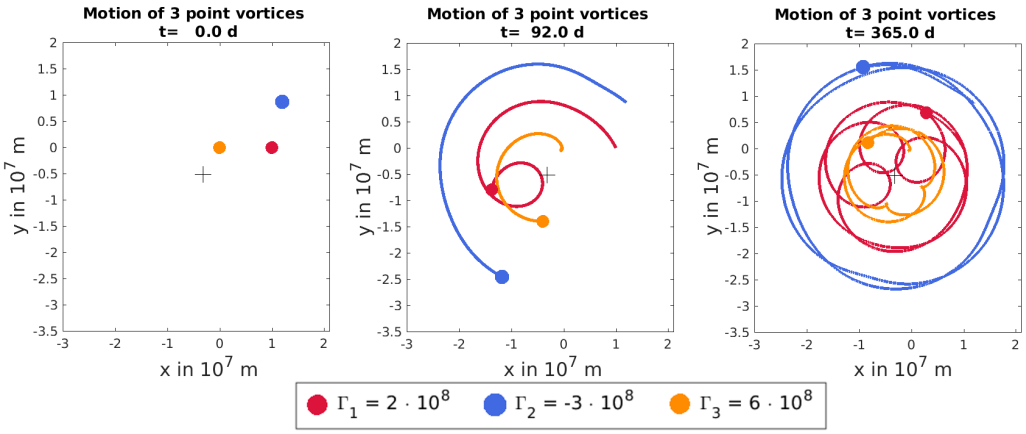

Figure 3.2: An example of the time evolution of a three point vortex system is shown.

tices (Makhaldiani, 1998; Névir, 1998). Whereas Makhaldiani picked up Nambu's general idea to represent the equations of motion in terms of the conserved quantities, we build on Névir's non-canonical classification and analysis of Nambu mechanics in the context of point vortex motion. In contrast to Hamiltonian mechanics, where the time evolution in any dimension is only based on one conserved quantity, the kinetic energy, we need a second conserved quantity to describe the time evolution in a $N = 3$-dimensional phase space in terms of Nambu mechanics. Based on the idea to formulate the time evolution in terms of the cross product (2.25), we will look for a suitable three dimensional phase space and two conserved quantities depending on the phase space coordinates for point vortex systems. That way, the point vortex trajectory is given by the intersection of two surfaces and the type of motion can be determined without explicitly solving the system of nonlinear differential equations.

Let $\mathbf{v}$ be a solenoidal vector field, i.e. $\nabla \cdot \mathbf{v} = 0$ and denote $\boldsymbol{\xi} = \nabla \times \mathbf{v}$ the vorticity vector. An important quantity in two-dimensional vortex dynamics is the circulation Γ that is defined by:

$$\Gamma = \oint_C \mathbf{v} \cdot d\mathbf{s} = \int_A \boldsymbol{\xi} \cdot \mathbf{n} \, dS, \tag{3.1}$$

where C is a closed curve on a material plane. To achieve the right hand side with area A and normal vector $\mathbf{n}$, Stokes theorem was applied. Moreover, assuming ideal incompressible fluids with conservative forces, Kelvin's circulation theorem states that the circulation Γ around a closed material

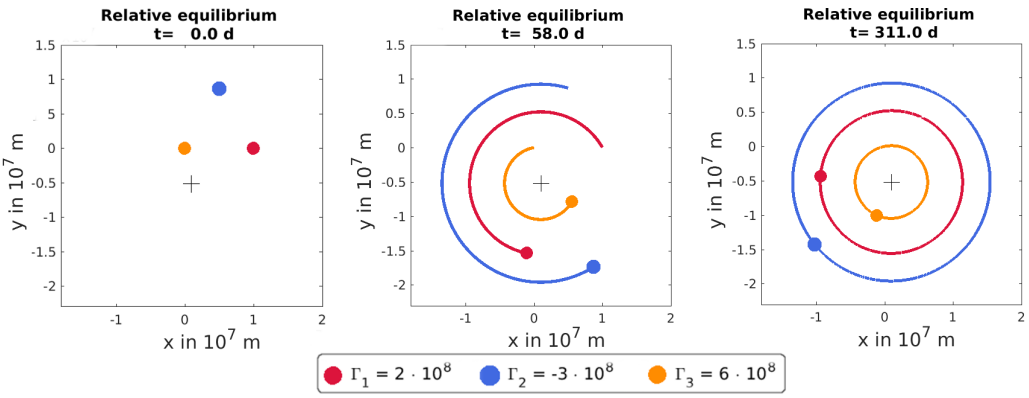

Figure 3.3: An example of the time evolution of a three point vortex equilibrium is shown.

curve moving with the fluid is constant, i.e.

$$\frac{d\Gamma}{dt} = 0 \quad \text{(Conservation of the circulation)}. \tag{3.2}$$

Denote $\mathbf{x}_i = (x_i \; y_i)^T$, $i = 1, \dots N$ the local coordinates of the i-th point vortex of a N-point vortex system in the plane. Each vortex is characterized by its circulation Γ_i, $i = 1, 2, \dots, N$. Further, denote $r_{ij} = ((x_i - x_j)^2 + (y_i - y_j)^2)^{1/2}$ the relative distance of the i-th and j-th point vortex $(i, j = 1, \dots, N)$. Then, the equations of motion derived by Helmholtz (1858) are given by:

$$\begin{aligned} \frac{dx_j}{dt} &= -\frac{1}{2\pi} \sum_{\substack{i \neq j \\ i,j=1}}^{N} \frac{\Gamma_i (y_j - y_i)}{r_{ij}^2}, \\ \frac{dy_j}{dt} &= +\frac{1}{2\pi} \sum_{\substack{i \neq j \\ i,j=1}}^{N} \frac{\Gamma_i (x_j - x_i)}{r_{ij}^2}. \end{aligned} \tag{3.3}$$

Kirchhoff (1876) established the Hamiltonian representation of these equations of motion as non-linear coupled system of $2N$ ordinary differential equations:

$$\begin{aligned} \Gamma_i \frac{dx_i}{dt} &= \frac{\partial H}{\partial y_i}, \\ \Gamma_i \frac{dy_i}{dt} &= -\frac{\partial H}{\partial x_i}. \end{aligned} \tag{3.4}$$

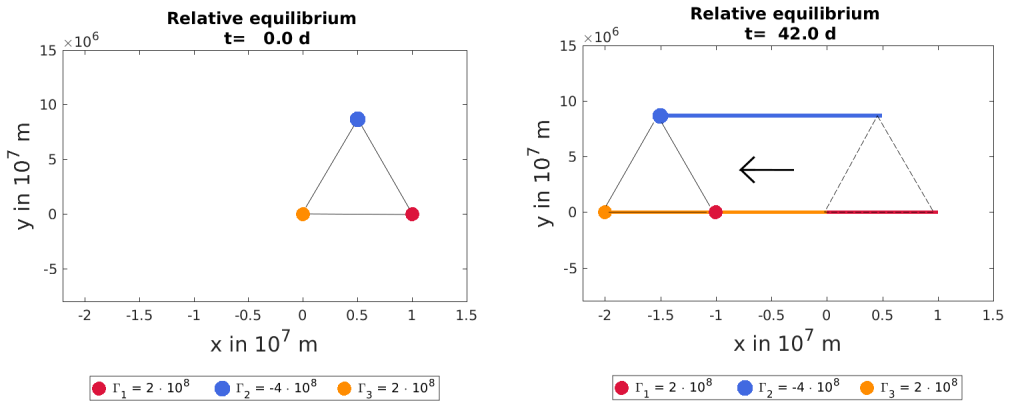

Figure 3.4: Three point vortex systems that form an equilateral triangle with vanishing total circulation translate.

where the total energy H of a N-vortex system is given by

$$H = -\frac{1}{4\pi} \sum_{\substack{i \neq j \\ i,j=1}}^{N} \Gamma_i \Gamma_j \ln(r_{ij}). \tag{3.5}$$

Because the energy depends on the relative distances, the relative distances seem suitable phase space coordinates to apply Nambu-mechanics. A second conserved quantity depending on the relative distances is needed to apply Nambu-mechanics to a three-dimensional phase space.

Kirchhoff showed the conservation of the *zonal momentum* P_x, the *meridional momentum* P_y and the vertical component of the *angular momentum* L_z (Kirchhoff, 1876)

$$P_x(x_i, y_i) = \sum_{i=1}^{N} \Gamma_i y_i \tag{3.6}$$

$$P_y(x_i, y_i) = -\sum_{i=1}^{N} \Gamma_i x_i \tag{3.7}$$

$$L_z(x_i, y_i) = -\frac{1}{2} \sum_{i=1}^{N} \Gamma_i (x_i^2 + y_i^2). \tag{3.8}$$

Moreover, Kelvin's circulation theorem allows us to conclude that the following scalars, the total circulation Γ and the double sum of all circulations, are conserved:

$$\Gamma_{\text{tot}} := \sum_{i=1}^{N} \Gamma_i, \qquad V := \frac{1}{2} \sum_{\substack{i,j=1 \\ i \neq j}}^{N} \Gamma_i \Gamma_j. \tag{3.9}$$

Fortak (1965) shows that the constant quantity V can be formulated with respect to the local coordinate $\mathbf{r}$ and the velocity $d\mathbf{r}/dt$. Let $\mathbf{k} = (0, 0, 1)$. Then V is equivalent to:

$$V = 2\pi \sum_{j=1}^{N} \Gamma_j \mathbf{k} \cdot \left(\mathbf{r}_j \times \frac{d\mathbf{r}_j}{dt} \right) = \frac{1}{2} \sum_{\substack{i,j=1 \\ i \neq j}}^{N} \Gamma_i \Gamma_j. \tag{3.10}$$

Moreover, deriving the point vortex equations (3.4) by a variational principle, the corresponding Lagrange-function is given by the sum of V and the total energy H (Chapman, 1978). Thus, the conservation of V is a non-trivial aspect of point vortex dynamics. A composition of P_x, P_y and Γ leads to a further important conserved quantity called the *center of circulation* $\mathbf{C}$:

$$\mathbf{C} = \frac{\sum_i^N \Gamma_i \boldsymbol{x}_i}{\sum_i^N \Gamma_i}. \tag{3.11}$$

Assuming that the total circulation is not equal to zero, point vortices move around their common center of circulation $\mathbf{C}$. Thereby, the orientation of a rotating N-vortex system depends on the sign of the total circulation. But a whole point vortex system can also have zero total circulation. For a vortex system with $\Gamma_{\text{tot}} \rightarrow 0$, $\mathbf{C}$ approaches infinity. Therefore, if $\Gamma_{\text{tot}} = 0$, each vortex may rotate, but the geometric central point of the N-vortex system translates. A point vortex system with vanishing total circulation will later be applied to describe blocked weather situations. Because of the conservation of the center of circulation, one single point vortex always remains in its initial condition.

Following for example Newton (2001), we can also define a Poisson bracket for point vortex dynamics.

Definition 1. Canonical Possion bracket for point vortex dynamics
The canonical Poisson bracket of two functions $f = f(x_i, y_i)$ and $g = g(x_i, y_i)$, $i = 1, \ldots, N$ of position variable (x_i, y_i) with respect to the i-th vortex with circulation Γ_i is defined by:

$$\{f, g\} = \sum_{i=1}^{N} \frac{1}{\Gamma_i} \left(\frac{\partial f}{\partial x_i} \frac{\partial g}{\partial y_i} - \frac{\partial f}{\partial y_i} \frac{\partial g}{\partial x_i} \right). \tag{3.12}$$

The bracket satisfies the properties of symmetry, linearity, Jacoby identity and Leibniz identity.

Definition 2. Casimir functions
Elements commuting with all other elements in the bracket are called Casimir functions.

Therefore, Casimir functions also commute with the energy. Thus, they are always conserved quantities. While, for general systems, the equations of motion are determined by the energy, the spatial conservation laws such as the momenta give further informations on the spatial structure of the systems. With respect to point vortex theory, the Kelvin momenta P_x, ,P_y, the angular momentum L_z and the energy H are the conserved quantities that further act as constraints on the systems. Moreover, $P_x,\ P_y$ and L_z form the conserved quantity M (cf. Aref (1979)), which can be identified as Casimir function of the system.

The non-trivial Poisson brackets of the global quantities P_x, P_y and L_z of the n-point vortex systems are summarized in the left column in table 3.1. They are compared with the mass-point bracket relation in the right column in table 3.1, where the Poisson-bracket and the conserved quantities for mass point dynamics can be derived from the canonical conjugate equation 2.19. It is defined as follows:

Definition 3. Poisson bracket for mass point dynamics
For two functions $F(\mathbf{p},\mathbf{q})$ and $G(\mathbf{p},\mathbf{q})$ the Poisson brackets for mass points reads as:

$$\{F,G\}_P = \sum_{i=1}^{N}\left(\frac{\partial F}{\partial \mathbf{q}_i}\cdot\frac{\partial G}{\partial \mathbf{p}_i} - \frac{\partial G}{\partial \mathbf{p}_i}\cdot\frac{\partial F}{\partial \mathbf{q}_i}\right), \tag{3.13}$$

where $\mathbf{q}_i$ and $\mathbf{p}_i$ are the 3D-local coordinate and 3D-momentum of the i-th mass point of a N-mass point system.

$$\begin{aligned}\mathbf{P} &= \sum_{i=1}^{N}\mathbf{p}_i && \text{(linear momentum)}\\ \mathbf{L} &= \sum_{i=1}^{N}\mathbf{q}_i\times\mathbf{p}_i && \text{(angular momentum)}\end{aligned} \tag{3.14}$$

Comparing the bracket relations of the constitutive quantities of point vortex systems with the bracket relations of classical mechanics in table 3.1, a major difference can be found for the bracket of the linear momenta. In classical mass point mechanics the momenta commute, but they do not commute regarding point vortex dynamics. This difference is important,

Point vortex dynamics	Mass point dynamics
$\{L_z, P_x\} = P_y$	$\{L_z, P_x\}_P = P_y$
$\{L_z, P_y\} = -P_x$	$\{L_z, P_y\}_P = -P_x$
$\{P_x, P_y\} = \Gamma$	$\{P_x, P_y\}_P = 0$

Table 3.1: The Poisson-bracket of point vortex dynamics compared to the Poisson-bracket of mass point dynamics (see def. 8.2, chapter 8), where L_z are the angular momenta and P_x and P_y are the momenta of the corresponding system

because it shows that a different algebraic description is needed for fluid dynamical systems regarding vortex dynamics. We will explore the algebraic view on fluid dynamics in part II of this thesis.

The total energy H commutes with these three quantities. A Casimir function of point vortex dynamics is the quantity M and given by:

$$M = -\Gamma L_z - \frac{1}{2}(P_x^2 + P_y^2) = \frac{1}{2}\sum_{i,j=1}^{N} \Gamma_i \Gamma_j r_{ij}^2. \tag{3.15}$$

This quantity commutes with the linear momenta P_x and P_y, the angular momentum L_z and the Hamilton function H, i.e.:

$$[M, P_x] = 0, \quad [M, P_y] = 0, \quad [M, L_z] = 0, \quad [M, H] = 0. \tag{3.16}$$

Because of the last relation, $[M, H] = 0$, M is a conserved quantity. [1] The energy H as well as the relative angular momentum M depend on the relative distances r_{ij} of the vortices. We recall that two conserved quantities are needed to describe a system of three degrees of freedom in terms of Nambu's formulation. Therefore, considering a three point vortex system in the phase space of their relative distances, the energy and the relative angular momentum can be chosen for a geometric classification of the motion of three point vortices. Moreover, three point vortices form an integrable system (see, e.g. Aref, 1979) and we will discuss the possible solutions of three point vortex systems in the following.

[1] In Müller and Névir (2014) we suggested to call M *squared relative angular momentum* with respect to the center of circulation, because it contains squared relative distances as well as the circulation as the rotational part. We will hold on to this notation in the following.

3.2 Geometric application of Nambu mechanics: the motion of three point vortices in the plane

In order to apply Nambu mechanics to three point vortex motion in the plane, we will consider the time evolution of the intervortical distances, see for example Aref (2007) or Névir (1998). Denote $A_{123} = A(r_{12}, r_{23}, r_{31})$ the area of the triangle with the intervortical distances as side lengths. Let σ the orientation of the triangle, where $\sigma = \sigma_{ijk} = 1$, if the point vortices with $\Gamma_i, \Gamma_j, \Gamma_k$ are arranged counter-clockwise and $\sigma = \sigma_{ijk} = -1$ if Γ_i, Γ_j and Γ_k are ordered clockwise. Further, let $i, j, k = 1, \ldots, n$ in cyclic order, $i \neq j \neq k$. Then, the time evolution of the squared relative distances $r_{ij}^2 = ((x_i - x_j)^2 + (y_i - y_j)^2)^{1/2}$ of three point vortices is given by

$$\frac{dr_{ij}^2}{dt} = \frac{2}{\pi}\sigma\Gamma_k A_{123} \cdot \left(\frac{1}{r_{jk}^2} - \frac{1}{r_{ik}^2}\right), \tag{3.17}$$

We apply the chain rule and denote

$$\rho := \rho(r_{ij}, r_{jk}, r_{ki}) = \frac{r_{ij}r_{jk}r_{ki}}{4A_{ijk}}, \tag{3.18}$$

which represents the inscribed circle radius of the triangle with side lengths r_{ij}, r_{jk} and r_{ki}. We get:

$$\boxed{\frac{dr_{ij}}{dt} = \frac{\sigma\Gamma_k}{4\pi\rho}\left(\frac{r_{ki}}{r_{jk}} - \frac{r_{jk}}{r_{ik}}\right),} \tag{3.19}$$

In the following, we will analyze the relative motion of three point vortices spanned by the phase space coordinates $r = (r_{12}, r_{23}, r_{31})$. Applying Nambu mechanics to a three-dimensional phase space, we need two conserved quantities to characterize the motion of three point vortices. We can find two conserved quantities that depend on the relative distances: M (3.15) and the total energy H (3.5). They can be formulated as follows:

$$\begin{aligned} M &= M(r_{12}, r_{23}, r_{31}) = \frac{1}{2}(\Gamma_1\Gamma_2 r_{12}^2 + \Gamma_2\Gamma_3 r_{23}^2 + \Gamma_3\Gamma_1 r_{31}^2) \\ H &= H(r_{12}, r_{23}, r_{31}) = -\frac{1}{2\pi}(\Gamma_1\Gamma_2 \ln(r_{12}) + \Gamma_2\Gamma_3 \ln(r_{23}) + \Gamma_3\Gamma_1 \ln(r_{31})) \end{aligned} \tag{3.20}$$

Using these definitions, the time evolution of the relative distances of three

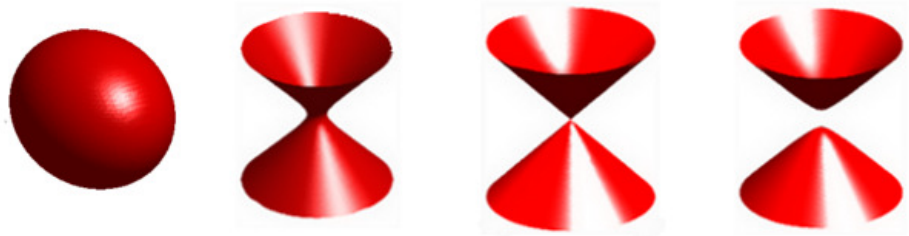

Figure 3.5: The M-surface represents one of the four types of quadrics (from lhs to rhs) an ellipsoid, a one-sheeted hyperboloid, a cone, or a two-sheeted hyperboloid

point vortices in Nambu representation can be written as:

$$\frac{dr_{ij}}{dt} = \frac{\sigma}{2\Gamma_1\Gamma_2\Gamma_3\rho}\left(\frac{\partial M}{\partial r_{jk}}\frac{\partial H}{\partial r_{ki}} - \frac{\partial M}{\partial r_{ki}}\frac{\partial H}{\partial r_{jk}}\right), \tag{3.21}$$

with $i, j, k = 1, 2, 3$ in cyclic order and $i \neq j \neq k$. In contrast to Makhaldiani, we scale the time t by a constant factor $t' = \alpha t$ with $\alpha = \sigma/2\Gamma_1\Gamma_2\Gamma_3$. Because the inscribed circle radius $\rho = \rho(r_{12}, r_{23}, r_{31})$ depends on the relative distances, we obtain a non-canonical Nambu representation of three point vortices:

$$\boxed{\rho\frac{d\mathbf{r}}{dt'} = \nabla M \times \nabla H} \tag{3.22}$$

This formulation of the equations of motion motivates the representation of the trajectory of three point vortices as intersection of two surfaces. The surfaces are given by the conserved quantities M and H leading to the phase space of intervortical distances, because both conserved quantities depend on the intervortical distances. Applying the generalized non-canonical Nambu-bracket (2.30) respectively (2.31), it follows that the Nambu-tensor for point vortices is given by:

$$N_{ijk}(r_{12}, r_{23}, r_{31}) = \frac{1}{\rho}\epsilon_{ijk},\ i, j, k = 1, 2, 3 \tag{3.23}$$

Therefore, we classify the relative motion of three point vortices as non-canonical Nambu dynamics.

Now, we will assign the conserved quantities M and H a surface to discuss the different kind of motions of three point systems from a geometrical point of view. Regarding (3.22), the time evolution of three point vortices, that is usually described in the two dimensional local coordinates, is here formulated in the phase space of the intervortical disctances $r =$

Sign of circulations	Surface of M	Possible motion
$\Gamma_1, \Gamma_2, \Gamma_3 > 0, c > 0$	Ellipsoid	Periodic motion Rel. equilibrium
$\Gamma_1, \Gamma_3 > 0, \Gamma_2 < 0, c > 0$	One-sheeted hyperboloid	Periodic motion Rel. equilibrium
$\Gamma_1, \Gamma_3 > 0, \Gamma_2 < 0, c = 0$	Cone	Collapse Expanding
$\Gamma_1, \Gamma_3 > 0, \Gamma_3 < 0, c < 0$	To-sheeted hyperboloid	Periodic motion Rel. equilibrium
$\Gamma_1, \Gamma_2, \Gamma_3 > 0, c < 0$		No real solution

Table 3.2: Geometry of the quantity M depending on the sign of the circulations of the point vortices

(r_{12}, r_{23}, r_{31}) using the relative angular momentum M and the energy H.

Set $b := -2\pi H/(\Gamma_1\Gamma_2\Gamma_3)$ and $c := 2M/(\Gamma_1\Gamma_2\Gamma_3)$. The energy and the relative angular momentum determine two surfaces:

$$H: \ \frac{\ln(r_{12})}{\Gamma_3} + \frac{\ln(r_{23})}{\Gamma_1} + \frac{\ln(r_{31})}{\Gamma_2} = b, \quad M: \ \frac{r_{12}^2}{\Gamma_3} + \frac{r_{23}^2}{\Gamma_1} + \frac{r_{31}^2}{\Gamma_2} = c \tag{3.24}$$

The surface of M represents a quadric and the sign of the circulations characterizes its topological structure. It can represent an ellipsoid, a one-sheeted hyperboloid, a cone, or a two-sheeted hyperboloid, see fig. 3.5. The different circulations and occurring motions are summarized in table 3.2).

Since both conserved quantities depend on the relative distances, we can apply (3.22) and the intersection $M \bigcap H$ yields the trajectory of the relative motion of the point vortices in the phase space. Because the relative distances r_{ij} $(i, j = 1, 2, 3, i \neq j)$ are positive, in each case the M-surface is a subsurface of the surfaces mentioned before. We can summarize the necessary conditions of the quantities M and H for the different kind of motions:

$$\begin{aligned} M \neq 0, \ H \neq 0: &\quad \text{Periodic motion} \\ M = \lambda H, \ \lambda \in \mathbb{R} \setminus \{0\}: &\quad \text{Relative equilibrium} \\ M = 0, \ H \neq 0, \sigma > 0: &\quad \text{Collapsed motion} \\ M = 0, \ H \neq 0, \sigma < 0: &\quad \text{Expanding motion} \end{aligned} \tag{3.25}$$

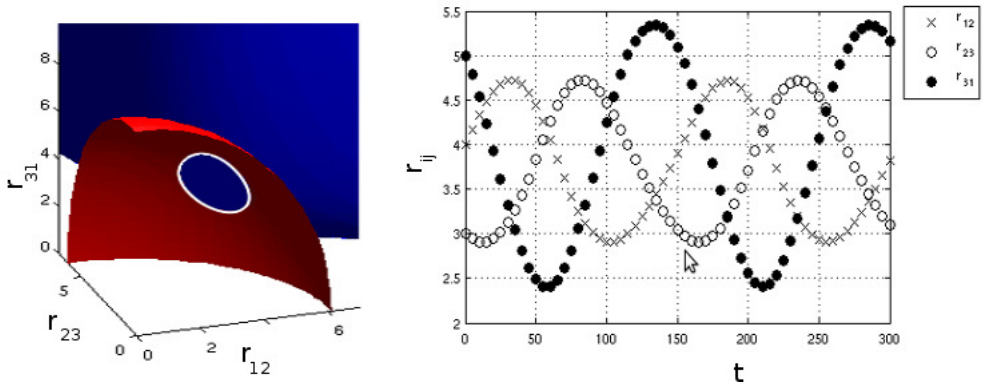

Figure 3.6: Left: the intersection of the M-surface (red surface, representing a subset of an ellipsoid) with the energy surface (blue) illustrates an example of periodic motion. Right: time evolution of three relative distances r_{ij} of a periodic three point vortex system.

Thus, the two conserved quantities the relative angular momentum, M, and the energy, H, determine the dynamics. In the following sections we will discuss the different classes of motions of three point vortex systems.

3.3 Periodic motion

Closed intersection lines in the phase space represent periodic point vortex motions. If the signs of the circulations are all positive and if the value of c is greater than zero, the surface of M becomes an ellipsoid (see (3.24) and table 3.2). H is an only slight curved surface. The slightly curvature is due to the logarithm. Therefore, the intersection of M and H is given by a closed line leading to a periodic motion. One example is given in fig. 3.6. Moreover, if the circulations have different signs, M represents a one-sheeted hyperboloid in case of $c > 0$ and a two-sheeted hyperboloid if $c < 0$. In this case, periodic motions can also occur. In fig. 3.6 an example of a periodic motion with initial circulations $\Gamma_1 = 1,\ \Gamma_2 = 2,\ \Gamma_3 = 1$ and initial distances $r_{12} = 4,\ r_{23} = 3,\ r_{31} = 5$ is shown. In fig. 3.6 on the left the point vortex trajectory in the phase space is given by the intersection line of the two surfaces of M (red surface) and H (blue surface). Because the signs of all circulations are positive, the M-surface represents a part of an ellipsoid. Therefore, the intersection line is a closed curve, i.e. the motion is periodic. Fig. 3.6 on the right represents the classical plot of time evolution of the relative displacements. To illustrate the temporal change of the inter-

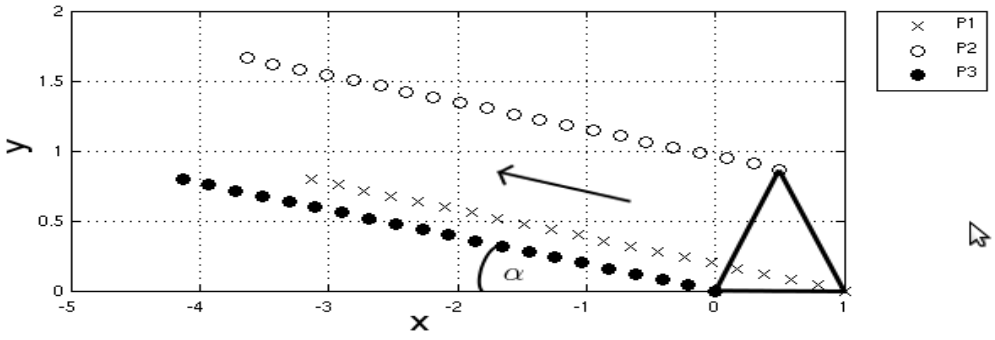

Figure 3.7: A three point vortex system translates in case of zero total circulation. Here we set $r_{12} = r_{23} = r_{32} = 1$ and $\Gamma_1 = 1,\ \Gamma_2 = -3$ and $\Gamma_3 = 2$. The translation angle α depends on the values of the circulations.

vortical distance in fig. 3.6, we used the Runge-Kutta method of 4. order to solve the nonlinear differential equations (3.19). We notice one benefit of the application of Nambu mechanics. Solving differential equations cost more computer effort than simply illustrating conserved quantities surfaces to classify different kind of motions.

3.4 Relative equilibrium

In case the two surfaces intersect in one point in the phase space, three point vortices generate a relative equilibrium configuration.

The relative equilibrium of three point vortices occur either for collinear initial states or for three point vortices forming an equilateral triangle. A three vortex system that forms an equilateral triangle and that has non-vanishing total circulation rotates about its center of circulation. Its rotation frequency is $\omega = \Gamma/2\pi r^2$, where r is the triangle side (Newton, 2001). In case of zero total circulation, the center of circulation (3.11) lies in infinity. In that case the vortices translate with velocity

$$v = |\mathbf{v}| = \frac{\sqrt{2(\Gamma_1^2 + \Gamma_2^2 + \Gamma_3^2)}}{4\pi r} \tag{3.26}$$

This translational velocity can be derived by inserting $r_{12} = r_{23} = r_{31} =: r$ in (3.3). One exemplary translating three point vortex system is shown in fig. 3.7. In Müller and Névir (2014) we have derived the formula for the translational angle α. Let the x-axis be on the line $\overline{\Gamma_1\Gamma_3}$, i.e. the straight line through the vortices of the same sign of circulation passing the origin (see

fig. 3.7). The point $P_0 = (x_0, y_0)$ with circulation Γ_1 lies at the origin. Set $r = r_{12} = r_{23} = r_{31}$. Applying (3.3), the velocity vector $\mathbf{v}$ in P_0 and the slope m of the line lying on the velocity vector are given by:

$$\mathbf{v} = \frac{1}{4\pi r}\begin{pmatrix}\sqrt{3}\Gamma_2\\ \Gamma_1 - \Gamma_3\end{pmatrix}, \quad m = \frac{dy/dt}{dx/dt} = \frac{\Gamma_1 - \Gamma_3}{\sqrt{3}\Gamma_2}. \tag{3.27}$$

Therefore, the angle of translation α between the velocity vector and the x-axis is given by:

$$\alpha = \arctan(m) = \arctan\left(\frac{\Gamma_1 - \Gamma_3}{\sqrt{3}\Gamma_2}\right) \tag{3.28}$$

To apply Nambu's formalism to an equilibrium state we take a look at the relevant conserved quantities H and M for equilateral triangles:

$$H = -\frac{\ln(r)}{2\pi}V, \quad M = \frac{r^2}{2}V \Longrightarrow H = \lambda \cdot M \tag{3.29}$$

In terms of Nambu mechanics for every energy level and an arbitrary but fixed V there is a solution of a relative equilibrium if and only if the M-surface is tangent to the H-surface. Because the intersection is given by a fixed point, no time evolution is possible.

3.5 Collapse and expanding state

Special cases are the collapse and the expanding motion that are characterized by self-similarity. An interesting question is how the self-similar motion can be expressed in terms of the geometrical view of Nambu mechanics. First, we will discuss the behavior of the conserved quantities. Necessary and sufficient conditions for the self-similar collapse of three vortices in general are shown in Aref (2010), Newton (2001) or Synge (1949). As first condition, M needs to be zero, i.e.

$$M = \frac{1}{2}\sum_{i,j=1,i\neq j}\Gamma_i\Gamma_j r_{ij}^2 = 0 \tag{3.30}$$

Second, the harmonic mean has to be zero, too:

$$h = \frac{1}{3}\left(\frac{1}{\Gamma_1} + \frac{1}{\Gamma_2} + \frac{1}{\Gamma_3}\right) = 0 \Longleftrightarrow V = \frac{1}{2}\sum_{i,j=1,i\neq j}\Gamma_i\Gamma_j = 0 \tag{3.31}$$

And, of course, the initial configuration must not be an equilibrium. Aref (2010) established the self-similarity of the collapse with respect to the intervortical distances:

$$r_{ij}(t) = f(t) r_{ij}(t=0),\ i,j = 1,2,3, \tag{3.32}$$

where $f(t) = \sqrt{1 - t/\tau}$ and τ is the collapse time. The energy is conserved during the whole collapse process, which can be shown using the self-similarity and the collapse condition $V = 0$ (Aref, 2010):

$$\begin{aligned} H &= -\frac{1}{4\pi} \sum_{i,j,i\neq j}^{N} \Gamma_i \Gamma_j \ln(f(t) r_{ij}(0)) \\ &= -\frac{1}{4\pi} \left[\ln(f(t)) \sum_{i,j,i\neq j}^{N} \Gamma_i \Gamma_j + \sum_{i,j,i\neq j}^{N} \Gamma_i \Gamma_j \ln(r_{ij}(0)) \right] \\ &= -\frac{1}{4\pi} \sum_{i,j,i\neq j}^{N} \Gamma_i \Gamma_j \ln(r_{ij}(0)) = \text{const.} \end{aligned} \tag{3.33}$$

To achieve the second line in (3.33), we used the product rule for logarithms $\ln(f(t) r_{ij}(0)) = \ln(f(t)) + \ln(r_{ij}(0))$. If these constraints are fulfilled and the vortices Γ_1, Γ_2 and Γ_3 appear counter-clockwise, the vortices expand ($\sigma = -1$). Otherwise they collapse ($\sigma = 1$). The orientation of the rotation of the whole vortex system is determined by the sign of the circulation of highest absolute value of the three vortices.

We have already derived the Nambu equation of the time evolution of three point vortices in (3.6):

$$\rho \frac{d\mathbf{r}}{dt} = \nabla M \times \nabla H. \tag{3.34}$$

Before we interpret the right-hand side of this equation for the geometrical Nambu representation, we apply Aref's self similarity condition of the relative distances (3.32) to the definition of ρ (3.18):

$$\rho = \frac{r_{12}(t') r_{23}(t') r_{31}(t')}{4A(t')} = f(t')\rho_0, \tag{3.35}$$

with $\rho_0 = \rho(t' = 0)$. Therefore, the left-hand side of (3.34) simplifies to:

$$\rho \frac{d\mathbf{r}}{dt'} = \rho_0 f(t') \frac{d\mathbf{r}_0 f(t')}{dt'} = -\frac{\rho_0}{2\tau'} \mathbf{r}_0. \tag{3.36}$$

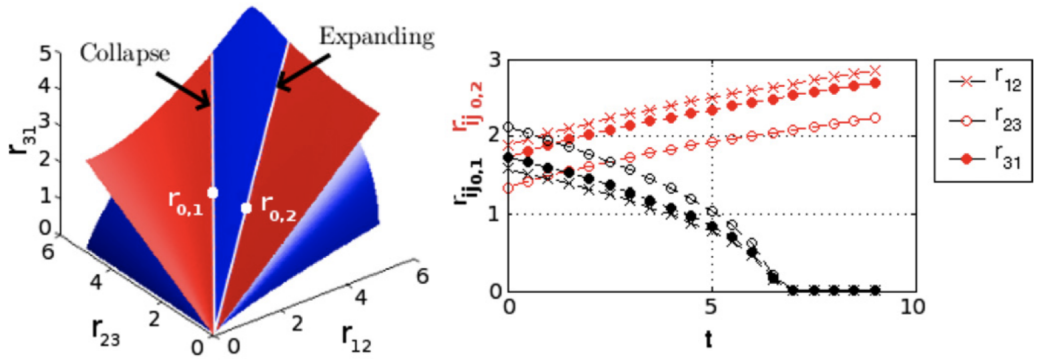

Figure 3.8: Left: two lines through the origin represent a collapse in the phase space given by the intersection of M (red surface, subset of a light cone) and H (blue surface). Right: time evolution of the intervortical distances with initial values $\mathbf{r}_{12}(0) = \sqrt{2.5}$, $\mathbf{r}_{23}(0) = \sqrt{4.5}$ and $\mathbf{r}_{12}(0) = \sqrt{3}$. The initial values $\mathbf{r}_{0,1} = (\sqrt{2.5}, \sqrt{4.5})$ for a collapse and $\mathbf{r}_{12}(0) = \sqrt{3}$ and $\mathbf{r}_{0,2} = (1.84, 1.33, \sqrt{3})$ for an expanding are marked on the geometric figure on the lhs.

Thus, the time evolution of the relative distances multiplied by ρ is constant and the phase space trajectory can not be a closed curve, i.e. periodic motion.

Now, we will analyze the right-hand side of equation (3.34) in terms of the geometrical interpretation. Because of the necessary condition, the quantities V and M are equal to zero. Therefore, the circulations have different signs. Then, in case of collapse/expanding the M-surface is given by

$$M : \frac{r_{12}^2}{\Gamma_3} + \frac{r_{23}^2}{\Gamma_1} + \frac{r_{31}^2}{\Gamma_2} = 0 \tag{3.37}$$

representing a cone; more precisely, since the relative distances are all positive, the upper part of a cone. The intersection of a cone with the H-surface in the phase space leads to two lines passing the origin representing the phase space trajectories. Fig. 3.8 shows the intersection lines of the two surfaces of the energy H (blue surface) and the quantity M (red surface). The circulations $\Gamma_1 = 12, \Gamma_2 = -3$ and $\Gamma_3 = 4$ satisfy the collapse-condition $V = 0$. By choosing the initial values of the intervortical distances $r_{12} = \sqrt{2.5}$, $r_{23} = \sqrt{4.5}, r_{31} = \sqrt{3}$, M is equal to zero, too. Therefore both collapse-conditions are satisfied. We see in fig. 3.8 that the M-surface represents the upper light cone and that the trajectory of three point vortices in the phase space consists of two lines. Since we know that the initial conditions lead to a collapse, the phase space coordinate $\mathbf{r}_{0,1} = (\sqrt{2.5}, \sqrt{4.5}, \sqrt{3})^T$ moves towards the origin. But why does the geometrical representation shows two

lines? Set $\Gamma_1, \Gamma_2, \Gamma_3$ and r_{31} as above and let r_{12}, r_{23} two arbitrary variables. Solving the H-equation (3.24) for r_{12}, we get $r_{12} = \exp(4b) r_{23}^{4/3} r_{13}^{-1/3}$. Now we insert r_{12} into the M-equation (3.37). On condition of $M = 0$ this leads to two solutions of $\mathbf{r}(0) = (r_{12}(0), r_{23}(0), r_{31}(0))^T$, namely, as expected the above solution

$$\mathbf{r}_1(0) = (\sqrt{2.5}, \sqrt{4.5}, \sqrt{3}) = (r_{1_{12}}, r_{1_{23}}, r_{1_{31}}) \tag{3.38}$$

and a second solution, numerically given by the approximated values

$$\mathbf{r}_2(0) = (1.84, 1.33, \sqrt{3}) = (r_{2_{12}}, r_{2_{23}}, r_{2_{31}}). \tag{3.39}$$

Therefore, the magnitude relative to the fixed value r_{31} interchanges, i.e. it is $r_{1_{12}} < r_{1_{31}} < r_{1_{23}}$, but $r_{2_{23}} < r_{2_{31}} < r_{2_{12}}$. Let the orientation of the vortices of these two solutions be fixed. Then, inserting these values in the equations of motion (3.17), we obtain:

$$\frac{d\mathbf{r}_1^2}{dt}|_{t=0} < 0, \quad \frac{d\mathbf{r}_2^2}{dt}|_{t=0} > 0. \tag{3.40}$$

Therefore, for fixed $\Gamma_1, \Gamma_2, \Gamma_3$ and r_{31} we obtain one solution leading to a collapse and another solution leading to an expanding of the three point vortices, see fig. 3.8 on the right-hand side. This explains that there are two intersection lines.

In contrast to solving a system of differential equations by time-stepping using a single initial condition, applying Nambu mechanics, we obtain a whole set of all possible initial conditions and trajectories for the collapse and expanding motions for fixed values of M and H. Moreover, beyond the well known effect of σ, we show, as a new aspect, that the order of magnitude of the intervortical distances also differentiates between the collapse and the expanding motion. In contrast to the change of σ that can be interpreted simply as time reversal, interchanging this order of magnitude leads to two structurally different collapse and expanding motions. In fig. 3.8 the intersection line on the left-hand side represents the collapse and the other intersection line represents the expanding state. We conclude that for every fixed r_{31} there are two initial configurations leading to a collapsing and an expanding at every energy level.

3.6 Nambu formulation for an arbitrary number of point vortices

It would be interesting to apply Nambu mechanics to $N \geq 4$ vortices. But on the one hand, there are $N-1$ conserved quantities needed to describe the motion of a N-vortex system. And not all needed conserved quantities might exist. On the other hand, a general $N \geq 4$-point vortex system is not integrable. Since the classical equations of motion (3.17) for a N-point vortex system depend on the area spanned by three point vortices, it is quite natural to describe the system by the time evolution of the area. A further motivation to use the area as dynamical variable is given by the circulation that is defined by a surface integral over the vortex vector. It is conserved on any material surface. Contracting this area to a point leads to the definition of the point vortex. Therefore, the dynamics of point vortices can also be classified by the evolution of material surfaces. Let now $A_{ijk} = A_{ijk}(r_{ij}(t), r_{jk}(t), r_{ki}(t))$ the area spanned by three vortices. Equation (3.17) for N vortices can be written as

$$\boxed{\frac{dr_{ij}^2}{dt} = \frac{64}{\pi} \sum_{k=1}^{N} \sigma_{ijk} A_{ijk} \frac{\partial(M,H)}{\partial(r_{jk}^2, r_{ki}^2)},} \tag{3.41}$$

where $\frac{\partial(M,H)}{\partial(r_{jk}^2, r_{ki}^2)}$ denotes the Jacobi-determinant.

We first derive the time evolution of the area for three point vortices. We denote $A = A_{123}$ and apply (3.41) to

$$\frac{dA}{dt} = \frac{\partial A}{\partial r_{12}^2}\frac{dr_{12}^2}{dt} + \frac{\partial A}{\partial r_{23}^2}\frac{dr_{23}^2}{dt} + \frac{\partial A}{\partial r_{31}^2}\frac{dr_{31}^2}{dt} \tag{3.42}$$

leading to:

$$\frac{dA}{dt} = \frac{192\ \sigma_{123} A}{\Gamma_1\Gamma_2\Gamma_3} \frac{\partial(A, M, H)}{\partial(r_{12}^2, r_{23}^2, r_{31}^2)} \tag{3.43}$$

Now we can generalize (3.43) to describe the interaction of $N \geq 4$ point vortices in terms of the two conserved quantities M and H. In this approach, applying (3.41) the nonlinear dynamics of the area of one triangle is determined by the time rate of change of all possible triangles spanned by the fixed ith and jth vortices:

$$\frac{dA_{ijk}}{dt} = \sum_{k=1}^{N} \frac{192\ \sigma_{ijk} A_{ijk}}{\Gamma_i\Gamma_j\Gamma_k} \frac{\partial(A_{ijk}, M, H)}{\partial(r_{ij}^2, r_{jk}^2, r_{ki}^2)}. \tag{3.44}$$

Analogously to (3.44), we can also derive the time evolution in dependency of the non-quadratical distances:

$$\boxed{\frac{dA_{ijk}}{dt} = \sum_{k=1}^{N} \frac{6\,\sigma_{ijk}}{\rho\Gamma_i\Gamma_j\Gamma_k} \frac{\partial(A_{ijk}, M, H)}{\partial(r_{ij}, r_{jk}, r_{ki})}.} \tag{3.45}$$

Even though we lose the information of the local position and the intervortical distances, we can still classify the special kinds of motion given by the relative equilibrium ($\dot{A} = 0$), collapse and expanding motion ($\dot{A} < 0$, $\dot{A} > 0$).

The Nambu-representation of N point vortices based on the area spanned by three point vortices is quite natural, because the dynamics can be understood as interactions of maximal integrable subsystems

3.7 Summary

In this chapter we have applied Nambu mechanics to three point vortex systems. Using this approach, only two conserved quantities (H, M) suffice for the integrability of a three point vortex system in a three-dimensional phase space. In contrast, using Hamiltonian mechanics, the integrability of the three point vortex system is assured by three conserved quantities $(H, L, P_x^2 + P_y^2)$ in a six-dimensional position space.

Applying Nambu mechanics, the phase space trajectory is generated geometrically by the intersection of two surfaces represented by two conserved quantities H and M, where both conserved quantities have equal status. Thus, in order to specify the motion, it is not necessary to solve the non-linear differential equations of motion. Topologically, the surface represented by M is a quadric giving rise to the different classes of motion. The trajectory of a periodic point vortex motion is always a closed line in the phase space. If the two surfaces intersect in one point, an equilibrium is given. Moreover, collapse and expanding motions are each represented by one line passing the origin. Moreover, in Müller and Névir (2014) we have shown that not only the orientation σ, but also the order of magnitude of the intervortical distances distinguishes between collapse and expanding motion.

This geometrical view on point vortex motion allows for a better understanding of the differences between the initial conditions for a collapse

and expanding motion. We see that small changes of the initial relative distances can lead to a change of motion. Systems of differential equations are typically solved by time-stepping methods with single initial conditions. Applying Nambu mechanics we obtain a whole set of all possible initial conditions and trajectories for fixed values of M and H. Especially, this is interesting for analyzing collapsed and expanding motion. Finally, we proposed an approach to generalize Nambu mechanics for an arbitrary number of point vortices, where the Nambu representation of N point vortices is based on the area spanned by three point vortex subsystems. Independent of the complexity of the surface, discrete Nambu mechanics offers a change from local numerical time stepping methods to global geometric solutions of phase space trajectories. In the next chapter we will apply point vortex theory to atmospheric blockings.

Chapter 4

Atmospheric blockings explained by point vortex theory

From a theoretical point of view, the classical and simplest way to describe motions on synoptic and planetary scale is a two-dimensional, barotropic, inviscid and non-divergent model that is mathematically represented by the corresponding vorticity equation; thereby, the property of being divergence-free is realized by the geostrophic wind. One concept that can be derived from the barotropic, inviscid, non-divergent vorticity equation is the classical point vortex theory. It is an idealized local and discrete model for two-dimensional vortex dynamics. Surprisingly, there are rather few publications on the application of point vortices to understand large-scale motions in the atmosphere, see for example Charney (1963), Obukhov et al. (1984), Morikawa and Swenson (1971), Friedlander (1975), Egger (1992), Polvani and Dritschel (1993) or Newton (2001). In this chapter we will show the applicability of point vortex theory to blocked weather situations as we have introduced and published in Müller et al. (2015).

Blockings are weather situations that often have devastating consequences, such as draughts or floods. Examples of these long lasting weather situations are blocked events in the extra-tropical regions of the midlatitudes that often last for several days up to months. In summer 2003 such a blocked weather situation caused the West-European heat wave; simultaneously there was strong precipitation in East-Europe. Also the heat wave around Moscow in summer 2010 was caused by a blocked situation (Friedrich and Bissolli, 2011). During the same time Pakistan had to struggle against floods. A recent blocked weather situation took place in July 2014, where a blocked high over Norway lead to the warmest July since the

beginning of weather recording in 1900 (NMI, 2014).

In general, Rossby-theory, which successfully describes propagating waves in a zonal flow dominates the thinking of large-scale atmospheric motions. A first explanation of blocked events is based on stationary Rossby waves in a zonal mean flow, which can be ascribed to Yeh (1949). A shortcoming of this global explanation is the missing description of non-periodic, local characteristics of blocked events. Therefore, a modern view on stationary patterns is based on Rossby-wave breaking giving rise to more local, cut-off structures diagnosed by PV-anomalies on isentropic surfaces (Altenhoff et al., 2008). In this context, we propose a physical model based on first principles considering the large-scale processes as local interactions of several discrete vortices. This approach is reasonable, because the observations show that blocked events are realized by two or three isolated vortices represented by high over low or omega-blocked weather patterns. In particular, we will use the concept of three point vortices building an relative equilibrium. We will follow our publication on the explanation of blockings by the point vortex model (Müller et al., 2015) and first discuss the atmospheric scales of the circulation (3.1), which measures the strength of rotation and is constant on material surfaces. Even though the circulation measures the strengths of vortices, this quantity is not often considered in fluid mechanical models. Then, we will show how the concept of point vortex equilibria can be applied to explain blocked weather situations and discuss two case studies. The first example deals with the severe drought over the European part of Russia in summer 2010, in the second example we will analyze an omega-block over the North Pacific in March 2011. Here, the calculations of the circulations are due to Schielicke et al. (2016) and Schielicke (2017), who introduced the algorithm to identify vortices with the kinematic vorticity number to calculate the circulation. In the meanwhile, in Hirt et al. (2018) we could corroborate our results statistically.

4.1 Atmospheric scales of circulation

A common approximation of large-scale atmospheric dynamics is to neglect dissipative processes. This approach is used in Rossby-wave theory as well as in vortex dynamics. However, to relate space and time scales of different vortex patterns we follow the principal idea of Kolmogorov (1941) taking dissipation into account.

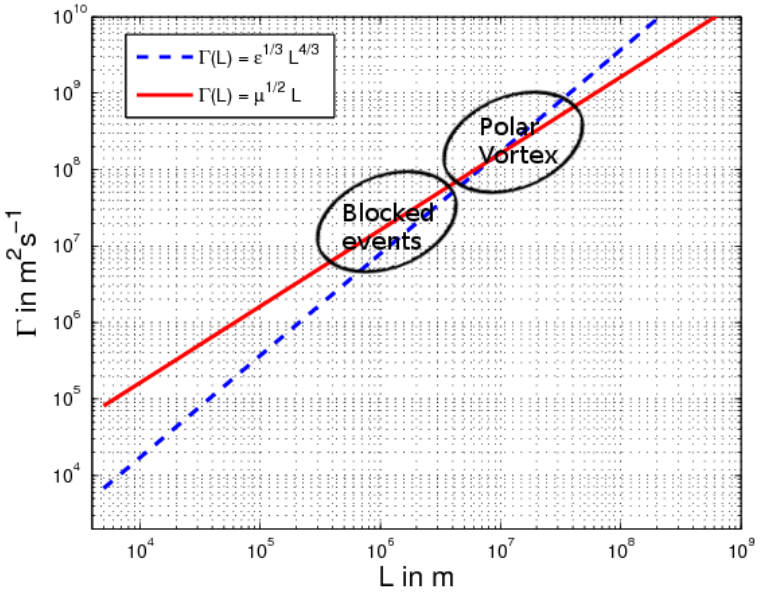

Figure 4.1: The order of magnitude of circulations with respect to different lengths scales for the dissipation of energy $\varepsilon = 5 \cdot 10^{-4}\ m^2\ s^{-3}$ (blue dashed line) and the dissipation of circulation $\mu = 264\ m^2 s^{-2}$ (red solid line).

One of the most important quantities in vortex theory is the circulation (3.1) that plays an important role in the point vortex equations (3.3). In order to analyze the atmospheric scales of circulation we regard dimensional analysis following the principal idea of Kolmogorov (1941). He considered constant dissipation of energy ε leading to a relation between the characteristic time T and the characteristic length L: $T = \varepsilon^{-1/3} L^{2/3}$. We now assume positive values of circulation $\Gamma > 0$. The dimension of Γ is given by $L^2 T^{-1}$. Thus, we can also formulate a power law of the characteristic circulation Γ in terms of L:

$$\Gamma = \varepsilon^{1/3} L^{4/3}. \tag{4.1}$$

Motivated by Kolmogorov's idea, we assume constant dissipation of circulation, i.e. $\dot{\Gamma} =: \mu = const.$, where the dissipation of circulation can also be formulated in terms of this characteristic quantities: $\mu = L^2 T^{-2}$. Thus, we obtain the relation of the characteristic time and the characteristic length L:

$$T = \mu^{-1/2} L. \tag{4.2}$$

In contrast to the assumption of a constant dissipation of energy (4.1), (4.2) represents a linear relation between T and L. Moreover, $\Gamma = L^2 T^{-1}$ and

(4.2) lead to the linear relationship

$$\Gamma = \mu^{1/2} L \tag{4.3}$$

which is illustrated in fig. 4.1. The dashed line indicates the circulation with respect to the characteristic lengths in terms of the dissipation of energy ($\varepsilon = 5 \cdot 10^{-4}\ m^2 s^{-3}$, Brunt (1939)) and the solid line illustrates the linear relation given in (4.3) in terms of the dissipation of circulation (with $\mu = 264\ m^2 s^{-2}$). This estimation of the dissipation of circulation follows from Schielicke et al. (2016). Fig. 4.1 indicates circulations in the order of magnitude $10^7 - 10^8\ m^2 s^{-1}$ for omega blockings and larger circulations for the polar vortex ($10^8 - 10^9\ m^2 s^{-1}$). Both lines show similar values of circulation for systems on the synoptic scale. In the following, we will see that these orders of magnitude coincide with our calculations of the circulations and distances of the real atmospheric vortices on this scale.

4.2 Relative point vortex equilibria

Point vortex motions can be classified into two different kinds of motions. For most initial conditions, the relative distances vary in time but in special cases they are constant in time. These cases are named relative equilibria. The first investigations of related equilibria took place more than one hundred years ago. Mayer (1878) studied equilibrium configurations of the interactions of floating magnets within a strong magnetic field. These configurations turned out to correspond to point vortex equilibria. Since then numerous studies on point vortex equilibria have followed, for example see Novikov (1975), Aref (1979), Dritschel (1985) or Aref et al. (2012).

In chapter 3, sec. 3.4 we have already discussed point vortex equilibria for a three point vortex system in terms of Nambu mechanics. In the following we will apply point vortex equilibria to flow patterns on synoptic and planetary scale characterized by a small number of distinguished vortices. On synoptic scale, dipole and tripole structures can be described as two or three point vortex systems. Denote Γ_1 and Γ_2 the circulations of a two vortex system. For $|\Gamma_1| \neq |\Gamma_2|$ the two point vortex system rotates around its center of circulation, while each vortex moves along a different circle. In case $\Gamma_1 = \Gamma_2$, both vortices rotate on the same circle. If $\Gamma_1 = -\Gamma_2$ the centre of circulation lies in infinity, and therefore, the two vortex system translates

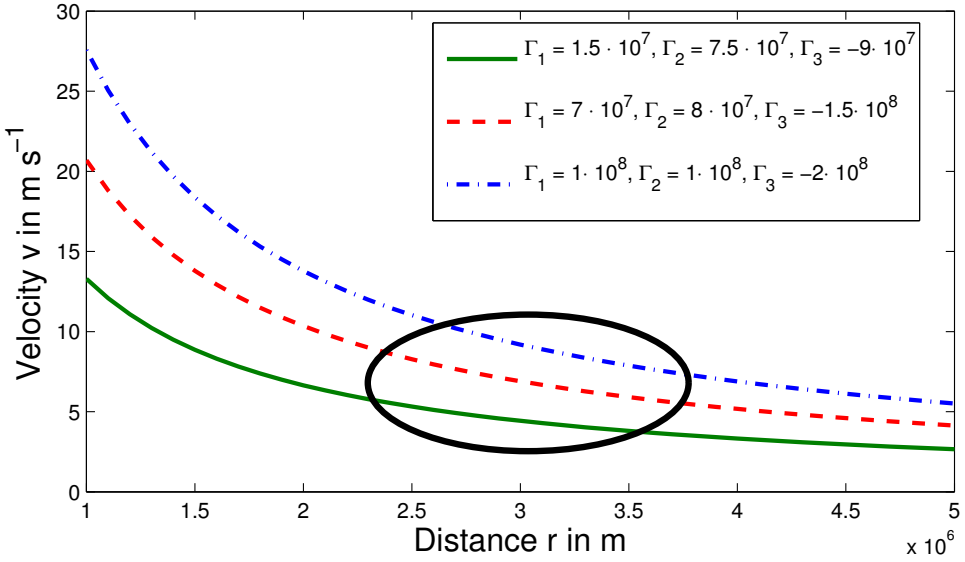

Figure 4.2: Translational velocity of a three point vortex system as function of the intervortical distances r for three different vortex configurations with vanishing total circulation is shown. For typical distances on synoptic scale of 2500-3500 km the absolute value of the analytical translation velocity of $5 - 10\ ms^{-1}$ of a three point vortex equilibrium which coincides with the typical basic westerly flow velocity.

with constant velocity. These two last cases are called relative equilibria and can be applied to atmospherical dipole structures (see Kuhlbrodt and Névir, 2000).

We will extend this idea and discuss Omega blocks by three point vortex equilibria. A first approach to study droughts was given by Obukhov et al. (1984) (in Russian) who realized the idea in terms of climatological geopotential anomalies. The relative equilibrium of three point vortices occur either for collinear initial states or for three point vortices forming an equilateral triangle. In case of an equilateral triangle and total circulation unequal to zero, the three vortex system rotates about its center of circulation with rotation frequency $\omega = (\Gamma_1 + \Gamma_2 + \Gamma_3)/2\pi r^2$, where r is the triangle side (Newton, 2001). In case of zero total circulation, the centre of circulation lies in infinity. Let now Δ_{123} be an equilateral triangle with the local point vortex coordinates as vertices and equal intervortical distances $r := r_{12} = r_{23} = r_{31}$. Applying (3.3) leads to the following translation velocity:

$$v = |\mathbf{v}| = \frac{\sqrt{2(\Gamma_3^2 + \Gamma_1^2 + \Gamma_2^2)}}{4\pi r}. \tag{4.4}$$

For $\Gamma_1 = \Gamma_2$ the system translates along the straight line through vortex 1

and vortex 2. As we have derived in Müller and Névir (2014), varying the circulations leads to the following translation angle:

$$\alpha = \arctan\left(\frac{\Gamma_1 - \Gamma_2}{\sqrt{3}\Gamma_3}\right). \tag{4.5}$$

In fig. 4.2 the velocity of a three point vortex equilibrium (4.4) with respect to the intervortical distance is illustrated indicating the applicability of the idealized point vortex concept to vortex systems on the synoptic scale. For intervortical distances of about 2500-3500 km the translation velocity of a three point vortex equilibrium coincides with the typical basic flow velocity. In section 4.4 we will use the translation velocity (4.4) of a three vortex system to explain the stationarity of blocked weather situations. Omega blocks are characterized by two low pressure areas south-east and south-west of an high pressure area (see figure 4.4). Thus, if both lows have equal circulations and are located on the same latitude and if the circulation of the high is twice as large as each low, the total sum of circulation is equal to zero. Therefore, the vortex system translates along a latitude.

4.3 Methods and data

To apply point vortex theory to large-scale atmospheric flow patterns, we discretize the dynamics by contracting the high and low pressure areas to points. Furthermore, to use the analytical equations of motion (3.3) we need to determine the circulations and the relative distances of the vortices. If the centers of the vortices are known, the relative distances can be easily measured. But the determination of the circulations Γ is more complicated and we will use both, a geometrical and a numerical method to calculate the circulations. Moreover, we use reanalysis data to apply the method to determine the circulation and to calculate the basic flow.

Geometrical method to calculate the circulations

To calculate the circulation Γ_i of a vortex geometrically to apply the point vortex concept, we use a method to estimate the circulation by integrating a loop around the geopotential field of the blocking high/low:

$$\Gamma_i = \frac{g}{f}\sum_k |\delta Z_k| \ \sin(\alpha_k) \tag{4.6}$$

with the Coriolis parameter f, the gravity acceleration g, the geopotential height Z and the angles α_k, where the $\sin(\alpha)$ is the line k-th line segment. For a more detailed description see Kuhlbrodt and Névir (2000).

Kinematic vorticity number method to calculate the circulations

Following Schielicke et al. (2016), the circulation of a vortex can also be determined numerically. The size of a vortex is estimated with help of the velocity gradient tensor and its invariants which describe the local motion around a point. The velocity gradient tensor $\nabla \mathbf{v}$ in two dimensions is given by

$$\nabla \mathbf{v} = \begin{pmatrix} \partial u/\partial x & \partial u/\partial y \\ \partial v/\partial x & \partial v/\partial y \end{pmatrix}, \tag{4.7}$$

where u and v are the horizontal wind components in zonal and meridional direction, respectively. The velocity gradient tensor can be decomposed into the sum of a symmetric tensor $\underline{\mathbf{S}}$ (rate-of-strain tensor) and an antisymmetric tensor $\underline{\mathbf{\Omega}}$ (vorticity tensor):

$$\nabla \mathbf{v} = \underline{\mathbf{S}} + \underline{\mathbf{\Omega}} \tag{4.8}$$

with

$$\underline{\mathbf{S}} = 1/2(\nabla \mathbf{v} + (\nabla \mathbf{v})^T) \ , \ \underline{\mathbf{\Omega}} = 1/2(\nabla \mathbf{v} - (\nabla \mathbf{v})^T) \tag{4.9}$$

While the rate-of-strain tensor $\underline{\mathbf{S}}$ describes the deformation of the flow field composed of expansion, shearing and stretching deformation, the vorticity tensor $\underline{\mathbf{\Omega}}$ describes the rotation of the flow. A vortex is identified as a connected region of grid points where the local rate of rotation $\|\underline{\mathbf{\Omega}}\|$ prevails over the local strain rate $\|\underline{\mathbf{S}}\|$. Truesdell (1954) introduced the kinematic vorticity number W_k as ratio of the local rate-of-strain and the local rate-of-rotation:

$$W_k = \frac{\|\mathbf{\Omega}\|}{\|\mathbf{S}\|}. \tag{4.10}$$

In case of $W_k > 1$, the local rate of rotation exceeds the local strain rate, $W_k = 1$ in case of a pure shearing motion and $W_k < 1$ if the deformation is larger than the rotation. With help of W_k the boundary of a vortex core is defined by $W_k = 1$ around a vorticity extremum. The circulation of the vortex is calculated by the integral (3.1).

	Russia/Europe (Summer 2010)
Points of initial trapezoid	(10°E, 80°N) (80°E, 80°N) (10°W, 35°N) (100°E, 35°N)
Adjustment of northern line	80° N $\rightarrow$ 70°N by $2.5°$
Adjustment of southern basis	25°N $\rightarrow$ 45°N by $2.5°$
Final averaged height	32.5°N $-$ 75°N

Table 4.1: Initial and final (averaged) configurations of the trapezoids of for the omega blocks over Russia in summer 2010 .

	North Pacific (March 2011)
Points of initial trapezoid	(160°E, 85°N) (220°E, 85°N) (140°E, 45°N) (240°E, 45°N)
Adjustment of northern line	85°N $\rightarrow$ 75°N by $2.5°$
Adjustment of southern basis	35°N $\rightarrow$ 55°N by $2.5°$
Final averaged height	46.9°N $-$ 80°N

Table 4.2: Initial and final (averaged) configurations of the trapezoids of for the omega block over North Pacific in March 2011.

Numerical implementation to determine omega blockings in gridded data

Schielicke et al. (2016) introduced a method to estimate the circulations of cyclonic and anticyclonic vortices such as low and high pressure systems. In the following we will summarize her method after Müller et al. (2015). In regularly gridded data (mercator projection), the shape of the tripole point vortex configuration is approximated by an isosceles trapezoid which at least includes parts of the polewards located high and of the two equatorwards located low pressure systems. The parallel sides of the trapezoid are aligned with two latitudes with the smaller side located polewards. Following Schielicke (2017), the aim of this pattern recognition method is to minimize the absolute value of the total circulation $|\Gamma|$. The circulations of the local coordinates of the centers of circulations and the intervortical distances are derived systematically by the following steps:

(1) A trapezoid is fixed to the lat-lon grid such that the vertical centerline of the trapezoid coincides with the approximated centre of the high pressure system and its West-East (width)/North-South (height) extent includes (at least most) of the high pressure area as well as parts of the two lows. See table 4.1 and 4.2 for more details on the initial

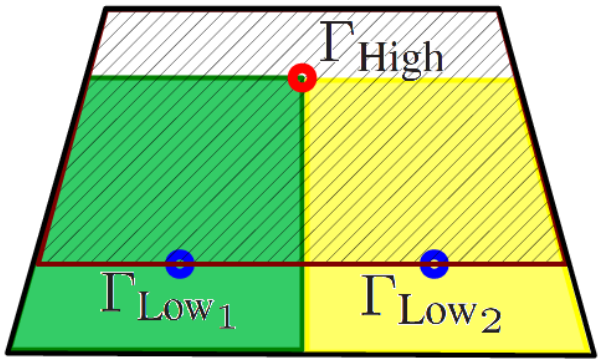

Figure 4.3: Trapezoid approximating the region of the omega block. In the green area the total cyclonic circulation Γ_{Low_1} is calculated and in the yellow area the total cyclonic circulation Γ_{Low_2} is determined. The total anticyclonic circulation Γ_{High} is calculated in the striped area (Müller et al, 2015, Schielicke, 2016).

configuration of the trapezoids for two real cases.

(2) We will use an ensemble of 45 trapezoid shapes derived by moving the southern baseline of the trapezoid by $\pm 10°$ latitude in $2.5°$ steps; and by moving the position of the northern line equatorwards by four steps each $2.5°$ latitude (summarized in tables 4.1 and 4.2).

(3) At each time step, the total circulation and the centre of positive and negative circulations associated with the three vortices inside the trapezoids are determined under the following conditions: Only positive circulations located south of the high pressure centroid and west (east) of the trapezoid centerline contribute to the southwesterly (southeasterly) low; only negative circulations polewards of the low pressure centroids contribute to the high (see fig. 4.3).

(4) For every time step the minimum absolute value of the total circulation, the centre of circulation, the trapezoid configuration, the translation velocity and the relative distances between the circulation centers are determined. Thereby, the local coordinates of the highs and lows are determined by calculating the centers of circulation (3.11) of each high and low pressure regions. An example is given in figure 4.6 where the local coordinates of the centers of the high and low pressure systems are indicated by the red/blue circles.

Finally, averaged values of the variables derived in step (4) are calculated for the whole blocked period. Moreover, the North-South extent of

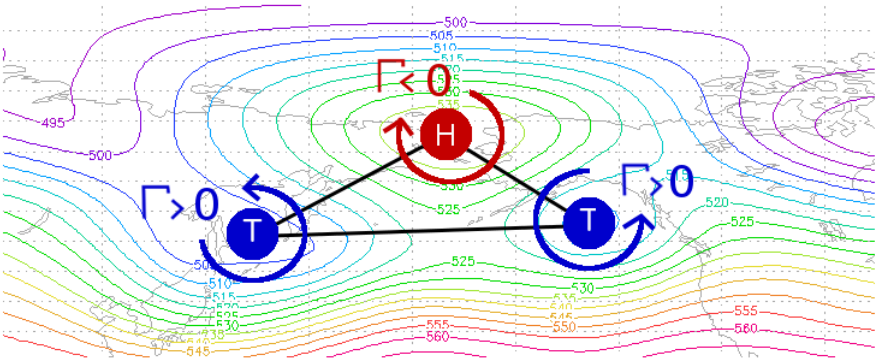

Figure 4.4: A three point vortex equilibrium describes an omega block (geopotential mean over North Pacific 01-12 March 2011).

the averaged trapezoid configuration is used to calculate the mean global wind speed averaged over the same latitudes and period.

Reanalysis data

In this chapter, we apply the concept of the explanation of blockings regarding three point vortex systems for two case studies. For the analysis of blocked weather events in summer (June-August) 2010 and March 2011, the horizontal wind field (u, v) and the geopotential height on the 500 hPa level from the NCEP/DOE Reanalysis 2 (R2) Project was used (NCEP, 2000; Kanamitsu et al., 2002). The data is available on a regular 2.5×2.5 degrees grid with a temporal resolution of 6 hours. In order to respect the differing perimeter of the latitudes on the sphere, we weight the velocity of the zonal mean flow in terms of its latitude, i.e. for the zonal mean flow u on the latitude φ_i with radius $R_i = R \cdot \cos(\varphi_i)$ and the earth radius R the weight is given by $(\sum_i u(\varphi_i) \cdot R_i) \cdot (\sum_i R_i)^{-1}$.

4.4 Application on synoptic scale: Atmospheric blockings

We will give two examples of the applicability of point vortex theory to omega blocks. During blocked events the basic flow is usually divided into different branches caused by a low number of isolated and persistent vortices. This large-scale feature of the atmospheric flow field was already recognized by Garriott (1904). In 1947, Namias (1947) mentioned that blocked situations are associated with a retardation in the zonal cir-

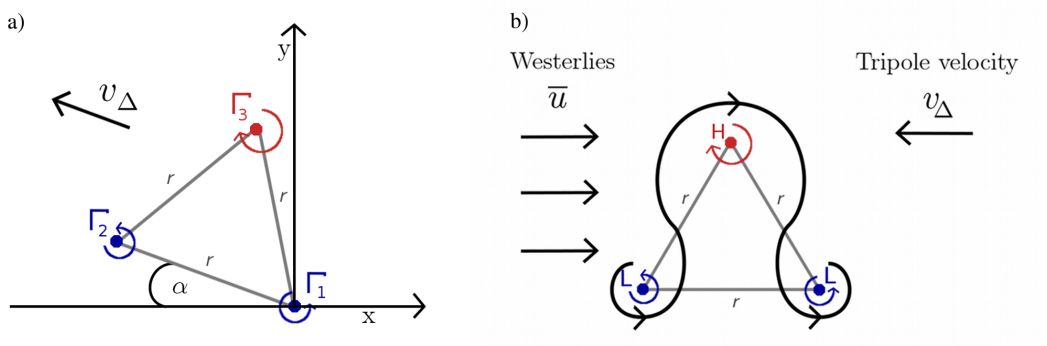

Figure 4.5: Regarding point vortex theory a three point vortex equilibrium translates, if the total circulation $\Gamma = \Gamma_1 + \Gamma_2 + \Gamma_3$ vanishes. In a) we see that the direction of translation depends on the local coordinate of the point vortices, and also on the strengths of the single circulations, as we have discussed in chapter 3. b) The idea of translating vortex systems can be transferred to atmospheric omega blocks. Stationarity can be explained, if the translation velocity v_Δ westwards is equal to the velocity of the zonal mean flow $\overline{u}$ eastwards denoted as westerlies in the meteorological context (Müller et al., 2015).

culation. Yeh (1949) explained blocking situations by the dispersion of an initial solitary wave and Elliott and Smith (1949) discussed the effects of large blocking highs on the general circulation in the northern-hemisphere westerlies. One year later, Rex (1950a,b, 1951) characterized in detail different blocked situations: the zonal basic flow should be divided into two branches at which each of the branches needs to transport mass. Moreover, following his definition, the block should remain for at last 6-10 days. Usually, during blocked situations a very strong high pressure area appears.

Bluestein characterizes three kinds of blocks (Bluestein, 1992): The simplest blocked event consists of a single high pressure area, another blocked event is described by a high pressure area north of a low pressure area (high-over-low). A further arrangement consists of a high pressure area and two low pressure areas located south-west and south-east. The latter weather situation is called omega-block, one example of such a weather situation is illustrated in figure 4.4, see also fig. 4.5. High temperatures and droughts can be caused by those persistent high pressure areas that can be stationary for several days or even for months. Moreover, the persistence of the low pressure areas can lead to heavy rainfalls and floods. See also the works of Pelly and Hoskins (2003) or Bott (2012). The first application to describe stationary, blocked weather situations by three point vortices was established by Obukhov et al. (1984) followed by Kuhlbrodt and Névir (2000), who applied blocked dipole structures to point vortex motion.

We will discuss analytically stationary solutions of a three point vortex system. The general applicability of two-dimensional point vortex theory to blocked events is indicated in fig. 4.2, where the analytical translation velocity (4.4) of a three point vortex equilibrium with respect to its inter-vortical distances is shown. Thereby, each curve represents a three point vortex system. We chose circulations that are typical for the synoptic scale and that sum up to zero. A main result of our approach is that the point vortex velocity of 5-10 m/s on the typical synoptic scale of 2000-3500 km coincides with the characteristic velocity of the atmospheric basic flow. This result leads to a natural explanation of the whole omega block consisting of the three vortices regarding the orientation. The tripole moves westwards with velocity v_Δ and the remaining interaction of vortices is parameterized as zonal mean flow leading to the eastwards velocity $\overline{u}$. If their absolute values coincide such that

$$v_\Delta = -\overline{u}, \tag{4.11}$$

the stationarity of blocked events can be explained (see figure 4.5(b)). Because the point vortex constellation should be a relative equilibrium, the total circulation of an ideal blocked event should vanish and therefore it should satisfy:

$$\Gamma_{\mathrm{Low}_1} + \Gamma_{\mathrm{Low}_2} = -\Gamma_{\mathrm{High}}. \tag{4.12}$$

If the local coordinates of the two lows, Γ_{Low_1} and Γ_{Low_2}, are lying on the same latitude, the whole three vortex system translates along this latitude with velocity (4.4). We do not explain the formation of blocked events, such as Rossby waves do, but we explain the stationarity by considering the local character, whereas wave theory is based on global features.

To include the β-effect the earth rotation has to be added. Therefore, from inertial-system perspective the absolute vorticity should be used leading to an absolute circulation (according to (3.1)) and to modifications of the equations of motion (3.3) considering the absolute point vortex velocity. Moreover, we have to add the effect of the earth rotation to the velocity of the basic flow. By applying (4.11) both terms considering the effects due to earth rotation would cancel. Therefore, in the following examples we calculate circulations and the velocities in terms of the relative frame of reference.

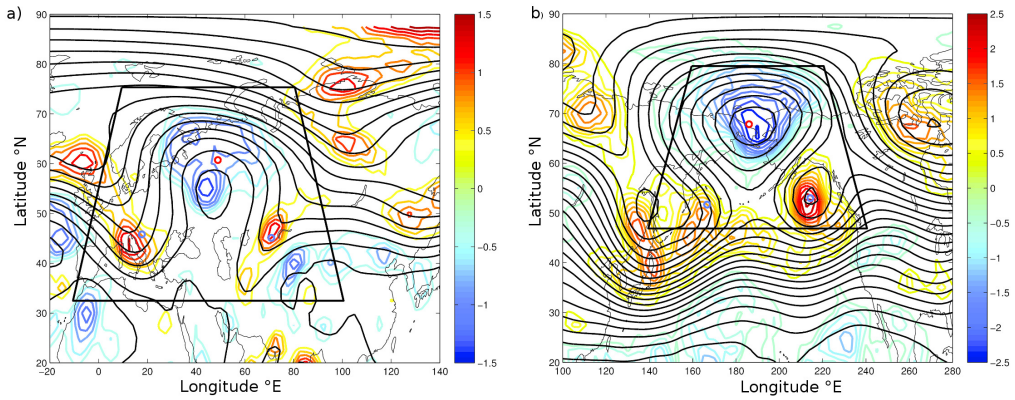

Figure 4.6: a) Temporal averages (24 July 2010 00 UTC – 7 August 2010 18 UTC and b) 1 March 2011 00 UTC – 11 March 2011 12 UTC of geopotential height (black contours) and relative vorticity (in $10^{-5}s^{-1}$, colored contours). The vorticity is shown in the field of kinematic vorticity number $W_k > 1$. The trapezoids encircle the area of zero total circulation and the blue and red circles mark centers of the low and high pressure areas, respectively. Note the different ranges of vorticity in the plots (Schielicke et al., 2016; Müller et al., 2015)

4.4.1 Example 1: Omega-block over Russia 2010

We will examine the blocked situation in summer 2010, where the blocked high caused a heat wave in the European part of Russia and surrounding countries. During this summer, low precipitation, low wind velocities and fatal forest fires were observed. In Moscow, more than 30 degrees Celsius were measured on more than 40 days; even on 15 days the temperature exceeded 35 degrees Celsius (Friedrich and Bissolli, 2011). Even though 2010 was one of the warmest years since weather recording, large parts of West-and Central Europe were colder than the average which could be ascribed to the two stationary low pressure areas.

During the time period 18 June 2010 until 23 July 2010 we recognize a blocked dipole structure followed by an omega block from 24 July 2010 until 07 August 2010. Even though the dipole structure can also be explained by a (two) point vortex equilibrium, we will concentrate on the omega block and explain the persistent structure by point vortex theory.

Thereby, to determine the circulations we first search for the trapezoidal area of approximately zero circulation as we described in section 4.1. The vertices of the initial trapezoid and the enlargement of the trapezoid-boundary are summarized in table 4.1. Figure 4.6a) shows the determined final configuration. To identify the low pressure systems Γ_{Low_1} and Γ_{Low_2} we use the lower part of the trapezoid, i.e. the area south of $60°$N. And for the deter-

	Russia/Europe (2010)	
	Circulation in m^2s^{-1}	Location $(^\circ N; ^\circ E)$
Γ_{Low_1}	$7.543 \cdot 10^7$	$(45.8; 17.7)$
Γ_{Low_2}	$5.424 \cdot 10^7$	$(45.1; 70.9)$
Γ_{High}	$-1.306 \cdot 10^8$	$(60.7; 48.9)$

Table 4.3: Values of the circulation of the tripole and the locations of the centers over Russia and Europe in summer 2010

	North Pacific (2011)	
	Circulation in m^2s^{-1}	Location $(^\circ N; ^\circ E)$
Γ_{Low_1}	$7.090 \cdot 10^7$	$(51.7; 166.7)$
Γ_{Low_2}	$8.322 \cdot 10^7$	$(53.0; 214.3)$
Γ_{High}	$-1.546 \cdot 10^8$	$(67.8; 186.0)$

Table 4.4: Values of the circulation of the tripole and the locations of the centers over North Pacific in March 2011

mination of the high pressure vortex we consider the area north of 45°N.

The values and local coordinates of the finally determined circulations are summarized in table 4.3. These values add up to the total circulation $\Gamma = -0.009 \cdot 10^8 m^2 s^{-1}$, which is only 0.71% of Γ_{High}. Thus, the total circulation is still small enough to apply formula (4.4). The averaged triangle side length, that means the intervortical distances are given by $\overline{r} = 2910$km. Applying formula (4.4) leads to the analytical solution of the tripole translation:

$$v_\Delta = -(6.3 \pm 2)\frac{m}{s}, \tag{4.13}$$

where the error tolerance is estimated by the calculated minima/maxima intervortical distances of the system. In the same time period, the zonal mean flow averaged in the area $32.5^\circ N - 75^\circ N$ [1] is given by:

$$\overline{u} = (6.5 \pm 1)\frac{m}{s}. \tag{4.14}$$

The sum of the mean flow and the analytical dipole velocity vanishes which explains the stationarity of the tripole.

[1] The error tolerance of the basic flow results from the calculation of the maxima/minima mean wind speeds.

4.4.2 Example 2: Omega-block over North Pacific 2011

As second example we will analyze an omega block during the time period 01-12 March 2011 that is shown in figure 4.6b). The circulations are again determined by the numerical method and its values and local coordinates are summarized in table 4.4. Here, the circulations of the two lows and the high sum up to $\Gamma = -0.005\ 10^8 m^2 s^{-1}$ which is 0.32% of the value of Γ_{High}. The averaged intervortical distance, i.e. the side length of the equilateral triangle is $\overline{r} = 2490$ km. Applying formula (4.4) and including the error estimation provides the tripole velocity

$$v_\Delta = -(8.8 \pm 2)\frac{m}{s}. \tag{4.15}$$

On the other hand, the mean flow ($45°N - 80°N$) is given by:

$$\overline{u} = (8.3 \pm 1)\frac{m}{s}. \tag{4.16}$$

Again, the sum of the flow velocity and the analytically determined point vortex velocity vanishes explaining the stationarity of the block.

4.5 Modes of disturbed equilibria

In principle, it is necessary to consider deviations of the perfect equilibrium tripole with vanishing total circulation and equal side lengths, because often we do not observe such perfect omega blocks. First, we disturb the equilateral triangle in terms of its side lengths by shifting one vertex by ε. This does not influence the circulations, i.e. the centre of circulation still lies in infinity. Therefore, the three vortex system still translates. But in case of perturbations of the local coordinate, the three vortices do not build a perfect equiangular triangle anymore; therefore, the trajectories of the vortices are given by cycloids with small amplitudes, which is simplified illustrated in figure 4.7. Here, the translational motion is superimposed by an additional pulsating mode. For $\varepsilon \to 0$, these amplitudes approach zero, i.e. the cycloid approaches a straight line. Moreover, the translation angle (4.5) is affected by the perturbation ε. Both effects, the pulsating mode and the varying angle only rarely affect the tripole velocity and therefore do not spoil the over all explanations of the persistence of blocked situations.

Second, we disturb one circulation leading to a non-vanishing total cir-

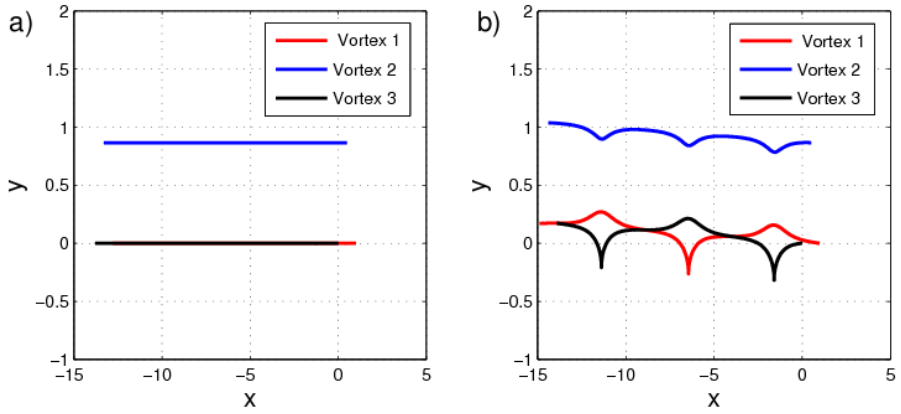

Figure 4.7: a) shows the equilibrium state for the initial states $\mathbf{x}_1 = (1, 0)$, $\mathbf{x}_2 = (0.5, \sqrt{.75})$, $\mathbf{x}_3 = (0, 0)$ and $\Gamma_1 = 1$, $\Gamma_2 = -2$, $\Gamma_3 = 1$, which builds an equilateral triangle with total sum of circulations equals zero. b) Small perturbations of $\mathbf{x}_3$ lead to cycloid motions (Müller et al., 2015).

culation. Thus, the center of circulation does not lie in infinity anymore. But for a small perturbation the centre of circulation still lies far away from the three point vortex system and therefore, the vortices move along a large circle, which locally can be assumed as linear translation.

We can summarize that small variations of both, the local coordinates and the circulations do not affect the applicability of point vortex theory to atmospheric blocked events.

4.6 Statistical corroboration of the applicability of the point vortex model

To corroborate the applicability of point vortex theory to blockings (Hirt et al., 2018) have automatized the algorithm we have discussed in section 4.3. In the first step blocking periods were identified using the instantaneous blocking index, short IBL. This blocking index was first introduced by Tibaldi and Molteni (1990) and, at the Institut für Meteoreologie, implemented by Richling et al. (2015). By applying this index to the Euro-Atlantic sector ($90°W - 90°E$ and $30 - 85°N$) for the time period 1990 to 2012 at the 500 hPa level, 347 blocking periods could be identified. In the next step, the positions of the high and low pressure system were determined by applying the kinematic vorticity number (Schielicke et al. (2016), Schielicke (2017), Müller et al. (2015)). Then, the blockings were further classified into

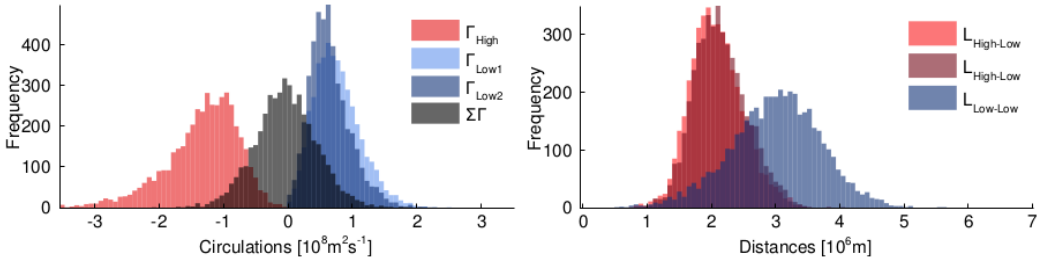

Figure 4.8: The circulation and the intervortical distances of the identified omega blockings are shown (Hirt et al., 2018)

high-over-low systems and omega blocks. In the last step the circulations and intervortical distances of the identified vortices were determined such that the point vortex tripole velocity for equilibria could be estimated. We will shortly discuss the identified omega blocks and their velocities that result from the trapezoid method, because it can be seen as a statistical corroboration of the results we have shown earlier in this chapter. For further details, e.g. the statistical results of the velocities of the high over low systems, the contour method, and the stability analysis see Hirt et al. (2018).

Examining the omega blocks Hirt et al. (2018) found that the condition of vanishing total circulation is approximately statistically satisfied, see fig. 4.8 left. But it is observed that the triangle spanned by the identified vortices deviates from the equilateral triangle, which is also shown in fig. 4.8 right. In fig. 4.9 the theoretical point vortex velocity and the averaged mean flow are compared. Here, the x-axis represents the zonal mean flow $\overline{u}$ averaged over $20 - 80°N$ and the y-axis shows the calculated point vortex velocity. Each dot represents one blocking period. The blue line shows the regression. Here, a correlation of 0.71 was found which confirms the applicability of the point vortex model to omega blocks. Moreover, the result of a multiple linear regression shows that the circulation of the high system is related to the zonal mean flow. In Hirt et al. (2018) very stable high pressure areas are observed, whereas the locations of the lows tend to change, which occasionally lead to a transition of high-over-lows to omega blocks and vice versa. This is also discussed in Schielicke (2017). Such a transition from a tripole to a dipole or vise versa happened, for instance, during the heatwave over the European part of Russia in 2001 that we have discussed in section 4.4, example 1. However, Hirt et al. (2018) also examined the effect of the deviations of the relative equilibrium. Based on the equation of motion for relative distances, the point vortex equilibrium is

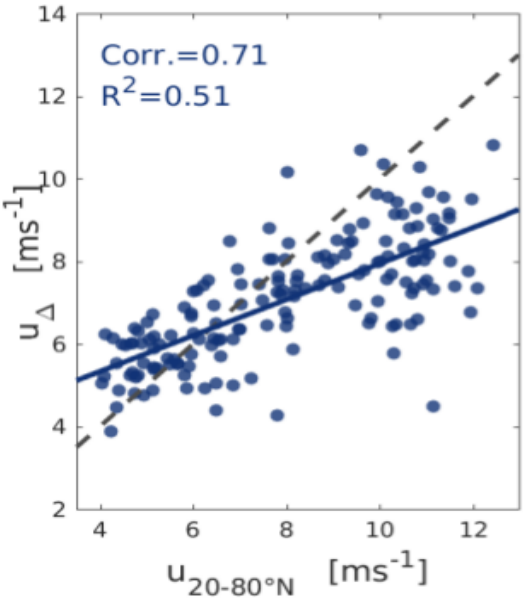

Figure 4.9: The x-axis shows the zonal mean flow and the the y-axis the tripole velocity of the omega block determined by the point vortex equations of motions for three vortex equilibria. Each dot illustrates a blocking period. A correlation coefficient of 0.71 was found (Hirt et al., 2018)

here regarded as one fix point in the phase space similar to the last chapter, where we discussed the three-dimensional phase space of the relative distances in terms of Nambu mechanics. Hirt et al. (2018) shows that this fix point corresponds to an unstable saddle point and come to the conclusion that atmospheric blockings, especially the high pressure systems behave similar to the idealized point vortex model.

4.7 Summary

We have shown the applicability of point vortex theory for a better understanding of atmospheric phenomena on the synoptic scale. By assuming constant dissipation of circulation, we could show a linear relation of the characteristic circulation and characteristic lengths on synoptic scale. Since the point vortex velocity of a three-vortex equilibrium and the mean zonal wind derived from reanalysis data coincide with respect to their absolute values, the stationarity of blocked situations can be explained. Evaluating omega blocks over the European part of Russia and over the North Pacific affirms the possibility to explain the stationarity of blocked events by this low-order point vortex model. These results have also been pub-

lished in Müller et al. (2015) and were further explored in our working group (Pueltz, 2014; Isernhagen, 2015; Braun, 2016; Schielicke, 2017; Hirt et al., 2018). Isernhagen (2015) examined further case studies to corroborate our concept to explain omega blocks. Moreover, Hirt et al. (2018) used data to confirm this concept statistically inventing an automatism to identify blockings based on the Tibaldi and Molteni (1990) blocking index. The characteristics (relative distances and circulation) of the high and low pressure systems are determined by applying Schielicke et al. (2016)'s kinematic vorticity number and it is shown statistically that the three point vortex theory is reasonable to describe blocked weather situations. Moreover, in Newton (2001), Pueltz (2014), Hirt (2016) and Braun (2016) point vortex dynamics on the sphere are discussed regarding synoptic as well as planetary scales. Pueltz (2014) discusses the differences of the applicability of point vortex dynamics to blockings on the sphere with the outcome that the point vortex velocities on the sphere and in the plane negligible differ from each other. Hirt (2016) analyzed the interaction between the equatorial stratosphere and the polar vortex by numerical simulations of 8+1 point vortex equilibria. Concerning the influence of reasonable perturbations, she could confirm instability of the QBO east phase and stability of QBO west phase during the north hemispheric winter periods. Thereby, as summarized in Müller et al. (2015), a dynamical explanation of the observed Holton Tan effect during the winter periods by point vortex theory is proposed. Therefore, point vortex theory seems to be suitable to explain different atmospheric processes on different scales.

Part II

Algebraic aspects of continuous fluid dynamics

Chapter 5

Introduction to algebraic aspects of vortex dynamics

So far, we have discussed discrete Nambu mechanics. In chapter 3, it was applied to the idealized point vortex model to classify planar point vortex motion. In chapter 4, this idealized point vortex concept was further used to explain blocked weather situations. In the following, we will consider continuous Nambu mechanics as basis for an algebraic approach to introduce a new concept to understand the spatial structures of splitting storms. This also leads to an alternative point of view of classical turbulence with respect to the helicity density field for conservative systems. Finally, in the last chapter we will show how continuous Nambu mechanics can be used to find shortest paths of point vortices moving from one point to another. In general, shortest routes between two points are called geodesics such that we call the shortest vortex paths vortex geodesics.

A common way to analyze fluid motions is the numerical examination of the Navier-Stokes equations. Here, we will discuss vortex dynamics algebraically, based on continuous Nambu mechanics. Considering the Nambu formulation, the kinetic energy and a vortex-related quantity play an equal role for the representation of the vortex motion. The choice of the vortex-related quantity depends on the spatial dimension. In two dimensions the conserved vortex-related quantity is given by the enstrophy; and in three dimensions the helicity is conserved. But, we notice that for continuous dynamics, two conserved quantities do not assure the integrability of a three-dimensional system.

There are several works addressing fluid dynamics algebraically. Based on the Hamiltonian structure the Poisson bracket is considered in order to

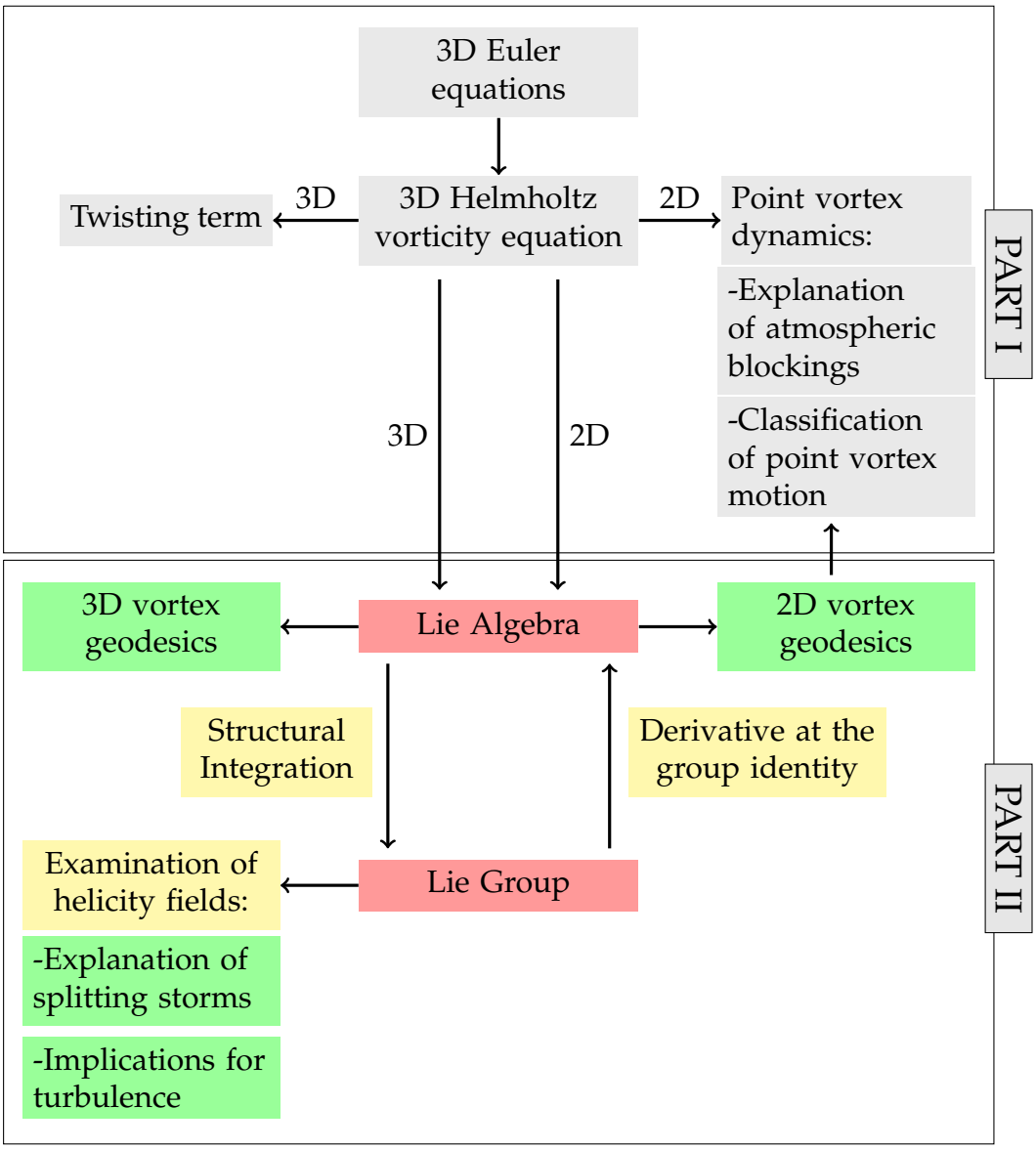

Figure 5.1: Thesis structure: In the first part of this thesis we have considered discrete vortex dynamics and in the second part we will explore vortex dynamics from an algebraic point of view.

derive variational principles and examine the stability of hydrodynamical systems. There are different algebraic formulations of fluid mechanical systems regarding continuous as well as discrete dynamical systems, see e.g. the works of Arnold (1969a), Arnold (1969b), Salmon (1982), Marsden and Weinstein (1983), Salmon (1988), Shepherd (1990), or Arnold and Khesin (1992). The commonly used Poisson brackets for hydrodynamical systems arose from the algebraic structure of mass point dynamics. The first Lagrangian formulations of mass point mechanics is based on the variational principles behind Newton's fundamental laws for force balance $\mathbf{F} = m\mathbf{a}$.

For Lagrangians that are purely kinetic energy, it was already known in 1840 that the corresponding solutions of the Euler-Lagrange equations are geodesics. Geodesics are shortest routes between two points that depend on the underlying topology. A summary of Jacobi's lecture notes are published in Jacobi (1866). By applying Legendre transformations, it can be shown that Hamilton's principle is equivalent to the Euler-Lagrange equations. Lagrange and Poincaré were the first who also took rotations – in terms of rigid body rotations – into account. They considered the Lie algebra of the classical rotation group in $\mathbb{R}^3$ leading to a representation of the Euler-Poincareé equations that can be seen as generalized Euler equations for rigid body rotations (Lagrange, 1788; Poincaré, 1901; Holm et al., 1998).

A Lagrangian and Hamilton formulation for the Euler equation of incompressible fluids, similar to the description for rigid body rotation, was introduced by Arnold (1966) and further studied, e.g. by Holm et al. (1998). They adapted the Lagrangian description of mass point dynamics to fluid mechanics. This leads to a Lagrangian description of vortex flows with a canonical Hamilton structure. In this approach, the Lie-Poisson-bracket for fluids is explored on a Poisson-manifold, which is associated to a cotangent bundle. This provides the natural structure of Lie algebras and Lie groups. To discuss Lagrangian mechanics the tangent space of the special orthogonal Lie group SO(3) is considered. The tangent space of SO(3), denoted $TSO(3)$, can be regarded as velocity-phase space (Holm et al., 1998; Arnold and Khesin, 1992). Applying the Legendre transformation this representation leads to a non-canonical Hamiltonian description on the tangent space. On this way it can be shown that Euler's rigid body equations are equivalent to a variational principle, the so-called rigid body action principle. A further Lie-Poisson representation for discrete dynamics is called *Heavy top* (Holm et al., 1998). It describes rigid body rotation with a fixed point in a gravitational field, where the underlying Lie algebra is the algebra of infinitesimal Euclidean motions in three-dimensional Euclidean space. Since rigid body rotations are considered, the basic phase space is also the cotangent bundle of $SO(3)$. The heavy top Hamiltonian is given by the total energy. Holm et al. (1998) point out that there are similar structures between the Poisson-bracket for compressible flow and that for heavy top.

By using the orthogonal decomposition of a wind field into a divergence-free part and a gradient, Holm et al. (1998) state that the Euler equations for an incompressible, homogeneous fluid moving in a region D are equiva-

lent to Poisson-bracket equations. Here, the Euler equations are formulated similar to the vorticity equation. In this way, the dynamics can be expressed by the kinetic energy providing a Hamiltonian structure. Holm et al. (1998) also regards the vorticity equation from an Hamiltonian point of view.

However, the above representation provides Hamilton's principle such that the associated curve satisfies the Euler-Lagrange equations, a *reduced* variational principle and *basic Euler-Poincaré equations* (Holm et al., 1998); Holm et al. (1998) also consider the vorticity as a dynamical variable formulated in the Hamiltonian structure. Additionally, they formulate Kelvin's circulation theorem in terms of this Lie-Poisson structure with respect to the vorticity. It is shown that Lie-Poisson systems can be applied to various physical problems: heavy top, compressible and stratified incompressible flow, magnetohydrodynamics as well as shallow water dynamics, and even quasi-geostrophic theory, see e.g. the works of Sudarshan and Mukunda (1974), Vinogradov and Kupershmidt (1977), Ratiu (1982), Holm and Kupershmidt (1983), or Marsden and Ratiu (2013).

We note two differences between the fluid mechanical Lie algebras that are based on Poisson brackets as shown above and the Lie algebras based on Nambu-mechanics derived by Névir and Blender (1993). On the one hand, the antisymmetric Poisson-Lie brackets yields a representation of the fluid dynamical equations in terms of the energy. The Nambu representation of the equations of fluid dynamics is formulated with respect to the energy and a vortex conservation law (2D: enstrophy, 3D: helicity) both determine the Lie-structure (see Névir, 1998). In previous studies, the algebraic approaches for the analysis of vortex motions are mostly based on Euler's equation of motion. Nambu mechanics is derived from the Helmholtz vorticity equation. Thus, we focus here only on those wind components that are related to vortex motions and express them in terms of vortex-related conserved quantities. Furthermore, the pressure is not given explicitly, but the Nambu formulation contains the conservation of mass by the incompressibility condition.

In this way, the Nambu-bracket allows for a compact and direct representation of vortex motions. Moreover, as we will discuss later in this thesis, the Nambu formulation of Névir and Blender (1993) takes the vortex rotations into account that differ from rigid body rotations.

After a short summary on the basic group theoretical and algebraic definitions in chapter 6, we will give an introduction to the Nambu formu-

lation of 2D and 3D continuous vortex dynamics in 7. In chapter 8 we will derive the Vortex-Heisenberg Lie algebra and the corresponding Lie group. In a second step we will introduce a novel Lie algebra that we will call Helmholtz Vortex algebra, where we include the angular momentum to the Vortex-Heisenberg Lie algebra. Based on the Vortex-Heisenberg Lie group and the Helmholtz Vortex Lie group we will explore the mechanism of splitting storms in terms of this Lie algebra in chapter 9. Here, we aim for a better understanding of the spatial structures of the wind fields that finally lead to splitting storms. Therefore, we will investigate the conditions on the spatial structures of a flow field that lead to splitted vortices. The trilinearity of the Nambu-bracket allows for an examination of the helicity field showing the existence of vortex splits. To the best of our knowledge, this is the first group theoretical approach to understand atmospheric phenomena. Already Arnold (1966) relates the Euler-Poincaré equations on a Lie algebra to geodesic motion on the corresponding Lie group. In chapter 10 we will show, how the novel Vortex-Heisenberg group provides a natural structure to derive point vortex geodesics via sub-Riemannian geometry. We will also introduce a concept to derive 3D vortex geodesics.

The Lie group operation itself was communicated with Peter Névir in private communication with Anton Schober in 2010. Based on their work and the algebraic Nambu formulation of vortex dynamics by Névir and Blender (1993), the novel contributions in this thesis that we will discuss in chapter 8 are:

(i.) Introducing a matrix representation of the Vortex-Heisenberg Lie algebra for 2D and 3D vortex dynamics.

(ii.) A derivation of the nilpotent Vortex-Heisenberg Lie group for 2D and 3D vortex dynamics.

(iii.) Extending the Vortex-Heisenberg group for three-dimensional vortex dynamics by the relative angular momentum to obtain a further spatial information of vortex motion. We will call this novel group Helmholtz Vortex group.

In chapter 9, based on steps (i)-(iii) we will

(iv.) Introduce a novel approach to understand the conditions for the development of splitting storms based on the Vortex-Heisenberg Lie group.

(v.) Apply the Helmholtz Vortex group to generate further vortex splits.

(vi.) Shortly discuss the implications of this algebraic approach for turbulence studies.

And, finally, in chapter 10, we will

(vii.) Apply Sub-Riemannian geometry to find vortex geodesics for point vortices and outline the concept for the derivation of vortex geodesics in three-dimensional fluids.

Chapter 6

Group theory of vortex dynamics

6.1 How can group theory be applied to atmospheric sciences?

In the following, we will consider an algebraic approach to introduce a new concept for the explanation of splitting storms and to describe point vortex geodesics. To this end, we will derive a group that is based on Helmholtz' vorticity equation. Mathematically, a group is a set M together with an operation $*$ that combines any two elements, say M_1 and $M_2 \in M$, to find a third element M_3 such that $M_1 * M_2 = M_3$. The closure-property of groups states that this third element M_3 also lies in the set M. This seemingly harmless property is important for the application of group theory to the atmosphere because of the following reason: The vortex groups we will derive in chapter 8 result from Helmholtz' vorticity equation, (cf. chapter 7, equation (7.31)). We consider the group elements M_1 and M_2 as solutions of the vorticity equation, where each element describes a state of a vortex flow. Then, the induced group element $M_3 = M_1 * M_2$ can be interpreted as a state, too. Furthermore, because of the closure-property, it yields an additional solution of the vorticity equation. Before we summarize the basic definitions of group theory, we will discuss the group of rotations which is a subset of the so-called orthogonal group and a classical example that we can observe in our daily life. We will use the following notations, see e.g. Hall (2003) or Baker (2012):

Let $M_{m,n}(\mathbb{K})$ be the set of $m \times n$ matrices whose entries are in the field $\mathbb{K}$ (see def. 6). For $n \times n$ matrices we will simply write $M(n, \mathbb{K})$. Then, the

common used notation for the set of invertible $n \times n$ matrices is

$$\mathrm{GL}(n, \mathbb{K}) = \{\underline{\mathbf{A}} \in M(n, \mathbb{K}) \mid \det(\underline{\mathbf{A}}) \neq 0\}, \tag{6.1}$$

where $\det(\underline{\mathbf{A}})$ denotes the determinant of the matrix $\underline{\mathbf{A}}$. The set of *unimodular matrices* is given by

$$\mathrm{SL}(n, \mathbb{K}) = \{\underline{\mathbf{A}} \in M(n, \mathbb{K}) \mid \det(\underline{\mathbf{A}}) = 1\} \tag{6.2}$$

Both sets are groups under matrix multiplication called

$$\begin{aligned} \mathrm{GL}(n, \mathbb{K}) &: \text{general linear group} \\ \mathrm{SL}(n, \mathbb{K}) &: \text{special linear group} \end{aligned} \tag{6.3}$$

where we will consider for $\mathbb{K}$ in the following the real numbers, the complex numbers and the quaternions, i.e. $\mathbb{K} = \mathbb{R}$, $\mathbb{K} = \mathbb{C}$ or $\mathbb{K} = \mathbb{H}$.

Definition 4. Matrix group
A matrix group is a closed subgroup of $\mathrm{GL}(n, \mathbb{K})$.

Examples of Matrix groups are the orthogonal and special orthogonal groups

The orthogonal group O(n)

The set of all $n \times n$ orthogonal matrices together with the usual matrix product is called *orthogonal group* $O(n) = O(n, \mathbb{R})$

$$O(n) = \{\underline{\mathbf{R}} \in \mathrm{GL}(n, \mathbb{R}) | \ \underline{\mathbf{R}}\underline{\mathbf{R}}^T = \underline{\mathbf{R}}^T\underline{\mathbf{R}} = \mathbb{1}\}, \tag{6.4}$$

where $\mathbb{1}$ denotes the unit matrix and $\underline{\mathbf{R}}^T$ transpose of the matrix $\underline{\mathbf{R}}$.

The special orthogonal group SO(n)

If the determinant of the matrices is one, this set is called *special orthogonal group* $SO(n, \mathbb{R})$:

$$SO(n) = \{\underline{\mathbf{R}} \in \mathrm{GL}(n, \mathbb{R}) | \ \underline{\mathbf{R}}\underline{\mathbf{R}}^T = \underline{\mathbf{R}}^T\underline{\mathbf{R}} = \mathbb{1}, \ \det(\underline{\mathbf{R}}) = 1\}. \tag{6.5}$$

Example 1. The special orthogonal group SO(3)
A well known subset of the orthogonal group is the set of three dimensional rotations. Its basis in matrix representation is given by the rotations around the x, y and z-axis by the angle ϕ:

$$\underline{\mathbf{R}}_x(\phi) = \begin{pmatrix} 1 & 0 & 0 \\ 0 & \cos(\phi) & -\sin(\phi) \\ 0 & \sin(\phi) & \cos(\phi) \end{pmatrix}, \underline{\mathbf{R}}_y(\phi) = \begin{pmatrix} \cos(\phi) & 0 & -\sin(\phi) \\ 0 & 1 & 0 \\ \sin(\phi) & 0 & \cos(\phi) \end{pmatrix}$$

and

$$\underline{\mathbf{R}}_z(\phi) = \begin{pmatrix} \cos(\phi) & -\sin(\phi) & 0 \\ \sin(\phi) & \cos(\phi) & 0 \\ 0 & 0 & 1 \end{pmatrix}$$

Now, we consider two planar rotations, both around the z-Axis, by the arbitrary but fixed angles ϕ_1 and ϕ_2. Since we use the matrix representation, the group operation $(*)$ is given by the matrix multiplication $(\cdot)$. Therefore, the group operation of the two group elements $\underline{\mathbf{R}}_z(\phi_1)$ and $\underline{\mathbf{R}}_z(\phi_2)$ induce the following third state $\underline{\mathbf{R}}_z(\phi_1)\underline{\mathbf{R}}_z(\phi_2)$ which, because of the closure-property, is an element of the orthogonal group, too:

$$\underline{\mathbf{R}}_z(\phi_1)\underline{\mathbf{R}}_z(\phi_2) = \begin{pmatrix} \cos(\phi_1) & -\sin(\phi_1) & 0 \\ \sin(\phi_1) & \cos(\phi_1) & 0 \\ 0 & 0 & 1 \end{pmatrix} \begin{pmatrix} \cos(\phi_2) & -\sin(\phi_2) & 0 \\ \sin(\phi_2) & \cos(\phi_2) & 0 \\ 0 & 0 & 1 \end{pmatrix}$$

$$= \begin{pmatrix} \cos(\phi_1)\cos(\phi_2) - \sin(\phi_1)sin(\phi_2) & -\cos(\phi_1)\sin(\phi_2) - \sin(\phi_1)\cos(\phi_2) & 0 \\ \cos(\phi_1)\sin(\phi_2) + \sin(\phi_1)\cos(\phi_2) & \cos(\phi_1)\cos(\phi_2) - \sin(\phi_1)sin(\phi_2) & \\ 0 & 0 & 1 \end{pmatrix}$$

Applying the trigonometric addition and subtraction theorems leads to:

$$\underline{\mathbf{R}}_z(\phi_1)\underline{\mathbf{R}}_z(\phi_2) = \begin{pmatrix} \cos(\phi_1+\phi_2) & -\sin(\phi_1+\phi_2) & 0 \\ \sin(\phi_1+\phi_2) & \cos(\phi_1+\phi_2) & 0 \\ 0 & 0 & 1 \end{pmatrix} = \underline{\mathbf{R}}_z(\phi_1+\phi_2). \quad (6.6)$$

Therefore, the group operation of two planar rotations can also be expressed by one rotation by the angle $\phi_1 + \phi_2$.

Next, we rotate around two axes, i.e. in three dimensions. We rotate by ϕ_1 about the x-axis and by ϕ_2 about the y-axis and calculate the group operation. For Matrix groups, the group operation is given by the usual matrix product. Considering each matrix $\underline{\mathbf{R}}_x(\phi_1)$ and $\underline{\mathbf{R}}_y(\phi_2)$ as group elements we

obtain:

$$\underline{\mathbf{R}}_x(\phi_1)\underline{\mathbf{R}}_y(\phi_2) = \begin{pmatrix} 1 & 0 & 0 \\ 0 & \cos(\phi_1) & -\sin(\phi_1) \\ 0 & \sin(\phi_1) & \cos(\phi_1) \end{pmatrix} \begin{pmatrix} \cos(\phi_2) & 0 & -\sin(\phi_2) \\ 0 & 1 & 0 \\ \sin(\phi_2) & 0 & \cos(\phi_2) \end{pmatrix} \tag{6.7}$$

$$\Longleftrightarrow \underline{\mathbf{R}}_x(\phi_1)\underline{\mathbf{R}}_y(\phi_2) = \begin{pmatrix} \cos(\phi_2) & 0 & -\sin(\phi_2) \\ -\sin(\phi_2)\sin(\phi_1) & \cos(\phi_1) & -\sin(\phi_1)\cos(\phi_2) \\ \cos(\phi_1)\sin(\phi_2) & \sin(\phi_1) & \cos(\phi_1)\cos(\phi_2) \end{pmatrix} \tag{6.8}$$

and leads to a third group element. As an example, we set $\phi_1 = \pi$ and $\phi_2 = \pi$, we obtain:

$$\underline{\mathbf{R}}_x(\pi)\underline{\mathbf{R}}_y(\pi) = \begin{pmatrix} -1 & 0 & 0 \\ 0 & -1 & 0 \\ 0 & 0 & 1 \end{pmatrix} = \underline{\mathbf{R}}_z(\pi) \tag{6.9}$$

which is equal to the rotation around the z-axis by the angle π. Both examples demonstrate the closure property.

In this chapter, we will outline the physical idea of a group for vortex dynamics and in chapter 8 we will show a mathematical derivation and definition of a vortex group for three dimensional inviscid flows. We regard two elements $\mathbf{A}$ and $\mathbf{A}'$ of the vortex group, where each element describes the state of an arbitrary but fixed region of a flow field. We assume a meteorological, atmospheric basic flow. State $\mathbf{A}$ is characterized by its shear field $\mathbf{v} \in \mathbb{R}^3$ with a vanishing vortex vector $\boldsymbol{\xi} = \nabla \times \mathbf{v} = \mathbf{0} \in \mathbb{R}^3$. We assign $\mathbf{A}$ the pair $(\mathbf{v}, \boldsymbol{\xi})$. The second state $\mathbf{A}'$ is characterized by the velocity field $\mathbf{v}'$ and the vortex vector $\boldsymbol{\xi}'$, where $\mathbf{v}'$ and $\boldsymbol{\xi}'$ are parallel causing a strong helical rotation. Thus, this state is characterized by large helicity density values, because the helicity density is defined by one and a half times the scalar product of the velocity and the vorticity vector. Therefore, we can regard $\mathbf{A}'$ as an idealized updraft in a supercell (we will discuss this case in more detail in chapter 9.)

The group operation $(*)$ of these two states induces a further group element $\mathbf{A}'' = \mathbf{A}' * \mathbf{A}$. Physically, the group operation can be seen as interaction, or state change. The outcome of the group operation $\mathbf{A}''$ is also an element of the group, which follows from the closure-property of groups; physically, it shows the change of the state of the fluid. The induced group element $\mathbf{A}''$ is also composed of a velocity and a vorticity part and we can determine the helicity (density) field of this state. In chapter 8 we will ex-

amine the plus-minus-structure of helicity density fields to investigate the split of vortices. Our previous two examples, the group of rotations and the group for atmospheric vortex dynamics can be sketched as follows:
Rotation group (O(3)):

$$\begin{pmatrix} \textit{Rotation by} \\ \textit{the angle } \phi_1 \end{pmatrix} \cdot \begin{pmatrix} \textit{Rotation by} \\ \textit{the angle } \phi_2 \end{pmatrix} = \begin{pmatrix} \textit{Rotation by} \\ \textit{the angle } \phi_1 + \phi_2 \end{pmatrix}$$

Vortex- group:

$$\begin{pmatrix} \textit{Initial field } \mathbf{A}: \\ \textit{helicity-free} \\ \textit{shear-flow} \end{pmatrix} \cdot \begin{pmatrix} \textit{Initial field } \mathbf{A}': \\ \textit{rotating flow} \\ \textit{with max. helicity} \end{pmatrix} = \begin{pmatrix} \textit{Induced field } \mathbf{A}'': \\ \textit{Splitted flow field} \\ \pm \textit{ helicity.} \end{pmatrix}$$

In chapter 8 we will introduce such a vortex group to explain atmospheric vortex splits by analyzing helicity fields in chapter 9.

6.2 Introduction to group theory

To investigate the Vortex-Heisenberg Lie group we will first introduce the main definitions and theorems of general group theory, then we will discuss the so-called Lie groups. Lie groups are groups that are characterized by an underlying topological structure. Finally, we will derive a matrix representation of the Vortex Heisenberg group and prove that the introduced group is indeed a Lie group. Here, we will follow Hall (2003), Wipf (2016) and Knapp (2013) and start with the basic definitions.

Definition 5. Group
A group is a set G together with an operation $G \times G$ into G. This group operation $*$ combines two group elements a and $b \in G$ by $a * b$ forming a third element which is also an element of the group. Every group $(G, *)$ satisfies the following properties:

i. Associativity:

$$(a * b) * c = a * (b * c),\ a, b, c \in G \tag{6.10}$$

ii. Existence of the identity element $e \in G$:

$$a * e = e * a = a,\ a \in G \tag{6.11}$$

iii. Existence of inverse elements $a^{-1} \in G$:

$$a^{-1} * a = e \tag{6.12}$$

Moreover, a group is called *abelian* if the group is commutative, i.e. if all $a, b \in G$ satisfy

$$a * b = b * a. \tag{6.13}$$

A classical example of a group is the set of integers with the addition as group operation. We see that the sum of two integers is an integer, too, and therefore the generated element lies in the group. Moreover, for three integers a, b, c it is $(a + b) + c = a + (b + c)$, therefore the associativity holds. Zero is the identity element and the inverse element of the element k in the group is $-k$. Therefore, all group properties are satisfied. We can also see that the set of integers with addition is an abelian group, because (6.13) is satisfied.

Definition 6. Field
A field is a set $\mathbb{K}$ together with operations $+$ and $*$ such that:

i. $(\mathbb{K}, +)$ is an abelian group, the identity element is 0.

ii. $(\mathbb{K} \setminus \{0\}, *)$ is an abelian group with identity element 1.

iii. The distributive law holds: Let $a, b \in \mathbb{K}$, then
$a * (b + c) = a * b + a * c,\ (a + b) * c = a * c + b * c.$

In this thesis we will primarily consider the fields $\mathbb{R}$ (real numbers) and $\mathbb{C}$ (complex numbers) as well as the quaternions that form a skew field. To identify and create different representations of the Vortex Heisenberg group we repeat the most important definitions dealing with maps between different (representations of) groups:

Definition 7. Group homomorphism, Isomorphism, Automorphism
Let $(G, *)$ and $(G', \star)$ be groups. A map $\varphi : G \longrightarrow G'$ such that

$$\varphi(g_1 * g_2) = \varphi(g_1) \star \varphi(g_2) \quad \forall g_1, g_2 \in G. \tag{6.14}$$

is called a *group homomorphism*. If the homomorphism is bijective, i.e. there exists a one-to-one correspondence[1], the map φ is called an *isomorphism*. If

[1] A bijective function is called one-to-one correspondence , because it is a function that it is a one-to-one (injective) and onto (surjective) mapping of a set M_1 to a set Y and therefore, it exists a unique inverse function from M_2 to M_1.

an isomorphism $\varphi : G \longrightarrow G'$ exists the groups G and G' are *isomorphic*, notation: $G \cong G'$. If $G' = G$ the map is called automorphism.

Moreover, we will define the kernel and image of a group homomorphism and use it for the definition of the special linear group. This group is important because we can find matrix representations for (subgroups of) the special linear group.

The *kernel* of a homomorphism $\varphi : G \longrightarrow G'$ is the set

$$\ker(\varphi) = \{g \in G \mid \varphi(g) = e'\} \tag{6.15}$$

where e' is the identity element in G'. The *image* of a homomorphism is the set

$$\mathrm{im}(\varphi) = \{\varphi(g) \mid g \in G\}. \tag{6.16}$$

We remark that the image is a subgroup of G' and the kernel a so called normal subgroup, which we will discuss later. Now, let $\mathbb{K}$ be a field, and let $\mathrm{GL}(n, \mathbb{K})$ be the matrix group with elements in the field $\mathbb{K}$. Then the determinant:

$$\det : \mathrm{GL}(n, \mathbb{K}) \longrightarrow (\mathbb{K}^*, *) \tag{6.17}$$

is a homomorphism, mapping from $\mathrm{GL}(n, \mathbb{K})$ to the multiplicative group $(\mathbb{K}^*, *)$ of the field $\mathbb{K}$. The kernel of the determinant is the *special linear group* we have defined in (6.2):

$$\mathrm{SL}(n, \mathbb{K}) = \ker(\det) = \{A \in \mathrm{GL}(n, \mathbb{K}) \mid \det A = 1\}. \tag{6.18}$$

Definition 8. Ring
A *ring* is a set R with two operations $R \times R \longrightarrow R$, usually called addition and multiplication and often denoted $(a, b) \mapsto a + b$ and $(a, b) \mapsto a * b$, such that

(i) $(R, +)$ is an abelian group

(ii) $(R, \cdot)$ is a monoid[2]

(iii) multiplication is associative in the sense that $a * (b * c) = (a * b) * c$ for all $a, b, c \in R$

[2]Assume a set S and a binary operation $S \times S \longrightarrow S$. Then, S together with the operation is called monoid if (i) the associativity property holds and (ii) if there exists a identity element for all elements in S.

(iiv) the two distributive laws $a * (b + c) = (a * c) + (b * c)$ and $(b + c) * a = (b * a) + (c * a)$ hold for all $a, b, c \in R$.

The sets $\mathbb{Z}, \mathbb{Q}, \mathbb{R}$ and $\mathbb{C}$ are examples of rings as well as the set of quadratic matrices with the usual matrix addition and matrix multiplication (Karpfinger and Meyberg, 2017). We remark that the set $\mathbb{Z}$ is a ring, but not a field, because there do not necessarily exist inverse and identity elements of ring elements.

Definition 9. Ideal of a ring
An ideal I of a ring R (or two-sided ideal in case of ambiguity) is an additive subgroup such that $a * b$ and $b * a$ are in I, whenever a is in I and b is in R.

Consider the following example of an ideal after Knapp (2006). Denote $\varphi : R \to R'$ a homomorphism of rings, where its image is a subring of R'. Now, we take two elements, one element a from the kernel, i.e. $\varphi(a) = 0$, and another element from the ring R. We can write $\varphi(a * b) = \varphi(a) * \varphi(b) = 0 * \varphi(b) = 0$. And analogously, $\varphi(b * a) = 0$. The kernel of a ring homomorphism is closed under products of members of the kernel with arbitrary members of the ring R. Following the definition, an ideal I of R is an additive subgroup such that $a * b$ and $b * a$ are in I, whenever a in I and b in I. It follows that the kernel of a homomorphism is an ideal.

Definition 10. Center of a group
The center Z of a group G is defined by the set

$$Z = \{z \in G |\ z * g = g * z \quad \forall g \in G\} \ \subset G. \tag{6.19}$$

It is a (non-empty) subgroup of G.

Thus, the center of a group is the set of all elements that commute with every element of the group and therefore, it is an abelian subgroup. A group is called centerless, if the center is trivial meaning that only consists of the identity element. We also introduce a very similar definition, the centralizer of a group. In contrast to the center, the centralizer of an element is the set of elements that commute with that element.

Definition 11. Centralizer of a group
The centralizer C of a group $(G, *)$ is defined by the set

$$C = C(g) = \{z \in G |\ z * g = g * z\} \ \subset G, \tag{6.20}$$

where g is in a fixed subset S of G. It is a non-empty subgroup of G.

Therefore, the centralizer always contains the center of the group. Moreover, we compare the definition of the so-called normalizer:

Definition 12. Normalizer
A normalizer of a subset S of the group G is defined to be:

$$N(S) = \{g \in G \mid g * S = S * g\} \tag{6.21}$$

Therefore, the normalizer of of a set S contains the centralizer as a subgroup. Both the normalizer and the centralizer contain the center of the group (see e.g. Cohen et al., 1999).

Definition 13. Normal subgroup
A normal subgroup N of G satisfies:

$$g * N * g^{-1} = N \quad \forall g \in G \tag{6.22}$$

Every group has at least two normal subgroups: the identity element of G and G itself. The center of a group and the commutator subgroup are further examples of a normal subgroup. If $\varphi : G \longrightarrow G'$ is a homomorphism, then the kernel $\ker(\varphi)$ is a normal subgroup of G. We also note that a normalizer is the largest intermediate subgroup in which the given subgroup is normal.

Definition 14. Commutator subgroup
The commutator subgroup $[G, G]$ is the group generated by all the commutators

$$\{[a, b] \equiv a * b * a^{-1} * b^{-1} |\ a, b \in G\} \tag{6.23}$$

of the group.

The commutator group $[G, G]$ is a normal subgroup of G. We will use commutator groups to define central series (see def. 16), which in turn is a basic ingredient to define the so-called nilpotent group. The group for vortex dynamics that we will derive in chapter 8 will turn out to be nilpotent. Nilpotency allows a simple transition between Lie groups and a Lie algebra and enables us to find vortex geodesics. Moreover, a quotient group G/N is abelian if and only if N contains the commutator subgroup. Therefore it can be interpreted as a measure of how far the group is from

being abelian: the larger the commutator subgroup is, the „less abelian“ the group is.

After the next definition, we can introduce the so-called nilpotent group, which is an important characterization of the group that we will derive later to describe vortex dynamics. A central series for a group can be seen as a witness for its nilpotency.

Definition 15. Central series,

A *central series* is a sequence of subgroups

$$\{1\} = G_0 \triangleleft G_1 \triangleleft \cdots \triangleleft G_n = G \tag{6.24}$$

such that $[G, G_{i+1}] \leqslant G_i,\ i = 1, 2, ..., n$, where the bracket $[G, H]$ denotes the commutator subgroup generated by all $g^{-1}h^{-1}gh$ for g in G and h in H as we have defined in (6.23). That means that the successive quotients are central. Therefore, we can write $[G, G_{i+1}] \leqslant G_i \leqslant G_{i+1}$. For each i, G_{i+1} is normal in G.

Definition 16. Lower central series
Given a group G, a *lower central series* is the inductively defined descending sequence

$$G = G_0 \trianglerighteq G_1 \trianglerighteq \cdots \trianglerighteq G_n \tag{6.25}$$

such that $G_{i+1} = [G_i, G],\ i = 0, 1, 2, ..., n-1$ is the commutator subgroup generated by all $g^{-1}h^{-1}gh$ for g in G and h in G_{i-1} as we have defined in (6.23). For a nilpotent group (see def. 17 below), this series terminates in finitely many steps at the trivial subgroup.

Definition 17. Nilpotent group
A group is called *nilpotent*, if its lower central series terminates in the trivial subgroup after finitely many steps. If there exist $n + 1$ different subgroups in the series (including the trivial subgroup and the whole group), we say that the length is n.

We remark that not every group has a lower central series, but if a group has a central series, it is called nilpotent group. And if we can find a lower central series of length n, where n is the smallest length, then n is called the *nilpotency class* of G. For example, the trivial group is the unique group of nilpotency class 0. Examples of groups of nilpotency class 1 are the non-trivial abelian groups. In chapter (8) we will introduce a further nilpotent

group the Vortex-Heisenberg group. The nilpotent group structure of the Vortex-Heisenberg group implies a nilpotent algebra, which in turn allows for the search for vortex geodesics. A classical example of a nilpotent group is the group of upper unitriangular $n \times n$ matrices such as the classical Heisenberg group.

Definition 18. Solvable group
A group G is a *solvable group* if there exists a sequence of subgroups $G_1, \ldots, G_k$ of G such that, for each j, $1 \leq j \leq k$, G_j is a normal subgroup of G_{j-1}, the quotient group G_{j-1}/G_j is abelian, and G_k is the identity.

In other words: A group is called solvable if it has a subnormal series whose factor groups (quotient groups) are all abelian.

For example, nilpotent groups are all solvable, but there are solvable groups that are not nilpotent, which underlines the importance of nilpotent groups. This relation does also hold for algebras, as we will briefly discuss later.

Definition 19. Simple group
A group G is said to be *simple* if the normal subgroups, the identity, and G itself are the only normal subgroups.

The following two definitions allow for combinations of two groups such that they form a common group. Either by defining the combination of the two groups component by component (direct product) or more generalized (indirect product).

Definition 20. Direct product
Let $(G, \cdot)$ and $(H, \circ)$ be two groups and consider their Cartesian product $G \times H$ and the set of ordered pairs (g, h) with $g \in G$ and $h \in H$. Then, we define a product operation as follows:

$$(g_1, h_1) * (g_2, h_2) = (g_1 \cdot g_2, h_1 \circ h_2), \tag{6.26}$$

which can be seen as a component by component composition. This operation makes the Cartesian product of G and H into a group, called the *direct product* of G and H and denoted $G \times H$.

A generalization of this concept ist called semidirect product. In chapter 8 we will introduce two groups that are based on Helmholtz' vorticity equation. The semidirect product can be used to show the relation of both vortex groups. The semidirect product of two groups is defined as:

Definition 21. Semidirect product
Let $(N, \cdot)$ and $(H, \circ)$ be two groups and let $\varphi : H \longrightarrow \mathrm{Aut}(N)$ be a group homomorphism mapping the group H to the set of all automorphisms of N. As in our last definition, the Cartesian product $G := N \times H$ of the sets N and H is the set of all pairs (n, h) with $n \in N$ and $h \in H$. This product together with the group operation $*$ defined by:

$$(n_1, h_1) * (n_2, h_2) := (n_1 \cdot \varphi(h_1)(n_2), h_1 \circ h_2) \tag{6.27}$$

forms a group. This product is called *semidirect product* and denoted by $H \ {}_{\varphi} \ltimes N$, where ${}_{\varphi}\ltimes$ is used for the notation of the semidirect product with respect to the homomorphism φ.

In the definition of the semidirect product the homomorphism φ has a large impact on the group structure. As an example, let us consider φ to be the trivial homomorphism, mapping every element of H to the identity automorphism of N, then $H_{\varphi} \ltimes N$ is equal to the direct product $H \times N$. But if φ is an arbitrary homomorphism, it has an impact on the structure of the semidirect product and we say that H acts on N and not vice versa.

So far, we have introduced the basic definitions of groups. But in order to apply groups to physical problems as atmospheric wind fields, we will consider matrix representations of groups. In this way, group elements can be represented as matrices forming a group together with the usual rule for matrix multiplication. Mathematically, a representation of a group is a linear map from the group to a $\mathbb{K}$-vector space V, such that each group element can be described by a matrix. For any finite-dimensional V, the group $\mathrm{GL}(n, V)$ is isomorphic to $\mathrm{GL}(n, \mathbb{K})$ (see e.g. Lorenz, 2018).

Definition 22. Group representation
A representation D of a group G on a linear space V is a group homomorphism

$$D : G \longrightarrow \mathrm{GL}(n, V), \quad g \mapsto D(g) \tag{6.28}$$

where the group structure of G with group operation $*$ is respected:

$$D(g_1 * g_2) = D(g_1) \cdot D(g_2),\ D(e) = \mathbb{1} \Longrightarrow D(g^{-1}) = D^{-1}(g). \tag{6.29}$$

The latter equation (6.29) follows from the assumption that the representation is a group homomorphism. Considering matrices as representations for group elements, the corresponding group composition, here denoted

with $\cdot$, is given by the usual matrix product.

A *trivial representation* maps all group elements to the unit matrix. Representations are called faithful if they are injective. (Then D is a group homomorphism $G \longrightarrow \mathrm{GL}(V)$, $\ker(D) = e \in G$). By Choosing a basis $D(G)$ become matrices. In case of faithful representations all properties of the group are conserved.

Definition 23. Left group action
We say a group G acts on a set X when there is a map $\varphi : G \times X \to X$ such that the following conditions hold:

i. $\varphi(e, x) = x$, for all $x \in X$ and with identity element e of G.

ii. $\varphi(g, \varphi(h, x)) = \varphi(gh, x)$ for all $g, h \in G$ and all $x \in X$.

Then, G is called a transformation group and the map φ is called the group action.

We can also think of a representation as a linear action of a group on a vector space, because to every group element g in a group G, there exist an operator $D(g)$, which acts on a vector space V (Hall, 2003). We will use the definition of group actions in particular in chapter 10, where we will search for vortex geodesics based on the Vortex-Heisenberg group we will derive in chapter 8.

Before we introduce Lie groups, that means groups with an underlying topological structure, we discuss two groups that are frequently applied in physics and other natural sciences. In (6.4) we have discussed planar and spatial rotations as subgroups of the orthogonal group $O(n)$. We extend this idea by including translations, too, leading to the Euclidean group. The Vortex-Heisenberg group that we will derive later also deals with rigid body rotations and translations, and the concept is quite similar to the Euclidean group although both groups result from very different physical concepts. For more details and further physical examples, see Hall (2003).

Example 2. The Euclidean group E(3)
The Euclidean group has two subgroups, the orthogonal group (see (6.4)) and the group of translations that have a matrix and a vector representation. As we will see in the next example, the Euclidean group is the semidirect product of the orthogonal group extended by the group of translations. For

now, let us consider the three-dimensional Euclidean space. Then, the Euclidean group describes motions that we can observe every day on every location — translations and rotations. We can define the *euclidean distance* between two points $\mathbf{x}_1$ and $\mathbf{x}_2$ in $\mathbb{R}^3$ by $d(\mathbf{x}_1, \mathbf{x}_2) = ||\mathbf{x}_1 - \mathbf{x}_2||$, which we know is a straight line and provides the shortest path between two objects in the three dimensional euclidean space. If we apply an affine transformation to $\mathbf{x} \in \mathbb{R}^3$ that is given by

$$\mathbf{x} \mapsto \underline{\mathbf{R}}\mathbf{x} + \mathbf{a}, \tag{6.30}$$

the distance of two points is invariant if and only if $\underline{\mathbf{R}}$ is a rotation, i.e. an element in O(3) and $\mathbf{a} \in \mathbb{R}^3$. Affine transformations (6.30) preserves points, straight lines and planes.

In chapter 8 we will introduce a group for three dimensional incompressible, inviscid fluids that contains the rigid body rotations and also the translation. Therefore, we will briefly recall the derivation of the matrix representation of the Euclidean group E(3). The three-dimensional Euclidean group E(3), which is the group of all one-to-one, onto, distance-preserving maps of $\mathbb{R}^3$ to itself, that is, maps $f : \mathbb{R}^3 \to \mathbb{R}^3$ such that $d(f(\mathbf{x}_1), f(\mathbf{x}_2)) = d(\mathbf{x}_1, \mathbf{x}_2)$ for all $\mathbf{x}_1, \mathbf{x}_2 \in \mathbb{R}^3$. We do not assume anything about the structure of f besides the above properties. Therefore, f does not need to be linear. The orthogonal group O(3) that we discussed earlier, is an example for a subgroup of E(3). It is the group of all linear distance-preserving maps of $\mathbb{R}^3$. Define a further subgroup of E(3): The *translation* of $\mathbf{x}$ by $\mathbf{a}$:

$$T_{\mathbf{a}}(\mathbf{x}) = \mathbf{a} + \mathbf{x}, \quad \mathbf{a}, \mathbf{x} \in \mathbb{R}^3. \tag{6.31}$$

Every element T of E(3) can be written uniquely as an orthogonal linear transformation followed by a translation of the form

$$T = T_{\mathbf{a}}\underline{\mathbf{R}} \quad \text{with } \mathbf{a} \in \mathbb{R}^3 \text{ and } \underline{\mathbf{R}} \in O(3). \tag{6.32}$$

The proof will lead to the group operation. We will prove that every one-to-one onto, distance preserving map of $\mathbb{R}^3$ to itself, which fixes the origin must be linear. We write an element $T = T_{\mathbf{a}}\underline{\mathbf{R}}$ of E(3) as a pair $\{\mathbf{a}, \underline{\mathbf{R}}\}$. For $\mathbf{x} \in \mathbb{R}^3$ we obtain:

$$\{\mathbf{a}, \underline{\mathbf{R}}\}\mathbf{x} = \underline{\mathbf{R}}\mathbf{x} + \mathbf{a} \tag{6.33}$$

and

$$\{\mathbf{a}, \underline{\mathbf{R}}\}\{\mathbf{a}', \underline{\mathbf{R}}'\}\mathbf{x} = \underline{\mathbf{R}}(\underline{\mathbf{R}}'\mathbf{x} + \mathbf{a}') + \mathbf{a} = (\mathbf{a} + \underline{\mathbf{R}}\mathbf{a}') + \underline{\mathbf{R}}\underline{\mathbf{R}}'\mathbf{x}. \tag{6.34}$$

Thus, the group operation of E(3) resulting from the latter equation reads as:

$$\boxed{(\mathbf{a}, \underline{\mathbf{R}}) * (\mathbf{a}', \underline{\mathbf{R}}') = (\mathbf{a} + \underline{\mathbf{R}}\mathbf{a}', \underline{\mathbf{R}}\underline{\mathbf{R}}') := (\mathbf{a}'', \underline{\mathbf{R}}'').} \tag{6.35}$$

Therefore, the three-dimensional Euclidean group is the semidirect product of the abelian group $\mathbb{R}^3$ of the translations and the group of rotations O(3). In chapter 8 we will first introduce a nilpotent group for vortex dynamics and later, we will include the Euclidean group into the vortex group such that the vortex group contains rigid-body rotations. The inverse of an element in E(3) is given by:

$$(\mathbf{a}, \underline{\mathbf{R}})^{-1} = (-\underline{\mathbf{R}}^{-1}\mathbf{a}, \underline{\mathbf{R}}^{-1}). \tag{6.36}$$

Since translations are not linear maps, E(3) is not a subgroup of the general linear group $\mathrm{GL}(3, K)$. But E(3) is isomorphic to a subgroup of $\mathrm{GL}(3+1, \mathbb{R})$ via the map that associates $(\mathbf{a}, \underline{\mathbf{R}}) \in E(3)$ to the following matrix:

$$\begin{pmatrix} & & a_1 \\ & \underline{\mathbf{R}} & a_2 \\ & & a_3 \\ 0 & 0 & 1 \end{pmatrix} \tag{6.37}$$

Thus, every vector $\mathbf{a}$ and every rotation $\underline{\mathbf{R}}$, $(\mathbf{a}, \underline{\mathbf{R}}) \in \mathrm{E}(3)$ is mapped one-to-one to a matrix. Moreover, direct computation shows that multiplication of elements of the form (6.37) follows the multiplication rule in (6.35) so that this map is a homomorphism. Therefore, $E(3)$ is isomorphic to the group of all matrices of the form (6.37), with $\underline{\mathbf{R}} \in O(3)$. Because the limit of (6.37) is again of that form, we have expressed the Euclidean group $E(3)$ as so-called matrix Lie group. We note that the previous calculations also hold for n-dimensions and we can replace '3' by n.

The last example is similar to our approach of the algebraization of Nambu fluid mechanics resulting in a matrix Lie group that we will discuss in chapter 8. The Galilei-group is a further physical example. It is based on Newton mechanics and the group of the Galilei-transformation in space and time that captures the symmetry properties of inertial systems in

classical physics.

Example 3. The Galilei-group
Consider a coordinate system formed by three dimensional spatial coordinates and one time coordinate. With $(t, \mathbf{x})$ and $(t', \mathbf{x}')$ we denote one state with respect to two inertial systems with origins O and O' and basis $\mathbf{e}_i,\ \mathbf{e}'_i$, $i, j = 1, \ldots, n$, ($\mathbf{x}, \mathbf{x}', \mathbf{e}_i, \mathbf{e}'_i \in \mathbb{R}^3$, $t, t' \in \mathbb{R}$). The following transformations between these two coordinate systems are possible:

Transformation	Time coordinate	Local coordinate
Translation of the origin	$t' = t$	$\mathbf{x}' = \mathbf{x} + \mathbf{a}$
Translation of the time-origin	$t' = t + \tau$	$\mathbf{x}' = \mathbf{x}$
Rotation of the systems	$t' = t$	$\mathbf{x}' = \underline{\mathbf{R}}\mathbf{x}$
Special Galilei-transformation	$t' = t$	$\mathbf{x}' = \mathbf{x} + \mathbf{u}t$

where $\mathbf{u}$ is a constant velocity, $\mathbf{x}, \mathbf{a}$ and $\mathbf{u}$ in $\mathbb{R}^3$, t and τ denote time, see (Wipf, 2016). The translation of the origin together with the rotation of the systems form the three-dimensional Euclidean group that we have discussed in our previous example. The rotations of the systems together with the special Galilei transformation provide a similar structure that is usually denoted $E_{\mathbf{u}}(3)$ The special Galilei-transformations build the so-called *Galilei group*. One element of this group is a composition of translations, rotations and special Galilei-transformations:

$$t' = t + \tau \quad \text{und } \mathbf{x}' = \underline{\mathbf{R}}\mathbf{x} + \mathbf{u}t + \mathbf{a}, \quad \mathbf{x}, \mathbf{a} \in \mathbb{R}^3, \quad \underline{\mathbf{R}}^T\underline{\mathbf{R}} = \mathbb{1}. \tag{6.38}$$

We note that the Galileo-transformation is determined by 10 parameters: $\tau, \mathbf{a}, \mathbf{u}$ and $\underline{\mathbf{R}}$. Now, we change the reference system I to the reference system I' by the transformations in (6.38); afterwards we switch from I' to I''. These transformations from $I \to I''$ can be expressed as:

$$\begin{aligned}(\tau', \mathbf{a}', \mathbf{u}', \underline{\mathbf{R}}') * (\tau, \mathbf{a}, \mathbf{u}, \underline{\mathbf{R}}) &= (\tau' + \tau, \mathbf{a}' + \underline{\mathbf{R}}'\mathbf{a} + \mathbf{u}'\tau, \mathbf{u}' + \underline{\mathbf{R}}'\mathbf{u}, \underline{\mathbf{R}}'\underline{\mathbf{R}}) \\ &= (\tau'', \mathbf{a}'', \mathbf{u}'', \underline{\mathbf{R}}'').\end{aligned} \tag{6.39}$$

Moreover, Galilei-transformation can be assigned to 5×5-matrices:

$$\begin{pmatrix} \mathbf{x}' \\ t' \\ 1 \end{pmatrix} = \begin{pmatrix} \underline{\mathbf{R}} & \mathbf{u}' & \mathbf{a}' \\ 0 & 1 & \tau \\ 0 & 0 & 1 \end{pmatrix} \begin{pmatrix} \mathbf{x} \\ t \\ 1 \end{pmatrix} \tag{6.40}$$

which is the matrix representation of the Galilei-group (see e.g Wipf, 2016)). Thus, the Galilei-group is a subgroup of $\mathrm{GL}(5,\mathbb{R})$. It has four normal subgroups. For the discussion of all twelve subgroups, especially for the four normal subgroups, see Lévy-Leblond (1971). Here, we will recall the two most frequently discussed normal subgroups after Wipf (2016): (1) the pure translations $(0,\mathbf{a},\mathbf{0},\mathbb{E})$ and (2) the translations and the special Galilei transformations $(0,\mathbf{a},\mathbf{u},\mathbb{E})$. We summarize that the Galilei-group can be formulated as the semidirect product of the group $\mathbb{R}^4$ representing the translations in time and space with elements $(\tau,\mathbf{a})$ and the Euclidean group $E_{\mathbf{u}}(3)$ with elements $(\mathbf{u},\underline{\mathbf{R}})$:

$$G = E_{\mathbf{u}}(3) \ltimes \mathbb{R}^4 \tag{6.41}$$

There are four possibilities to express the Galilei-group in terms of a semidirect product of groups. There are five ideals, but only four ideal can be used to formulate a semidirect product. Finally, the action of $(\mathbf{u},\underline{\mathbf{R}}) \in E(3)$ on $(\tau,\mathbf{a}) \in \mathbb{R}^4$ is given by:

$$\varphi(\mathbf{u},\underline{\mathbf{R}})(\tau,\mathbf{a}) = (\tau, \underline{\mathbf{R}}\mathbf{a} + \tau\mathbf{u}). \tag{6.42}$$

For further details on the Galilei group see e.g. Wipf (2016) or Lévy-Leblond (1971).

6.2.1 Lie group

Lie groups are groups with topological structure, so-called manifolds. In order to introduce a Lie group that is based on Helmholtz' vorticity equations, we will give a short introduction to differential geometry of manifolds, and the structure of Lie groups and Lie algebras.

Definition 24. Differentiable manifold
An n-dimensional manifold M is a topological space that is a second countable Hausdorff space and locally homeomorphic to $\mathbb{R}^n$.

In other words, a n-dimensional manifold looks locally like a piece of $\mathbb{R}^n$. Let us assume, we are standing on a sphere, for instance, the Earth; locally, it could feel like standing on a two dimensional surface. This is an example of a two-dimensional manifold embedded in three-dimensional Euclidean space. We will follow the definitions and examples given in Hall (2003).

Definition 25. (Normal, sub-) Lie group
A *Lie group* is a differentiable manifold G which is also a group and such that the group product

$$G \times G \to G \tag{6.43}$$

and the inverse map $g \to g^{-1}$ are differentiable. A *Lie subgroup* H of the group G is a submanifold H of G that also is a subgoup of G. A normal subgroup N of G is also a Lie subgroup. It is called *Lie normal subgroup*.

In Hall (2003), p. 313, it is proven that every matrix Lie group is a smooth embedded submanifold of the vector space $V = M_n(\mathbb{C})$, where we think of $V = M_n(\mathbb{C})$ as a real vector space of dimension $2n^2$. Because the matrix product and the matrix inverse are smooth on the open subset $\mathrm{GL}(n, \mathbb{C})$ of $V = M_n(\mathbb{C})$, every matrix Lie group is indeed a Lie group.

Definition 26. Lie group action, left invariance
An action of a Lie group G on a smooth manifold M is a group homomorphism into the group of diffeormorphism on M

$$G \longrightarrow \mathrm{Diff}(M) \tag{6.44}$$

such that the action map

$$G \times M \longrightarrow M \tag{6.45}$$

is smooth.

Define the map $L_G \to \mathrm{Diff}(G)$, $g \mapsto L_g$ by $L_g(g') = gg'$. Then L_g is a homomorphism for each $g \in G$ and represents the usual action of G on itself. Let now $\mathbf{X}$ be a vector field on a Lie group G, i.e. on the underlying manifold. $\mathbf{X}$ is *left invariant* if

$$(dL_g)(\mathbf{X}(x)) = \mathbf{X}(L_g(x)) = \mathbf{X}(gx) \tag{6.46}$$

for each $x, g \in G$.

Left invariance means that the vector field is left invariant under the derivative of the group action, which means that the vector field is completely determined by the vector at the unit element of the Lie group. The main difference of the definition of a Lie group action compared to the definition 23 of a group action is that the Lie group action is defined for (Lie) groups on smooth manifolds.

Here, we will give some examples of matrix Lie groups that are often applied in different fields, especially in physics. In chapter 7, we will introduce the Vortex-Heisenberg matrix Lie group.

Example 4. O(n) and SO(n)
The orthogonal group O(n) and the special orthogonal group SO(n) with determinant equal to ± 1, which is a subgroup of the orthogonal group O(n).

Example 5. Symplectic group
Let $B[\mathbf{x}, \mathbf{y}]$ be the skew-symmetric bilinear form on $\mathbb{R}^{2n}$ given by $B[\mathbf{x}, \mathbf{y}] = \sum_{k=1}^{n}(x_k y_{n+k} - x_{n+k} y_k)$. Let $\underline{\mathbf{J}}$ be the $2n \times 2n$ matrix

$$\underline{\mathbf{J}} = \begin{pmatrix} 0 & \underline{\mathbb{1}}_n \\ -\underline{\mathbb{1}}_n & 0 \end{pmatrix}. \tag{6.47}$$

Then for all $\mathbf{x}, \mathbf{y} \in \mathbb{R}^n$ we can write the bilinear form as:

$$B[\mathbf{x}, \mathbf{y}] = \mathbf{x} \cdot \underline{\mathbf{J}}\mathbf{y}. \tag{6.48}$$

And the symplectic group is given by:

$$Sp(2n, \mathbb{K}) = \{\underline{\mathbf{M}} \in \mathrm{GL}(2n, \mathbb{K}) \mid \underline{\mathbf{M}}^T \underline{\mathbf{J}}\underline{\mathbf{M}} = \underline{\mathbf{J}}\} \tag{6.49}$$

We remark that $Sp(n, \mathbb{R})$ is a subgroup of $\mathrm{GL}(2n, \mathbb{R})$ and a matrix Lie group.

A classical physical application of symplectic geometry is given by Hamilton's equations of motion. Consider a single particle moving in the two-dimensional real space. The state of the system is given by the two position coordinates (q_1, q_2) and the momentum (p_1, p_2), which build the 4-dimensional phase space. The so-called Hamiltonian H provides the time evolution of this system. The Hamiltonian for one particle of mass m in a potential $V(q_1, q_2)$ is given by:

$$H = \frac{1}{2m}(p_1^2 + p_2^2) + V(q_1, q_2) \tag{6.50}$$

satisfying Hamilton's equations:

$$\frac{dp_i}{dt} = -\frac{\partial H}{\partial q_i}, \quad \frac{dq_i}{dt} = \frac{\partial H}{\partial p_i}, \quad i = 1, 2. \tag{6.51}$$

and describing the time evolution of one state of the system. It can be extended to any $2n$-dimensional phase space $\mathbb{R}^{2n}$. In (2.20) we have already

written the Hamilton equations with respect to the two-dimensional skew-symmetric tensor $\underline{\mathbf{J}}$:

$$\begin{pmatrix} \frac{d\mathbf{p}}{dt} \\ \frac{d\mathbf{q}}{dt} \end{pmatrix} = \begin{pmatrix} 0 & \underline{\mathbb{1}}_n \\ -\underline{\mathbb{1}}_n & 0 \end{pmatrix} \cdot \begin{pmatrix} \frac{\partial H}{\partial \mathbf{p}} \\ \frac{\partial H}{\partial \mathbf{p}} \end{pmatrix}. \tag{6.52}$$

Example 6. (Special) unitary group
The set of unitary matrices:

$$U(2,\mathbb{C}) \equiv U(2) = \{\underline{\mathbf{U}} \in GL(2,\mathbb{C}) |\ \underline{\mathbf{U}}^\dagger \underline{\mathbf{U}} = \underline{\mathbb{I}}\} \tag{6.53}$$

and the special unitary group:

$$SU(2) = \{\underline{\mathbf{U}} = \begin{pmatrix} a & b \\ -\bar{b} & \bar{a} \end{pmatrix} |\ a, b \in \mathbb{C},\ a\bar{a} + b\bar{b} = 1\} \tag{6.54}$$

are further examples of Lie groups. Here, the overline denotes complex conjugation. Moreover, $SU(2)$ is a normal subgroup of $U(2)$ and $SU(2)$ can be identified with S^3. The center of $SU(2)$ is $Z = \{1, -1\}$ and the factor group $SU(2)/Z$ is isomophic to the group of rotations $SO(3)$ in three dimensions.

6.2.2 Lie algebra

The tangent space to a linear Lie group G at the identity[3], that we denote with $\mathfrak{g} = T_eG$, has special properties. It is equipped with a multiplication operation – the Lie bracket – such that $\mathfrak{g}$ can be defined as a Lie algebra. Because Lie algebras are linear spaces, they can be easier applied to many problems than Lie groups.

„The miracle of Lie theory is that a curved object, a Lie group G, can be almost completely captured by a flat one, the Tangent space T_eG of G at the identity.“ (Stillwell, 2008):

We start with the definition of an algebra

Definition 27. Algebra
An algebra A (also called algebraic structure) over a field is a $\mathbb{K}$-vector field with a K-linear operation $(A, *)$: $A \times A \to A$. Let $x, y, z \in A,\ \lambda \in K$:

[3] A closed subgroup $G \subseteq GL(n;\mathbb{K})$ is called linear group.

1. $(x + y) * z = x * z + y * z$
2. $x * (y + z) = x * y + y * z$
3. $\lambda\,(x * y) = (\lambda x) * y = x * (\lambda y)$

We notice that an algebra does not need to be associative. Moreover, an algebra is called *unitary*, if the identity element of the corresponding group is also the identity element of the algebra.

Definition 28. Lie Algebra
A *Lie Algebra* is a vector space g over some field F together with a binary operation $[\cdot, \cdot] :\ g \times g \to g$ called the *Lie bracket*. For $\forall a, b \in F.\ \forall x, y, z \in g$ the Lie bracket satisfies the following axioms:

1. $[ax + by, z] = a[x, z] + b[y, z], \quad [z, ax + by] = a[z, x] + b[z, y]$ (bilinearity)
2. $[x, x] = 0$
3. $[x, [y, z]] + [z, [x, y]] + [y, [z, x]] = 0$ (Jacobi identity)

A *sub Lie algebra* $\mathfrak{h}$ of a Lie algebra $\mathfrak{g}$ is a subvector space $\mathfrak{h} \subseteq \mathfrak{g}$ that is closed with respect to the Lie bracket. I.e. for all $X, Y \in \mathfrak{h}$ it is $[X, Y] \in \mathfrak{h}$.

The Lie algebra $\mathfrak{g}$ of a matrix Lie group G is just the tangent space of G at the identity. Furthermore, the exponential map as it is defined in the matrix case coincides with the exponential map for general Lie groups (see e.g. Hall, 2003). Let now $\mathbf{X}_1, \ldots, \mathbf{X}_n$ a basis of a n-dimensional vector space $\mathfrak{g}$ with $[\mathbf{X}_i, \mathbf{X}_j] = f_{ij}^k \mathbf{X}_k$. Then f_{ij}^k are called *structure constants*, where the Einstein summation convention is used.

Definition 29. Abelian Lie-Algebra
A Lie algebra $\mathfrak{g}$ is called abelian if $[\mathbf{X}, \mathbf{Y}] = 0$ for all $\mathbf{X}, \mathbf{Y}$ in $\mathfrak{g}$.

We notice that abelian Lie algebras are related to abelian connected Lie groups. They are n-dimensional vector spaces with the trivial Lie brackets.

Definition 30. Ideal
A Lie subalgebra $\mathcal{I} \subset \mathfrak{g}$ is called invariant Lie-subalgebra or ideal of $\mathfrak{g}$ if

$$[\mathcal{I}, \mathfrak{g}] \subseteq \mathcal{I} \tag{6.55}$$

We remark that a normal subgroup of the Lie group is analogously to an ideal of a Lie algebra (see e.g. Kühnel, 2011).

Definition 31. Center
The center of a lie algebra $\mathfrak{g}$ is the set of elements Z that commutes with all elements of the Lie algebra, i.e.

$$\mathfrak{z} := \{Z \in \mathfrak{g} |\ [Z, \mathfrak{g}] = 0\} \tag{6.56}$$

Thus, the center is an ideal of $\mathfrak{g}$.

Definition 32. Centralizer
The *centralizer* of a subset $m \subset \mathfrak{g}$ is the set of elements of $\mathfrak{g}$ with

$$\mathfrak{z}_g(m) : \{\mathbf{X} \in \mathfrak{g} |\ [\mathbf{X}, m] = 0\} \tag{6.57}$$

This set is a linear space and it is closed with respect to the Lie-product. The centralizer of m contains all elements that commute (only) with m. Whereas the center contains all elements commuting with $\mathfrak{g}$. Therefore, it is easy to proof that

$$\mathfrak{z} = \bigcap_{m \in \mathfrak{g}} \mathfrak{z}_{\mathfrak{g}}(m), \tag{6.58}$$

where $\bigcap$ denotes the intersection. The centralizer is defined for all elements and therefore, the centralizer of the whole Lie algebra $\mathfrak{z}_{\mathfrak{g}}(\mathfrak{g})$ is the center of the Lie algebra.

Definition 33. Lower central series, nilpotent Lie-Algebra
Let $\mathfrak{g}$ be a Lie algebra. The *lower central series* of $\mathfrak{g}$ is defined recursively as $\mathfrak{g} = \mathfrak{g}^1$ and $\mathfrak{g}^n = [\mathfrak{g}, \mathfrak{g}^{n-1}]$. The Lie algebra $\mathfrak{g}^n$ is called *nilpotent* if the lower central series vanishes. The smallest value of $m \in \mathbb{N}$ for which $\mathfrak{g}^{m+1} = 0$ is called *degree of nilpotency*.

We will introduce the vortex-Heisenberg Lie algebra in chapter 8 which is an example of a nilpotent Lie algebra. This characterization simplifies the transition of a Lie group to a Lie algebra and it also allows for finding vortex geodesics by applying sub-Riemannian geometry.

Definition 34. Derived series, solvable Lie Algebra
Let $\mathfrak{g}$ be a Lie algebra. The recursively defined series $\mathfrak{g} = \mathfrak{g}^{(1)}$ and $\mathfrak{g}^{(n)} = [\mathfrak{g}^{(n-1)}, \mathfrak{g}^{(n-1)}]$ is called *derived series* of $\mathfrak{g}$

The Lie algebra $\mathfrak{g}$ is called solvable if the derived series terminates, i.e. if there exists a $m \in \mathbb{N}$ such that $\mathfrak{g}^{(m)} = 0$

We notice that every finite-dimensional Lie algebra has a unique maximal solvable ideal, the so-called radical and any finite-dimensional real Lie algebra can be decomposed into the semidirect product of a solvable ideal and a semisimple subalgebra. This decomposition is called Levi decomposition. It follows that any finite-dimensional Lie algebra is a semidirect product of a solvable Lie algebra and a semisimple Lie algebra. We also remark that every nilpotent (solvable) Lie group can be related to a nilpotent (solvable) Lie algebra (see, e.g. Hall, 2003).

Let us assume that we are looking for a representation of a group G on a vector space and let this vector space be the tangent vector space at the identity T_eG. It is the Lie algebra of the group and the representation is called adjoint representation. The elements of the Lie algebra act on a space as linear transformation represented by the adjoint representation. The linearization results from taking the differential of the action of a Lie group G. There is an invariant bilinear form on the Lie algebra that comes with the adjoint representation. It is the so-called „Killing form“, named after the mathematician Wilhelm Killing (1847-1823). Especially for nilpotent Lie groups and Lie algebra this concept leads to a simple transition from the Lie algebra to the associated Lie group as we will show in terms of the Vortex-Heisenberg-Lie algebra in chapter 8.

Definition 35. Adjoint representation of a Lie group
Let G be a matrix Lie group with Lie algebra $\mathfrak{g}$. For each $A \in G$ the adjoint mapping is a linear map defined by

$$Ad_A : G \longrightarrow \mathrm{GL}(\mathfrak{g}) \tag{6.59}$$

with

$$Ad_A(X) = AXA^{-1}. \tag{6.60}$$

The map $A \to Ad_A$ is a Lie group homomorphism from the group G into the group of invertible operators GL($\mathfrak{g}$) (see e.g. Hall, 2003). Moreover, the adjoint mapping Ad is a representation of the group G that acts on the space $\mathfrak{g}$. That is the reason, why Ad is called *adjoint representation* of G. It is a real representation of the Lie group G.

Definition 36. Adjoint representation of a Lie algebra
Furthermore, if $\mathfrak{g}$ is a Lie Algebra, the map

$$ad : \mathfrak{g} \longrightarrow gl(\mathfrak{g}) \tag{6.61}$$

given by

$$ad_{\mathbf{X}}(\mathbf{Y}) = [\mathbf{X}, \mathbf{Y}] \tag{6.62}$$

is a Lie algebra homomorphism that is a representation of $\mathfrak{g}$. It is also called *adjoint representation*. Here, $\mathfrak{g}$ is the Lie algebra of some matrix Lie group G and $gl(\mathfrak{g})$ denotes the general linear Lie algebra of the general linear group.

Both representations, Ad and ad are related by $\exp(ad_x) = Ad_e x$. For further details, also on the following definitions, see e.g. Hall (2003).

Theorem 1. Engel's theorem
Let $\mathfrak{g}$ be a finite-dimensional complex Lie-Algebra. Then the following statements are equivalent:

1. The Lie algebra $\mathfrak{g}$ is nilpotent.
2. For all $\mathbf{X} \in \mathfrak{g}$ the map $\mathrm{ad}_X : \mathfrak{g} \to \mathfrak{g}$ with $\mathrm{ad}_X(Y) = [X, Y]$ is a nilpotent linear map.

Definition 37. Exponential map
Let G be a Lie group and $\mathfrak{g}$ be its Lie algebra. The exponential map is the map

$$\exp\colon \mathfrak{g} \to G.$$

Further, let G be a matrix Lie group and let $\underline{\mathbf{X}}$ be a $n \times n$ real or complex matrix. Then the exponential map coincides with the matrix exponential. It is defined by the Taylor series:

$$\exp(\underline{\mathbf{X}}) = \sum_{k=0}^{\infty} \frac{\underline{\mathbf{X}}^k}{k!} = \mathbb{E} + \underline{\mathbf{X}} + \frac{1}{2}\underline{\mathbf{X}}^2 + \frac{1}{6}\underline{\mathbf{X}}^3 + \cdots \tag{6.63}$$

with the identity matrix $\mathbb{E}$.

Let us consider a matrix $\underline{\mathbf{M}}$ as representative of a nilpotent algebra (6.63), where $\underline{\mathbf{M}}^2$ is a matrix that entries are all zeroes leading to a simplified exponential map and thus, to a simplified transition from the Lie group to the Lie algebra. We will apply the so-called Baker-Campbell-Hausdorff-formula based on the exponential map to derive the group operation of the Vortex-Heisenberg group.

Theorem 2. Baker-Campbell-Hausdorff-formula
Suppose $\underline{\mathbf{X}}$ and $\underline{\mathbf{Y}}$ are finite dimensional complex or real $n \times n$ matrices, then

$$e^{\underline{\mathbf{X}}} e^{\underline{\mathbf{Y}}} = e^{\underline{\mathbf{X}} + \underline{\mathbf{Y}} + \frac{1}{2}[\underline{\mathbf{X}}, \underline{\mathbf{Y}}] + \frac{1}{12}[\underline{\mathbf{X}}, [\underline{\mathbf{X}}, \underline{\mathbf{Y}}]] - \frac{1}{12}[\underline{\mathbf{Y}}, [\underline{\mathbf{X}}, \underline{\mathbf{Y}}]] + \cdots}. \tag{6.64}$$

Moreover if $\underline{\mathbf{X}}$ and $\underline{\mathbf{Y}}$ commute with their commutator, i.e.

$$[\underline{\mathbf{X}}, [\underline{\mathbf{X}}, \underline{\mathbf{Y}}]] = [\underline{\mathbf{Y}}, [\underline{\mathbf{X}}, \underline{\mathbf{Y}}]] \tag{6.65}$$

the last equation simplifies to:

$$e^{\underline{\mathbf{X}}} e^{\underline{\mathbf{Y}}} = e^{\underline{\mathbf{X}} + \underline{\mathbf{Y}} + \frac{1}{2}[\underline{\mathbf{X}}, \underline{\mathbf{Y}}]}. \tag{6.66}$$

The proof is for example given in Hall (2003). Regarding the matrix representation of groups, the group operation is given by the usual matrix product. Last formula (6.66) leads to the group operation, which can be expressed using the matrix representation for two matrices $\underline{\mathbf{X}}$ and $\underline{\mathbf{Y}}$ and the usual matrix product:

$$\text{The matrix group operation} \quad \underline{\mathbf{X}} \cdot \underline{\mathbf{Y}} \ \text{ is given by } \quad \underline{\mathbf{X}} + \underline{\mathbf{Y}} + \frac{1}{2}[\underline{\mathbf{X}}, \underline{\mathbf{Y}}] \tag{6.67}$$

Here, the first sum on the right hand side in (6.67) results from the exponential map, because the product of two exponential maps is given by a sum of the exponents.

We note that Lie algebras are usually non-associative (except if the commutator always vanishes) (Knapp, 2006). Embedding a Lie algebra $\mathfrak{g}$ into an associative algebra $\mathfrak{a}$ leads to the definition of the universal enveloping.

Definition 38. Universal enveloping
Let $\mathfrak{g}$ be an arbitrary Lie algebra over the field $\mathbb{K}$. An universal enveloping algebra of $\mathfrak{g}$ (or simply enveloping algebra of $\mathfrak{g}$) is a pair $(U(\mathfrak{g}), \varepsilon)$ where $U(\mathfrak{g})$ is an associative, unital $\mathbb{K}$-algebra[4] and $\varepsilon : \mathfrak{g} \to \mathrm{Lie}(U(\mathfrak{g}))$ a homomorphism of Lie algebras such that the following universal property holds: for any associative unital $\mathbb{K}$-algebra $\mathfrak{a}$ and any homomorphism of Lie algebras $\varphi : \mathfrak{g} \to \mathrm{Lie}(\mathfrak{a})$, there exists a unique homomorphism $\tilde{\varphi} : U(\mathfrak{g}) \to \mathfrak{a}$ of *associative* algebras such that $\varphi = \tilde{\varphi} \circ \varepsilon$ (Gobet, 2017) as it is summarized in the diagram below:

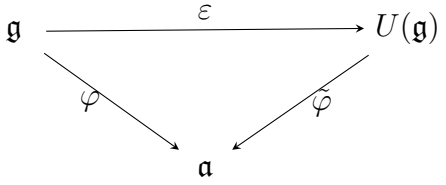

[4] An algebra is called unital or unitary if it has a unit or identity element for all elements in the algebra.

A universal enveloping algebra is unique up to a unique isomorphism.

Definition 39. Casimir elements
The Casimir elements of a Lie algebra are the elements of the center of its enveloping algebra.

Casimir elements play a crucial role in theoretical physics as well as in mathematics. Being elements of the center of the enveloping Lie algebra means that they commute with every element in the Lie algebra which makes them to distinguished elements. Concerning vortex dynamics, we will see that Casimir elements play a role that is comparable to the role of the energy (cf. chapter 7).

6.3 Summary

In this chapter, we have repeated the necessary definitions and properties of groups, Lie groups and Lie algebras such that we can derive Lie groups and a Lie algebras based on Helmholtz' vorticity equation. We close this chapter by summarizing the main differences between the main definitions of Lie groups and Lie algebras in table 6.1 and 6.2:

Lie group (G)	**Lie algebra** ($\mathfrak{g}$)
Commutator subgroup (see (6.23)) $\{[a,b] = a*b*a^{-1}*b^{-1},\ a,b \in G\}$	Lie bracket (see Def. 28) $[\mathcal{A},\mathcal{B}] = \mathcal{AB} - \mathcal{BA}$
Center (see (6.19)) $Z = \{z \in G \mid z*g = g*z\ \forall g \in G\}$	Center (see (6.56)) $\mathfrak{z} = \{\mathbf{z} \in \mathfrak{g} \mid [\mathbf{z},\mathfrak{g}] = 0\}$
Centralizer (see (6.20)) $Z(g) = \{z \in G \mid z*g = g*z\}$	Centralizer (see (6.57)) $\mathfrak{z}(m) = \{\mathbf{X} \in \mathfrak{g} \mid [\mathbf{X}, m] = 0\}$
Normal subgroup $N \subset G$ (see (6.22)) $\{g*N*g^{-1} = N \quad \forall g \in G\}$	Ideal $\mathcal{I}$ (see (6.55)) $[\mathcal{I},\mathfrak{g}] \subseteq \mathcal{I}$

Table 6.1: Main definition for Lie groups and Lie algebras.

We note that there is no analogous concept of the ideals for Lie groups. Regarding Lie groups, the concept of ideals can be compared to normal subgroups. There are ideals for rings:

Ring (R)	**Algebra** ($\mathfrak{a}$)
Ideal I (w.r.t. rings R, see Def. 9) $a * b \in I,\ b * a \in I,\ \forall a \in I,\ b \in R$	Ideal $\mathcal{I}$ (see (6.55)) $\mathcal{I} \cdot \mathfrak{a} \subseteq \mathcal{I}$ and $\mathfrak{a} \cdot \mathcal{I} \subseteq \mathcal{I}$

Table 6.2: Comparison of the definition of an ideal for a ring and an algebra.

Chapter 7

Continuous Nambu mechanics

In the beginning of this chapter, we will follow Névir and Blender (1993) and derive the Nambu representation of the 2D and 3D vorticity equations. At the end of this chapter, we will summarize the bracket relations of all related conserved quantities after Névir (1998). These brackets form a Lie algebra that is based on the Helmholtz vorticity equation. In chapter 8 we will start at this Lie algebra for vortex dynamics and derive a Lie group for vortex dynamics. In chapter 9 we will use this group operation to represent splitting storms in terms of the helicity field. In this way, we can propose conditions for a helicity cascade for special initial conditions. Finally, in chapter 10 we will use this Lie algebra from this chapter to search for shortest paths of vortices.

7.1 Nambu formulation of 2D vortex dynamics

The 2D-equation of motion for incompressible inviscid fluids in an inertial system is given by

$$\frac{d\mathbf{v}_h}{dt} = -\frac{1}{\rho_0}\nabla_h p \tag{7.1}$$

with the horizontal velocity $\mathbf{v}_h$, constant density ρ_0 of the fluid and pressure p. The continuity equation is given by the condition of incompressibility:

$$\nabla_h \cdot \mathbf{v}_h = 0. \tag{7.2}$$

To reformulate (7.1) we first use Euler's decomposition for the material derivative:

$$\frac{d\mathbf{v}_h}{dt} = \frac{\partial \mathbf{v}_h}{\partial t} + \mathbf{v}_h \cdot \nabla_h \mathbf{v}_h, \tag{7.3}$$

where the advection can be written as:

$$\mathbf{v}_h \cdot \nabla_h \mathbf{v}_h = \nabla_h \frac{1}{2}\mathbf{v}_h^2 + \zeta\ \mathbf{k} \times \mathbf{v}_h. \tag{7.4}$$

Using (7.3) and (7.4), the equation for incompressible inviscid flows reads as:

$$\frac{\partial \mathbf{v}_h}{\partial t} + \zeta\ \mathbf{k} \times \mathbf{v}_h = -\nabla_h \left(\frac{p}{\rho_0} + \frac{1}{2}\mathbf{v}_h^2, \right) \tag{7.5}$$

where $\zeta = \mathbf{k} \cdot \nabla \times \mathbf{v}$ denotes the vorticity. Thus, multiplying the last equation by the cross product $\mathbf{k} \cdot \nabla_h \times$ leads to the vorticity equation that can be formulated as Lagrangian conservation of the vorticity:

$$\frac{\partial \zeta}{\partial t} + \mathbf{v}_h \cdot \nabla_h \zeta = 0 \quad \longleftrightarrow \quad \frac{\mathrm{d}\zeta}{\mathrm{d}t} = 0. \tag{7.6}$$

Note that the 2D vorticity equation for incompressible and inviscid flows states that local vorticity changes are only dedicated to redistributions of vorticity, i.e. advection. Using the condition of a solenoidal vector field, a stream function $\psi(x, y)$ can be defined

$$\boldsymbol{\nabla_h} \cdot \mathbf{v}_h = 0 \quad \longleftrightarrow \quad \mathbf{v}_h = \mathbf{k} \times \nabla_h \psi(x, y). \tag{7.7}$$

Then, the vorticity ζ can also be expressed via the stream function:

$$\zeta = \mathbf{k} \cdot \nabla_h \times \mathbf{v}_h = \Delta_h \psi, \tag{7.8}$$

where $\mathbf{k}$ denotes the unit-vector $(0, 0, 1)$. Now, we can write the horizontal advection of the vorticity in terms of the Jacobi-operator $J(\psi, \zeta)$ of the stream function and the vorticity:

$$(\mathbf{k} \times \nabla_h \psi) \cdot \nabla_h \zeta = J(\psi, \zeta) = \frac{\partial \psi}{\partial x}\frac{\partial \zeta}{\partial y} - \frac{\partial \psi}{\partial y}\frac{\partial \zeta}{\partial x} \tag{7.9}$$

We notice the Jacobian-operator of this nonlinear advection term is anti-symmetric. With the last equations, we can write the 2D incompressible inviscid vorticity equation as:

$$\boxed{\frac{\partial \zeta}{\partial t} = -J(\psi, \zeta)} \tag{7.10}$$

In incompressible, two-dimensional fluids there are two global conserved quantities that are constitutive for the time evolution of fluids, the kinetic

energy $\mathcal{H}$ and the enstrophy $\mathcal{E}$:

$$\begin{aligned} \mathcal{H} &= \frac{1}{2}\int_F df\ \mathbf{v}_h \quad \text{(Kinetic energy)} \\ \mathcal{E} &= \frac{1}{2}\int_F df\ \zeta^2 \quad \text{(Enstrophy)} \end{aligned} \tag{7.11}$$

The functional derivative of the energy and enstrophy with respect to the vorticity are given by

$$\frac{\delta\mathcal{H}}{\delta\zeta} = -\psi, \quad \frac{\delta\mathcal{E}}{\delta\zeta} = \zeta. \tag{7.12}$$

See Névir (1998) for the derivation of the functional derivatives. Using the functional derivative of the energy, a non-canonical Hamilton representation of the vorticity equation can be found. First, we define the operator $D(\zeta)$ as

$$D(\zeta) = -J(\zeta, \dot{}) = -\left(\frac{\partial\zeta}{\partial x}\frac{\partial}{\partial y} - \frac{\partial\zeta}{\partial y}\frac{\partial}{\partial x}\right). \tag{7.13}$$

Then, we can write the vorticity equation as follows:

$$\frac{\partial\zeta}{\partial t} = D(\zeta)\frac{\delta\mathcal{H}}{\delta\zeta} =: \{\zeta, \mathcal{H}\}. \tag{7.14}$$

We note that the operator $D(\zeta)$ is singular. There is an infinite number of Casimirs $\mathcal{C}$ that depend on the vorticity ζ. And, using the above representation the time evolution reads:

$$\frac{\partial\mathcal{C}}{\partial t} = D(\zeta)\frac{\delta\mathcal{C}[\zeta]}{\delta\zeta} = -J\left(\zeta, \frac{\delta\mathcal{C}[\zeta]}{\delta\zeta}\right) = 0. \tag{7.15}$$

Therefore, the Casimirs $\mathcal{C}[\zeta]$ are conserved. [1]

7.1.1 Casimir functionals

Casimir functionals are global conserved quantities. Regarding two-dimensional fluid dynamics, they can be expressed by surface integrals. In this context they are functionals $\phi(\zeta)$ depending on the vorticity. Let F denote a surface. Then, the Casimir functionals are given by:

$$\mathcal{C}_\phi[\zeta] = \int_F df\ \phi(\zeta), \quad \text{with} \quad \frac{\delta\mathcal{C}}{\delta\zeta} = \frac{d\phi(\zeta)}{d\zeta} = \phi'(\zeta), \tag{7.16}$$

[1] We remark that functional derivatives or variational derivatives can be seen as generalized gradients of functions.

where $\phi'(\zeta)$ denotes the derivative with respect to the vorticity. We obtain

$$J\left(\zeta, \frac{\delta\phi}{\delta\zeta}\right) = \frac{\partial\zeta}{\partial x}\frac{\partial\phi'(\zeta)}{\partial y} - \frac{\partial\zeta}{\partial y}\frac{\partial\phi'(\zeta)}{\partial x} = \phi''(\zeta)\left(\frac{\partial\zeta}{\partial x}\frac{\partial\zeta}{\partial y} - \frac{\partial\zeta}{\partial y}\frac{\partial\zeta}{\partial x}\right) = 0 \quad (7.17)$$

Using $\phi = \zeta$ (7.16) provides the definition of the circulation and for $\phi = \frac{1}{2}\zeta^2$ we obtain the enstrophy. However, we can raise ζ to any higher power $n \in \mathbb{N}$ to derive further Casimir functionals:

$$\begin{aligned}
\mathcal{C}_{\phi=\zeta} &= \mathcal{Z} = \int_F df\ \zeta && \text{(Circulation)} \\
\mathcal{C}_{\phi=\frac{1}{2}\zeta^2} &= \mathcal{E} = \frac{1}{2}\int_F df\ \zeta^2 && \text{(Enstrophy)} \\
\mathcal{C}_{\phi=\frac{1}{n}\zeta^n} &= \frac{1}{n}\int_F df\ \zeta^n && \text{(Further Casimir functionals)} \\
\mathcal{C}_{\phi(\zeta)} &= \int_F df\ \phi(\zeta) && \text{(General Casimir functionals)}
\end{aligned} \quad (7.18)$$

(see Névir, 1998). The circulation and the enstrophy are the most known and most important Casimir functions of the vorticity equation. Casimir functionals are distinctive functionals, because they commute with every functional of the bracket:

$$\{\mathcal{F}, \mathcal{C}_\phi\} = -\int_F df \frac{\delta\mathcal{F}}{\delta\zeta} J\left(\zeta, \frac{\delta\mathcal{C}_\phi}{\delta\zeta}\right) = 0 \quad (7.19)$$

Thus, they also commute with the energy and therefore, they are conserved quantities.

We show, why the above Casimir functionals (7.18) commute with every functional of the vorticity. First, we use the Lagrangian conservation of the vorticity (7.20):

$$\frac{d\zeta}{dt} = 0 \quad \Longrightarrow \quad \frac{d\phi(\zeta)}{dt} = \frac{d\phi}{d\zeta}\frac{d\zeta}{dt} = \phi'\frac{d\zeta}{dt} = 0 \quad (7.20)$$

Then, we apply Euler's decomposition (7.3) and include the horizontal solenoidal condition $\nabla_h \cdot \mathbf{v}_h = 0$, we obtain the local conservation law of the vorticity-Casimir functionals:

$$\frac{\partial\phi(\zeta)}{\partial t} + \nabla_h \cdot (\mathbf{v}_h\phi(\zeta)) = 0 \quad (7.21)$$

Integrating the last equation about a closed surface leads to the conserva-

tion of the vorticity-Casimir functionals:

$$\boxed{\frac{\partial \mathcal{C}_\phi}{\partial t} = \frac{\partial}{\partial t} \int_F df\ \phi(\zeta) = 0} \tag{7.22}$$

as stated above.

Now, we would like to formulate the vorticity equation in terms of the Nambu formalism with respect to a Casimir functional. Thus we insert the Casimir functional of the enstrophy in the non-canonical representation leading to the Nambu formulation of the vorticity equation:

$$\boxed{\frac{\partial \zeta}{\partial t} = -J\left(\frac{\delta \mathcal{E}}{\delta \zeta}, \frac{\delta \mathcal{H}}{\delta \zeta}\right)} \tag{7.23}$$

In contrast to Hamiltonian dynamics Nambu's formulation for two-dimensional incompressible fluid dynamics is based on two conserved quantities that characterize 2D turbulence – energy and enstrophy – that have equal status. Analogously to discrete Nambu mechancis, a Nambu bracket can be defined. Consider a functional with respect to the vorticity $\mathcal{F} : \mathbb{R}^n \to \mathbb{R}^n$. Then, the time evolution of the functional $\mathcal{F}[\zeta]$ can be formulated as:

$$\frac{\partial \mathcal{F}[\zeta]}{\partial t} = \int_F df\ \frac{\delta \mathcal{F}}{\delta \zeta}\frac{\partial \zeta}{\partial t} = -\int_F df\ \frac{\delta \mathcal{F}}{\delta \zeta} J\left(\frac{\delta \mathcal{E}}{\delta \zeta}, \frac{\delta \mathcal{H}}{\delta \zeta}\right) \tag{7.24}$$

We summarize: For two-dimensional incompressible, inviscid fluids, the time evolution of a function $\mathcal{F} : \mathbb{R}^n \to \mathbb{R}^n$ is given by the trilinear Nambu bracket, introduced by Névir and Blender (1993):

$$\boxed{\{\mathcal{F}, \mathcal{E}, \mathcal{H}\} := -\int_F df\ \frac{\delta \mathcal{F}}{\delta \zeta} J\left(\frac{\delta \mathcal{E}}{\delta \zeta}, \frac{\delta \mathcal{H}}{\delta \zeta}\right)} \tag{7.25}$$

The Nambu bracket (7.25) is antisymmetric and the calculating the Nambu bracket of three conserved quantities results in a conserved quantity, too (see Névir, 1998).

Inserting the vorticity in the above defined bracket, we obtain the Nambu formulation of the vorticity equation:

$$\boxed{\frac{\partial \zeta}{\partial t} = \{\zeta, \mathcal{E}, \mathcal{H}\}} \tag{7.26}$$

We notice that the time evolution of the vorticity depends as well on the

energy as on the enstrophy. We can also express an arbitrary function $\mathcal{F}[\zeta]$ in terms of these two conserved quantities:

$$\boxed{\frac{\partial \mathcal{F}[\zeta]}{\partial t} = \{\mathcal{F}, \mathcal{E}, \mathcal{H}\}} \tag{7.27}$$

(see Névir, 1998). The Nambu bracket as defined above is trilinear, because the Jacobi-Operator as well as the functional derivative are (multi-)linear Moreover, the Jacobi-operator is anti-symmetric. Therefore, the Nambu-bracket is antisymmetric in all three arguments. The Nambu bracket satisfies the Jacobi identity when they are reduced to a Poisson bracket by keeping one argument fixed (cf. Névir and Blender, 1993). In the next section we will derive the Nambu representation of the three-dimensional Helmholtz equation.

7.2 Nambu formulation of 3D vortex dynamics

Regarding Nambu mechanics, a main difference between two- and three dimensional fluid dynamics are the vortex-related conserved quantities. In the last section, we have shown how the conservation of the enstrophy is used to formulate the 2D-vorticity equation. In three dimensions, the 3D vorticity equation will be expressed by the Nambu bracket with respect to the helicity, because the enstrophy is not conserved. Comparing both quantities, the enstrophy is positive definite, whereas the helicity can also be negative. The sign structure of the helicity density field will allow for the investigation of splitting storms in the next chapter.

7.2.1 Equations of motion

The Nambu bracket for three-dimensional vortex dynamics is based on the Euler equation for incompressible flows that is given by

$$\frac{d\mathbf{v}}{dt} = -\frac{1}{\rho_0}\nabla p - \nabla\phi \tag{7.28}$$

with velocity vector $\mathbf{v}$, constant density ρ_0, pressure p and potential of the gravitational force ϕ. For the condition to be incompressible, the second

equation is given by the continuity equation:

$$\nabla \cdot \mathbf{v} = 0. \tag{7.29}$$

Applying Euler's decomposition $\frac{d\mathbf{v}}{dt} = \frac{\partial \mathbf{v}}{\partial t} + \mathbf{v} \cdot \nabla \mathbf{v}$, and dividing the advection term into two expressions $\mathbf{v} \cdot \nabla \mathbf{v} = \nabla \frac{1}{2}\mathbf{v}^2 + \boldsymbol{\xi} \times \mathbf{v}$ with the three-dimensional vorticity vector $\boldsymbol{\xi} = \nabla \times \mathbf{v}$, we can formulate Euler's equation as follows:

$$\frac{\partial \mathbf{v}}{\partial t} + \boldsymbol{\xi} \times \mathbf{v} = -\nabla \left(\frac{p}{p_0} + \frac{1}{2}\mathbf{v}^2 + \phi \right). \tag{7.30}$$

The rotation of last equation $\nabla\times$ (7.30) leads to the well-known three-dimensional Helmholtz vorticity equation:

$$\begin{aligned} \frac{\partial \boldsymbol{\xi}}{\partial t} &= -\nabla \times (\boldsymbol{\xi} \times \mathbf{v}) = -\nabla \cdot [\mathbf{v}\boldsymbol{\xi} - \boldsymbol{\xi}\mathbf{v}] \\ \frac{\partial \boldsymbol{\xi}}{\partial t} &= \underbrace{\boldsymbol{\xi} \cdot \nabla \mathbf{v}}_{\text{Twisting term}} - \underbrace{\mathbf{v} \cdot \nabla \boldsymbol{\xi}}_{\text{Advection term}} \end{aligned} \tag{7.31}$$

The Helmholtz equation form the basis of the Lie algebra and the Lie group, as we will show in the following. For further reading on the vorticity equation see e.g. Lange (2002) or Hantel (2013).

7.2.2 Formulating the Energy and the Helicity in terms of the vorticity vector

The condition of incompressibility allows the definition of a vector potential as solution of the continuity equation (7.29):

$$\nabla \cdot \mathbf{v} = 0 \quad \longrightarrow \quad \mathbf{v} = -\nabla \times \mathbf{A}. \tag{7.32}$$

Which leads to the following formulation of the vorticity vector

$$\boldsymbol{\xi} = \nabla \times \mathbf{v} = -\nabla \times (\nabla \times \mathbf{A}) = -\nabla \cdot [\mathbf{A}\nabla - \nabla \mathbf{A}] = -\nabla (\nabla \cdot \mathbf{A}) + \nabla^2 \mathbf{A}. \tag{7.33}$$

Assuming $\nabla \cdot \mathbf{A} = 0$ we can write the vorticity as Laplace-operator of the vector potential:

$$\boldsymbol{\xi} = \nabla^2 \mathbf{A} = \Delta \mathbf{A}. \tag{7.34}$$

Thus, we can formulate the 3D vorticity equation (7.31)

$$\frac{\partial \boldsymbol{\xi}}{\partial t} = \nabla \times (\boldsymbol{\xi} \times (\nabla \times \mathbf{A})) \tag{7.35}$$

with respect to the vector potential $\mathbf{A}$.

By multiplying the equation of motion (7.30) with the velocity vector $\mathbf{v}$ it can be shown that the kinetic energy is given by the volume integral

$$\boxed{\mathcal{H} = \frac{1}{2}\int_V d\tau\ \mathbf{v}^2 \quad \text{(Energy)}} \tag{7.36}$$

and conserved in incompressible, inviscid three-dimensional flows. Moreover, multiplying the vorticity equation (7.31) with the velocity vector $\mathbf{v}$ and the equation of motion (7.30) with the vorticity vector $\boldsymbol{\xi}$ leads to the conservation of the helicity h_V in incompressible, inviscid three-dimensional flows. The helicity reads as:

$$\boxed{h_V = \frac{1}{2}\int_V d\tau\ \mathbf{v} \cdot \boldsymbol{\xi} \quad \text{(Helicity)}} \tag{7.37}$$

The functional derivatives of these quantities are given by (after Névir, 1998)

$$\frac{\delta \mathcal{H}}{\delta \boldsymbol{\xi}} = -\mathbf{A} \quad \text{and} \quad \frac{\delta h_V}{\delta \boldsymbol{\xi}} = \mathbf{v}. \tag{7.38}$$

(Névir, 1998). The anti-symmetric matrix differential operator with respect to the vorticity vector is given by:

$$\mathbf{D}(\boldsymbol{\xi}) = -\nabla \times [\boldsymbol{\xi} \times [\nabla \times (\ \cdot\ )]]. \tag{7.39}$$

Thus, the non-canonical representation of the 3D vorticity equation (7.31) can be written as

$$\frac{\partial \boldsymbol{\xi}}{\partial t} = \mathbf{D}(\boldsymbol{\xi}) \cdot \frac{\delta \mathcal{H}}{\delta \boldsymbol{\xi}} =: \{\boldsymbol{\xi}, \mathcal{H}\}. \tag{7.40}$$

We recall that a so-called Casimir element or invariant is an distinguished element, because they commute with all other basis elements of a Lie algebra. The Casimir functional of three-dimensional vorticity dynamics is given by the helicity that we defined in (7.37):

$$\mathcal{C}\,[\boldsymbol{\xi}] = \frac{1}{2}\int_V d\tau\ \boldsymbol{\xi} \cdot \mathbf{v} = h_V. \tag{7.41}$$

Moreover, we note that the helicity is the only existing non-trivial Casimir functional. For more detailed calculations see Névir and Blender (1993) or Névir (1998).

7.2.3 The Nambu bracket of 3D vortex dynamics

In this section we will formulate the vorticity equation in terms of the two, equally treated conserved quantities helicity and energy. This is in contrast to classical mechanics, where only one conserved quantity, the energy, determines the time evolution of the system. Therefore we write the vorticity equation formulation (7.40) in terms of the functional derivative of the helicity and the energy:

$$\frac{\partial \boldsymbol{\xi}}{\partial t} = -\nabla \times \left(\left(\nabla \times \frac{\delta h_V}{\delta \boldsymbol{\xi}} \right) \times \left(\nabla \times \frac{\delta \mathcal{H}}{\delta \boldsymbol{\xi}} \right) \right). \tag{7.42}$$

We remark that this representation of the vorticity equation underlines the equal status of the energy and the helicity.

To simplify the notation, we define a constant bilinear and anti-symmetric differential operator $\mathbf{K}$

$$\mathbf{K}(\mathbf{a}, \mathbf{b}) := -\nabla \times ((\nabla \times \mathbf{a}) \times (\nabla \times \mathbf{b})) \tag{7.43}$$

for $\mathbf{a}$ and $\mathbf{b}$ in $\mathbb{R}^3$. Finally, we obtain the continuous Nambu representation of the three-dimensional Helmholtz equation for incompressible, inviscid flows:

$$\frac{\delta \boldsymbol{\xi}}{\delta t} = \mathbf{K} \left(\frac{\partial h_V}{\partial \boldsymbol{\xi}}, \frac{\delta \mathcal{H}}{\delta \boldsymbol{\xi}} \right), \tag{7.44}$$

see Névir and Blender (1993) and Névir (1998). Then, the trilinear Nambu bracket can be defined as:

$$\frac{\partial \mathcal{F}}{\partial t} = \{\mathcal{F}, h_V, \mathcal{H}\} := \int_V d\tau \frac{\delta \mathcal{F}}{\delta \boldsymbol{\xi}} \cdot \frac{\delta \boldsymbol{\xi}}{\delta t} = \int_V d\tau \frac{\delta \mathcal{F}}{\delta \boldsymbol{\xi}} \cdot \mathbf{K} \left(\frac{\delta h_V}{\delta \boldsymbol{\xi}}, \frac{\delta \mathcal{H}}{\delta \boldsymbol{\xi}} \right). \tag{7.45}$$

See Névir and Blender (1993) and Névir (1998) for more details and the proofs of the algebraic properties of the Nambu bracket for fluid dynamics. We notice that h_V and $\mathcal{H}$ denote the helicity and the energy as defined in (7.37) and (7.36), which are conserved for incompressible, inviscid flows. Now, the 3D vorticity equation for incompressible inviscid flows can be

formulated in terms of the Nambu bracket:

$$\boxed{\frac{\partial \boldsymbol{\xi}}{\partial t} = \{\boldsymbol{\xi}, h_V, \mathcal{H}\}.} \tag{7.46}$$

Last representation shows that Helmholtz' vorticity equation also contains the trilinear Nambu structure. Furthermore, the Nambu bracket can be applied to express the time evolution of any functional that depends on the vorticity vector $\mathcal{F}[\boldsymbol{\xi}]$:

$$\frac{\partial \mathcal{F}}{\partial t} = \{\mathcal{F}, h_V, \mathcal{H}\}, . \tag{7.47}$$

where, under the assumption of suitable boundary conditions, the Nambu bracket is given by:

$$\boxed{\{\mathcal{F}, h_V, \mathcal{H}\} = -\int_V d\tau \left(\left(\nabla \times \frac{\delta \mathcal{F}}{\delta \boldsymbol{\xi}} \right) \cdot \left(\nabla \times \frac{\delta h_V}{\delta \boldsymbol{\xi}} \right) \times \left(\nabla \times \frac{\delta \mathcal{H}}{\delta \boldsymbol{\xi}} \right) \right).} \tag{7.48}$$

The Nambu bracket is antisymmetric in all argument, which follows from the triple and cross products in (7.48). It is also multilinear. Moreover, keeping one argument, i.e. h_V fixed, it can be reduced to a Poisson bracket that satisfies the Jacobi identity.

Example 7. Enstrophy's time evolution
The enstrophy is defined by the integration over the squared vorticity vector

$$\mathcal{E} = \mathcal{E}[\boldsymbol{\xi}] = \frac{1}{2}\int_V d\tau\, \boldsymbol{\xi}^2 \quad \text{(Enstrophy)} \tag{7.49}$$

Applying the above defined Nambu bracket (7.48) and using the functional derivatives (7.38) the time evolution of the enstrophy reads as:

$$\frac{\partial}{\partial t}\mathcal{E} = \{\mathcal{E}, h_V, \mathcal{H}\} = \frac{\partial}{\partial t}\left(\frac{1}{2}\int_V d\tau \boldsymbol{\xi}^2\right) = -\int_V d\tau \left[(\nabla \times \boldsymbol{\xi}) \cdot (\boldsymbol{\xi} \times \mathbf{v}) \right]. \tag{7.50}$$

This expression can be further simplified by applying Gauß's theorem. Assuming suitable boundary conditions we obtain a more compact representation of the time evolution of the enstrophy. But the whole integral does not vanish, because the enstrophy is not conserved in three dimensions.

7.3 A Lie algebra for 3D vortex dynamics

In the beginning of this chapter we have summarized how the 2D and 3D vorticity equations for incompressible, inviscid flows can be formulated regarding Nambu mechanics. This leads to the definitions of the Nambu bracket for two- and three-dimensional fluid dynamics. In the second part of this chapter we will discuss a Lie algebra for vortex dynamics based on the Nambu bracket (after Névir, 1998). In chapter 8 we will derive the corresponding Lie group.

To derive the Lie algebra for 3D inviscid, incompressible vortex dynamics we first need to calculate the Nambu bracket of the basic conserved quantities. Therefore, in the first step all quantities should be written in terms of the vorticity vector:

$$\mathcal{H}[\mathbf{v}] \to \mathcal{H}[\boldsymbol{\xi}], \quad \mathbf{P}[\mathbf{v}] \to \mathbf{P}[\boldsymbol{\xi}], \quad \mathbf{L}[\mathbf{v}] \to \mathbf{L}[\boldsymbol{\xi}], \tag{7.51}$$

such that in the second step, all functional derivatives with respect to the vorticity vector can be determined under the assumption of suitable boundary conditions (Névir, 1998). Step one results in the following representation of the conserved quantities for three-dimensional incompressible, inviscid vortex dynamics:

$$\begin{aligned}
\mathcal{H} &= \frac{1}{2}\int_V d\tau\ \mathbf{v}^2 = -\frac{1}{2}\int_V d\tau\ \boldsymbol{\xi}\cdot\mathbf{A} && \text{(kinetic energy)}\\
\mathbf{P} &= \int_V d\tau\ \mathbf{v} = \frac{1}{2}\int_V d\tau\ (\mathbf{r}\times\boldsymbol{\xi}) && \text{(Momentum)}\\
\mathbf{L} &= \int_V d\tau\ (\mathbf{r}\times\mathbf{v}) = -\frac{1}{2}\int_V d\tau\ r^2\boldsymbol{\xi} && \text{(Angular momentum)}\\
h_V &= \frac{1}{2}\int_V d\tau\ \mathbf{v}\cdot\boldsymbol{\xi} && \text{(Helicity)}\\
\mathbf{Z} &= \int_V d\tau\ \boldsymbol{\xi} && \text{(Total flux of vorticity)},
\end{aligned} \tag{7.52}$$

We will follow Majda and Bertozzi (2002) and call Z the *total flux of vorticity*. The functional derivatives of the quantities that determine the Vortex-Heisenberg algebra are given by:

$$\begin{aligned}
\frac{\delta\mathcal{H}[\boldsymbol{\xi}]}{\delta\boldsymbol{\xi}} &= -\mathbf{A} && \text{(Functional derivative of the kinetic energy)}\\
\frac{\delta h_V[\boldsymbol{\xi}]}{\delta\boldsymbol{\xi}} &= \mathbf{v} && \text{(Functional derivative of the helicity)}
\end{aligned} \tag{7.53}$$

and

$$\frac{\delta \mathcal{P}[\boldsymbol{\xi}]}{\delta \boldsymbol{\xi}} = -\frac{1}{2}(\mathbf{r} \times \underline{\mathbf{E}}) \quad \text{(Functional derivative of the momentum)} \tag{7.54}$$

with unit tensor $\underline{\mathbf{E}}$ and local coordinate $\mathbf{r}$. Moreover, in chapter 8, section 8.4 we will extend the vortex Lie algebra generated by the linear momenta by including the angular momentum. But compared to the Vortex-Heisenberg algebra, the novel algebra looses its property of nilpotency. We will call it Helmholtz Vortex algebra, respectively Helmholtz Vortex group, because it does not hold the typical Heisenberg-structure but it is constructed from Helmholtz' vorticity equation. However, to derive Helmholtz Vortex group we also need the functional derivative of the angular momentum given by:

$$\frac{\delta \mathbf{L}[\boldsymbol{\xi}]}{\delta \boldsymbol{\xi}} = -\frac{1}{2} r^2 \underline{\mathbf{E}} \quad \text{(Functional derivative of the angular momentum)} \tag{7.55}$$

Determining the Nambu bracket of the momentum $\mathbf{P} = (P_x, P_y, P_z)$ and the total flux of vorticity $\mathbf{Z} = (Z_x, Z_y, Z_z)$, given in (7.52), with respect to the helicity h_V leads to the following relations:

$$\{P_i, h_V, P_j\} = \varepsilon_{ijk} Z_k, \quad \{Z_i, h_V, Z_j\} = 0, \quad \{Z_i, h_V, P_j\} = 0. \tag{7.56}$$

Moreover, the momentum and the total flux of circulation commute with the energy:

$$\{P_i, h_V, \mathcal{H}\} = 0 \qquad \{\mathcal{H}, h_V, Z_i\} = 0. \tag{7.57}$$

The Nambu bracket of the total flux of vorticity and the momentum with respect to the helicity (7.56) generate a Lie algebra for vortex dynamics. It is multi-linear, antisymmetric and the Jacobi-identity

$$\{Z_i, h_v, \{P_i, h_V, P_j\}\} + \{P_j, h_v, \{Z_i, h_V, P_i\}\} + \{P_i, h_v, \{P_j, h_V, Z_i\}\} = 0 \tag{7.58}$$

is satisfied, because each summand vanishes:

$$\{Z_i, h_v, \{P_i, h_V, P_j\}\} = \{P_j, h_v, \{Z_i, h_V, P_i\}\} = \{P_i, h_v, \{P_j, h_V, Z_i\}\} = 0. \tag{7.59}$$

We also recall that a vector space is a nonempty set with a scalar multiplication and a vector addition. Functions $X \to V$ that satisfy these two properties locally, also form a vector space (Akcoglu et al., 2011). Therefore, all properties of a Lie algebra (28) are satisfied. In the next chapter, we

will first derive a novel matrix representation of this Lie algebra leading to a novel matrix representation of the corresponding Lie group.

Moreover, the Nambu brackets of the components $L_i,\ i = 1, 2, 3$, of the angular momentum $\mathbf{L}$ and the momentum $\mathbf{P}$ with respect to the helicity read as:

$$\begin{aligned} \{L_i, h_V, P_j\} &= \varepsilon_{ijk} P_k, \quad & \{L_i, h_V, L_j\} &= \varepsilon_{ijk} L_k \\ \{L_i, h_V, \mathcal{H}\} &= 0, & \{L_i, h_V, Z_i\} &= 0. \end{aligned} \tag{7.60}$$

For further calculations see Névir (see 1998). This extension of the Lie algebra by the linear momentum (7.60) leads to a novel vortex group. In chapter 9 we will use both vortex groups to explain the split of storms.

For the derivations of the vortex groups for two- and three dimensional incompressible vortex dynamics, we will use different mathematical concepts and tools. But our objective is to transfer these mathematical representations to vortex dynamics and atmospheric processes. Therefore, we will have to give the novel Lie groups and Lie algebras a physical meaning. Thus, we will shortly recall the Biot-Savart law after Adams (2015) and Wu et al. (2007) to adapt this concept to our algebraic approach in the next chapter.

7.3.1 The law of Biot-Savart

In part I chapter 3 (3.1) we have already discussed the circulation, a quantity that is conserved on two-dimensional material surfaces that can be embedded in higher dimensions. We recall that by applying Stoke's theorem we can formulate the circulation with respect to the enclosed domain A or the boundary S:

$$\Gamma(S) = \oint_S \mathbf{v} \cdot \mathbf{ds} = \int_A (\nabla \times \mathbf{v}) \cdot \mathbf{n}\, dA. \tag{7.61}$$

as it is illustrated in fig. 7.1 a). A *vortex line* is defined as an integral curve of the vorticity field $\boldsymbol{\xi} = \nabla \times \mathbf{v}$, i.e.:

$$\frac{d\mathbf{x}_{\boldsymbol{\xi}}}{ds} = \boldsymbol{\xi}(\mathbf{x}(s), t), \quad \mathbf{x}_{\boldsymbol{\xi}}(s = 0) = \mathbf{x}_0 \tag{7.62}$$

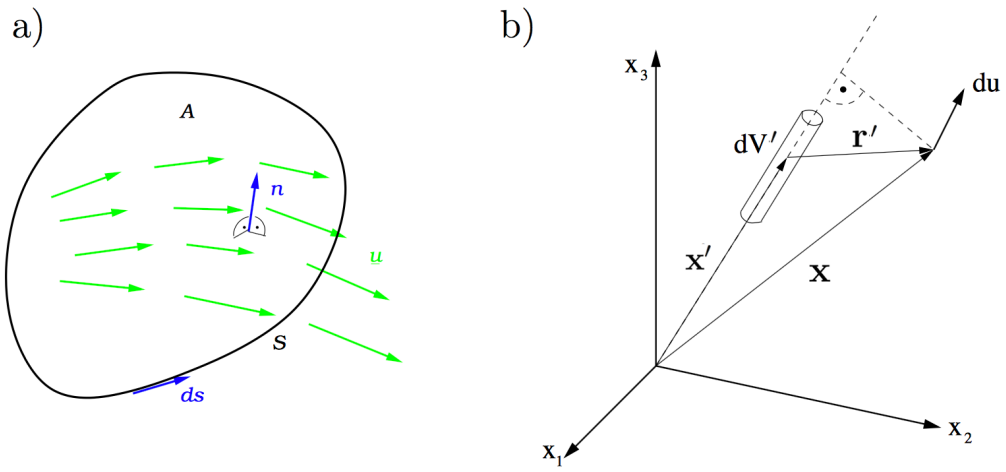

Figure 7.1: a) The quantities that define the circulation Γ are shown. The green arrows denote the velocity field, the vector $\mathbf{n}$ is normal to the surface A und ds denotes an infinitesimal element of the contour S. b) Assuming a straight vortex line with finite length. The vector $\mathbf{x}$ denotes the reference point and $\mathbf{x}'$ a point of the volume V' of the vortex tube. Then, $\mathbf{r}'$ is the vector from $\mathbf{x}'$ to the reference point $\mathbf{x}$. The Biot-Savart law provides the velocity $d\mathbf{u}$ at $\mathbf{x}$ induced at $\mathbf{x}'$ [adapted from Adams (2015)].

It is the line (green line, fig. 7.1 c), or red lines, fig. **??**) that is everywhere tangent to the local vorticity vector satisfying the following relation:

$$\frac{dx}{\xi_x} = \frac{dy}{\xi_y} = \frac{dz}{\xi_z}. \tag{7.63}$$

A *vortex tube* is a surface formed by vortex lines, where the vortex lines are characterized by the circulation Γ. An infinitesimal thin vortex tube can be seen as a vortex line as indicated in fig. 7.1 c,d and **??** .

Helmholtz (1858) stated that any velocity field can be decomposed into the sum of a solenoideal (divergence-free: $\nabla \cdot \mathbf{v}^{\xi} = 0$) and an irrotational (curl-free: $\nabla \times \mathbf{v}^{\phi} = 0$) vector field. It is called Helmholtz' decomposition:

$$\mathbf{v} = \mathbf{v}^{\xi} + \mathbf{v}^{\phi}, \tag{7.64}$$

where the rotational part satisfies the following equation:

$$\Delta \mathbf{v}^{\xi} = -\nabla \times \boldsymbol{\xi}. \tag{7.65}$$

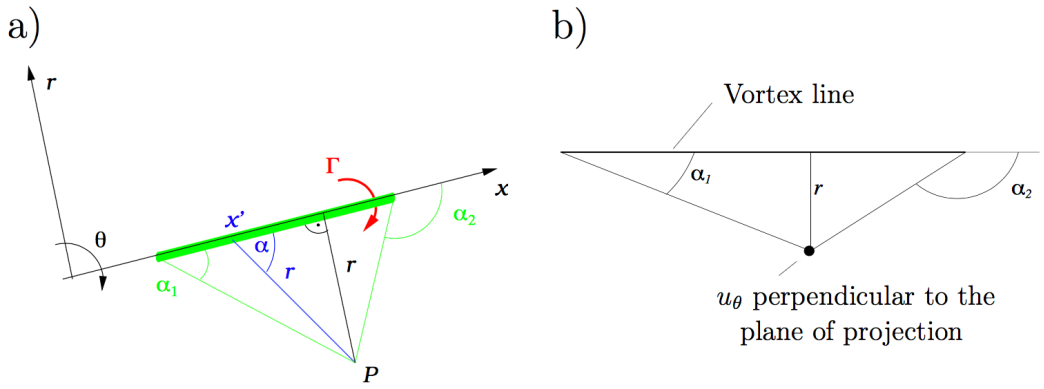

Figure 7.2: a) Considering infinitesimal radius of a vortex tube, we obtain a vortex line (marked in green) characterized by the circulation Γ. $\mathbf{x}'$ is a point on the vortex line, and $\mathbf{r}$ denote distances (blue: blue from $\mathbf{x}'$ to the reference point, black: the vector perpendicular to the vortex line to the reference point), see also fig. 7.1. b) The induced velocity depends on the angles α_1 and α_2 [adapted from Adams (2015)]

The solution of (7.65) is called the law of Biot-Savart. It can derived with respect to the Green function (see e.g. Wu et al., 2007). We obtain:

$$\mathbf{v}^{\xi}(\mathbf{x}) = -\frac{1}{4\pi}\int_{V'}\frac{\mathbf{r}\times\boldsymbol{\xi}'}{|\mathbf{r}|^3}\,dV' \tag{7.66}$$

for an unbounded domain V', under the assumption that $\boldsymbol{\xi} = 0$ everywhere else, $\boldsymbol{\xi}' = \boldsymbol{\xi}(\mathbf{x}')$ and $\mathbf{r} = \mathbf{x} - \mathbf{x}'$, where $\mathbf{x}$ is a fixed reference point and $\mathbf{x}'$ the point of the integration volume V', as illustrated in fig. 7.1 b). Considering a vortex line S' instead of a vortex tube with constant circulation, as illustrated in fig. 7.1 c), equation (7.66) can be reduced to

$$\mathbf{v}(\mathbf{x}) = \frac{\Gamma}{4\pi}\int_{S'}\frac{d\mathbf{s}'\times\mathbf{r}}{|\mathbf{r}|^3} \tag{7.67}$$

(Adams, 2015). In the next step, we consider a straight vortex line segment with finite lengths $r = l\tan(\alpha)$, see fig. 7.1 c) and d). Then, the velocity field with respect to cylindrical coordinates further simplifies to

$$u_\theta = -\frac{\Gamma}{4\pi r}(\cos(\alpha_2) - \cos(\alpha_1)) \tag{7.68}$$

(see fig. 7.1 d)). Thus, for an infinite straight vortex line with $\alpha_1 \to 0$ and $\alpha_2 \to \pi$ we obtain

$$u_\theta = \frac{\Gamma}{2\pi r} \tag{7.69}$$

We note that point vortex dynamics we have discussed in chapters 3 and 4 can be related to 7.69. We can consider 2D point vortices dynamics as motion of intersection points of a plane with straight vortex lines. Then, assuming a point vortex dipole with equal but opposite strength of rotation, i.e. $\pm\Gamma$, the vortex pair translates with velocity (7.69). This follows from the equations of motion (3.3). In chapter 8 we will discuss the Lie group for vortex dynamics and relate the group elements to the Law of Biot-Savart.

7.4 Summary

In this chapter we have summarized Névir's and Blender's (1993) formulation of 2D and 3D vortex dynamics in terms of Nambu mechanics. In contrast to Hamiltonian dynamics, the Nambu bracket is trilinear, and two conserved quantities have equal status. This Nambu bracket leads to a Lie algebra that we will explore further in the next chapters.

Chapter 8

The Vortex groups

8.1 Introduction

In the first part of this thesis we have considered discrete Nambu mechanics showing that this formulation allows for the classification of point vortex motions. Then, we have applied the discrete vortex model to explain atmospheric blockings. In the last chapters we have explored continuous Nambu mechanics and showed how the 2D and 3D vorticity equations for incompressible, inviscid flows can be represented with respect to the Nambu brackets. As we have explored in the last chapter, these brackets imply Lie algebras for 2D ans 3D vortex dynamics.

In this chapter, we will start from these algebras and introduce a matrix representation of these Lie algebras. From these representations we will derive a vector Lie group representation as well as a matrix Lie group representation for two-and three-dimensional incompressible, inviscid vortex dynamics. The group structure itself was communicated with Peter Névir in private communication with Anton Schober in 2010. But so far, no matrix representation of the Lie algebra and Lie group and no derivation has been introduced.

In the last part of this chapter, we will further extend this Lie group and derive it from a Lie algebra that additionally contains the bracket of the angular momentum. In this way, we will obtain a novel group for vortex dynamics that contains two kinds of rotations, vortical and rigid body rotations. Here, we do not consider the bracket representation with respect to the energy. Therefore, we only regard the spatial aspect on the dynamics, not the time evolution. We will call it the Helmholtz Vortex group and show that it can be represented as a semi-direct product of the Lie group

from the first part of this chapter and the rigid body rotations SO(3).

Thus far, the rotational part of the fluid dynamical equations of motions are – similar to classical mass point mechanics – are included in the equations as rigid body rotations, see e.g. Arnold (1969a), Arnold (1969b), Salmon (1982), Marsden and Weinstein (1983), Salmon (1988), Holm et al. (1998), Shepherd (1990), or Arnold and Khesin (1992). The algebraic representations of fluid dynamics are commonly derived from the incompressible Navier-Stokes equations, which are equations for the time evolution of the velocity.

Here we will start from the equation for the vortex flow itself, from the Helmholtz vorticity equation, which provides a more direct approach to describe vortex dynamics. We think that vortical rotations – not just rigid body rotations – play a crucial role in vortex dynamics. The Helmholtz vorticity equation is derived by the mathematical rotation of the Euler equation. The rotation of gradients vanish. Therefore, using the Helmholtz vorticity equation as the basis of our approach, we only regard the rotational part of the velocity field and exclude the divergent part of the velocity field. Thus, we consider an algebra that is directly based on the vorticity field and not on the velocity field. Moreover, the Nambu formulation is based on conserved quantities that are expressed by the vorticity, we will explore the Nambu bracket with respect to the enstrophy in two-dimensions and with respect to the helicity to formulate three-dimensional vortex dynamics. Comparing vortex dynamics to the evolution of mass points, we see that mass points are characterized by their mass m, a positive definite quantity. And assuming idealized systems, mass points move along straight lines. In two dimensions vortices are characterized by the circulation, a quantity that can have positive and negative sign. In 3D, vortices are characterized by the total flux of vorticity in 3D; both quantities describe the strength of the vortex rotation. Distinguishing between vortex rotations and rigid body rotations and regarding the different sign structures, it seems reasonable that vortex dynamics provides a different group structure than mass point dynamics.

After the derivations of the vortex groups for two-and three-dimensional vortex dynamics in this chapter, we will apply these groups to atmospheric flow fields in chapter 9 to demonstrate the existence of storm splits. Before we derive the groups for vortex flows, we will discuss the Heisenberg algebra for mass point dynamics to demonstrate a transition from a Lie algebra

to a Lie group. There are different approaches to represent mass point dynamics algebraically. One more mathematical approach starts with the $2n$-dimensional phase space with the n-dimensional position coordinate and the n-dimensional momentum vector. A more physical approach is given by the Galilei algebra which can be extended by the mass, algebraically it is called a 'central extension'. This leads to the nilpotent, so-called Standard-Heisenberg algebra. Physically, this algebra is formed by the momentum, the special Galilei transformations and the mass such that it has dimension $2n + 1$. We will discuss this example for $n = 3$ in subsection 8.1.1.

The vortex algebras and groups that we will derive in this chapter are also nilpotent. Furthermore, it will turn out that the group for two-dimensional incompressible, inviscid flows can also be represented as a Heisenberg matrix, where the group operation can be compared with the Standard-Heisenberg group operation – although both groups have different physical meaning.

A further physical example of a nilpotent Lie algebra is the algebra for quantum mechanics. The Lie bracket relations of the state space coordinates were first discovered by Werner Karl Heisenberg and lead to the beginning of quantum mechanics. He introduced the uncertainty principle. Already in 1929 Hermann Weyl derived from this algebra a group for quantum mechanical systems that was published 21 years later (Weyl, 1950).

8.1.1 The Heisenberg Algebra and Heisenberg group of mass point mechanics

In this example, we will discuss the algebraic representation of mass point dynamics with respect to the Galilei transformation. Consider the six-dimensional phase space given by the position vector $\mathbf{p} \in \mathbb{R}^3$ and the momentum $\mathbf{q} \in \mathbb{R}^3$ to describe the state of a point with mass m at a given time t. Then, the Hamiltonian representation of the set of equations is given by:

$$\frac{dp_i}{dt} = -\frac{\partial H}{\partial q_i}, \quad \frac{dq_i}{dt} = \frac{\partial H}{\partial p_i}, \tag{8.1}$$

where the index $i = 1, 2, 3$ denotes the direction in the three-dimensional configuration space; H is the Hamiltonian, which is the total energy and given by the sum of the kinetic and potential energy. This set of equations

leads to the classical canonical Poisson bracket:

$$\{F, G\}_{\mathrm{P}} = \sum_{i=1}^{3} \left(\frac{\partial F}{\partial q_i} \frac{\partial G}{\partial p_i} - \frac{\partial F}{\partial p_i} \frac{\partial G}{\partial q_i}, \right). \tag{8.2}$$

which we have already compared to the bracket for point vortices in table 3.1 chapter 3. We consider the special Galilei transformation, where the local coordinate is now expressed in terms of the total mass m:

$$q_i \mapsto g = mq_i. \tag{8.3}$$

Adding the mass to the six-dimensional phase space of the momentum and position vector the dimension of the phase space becomes seven. Algebraically, we can speak of the central extension of the Galilei-group that we have explored in example 3, chapter 6. We obtain the following relations of the components of the momentum, position vector and the mass:

$$\{g_i, p_j\}_{\mathrm{P}} = \delta_{ij} m,\ \{g_i, g_j\}_{\mathrm{P}} = 0,\ \{p_i, p_j\}_{\mathrm{P}} = 0,\ \{m, g_i\}_{\mathrm{P}} = 0,\ \{m, p_i\}_{\mathrm{P}} = 0, \tag{8.4}$$

for $i, j = 1, 2, 3$. We can find a matrix representation for states in the phase space characterized by the momentum $\mathbf{q} = (q_1, q_2, q_3)$, the position vector $\mathbf{p} = (p_1, p_2, p_2)$ and the total mass m, such that they satisfy the bracket relations (8.4) with respect to the matrix commutator as we have discussed in chapter 6.

$$\begin{aligned} \text{Poisson-bracket} &\longrightarrow \text{Matrix commutator} \\ \{a, b\}_{\mathrm{P}} &\longrightarrow [A, B] = A \cdot B - B \cdot A \end{aligned} \tag{8.5}$$

where A and B denote two $n \times n$ matrices and '$\cdot$' is the usual matrix multiplication. We will use the following notation:

$$\begin{aligned} \text{Galilei transformation} \quad g &\rightarrow \text{matrix representation} \quad G \\ \text{Momentum} \quad p &\rightarrow \text{matrix representation} \quad P \\ \text{Mass} \quad m &\rightarrow \text{matrix representation} \quad M \end{aligned} \tag{8.6}$$

And the matrix representations are given by:

$$\underline{\mathcal{G}} = \begin{pmatrix} 0 & 1 & 0 \\ 0 & 0 & 0 \\ 0 & 0 & 0 \end{pmatrix}, \quad \underline{\mathcal{P}} = \begin{pmatrix} 0 & 0 & 0 \\ 0 & 0 & 1 \\ 0 & 0 & 0 \end{pmatrix}, \quad \underline{\mathcal{M}} = \begin{pmatrix} 0 & 0 & 1 \\ 0 & 0 & 0 \\ 0 & 0 & 0 \end{pmatrix}, \tag{8.7}$$

Applying the matrix commutator (8.5), we obtain the same bracket relations as in (8.4). Then, the linear combination $\underline{\mathcal{C}}$ of the matrix representations (8.7) reads as:

$$\underline{\mathcal{C}} := v\underline{\mathcal{G}} + r\underline{\mathcal{P}} + \theta\underline{\mathcal{M}} = \begin{pmatrix} 0 & v & \theta \\ 0 & 0 & r \\ 0 & 0 & 0 \end{pmatrix}, \tag{8.8}$$

where r is a constant displacement in direction of the momentum, v a constant velocity generated by g and the variable θ is conjugated to the mass with respect to the action. In this context, it is interesting to note that θ has the dimension of a circulation. Thus, the dimension in all summands is the action. Matrices of form $\underline{\mathcal{C}}$ build a subgroup of the so-called Heisenberg group, which is defined as the set of upper triangular matrices. The above matrix $\underline{\mathcal{C}}$ is nilpotent, because $\underline{\mathcal{C}}^3 = 0$. Sudarshan and Mukunda (1974) consider the following componentwise transition from the algebra to the group:

$$\begin{array}{ccccccc} \text{algebra} & & & & & & \text{group} \\ p & \longrightarrow & \exp(\widetilde{r \cdot p}) & \longrightarrow & r \\ g & \longrightarrow & \exp(\widetilde{v \cdot g}) & \longrightarrow & v \\ m & \longrightarrow & \exp(\widetilde{\theta \cdot m}) & \longrightarrow & \theta, \end{array} \tag{8.9}$$

where the tilde denotes the scaling by the action to obtain dimensionless exponents.

In order to derive the group operation, we first calculate the Lie bracket of two states, where each is given by the tuple of the phase space coordinate and the corresponding mass (r, v, θ) and (r', v', θ') and represented by the matrices $\underline{\mathbf{X}}$ and $\underline{\mathbf{Y}}$:. We will use the following notations for the matrices representation of our physical states

$$(r, v, \theta) \mapsto \begin{pmatrix} 0 & v & \theta \\ 0 & 0 & r \\ 0 & 0 & 0 \end{pmatrix} := \underline{\mathbf{X}} \quad \text{and} \quad (r', v', \theta') \mapsto \begin{pmatrix} 0 & v' & \theta' \\ 0 & 0 & r' \\ 0 & 0 & 0 \end{pmatrix} := \underline{\mathbf{Y}} \tag{8.10}$$

Calculating the matrix commutator $[\underline{\mathbf{X}}, \underline{\mathbf{Y}}]$ leads to

$$\left[\begin{pmatrix} 0 & v & \theta \\ 0 & 0 & r \\ 0 & 0 & 0 \end{pmatrix}, \begin{pmatrix} 0 & v' & \theta' \\ 0 & 0 & r' \\ 0 & 0 & 0 \end{pmatrix} \right] = \begin{pmatrix} 0 & 0 & v \cdot r' - v' \cdot r \\ 0 & 0 & 0 \\ 0 & 0 & 0 \end{pmatrix}. \tag{8.11}$$

If we calculate the matrix commutator of the last result (8.11) and an additional state (r'', v'', θ''), represented by the matrix $\underline{\mathbf{Z}}$, the outcome will be zero:

$$[[\underline{\mathbf{X}}, \underline{\mathbf{Y}}], \underline{\mathbf{Z}}] = 0 \tag{8.12}$$

Thus, this algebraic structure is nilpotent. And this property allows for a smooth transition from the bracket, i.e. the algebra, to the group.

Transition from the Lie algebra to the Lie group

We apply the Baker-Campbell-Hausdorff-formula (6.66) to obtain the group operation directly from the Lie algebra matrix representation. For non-nilpotent algebras, the exponent of (8.13) would have infinitely many terms. But, because this algebraic structure is nilpotent (8.12), the Baker-Campbell-Hausdorff-formula reduces to:

$$e^{\underline{\mathbf{X}}} e^{\underline{\mathbf{Y}}} = e^{\underline{\mathbf{X}} + \underline{\mathbf{Y}} + \frac{1}{2}[\underline{\mathbf{X}}, \underline{\mathbf{Y}}]}, \tag{8.13}$$

with the usual matrix addition and the matrix commutator (8.5).

We obtain the Lie group by regarding the exponents of (8.13) by applying the matrix representations (8.10) and the matrix commutator (8.11) to (8.13). Then, the vector representation of the Heisenberg Lie group for mass point dynamics is given by the exponent on the right hand side of (8.13): The exponent of (8.13) reads as:

$$X + Y + \frac{1}{2}[X, Y] = \begin{pmatrix} 0 & v + v' & \theta + \theta' + \frac{1}{2}(v \cdot r' - r \cdot v') \\ 0 & 0 & r + r' \\ 0 & 0 & 0 \end{pmatrix} \tag{8.14}$$

Then, $\ln(\exp(X)\exp(Y))$ provides the associated group operation of the Heisenberg Lie group for mass point dynamics:

$$(v, r, \theta) * (v', r', \theta') = \left(v + v', r + r', \theta + \theta' + \frac{1}{2}(v \cdot r' - r \cdot v') \right). \tag{8.15}$$

(see also, e.g. Kisil, 2012). We call this group for mass point dynamics together with the group operation (8.15) Standard-Heisenberg algebra and use the notation sh(2). As we will see later in this chapter, last example of the matrix representation and group operation of mass point dynamics is isomorphic the two-dimensional Vortex-Heisenberg group that we will derive in the following. Even though both groups are derived from different sets of equations! This difference is reflected in the physical meaning of the quantities.

In order to derive the group operations for two-and three dimensional incompressible and inviscid vortex flows, we will shortly summarize the concept of the so-called quaternions. We will use the quaternions for the matrix representation of the Lie algebras and Lie groups and represent the physical quantities that form the basis of the Lie algebra with respect to quaternions.

8.1.2 The concept of Quaternions

Quaternions can be seen as a generalization of the complex numbers. The algebra of quaternions is denoted $\mathbb{H}$ to honor William R. Hamilton who introduced the quaternions in 1843. A quaternion q can be written as $\mathbf{q} = ai + bj + ck + d$ and its conjugate is given by $\overline{\mathbf{q}} = -ai - bj - ck + d$. We can write $\mathbb{H}$ as set

$$\mathbb{H} = \{(a, b, c, d) \mid a, b, c, d \in \mathbb{R}\} \tag{8.16}$$

with basis elements

$$\begin{aligned} i &= (1, 0, 0, 0) \\ j &= (0, 1, 0, 0) \\ k &= (0, 0, 1, 0) \\ 1 &= (0, 0, 0, 1) \end{aligned} \tag{8.17}$$

Thus, the set $\mathbb{H}$ is isomorphic to $\mathbb{R}^4$. But, in contrast to multiplication of real numbers the multiplication of quaternions is not commutative. The multiplication of the basic elements can be summarized in the following table

·	1	i	j	k
1	1	i	j	k
i	i	-1	k	-j
j	j	-k	-1	i
k	k	j	-i	-1

Let now $\mathbf{q}_1 = a_1 i + b_1 j + c_1 k + d_1$ and $\mathbf{q}_2 = a_2 i + b_2 j + c_2 k + d_2$ two quaternions. Then the following compositions of two quaternions hold:

1. Addition:

$$\mathbf{q}_1 + \mathbf{q}_2 = (a_1 + a_2)i + (b_1 + b_2)j + (c_1 + c_2)k + (d_1 + d_2) \tag{8.18}$$

2. The imaginary part of quaternions can be identified with $\mathbb{R}^3$. Let us only consider the imaginary part and set $\mathbf{h}_1 = (a_1\ b_1\ c_1)^T$ and $\mathbf{h}_2 = (a_2\ b_2\ c_2)^T$. Then, the cross product for the imaginary part reads

$$\mathbf{h}_1 \times \mathbf{h}_2 = (b_1 c_2 - b_2 c_1)i + (c_1 a_2 - c_2 a_1)j + (a_1 b_2 - a_2 b_1)k \tag{8.19}$$

3. Using the above notation, we again divide a quaternion into a real part $d \in \mathbb{R}$ and a imaginary part $\mathbf{h} \in \mathbb{R}^3$. We denote with the symbol $\cdot$ the usual dot-product and with $\times$ the cross product. Then, the multiplication of two quaternions $\mathbf{q_1} = (\mathbf{h}_1, d_1)$ and $\mathbf{q_2} = (\mathbf{h}_2, d_2)$ is given by:

$$(\mathbf{h}_1, d_1)(\mathbf{h}_2, d_2) = (d_1 \mathbf{h}_2 + d_2 \mathbf{h}_1 + \mathbf{h}_1 \times \mathbf{h}_2, d_1 d_2 - \mathbf{h}_1 \cdot \mathbf{h}_2) \tag{8.20}$$

In the next section, we will use this concept of the generalization of the complex numbers for the derivation of a group for two-dimensional incompressible, inviscid vortex flows.

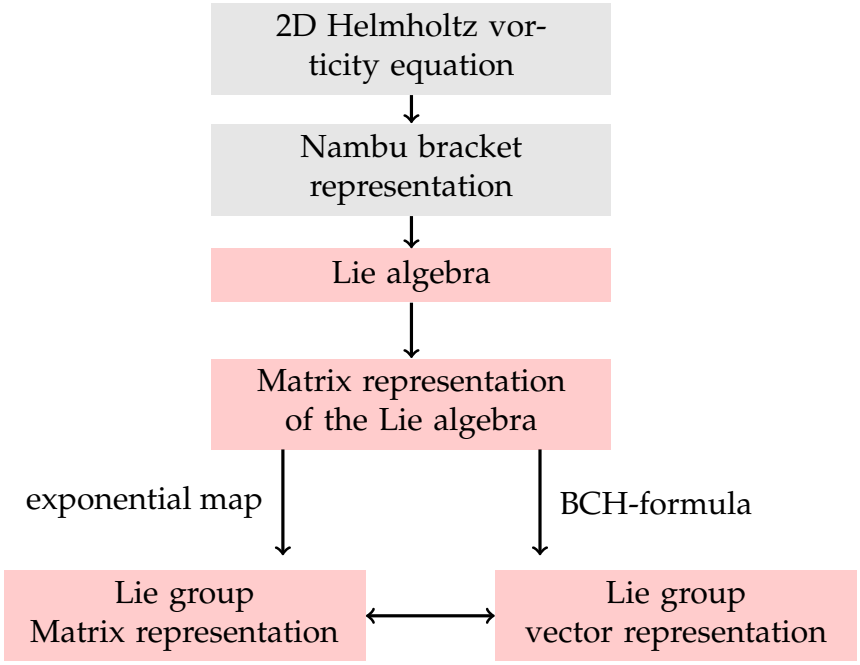

Figure 8.1: The steps are sketched, how we will derive the vortex groups for two dimensional inviscid, vortex dynamics. The Nambu bracket representation of the 2D Helmholtz vorticity equation were introduced by Névir (1998). The red boxes mark the novel contributions in this thesis noting that the vector representation of the vortex Lie group was also communicated with Peter Névir in private communication with Anton Schober in 2010. Here, we show how different group representations can be derived.

8.2 A vortex algebra and group for 2D flows

In the last section we have discussed the Heisenberg group for the dynamics of discrete mass points. Now, we will derive a group based on the continuous 2D incompressible vorticity equation. Névir (1998) has shown that the bracket relations for continuous, incompressible flows are comparable to the bracket relations of the discrete point vortex model of incompressible flows in two dimension. Therefore, a group for 2D vortex dynamics can be derived that provides a structure similar to the Heisenberg group for mass points. Because of the isomorphic structures, we call the vortex group *Vortex-Heisenberg group*, short VH(2), and the corresponding Lie algebra *Vortex-Heisenberg Lie algebra* (vh(2)). In fig. 8.1 the steps are summarized how we will proceed to derive the group for 2D incompressible, inviscid fluids. In chapter 7 we have shown the Nambu formulation of the vorticity equation. The resulting bracket formulation generates the Vortex-Heisenberg Lie algebra. The brackets are introduced by Névir and Blender (1993) and Névir (1998). The novel aspect in the thesis is the introduction

of a basis matrix representation of the physical quantities that satisfy the bracket relation. First, we will introduce matrices that represent conserved quantities for two-dimensional, inviscid incompressible flows given by the linear momenta P_x and P_y and the circulation Γ. In this way, we can easily calculate the matrix commutator to obtain the corresponding bracket relations.

$$\begin{array}{ccc} \text{Nambu-bracket} & \longrightarrow & \text{Matrix commutator} \\ \{\mathcal{F}, \mathcal{E}, \mathcal{G}\} & \longrightarrow & [\underline{\mathcal{F}}, \underline{\mathcal{G}}] \end{array} \tag{8.21}$$

We will obtain a matrix representation of the Vortex-Heisenberg algebra such that we can derive a matrix representation as well as a vector representation of a Lie group for vortex dynamics.

8.2.1 Introducing a matrix representation of vh(2)

To derive the matrix representation of a an algebra for two-dimensional incompressible, inviscid fluids, we first recall the formulation of the following conserved quantity via the vorticity ζ:

$$\begin{aligned} \mathcal{H}[\zeta] &= -\frac{1}{2}\int_F df\ \zeta\psi \qquad \text{(Energy)} \\ \mathcal{E}[\zeta] &= \frac{1}{2}\int_F df\ \zeta^2 \qquad \text{(Enstrophy)} \\ P_x[\zeta] &= \int_F df\ \zeta y \qquad \text{(zonal momentum)} \\ P_y[\zeta] &= -\int_F df\ \zeta x \qquad \text{(meridional momentum).} \end{aligned} \tag{8.22}$$

Névir (1998) shows that the Nambu bracket of these global, continuous conserved quantities with respect to the enstrophy $\mathcal{E}$ results in the same relations that we obtained for the discrete point vortex model regarding discrete vortex quantities and the Lie-Poisson bracket for point vortex dynamics, see chapter 3.

In the first part of this thesis, we have already discussed the conserved quantities for two-dimensional discrete point vortex dynamics and compared the different Lie brackets for mass points and point vortices (see chapter 3). In contrast to the algebraic structure of mass point dynamics,

the momenta do not commute:

$$\{P_x, \mathcal{E}, P_y\} = \Gamma, \quad \{\Gamma, \mathcal{E}, P_x\} = 0, \quad \{\Gamma, \mathcal{E}, P_y\} = 0. \tag{8.23}$$

where the bracket here is the Nambu bracket for two-dimensional incompressible vortex dynamics.

We compare the Vortex-Heisenberg algebra VH(2) with the Standard Heisenberg algebra that we discussed in the last example.

$$\begin{array}{ccc} \text{Vortex-Heisenberg algebra VH(2)} & \cong & \text{Standard Heisenberg algebra sh(1)} \\ \{P_x, \mathcal{E}, P_y\} = \Gamma & & \{g, p\}_P = M \end{array} \tag{8.24}$$

Thus, the two-dimensional vortex algebra is isomorphic to the Heisenberg structure of the Galilei algebra.

We will first introduce the following novel matrix representation of the two linear momenta and the circulation with respect to the quaternions with i, j, k in $\mathbb{H}$. We will denote the corresponding matrix representations of the momenta and the circulation by $\underline{P_x}, \underline{P_y}$ and $\underline{\Gamma}$. Then, we will show that these matrix representations satisfy the bracket relations (8.23) with respect to the matrix commutator.

$$\begin{array}{ccc} \text{Nambu-bracket} & \longrightarrow & \text{Matrix commutator} \\ \{\mathcal{F}, \mathcal{E}, \mathcal{G}\} & \longrightarrow & [\underline{\mathcal{F}}, \underline{\mathcal{G}}] \end{array} \tag{8.25}$$

The novel matrix representations of the conserved quantities are given by:

$$\underline{P_x} = \begin{pmatrix} 0 & i & 0 \\ 0 & 0 & 0 \\ 0 & 0 & 0 \end{pmatrix}, \quad \underline{P_y} = \begin{pmatrix} 0 & 0 & 0 \\ 0 & 0 & j \\ 0 & 0 & 0 \end{pmatrix}, \quad \underline{\Gamma} = \begin{pmatrix} 0 & 0 & k \\ 0 & 0 & 0 \\ 0 & 0 & 0 \end{pmatrix}. \tag{8.26}$$

We see that determining the bracket in terms of these matrix representations leads to the same relations as in (8.23):

$$[\underline{P_x}, \underline{P_y}] = \underline{P_x}\underline{P_y} - \underline{P_y}\underline{P_x} = \begin{pmatrix} 0 & i & 0 \\ 0 & 0 & 0 \\ 0 & 0 & 0 \end{pmatrix} \begin{pmatrix} 0 & 0 & 0 \\ 0 & 0 & j \\ 0 & 0 & 0 \end{pmatrix} - \begin{pmatrix} 0 & 0 & 0 \\ 0 & 0 & j \\ 0 & 0 & 0 \end{pmatrix} \begin{pmatrix} 0 & i & 0 \\ 0 & 0 & 0 \\ 0 & 0 & 0 \end{pmatrix} \tag{8.27}$$

$$\Longleftrightarrow \quad [\underline{P_x}, \underline{P_y}] = \begin{pmatrix} 0 & 0 & k \\ 0 & 0 & 0 \\ 0 & 0 & 0 \end{pmatrix} = \underline{\Gamma} \tag{8.28}$$

and

$$\begin{aligned} [\underline{P_y}, \underline{P_x}] = \underline{P_y}\underline{P_x} - \underline{P_x}\underline{P_y} &= \begin{pmatrix} 0 & 0 & 0 \\ 0 & 0 & j \\ 0 & 0 & 0 \end{pmatrix} \begin{pmatrix} 0 & i & 0 \\ 0 & 0 & 0 \\ 0 & 0 & 0 \end{pmatrix} - \begin{pmatrix} 0 & i & 0 \\ 0 & 0 & 0 \\ 0 & 0 & 0 \end{pmatrix} \begin{pmatrix} 0 & 0 & 0 \\ 0 & 0 & j \\ 0 & 0 & 0 \end{pmatrix} \\ &= \begin{pmatrix} 0 & 0 & -k \\ 0 & 0 & 0 \\ 0 & 0 & 0 \end{pmatrix} = -\underline{\Gamma}. \end{aligned} \tag{8.29}$$

Thus, these matrices satisfy the bracket relations (8.23)! Their linear combination reads as:

$$\underline{\mathcal{A}} = \alpha \underline{P_x} + \beta \underline{P_y} + \gamma \underline{\Gamma} = \begin{pmatrix} 0 & \alpha i & \gamma k \\ 0 & 0 & \beta j \\ 0 & 0 & 0 \end{pmatrix}, \quad \alpha, \beta, \gamma \in \mathbb{R} \tag{8.30}$$

which satisfies the Heisenberg structure and can be compared with the above example of the matrix Standard-Heisenberg algebra sh(2) for mass point dynamics.

8.2.2 Derivation of the Vortex-Heisenberg Lie group VH(2)

To derive the matrix representation of the Vortex-Heisenberg Lie group, we recall the exponential map (6.63), which maps the matrix algebra (8.30) to a matrix group:

$$\exp \underline{\mathcal{A}} = \sum_{k=0}^{\infty} \frac{\underline{\mathcal{A}}^k}{k!} = \mathbb{I} + \underline{\mathcal{A}} + \frac{1}{2}\underline{\mathcal{A}}^2 + \frac{1}{6}\underline{\mathcal{A}}^3 + \cdots \tag{8.31}$$

Using the quaternionian relations $ij = k$ we obtain for $\underline{\mathcal{A}}^2 = 0$ and $\underline{\mathcal{A}}^3 = 0$:

$$\underline{\mathcal{A}} = \begin{pmatrix} 0 & \alpha i & \gamma k \\ 0 & 0 & \beta j \\ 0 & 0 & 0 \end{pmatrix} \quad \longrightarrow \quad \underline{\mathcal{A}}^2 = \begin{pmatrix} 0 & 0 & \alpha i \beta j \\ 0 & 0 & 0 \\ 0 & 0 & 0 \end{pmatrix} = \begin{pmatrix} 0 & 0 & \alpha\beta k \\ 0 & 0 & 0 \\ 0 & 0 & 0 \end{pmatrix} \tag{8.32}$$

and

$$\underline{\mathcal{A}}^3 = \begin{pmatrix} 0 & 0 & 0 \\ 0 & 0 & 0 \\ 0 & 0 & 0 \end{pmatrix}. \tag{8.33}$$

Thus, we obtain the following matrix representation of a group for vortex dynamics:

$$\begin{aligned} \exp \underline{\mathcal{A}} &= \begin{pmatrix} 1 & 0 & 0 \\ 0 & 1 & 0 \\ 0 & 0 & 1 \end{pmatrix} + \begin{pmatrix} 0 & \alpha i & \gamma k \\ 0 & 0 & \beta j \\ 0 & 0 & 0 \end{pmatrix} + \frac{1}{2} \begin{pmatrix} 0 & 0 & \alpha\beta k \\ 0 & 0 & 0 \\ 0 & 0 & 0 \end{pmatrix} \\ &= \begin{pmatrix} 1 & \alpha i & \gamma' k \\ 0 & 1 & \beta j \\ 0 & 0 & 1 \end{pmatrix}, \end{aligned} \tag{8.34}$$

where the property of quaternions $ij = k$ was used in the third term on the right hand side and $\gamma' = (\gamma + \frac{1}{2}\alpha\beta)$. From physical perspective, group elements have a different meaning than the elements of the Lie algebra that 'live' on the tangent space of the neutral element of the group. In order to interpret the coefficients physically, we will rename the constants $\alpha,\ \beta$ and γ in (8.34):

$$\alpha \to a_x, \quad \beta \to a_y, \quad \gamma' \to A, \tag{8.35}$$

where $\mathbf{a}$ denotes the vector tangent to the streamlines of an infinitesimal vortex tube, indicating a local displacement, and A is the change of the area enclosed by the vortex. Here, we focus on the mathematical formulation of the vortex algebra group and vortex group for two-dimensional flows. After the derivation of the 3D vortex group we will explain the physical interpretation more in detail in section 8.5. We can formulate the basis matrix representation of a vortex Lie group for two-dimensional fluid dynamics:

$$\boxed{(\mathbf{a}, A) = (a_x, a_y, A) \mapsto \begin{pmatrix} 1 & a_x i & Ak \\ 0 & 1 & a_y j \\ 0 & 0 & 1 \end{pmatrix}}, \tag{8.36}$$

This representation is isomorphic to the matrix group representation of the Heisenberg algebra of classical mass point dynamics that we have discussed in the beginning of this chapter.

But we also aim for the group operation for group elements represented as vectors. To achieve this goal, we start again from the matrix representation of the Lie algebra (8.30). Then, the group operation can be derived by applying the Baker-Campbell-Hausdorff-formula (6.66)

$$e^{\underline{\mathcal{A}}}e^{\underline{\mathcal{B}}} = e^{\underline{\mathcal{A}}+\underline{\mathcal{B}}+\frac{1}{2}[\underline{\mathcal{A}},\underline{\mathcal{B}}]}. \tag{8.37}$$

to our matrix representation (8.36). Let $\underline{\mathcal{A}}$ and $\underline{\mathcal{B}}$ be two elements of the vortex group given by:

$$\underline{\mathcal{A}} = \begin{pmatrix} 0 & a_x i & Ak \\ 0 & 0 & a_y j \\ 0 & 0 & 0 \end{pmatrix} \quad \text{and} \quad \underline{\mathcal{B}} = \begin{pmatrix} 0 & a'_x i & A'k \\ 0 & 0 & a'_y j \\ 0 & 0 & 0 \end{pmatrix}. \tag{8.38}$$

Now, we apply the Baker-Campbell-Hausforff-formula (8.37) to $\underline{\mathcal{A}}$ and $\underline{\mathcal{B}}$ and obtain:

$$\underline{\mathcal{A}} + \underline{\mathcal{B}} + \frac{1}{2}[\underline{\mathcal{A}}, \underline{\mathcal{B}}] = \begin{pmatrix} 0 & (a_x + a'_x)i & A + A' + \frac{1}{2}(a_x a'_y - a_y a'_x) \\ 0 & 0 & (a_y + a'_y)j \\ 0 & 0 & 0 \end{pmatrix}. \tag{8.39}$$

We compare the entries of the matrix (8.39) with the entries in $\underline{\mathcal{A}}$. We see that the components that denote the displacement add: $(a_x + a'_x)$, $(a_y + a'_y)$ and the A-entry becomes $A + A' + \frac{1}{2}(a_x a'_y - a_y a'_x)$. Therefore, we obtain the the following group operation for 2D incompressible, inviscid vortex dynamics:

$$\boxed{(\mathbf{a}, A) * (\mathbf{a}', A') = (\mathbf{a} + \mathbf{a}', A + A' + \frac{1}{2}(a_x a'_y - a_y a'_x)) =: (\mathbf{a}'', A'').} \tag{8.40}$$

This representation is isomorphic to the matrix group representation of the Heisenberg group of classical mass point dynamics that we have discussed in the previous section. Because of this isomorphic structure, we call the here derived group *Vortex-Heisenberg group* and denote it VH(2).

In the next section, we will analogously derive a group for three-dimensional incompressible, inviscid vortex flows. To compare the group operations of the two-and three-dimensional Vortex-Heisenberg groups, we reformulate (8.40) as follows:

$$(\mathbf{a}, A) * (\mathbf{a}', A') = (\mathbf{a} + \mathbf{a}', A + A' + \frac{1}{2}\mathbf{k} \cdot (\mathbf{a} \times \mathbf{a}')) \tag{8.41}$$

where $\mathbf{k}$ denotes the unit vector in z-direction, and the displacement vectors (a_x, a_y) and (a'_x, a'_y) are embedded in three dimensions $\mathbf{a} = (a_x, a_z, 0)$ and $\mathbf{a}' = (a'_x, a'_z, 0)$. We will see that the Vortex-Heisenberg group VH(3) for incompressible, inviscid three-dimensional vortex dynamics has the same structure as (8.41).

Claim 1. We state that the Vortex-Heisenberg group with operation (8.41) is indeed a group, where the identity element is given by $e = (\mathbf{0}, 0)$ and the inverse of an element $(\mathbf{a}, A) \in$ VH(2) by $(-\mathbf{a}, -A) \in$ VH(2)

Proof.

$$(\mathbf{a}, A) * (\mathbf{0}, 0) = (\mathbf{a} + 0, A + 0 + \frac{1}{2}\mathbf{k} \cdot (\mathbf{a} \times \mathbf{0})) = (\mathbf{a}, A) \tag{8.42}$$

and

$$\begin{aligned} (\mathbf{a}, A) * (-\mathbf{a}, -A) &= (\mathbf{a} - \mathbf{a}, A - A + \frac{1}{2}\mathbf{k} \cdot (\mathbf{a} \times (-\mathbf{a}))) = (\mathbf{0}, 0) \\ (-\mathbf{a}, -A) * (\mathbf{a}, A) &= (-\mathbf{a} + \mathbf{a}, -A + A + \frac{1}{2}\mathbf{k} \cdot (-\mathbf{a} \times \mathbf{a})) = (\mathbf{0}, 0) \end{aligned} \tag{8.43}$$

Moreover, the associative property is satisfied:

$$\begin{aligned} &(\mathbf{a}'', A'') * ((\mathbf{a}', A') * (\mathbf{a}, A)) \\ &\quad = \left(\mathbf{a}'' + \mathbf{a}' + \mathbf{a}, A'' + (A' + \frac{1}{2}\mathbf{a}' \times \mathbf{a}) + A + \frac{1}{2}\mathbf{a}'' \times (\mathbf{a}' + \mathbf{a})\right) \\ &\quad = \left(\mathbf{a}'' + \mathbf{a}' + \mathbf{a}, A'' + A' + A + \frac{1}{2}(\mathbf{a}' \times \mathbf{a} + \mathbf{a}'' \times \mathbf{a}' + \mathbf{a}'' \times \mathbf{a})\right) \\ &\quad = ((\mathbf{a}'', A'') * (\mathbf{a}', A')) * (\mathbf{a}, A) \end{aligned} \tag{8.44}$$

Therefore, VH(2) with group operation (8.41) forms a group. □

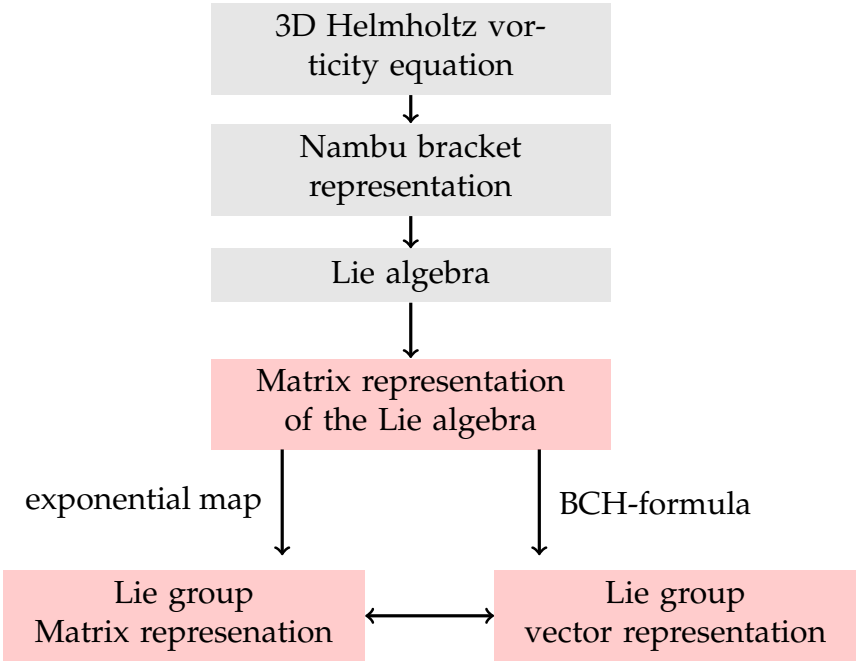

Figure 8.2: The steps, how we will derive the different vortex group representations for three-dimensional inviscid, incompressible vortex flows are shown. The Lie algebra was derived by Névir (1998). The red boxes mark the novel contributions in this thesis noting that the vector representation of the vortex Lie group was also communicated with Peter Névir in private communication with Anton Schober in 2010. Here, we show the derivation of the vortex group operation.

8.3 A vortex algebra and group for 3D flows

8.3.1 Introducing a matrix representation for vh(3)

In the following, we will derive the group for incompressible, inviscid three-dimensional vortex dynamics and proceed analogously to last section. The steps are sketched in fig. 8.2. In chapter 7 we have introduced the Nambu bracket for the 3D Helmholtz vorticity equation that generate a Lie algebra for fluid motion. Here, will introduce a matrix representation of the Lie algebra such that we can derive (i) a matrix Lie group for 3D incompressible, inviscid fluids, and (ii) a vector-valued Lie group representation 3D incompressible, inviscid fluids. A group is always defined by a set together with an operation. For matrix Lie groups, such as (i), the group operation is simply given by the matrix product. Here, the challenge is to find a matrix that represents the elements. Whereas the challenge of (ii) is the derivation of the vector valued group operation itself. Regarding application-oriented aspects, the matrix representation might be useful for numerical investigations of the group, whereas the vector representation of the group and

the corresponding group operation might be helpful for a better process-related understanding of vortex flows.

First, we will introduce a matrix representation of the basis elements of the Vortex-Heisenberg algebra vh(3) with respect to the basis of quaternions $\mathbb{H}$. For this approach, we recall the definitions of the helicity h_V, the momentum $\mathbf{P} = (P_x, P_y, P_z)$ and the total flux of vorticity $\mathbf{Z} = (Z_x, Z_y, Z_z)$:

$$\begin{aligned} h_V &= \frac{1}{2}\int_V d\tau\ \mathbf{v}\cdot\boldsymbol{\xi} \quad \text{(Helicity)} \\ \mathbf{P} &= \frac{1}{2}\int_V d\tau\ (\mathbf{a}\times\boldsymbol{\xi}) \quad \text{(Momentum)} \\ \mathbf{Z} &= \int_V d\tau\ \boldsymbol{\xi} \quad \text{(Total flux of vorticity)}, \end{aligned} \tag{8.45}$$

As we have discussed in chapter 7, the Vortex-Heisenberg algebra for three-dimensional incompressible, inviscid vortex flows is based on the Nambu-bracket, expressed with respect to the helicity:

$$\{P_i, h_V, P_j\} = \epsilon_{ijk} Z_k, \quad \{Z_i, h_V, P_j\} = \{Z_i, h_V, Z_j\} = 0. \tag{8.46}$$

We propose matrix representations for the momentum and the total flux of vorticity for three dimensional fluids, where we will denote the corresponding matrix representations of the components of the momentum and the total flux of vorticity by $\underline{P_x}, \underline{P_y}, \underline{P_z}$ and $\underline{Z_x}, \underline{Z_y}, \underline{Z_z}$. We will represent these quantities with respect to quaternions. We will show that these matrices together with the matrix commutator satisfy the bracket relations (8.46) for 3D incompressible vortex dynamics, i.e.

$$\begin{array}{ccc} \text{Nambu-bracket} & \longrightarrow & \text{Matrix commutator} \\ \{\mathcal{F}, h_V, \mathcal{G}\} & \longrightarrow & [\underline{\mathcal{F}}, \underline{\mathcal{G}}] \end{array} \tag{8.47}$$

The matrices that represent the components of the momentum and the total flux of vorticity are given by:

$$\underline{P_x} = \frac{1}{\sqrt{2}}\begin{pmatrix} 0 & 0 & 0 & 0 & 0 & 0 & i \\ 0 & 0 & 0 & 0 & 0 & 0 & 0 \\ 0 & 0 & 0 & 0 & 0 & 0 & 0 \\ 0 & 0 & 0 & 0 & 0 & 0 & 0 \\ 0 & 0 & -i & 0 & 0 & 0 & 0 \\ 0 & i & 0 & 0 & 0 & 0 & 0 \\ 0 & 0 & 0 & 0 & 0 & 0 & 0 \end{pmatrix}, \underline{Z_x} = \frac{1}{\sqrt{2}}\begin{pmatrix} 0 & 0 & 0 & 0 & 0 & 0 & 0 \\ 0 & 0 & 0 & 0 & 0 & 0 & 0 \\ 0 & 0 & 0 & 0 & 0 & 0 & 0 \\ 0 & 0 & 0 & 0 & 0 & 0 & i \\ 0 & 0 & 0 & 0 & 0 & 0 & 0 \\ 0 & 0 & 0 & 0 & 0 & 0 & 0 \\ 0 & 0 & 0 & 0 & 0 & 0 & 0 \end{pmatrix} \tag{8.48}$$

$$\underline{P_y} = \frac{1}{\sqrt{2}} \begin{pmatrix} 0 & 0 & 0 & 0 & 0 & 0 & 0 \\ 0 & 0 & 0 & 0 & 0 & 0 & j \\ 0 & 0 & 0 & 0 & 0 & 0 & 0 \\ 0 & 0 & j & 0 & 0 & 0 & 0 \\ 0 & 0 & 0 & 0 & 0 & 0 & 0 \\ -j & 0 & 0 & 0 & 0 & 0 & 0 \\ 0 & 0 & 0 & 0 & 0 & 0 & 0 \end{pmatrix}, \ \underline{Z_y} = \frac{1}{\sqrt{2}} \begin{pmatrix} 0 & 0 & 0 & 0 & 0 & 0 & 0 \\ 0 & 0 & 0 & 0 & 0 & 0 & 0 \\ 0 & 0 & 0 & 0 & 0 & 0 & 0 \\ 0 & 0 & 0 & 0 & 0 & 0 & 0 \\ 0 & 0 & 0 & 0 & 0 & 0 & j \\ 0 & 0 & 0 & 0 & 0 & 0 & 0 \\ 0 & 0 & 0 & 0 & 0 & 0 & 0 \end{pmatrix} \tag{8.49}$$

$$\underline{P_z} = \frac{1}{\sqrt{2}} \begin{pmatrix} 0 & 0 & 0 & 0 & 0 & 0 & 0 \\ 0 & 0 & 0 & 0 & 0 & 0 & 0 \\ 0 & 0 & 0 & 0 & 0 & 0 & k \\ 0 & -k & 0 & 0 & 0 & 0 & 0 \\ k & 0 & 0 & 0 & 0 & 0 & 0 \\ 0 & 0 & 0 & 0 & 0 & 0 & 0 \\ 0 & 0 & 0 & 0 & 0 & 0 & 0 \end{pmatrix}, \underline{Z_z} = \frac{1}{\sqrt{2}} \begin{pmatrix} 0 & 0 & 0 & 0 & 0 & 0 & 0 \\ 0 & 0 & 0 & 0 & 0 & 0 & 0 \\ 0 & 0 & 0 & 0 & 0 & 0 & 0 \\ 0 & 0 & 0 & 0 & 0 & 0 & 0 \\ 0 & 0 & 0 & 0 & 0 & 0 & 0 \\ 0 & 0 & 0 & 0 & 0 & 0 & k \\ 0 & 0 & 0 & 0 & 0 & 0 & 0 \end{pmatrix} \tag{8.50}$$

Applying the matrix commutator $[\underline{\mathcal{A}}, \underline{\mathcal{B}}] = \underline{\mathcal{A}} \cdot \underline{\mathcal{B}} - \underline{\mathcal{B}} \cdot \underline{\mathcal{A}}$ to $n \times n$ matrices $\underline{\mathcal{A}}$ and $\underline{\mathcal{B}}$ with matrix product $\cdot$ to the basis representation introduced above, we obtain:

$$[\underline{P_x}, \underline{P_y}] = \frac{1}{2} \begin{pmatrix} 0 & 0 & 0 & 0 & 0 & 0 & 0 \\ 0 & 0 & 0 & 0 & 0 & 0 & 0 \\ 0 & 0 & 0 & 0 & 0 & 0 & 0 \\ 0 & 0 & 0 & 0 & 0 & 0 & 0 \\ 0 & 0 & 0 & 0 & 0 & 0 & 0 \\ 0 & 0 & 0 & 0 & 0 & 0 & ij - ji \\ 0 & 0 & 0 & 0 & 0 & 0 & 0 \end{pmatrix} = \frac{1}{2} \begin{pmatrix} 0 & 0 & 0 & 0 & 0 & 0 & 0 \\ 0 & 0 & 0 & 0 & 0 & 0 & 0 \\ 0 & 0 & 0 & 0 & 0 & 0 & 0 \\ 0 & 0 & 0 & 0 & 0 & 0 & 0 \\ 0 & 0 & 0 & 0 & 0 & 0 & 0 \\ 0 & 0 & 0 & 0 & 0 & 0 & 2k \\ 0 & 0 & 0 & 0 & 0 & 0 & 0 \end{pmatrix} = \underline{Z_z} \tag{8.51}$$

$$[\underline{P_y}, \underline{P_z}] = \frac{1}{2} \begin{pmatrix} 0 & 0 & 0 & 0 & 0 & 0 & 0 \\ 0 & 0 & 0 & 0 & 0 & 0 & 0 \\ 0 & 0 & 0 & 0 & 0 & 0 & 0 \\ 0 & 0 & 0 & 0 & 0 & 0 & 2i \\ 0 & 0 & 0 & 0 & 0 & 0 & 0 \\ 0 & 0 & 0 & 0 & 0 & 0 & 0 \\ 0 & 0 & 0 & 0 & 0 & 0 & 0 \end{pmatrix} = \underline{Z_x}, \tag{8.52}$$

$$[\underline{P_z}, \underline{P_x}] = \frac{1}{2}\begin{pmatrix} 0 & 0 & 0 & 0 & 0 & 0 & 0 \\ 0 & 0 & 0 & 0 & 0 & 0 & 0 \\ 0 & 0 & 0 & 0 & 0 & 0 & 0 \\ 0 & 0 & 0 & 0 & 0 & 0 & 0 \\ 0 & 0 & 0 & 0 & 0 & 0 & 2j \\ 0 & 0 & 0 & 0 & 0 & 0 & 0 \\ 0 & 0 & 0 & 0 & 0 & 0 & 0 \end{pmatrix} = \underline{Z_y} \tag{8.53}$$

Thus, we can summarize the bracket relations with respect to the matrix commutator $[\cdot, \cdot]$:

$$[\underline{P_i}, \underline{P_j}] = \epsilon_{ijk}\underline{Z_k}, \quad [\underline{P_i}, \underline{Z_j}] = 0, \quad \text{and} \quad [\underline{Z_i}, \underline{Z_j}] = 0 \tag{8.54}$$

for $i, j, k \in \{x, y, z\}$. These relations coincide with the Nambu-bracket (7.56) with respect to the helicity h_V:

$$\{P_i, h_V, P_j\} = \epsilon_{ijk}Z_k, \quad \{Z_i, h_V, Z_j\} = 0 \quad \text{and} \quad \{Z_i, h_V, P_j\} = 0 \tag{8.55}$$

Thus, the above proposed basis is indeed a basis and yields a matrix representation of the vortex-Heisenberg Lie algebra. To the best of our knowledge, the above presented matrix representations are the first matrix representations for the momentum and the circulation. The linear combination of the basis elements reads:

$$\underline{\mathcal{A}} = \alpha_x\underline{P_x} + \alpha_y\underline{P_y} + \alpha_z\underline{P_z} + \gamma_x\underline{Z_x} + \gamma_y\underline{Z_y} + \gamma_z\underline{Z_z} \tag{8.56}$$

with $\alpha_x, \alpha_y, \alpha_z, \gamma_x, \gamma_y, \gamma_z \in \mathbb{R}$. In terms of the matrix representation, inserting (8.48), (8.49) and (8.50) in (8.56) results in:

$$\underline{\mathcal{A}} = \frac{1}{\sqrt{2}}\begin{pmatrix} 0 & 0 & 0 & 0 & 0 & 0 & \alpha_x i \\ 0 & 0 & 0 & 0 & 0 & 0 & \alpha_y j \\ 0 & 0 & 0 & 0 & 0 & 0 & \alpha_z k \\ 0 & -\alpha_z k & \alpha_y j & 0 & 0 & 0 & \gamma_x i \\ \alpha_z k & 0 & -\alpha_x i & 0 & 0 & 0 & \gamma_y j \\ -\alpha_y j & \alpha_x i & 0 & 0 & 0 & 0 & \gamma_z k \\ 0 & 0 & 0 & 0 & 0 & 0 & 0 \end{pmatrix} \tag{8.57}$$

We relate the coefficients in (8.57) to the components of the global momentum and the components of the flux of vorticity:

$$(\alpha_x, \alpha_y, \alpha_z) \longrightarrow (v_x, v_y, v_z) \quad \text{and} \quad (\gamma_x, \gamma_y, \gamma_z) \longrightarrow (\xi_x, \xi_y, \xi_z). \tag{8.58}$$

We will discuss the physical meaning of the group and the algebra at the end of this chapter in section 8.5. For now, we use these notations to formulate the matrix representation of the Vortex-Heisenberg algebra as follows:

$$\underline{\mathcal{A}}_{\mathbf{v},\boldsymbol{\xi}} = \frac{1}{\sqrt{2}} \begin{pmatrix} 0 & 0 & 0 & 0 & 0 & 0 & v_x i \\ 0 & 0 & 0 & 0 & 0 & 0 & v_y j \\ 0 & 0 & 0 & 0 & 0 & 0 & v_z k \\ 0 & -v_z k & v_y j & 0 & 0 & 0 & \xi_x i \\ v_z k & 0 & -v_x i & 0 & 0 & 0 & \xi_y j \\ -v_y j & v_x i & 0 & 0 & 0 & 0 & \xi_z k \\ 0 & 0 & 0 & 0 & 0 & 0 & 0 \end{pmatrix} \tag{8.59}$$

In the next step, we will start from this matrix algebra and derive a matrix Lie group representation for three dimensional vortex flows.

8.3.2 Derivation of the matrix vortex Lie group VH(3)

In order to apply Baker-Campbell-Hausdorff's formula (6.66) to derive the Vortex-Heisenberg group operation, we first calculate the Lie bracket in terms of the matrix commutator. We recall that a $n \times n$-matrix $\underline{\mathbf{X}}$ is called nilpotent if $\underline{\mathbf{X}}^m = 0$ for some $m \in \mathbb{N}, m > 0$. Such a matrix $\underline{\mathbf{X}}$ is called m-th-order nilpotent. Therefore, the matrices of form $\underline{\mathcal{A}}$ representing the linear combination of the basis elements of the Vortex-Heisenberg Lie algebra as given in (8.57) are second-order nilpotent, i.e.:

$$\underline{\mathcal{A}}^2 = \mathbf{0}.$$

For $\underline{\mathcal{A}}$ and $\underline{\mathcal{A}}'$ in the Vortex-Heisenberg Lie algebra vh(3) the matrix commutator reads as:

$$[\underline{\mathcal{A}}', \underline{\mathcal{A}}] = \underline{\mathcal{A}}' \cdot \underline{\mathcal{A}} - \underline{\mathcal{A}} \cdot \underline{\mathcal{A}}' = \frac{1}{2} \begin{pmatrix} 0 & 0 & 0 & 0 & 0 & 0 & 0 \\ 0 & 0 & 0 & 0 & 0 & 0 & 0 \\ 0 & 0 & 0 & 0 & 0 & 0 & 0 \\ 0 & 0 & 0 & 0 & 0 & 0 & (v'_y \cdot v_z - v_y \cdot v'_z)i \\ 0 & 0 & 0 & 0 & 0 & 0 & (v'_z \cdot v_x - v_z \cdot v'_i)j \\ 0 & 0 & 0 & 0 & 0 & 0 & (v'_x \cdot v_y - v_x \cdot v'_y)k \\ 0 & 0 & 0 & 0 & 0 & 0 & 0 \end{pmatrix}, \tag{8.60}$$

where the quaternion multiplication of the basis elements $ij = -ji = k$, $ik = -ki = j$ and $jk = -kj = i$ is used. We notice that the non-

vanishing terms can be summarized as cross product $\mathbf{v}' \times \mathbf{v}$. Moreover, if we calculate the bracket of last outcome (8.60) and a further element of the Vortex-Heisenberg Lie algebra, the bracket will vanish, i.e. the Lie algebra is nilpotent.

In the first step, we will apply the exponential map (6.63) to the Vortex-Heisenberg algebra representation to derive the matrix representation of the Vortex-Heisenberg group. Then, the group elements, given by the matrices, together with the usual matrix product form the Vortex-Heisenberg group VH(3). In the second step, we will start again from the matrix representation of the Vortex-Heisenberg algebra and derive the the vector representation of the group.

Let $\underline{\mathcal{A}}$ be of form (8.57). We recall that $\underline{\mathcal{A}}$ is second-order nilpotent, i.e. $\underline{\mathcal{A}}^2 = 0$. Then, the exponential map reduces to

$$\begin{aligned} \exp \underline{\mathcal{A}} &= \sum_{m=0}^{\infty} \frac{\underline{\mathcal{A}}^m}{m!} = \mathbb{I} + \underline{\mathcal{A}} + \frac{1}{2}\underline{\mathcal{A}}^2 + \frac{1}{6}\underline{\mathcal{A}}^3 + \cdots \\ &= \mathbb{I} + \underline{\mathcal{A}}. \end{aligned} \tag{8.61}$$

And we obtain the matrix:

$$\exp \underline{\mathcal{A}} = \begin{pmatrix} 1 & 0 & 0 & 0 & 0 & 0 & \hat{\alpha}_x i \\ 0 & 1 & 0 & 0 & 0 & 0 & \hat{\alpha}_y j \\ 0 & 0 & 1 & 0 & 0 & 0 & \hat{\alpha}_z k \\ 0 & -\hat{\alpha}_z k & \hat{\alpha}_y j & 1 & 0 & 0 & \hat{\gamma}_x i \\ \hat{\alpha}_z k & 0 & -\hat{\alpha}_x i & 0 & 1 & 0 & \hat{\gamma}_y j \\ -\hat{\alpha}_y j & \hat{\alpha}_x i & 0 & 0 & 0 & 1 & \hat{\gamma}_z k \\ 0 & 0 & 0 & 0 & 0 & 0 & 1 \end{pmatrix} \tag{8.62}$$

with $\hat{\alpha}_i = \frac{\alpha_i}{\sqrt{2}}$, $\hat{\gamma}_i = \frac{\gamma_i}{\sqrt{2}}, \in \mathbb{R}$. Thus, we have derived a matrix representation of the Vortex-Heisenberg Lie group. In order to apply this algebraic representations to atmospheric phenomena in the next chapter, we set

$$(\hat{\alpha}_x, \hat{\alpha}_y, \hat{\alpha}_z) \longrightarrow (a_x, a_y, a_z) \quad \text{and} \quad (\hat{\gamma}_x, \hat{\gamma}_y, \hat{\gamma}_z) \longrightarrow (A_x, A_y, A_z), \tag{8.63}$$

where $(A_x, A_y, A_z) = \mathbf{A}$ and $\mathbf{a} = (a_x, a_y, a_z)$. After the mathematical derivations of the vortex group we will outline our physical interpretation more in detail in section 8.5.

We summarize that each element of the Vortex-Heisenberg Lie group is given by a tuple $(\mathbf{a}, \mathbf{A})$. Furthermore, we can assign each element to a

matrix:

$$\boxed{(\mathbf{a},\mathbf{A}) = (a_x, a_y, a_z, A_x, A_y, A_z) \mapsto \begin{pmatrix} 1 & 0 & 0 & 0 & 0 & 0 & a_x i \\ 0 & 1 & 0 & 0 & 0 & 0 & a_y j \\ 0 & 0 & 1 & 0 & 0 & 0 & a_z k \\ 0 & -a_z k & a_y j & 1 & 0 & 0 & A_x i \\ a_z k & 0 & -a_x i & 0 & 1 & 0 & A_y j \\ -a_y j & a_x i & 0 & 0 & 0 & 1 & A_z k \\ 0 & 0 & 0 & 0 & 0 & 0 & 1 \end{pmatrix}}, \tag{8.64}$$

respectively,

$$\underline{\mathcal{A}} : VH \longrightarrow \mathrm{SL}(7,\mathbb{H}),\ (\mathbf{a},\mathbf{A}) \mapsto \underline{\mathcal{A}}((\mathbf{a},\mathbf{A})), \tag{8.65}$$

where SL is the set of special linear matrices (6.3). Therefore, we have derived a matrix representation for the Vortex-Heisenberg group VH(3). As we have outlined in fig. 8.2, we will show next how the vector representation of VH(3) can be derived from the Vortex-Heisenberg Lie algebra vh(3).

8.3.3 Derivation of the vector representation of VH(3)

After the introduction the matrix representation of the Vortex-Heisenberg group we again start from the Vortex-Heisenberg algebra to derive the group operation vie the Baker-Campbell-Hausdorff-formula (6.66). Let now $\underline{\mathcal{A}}, \underline{\mathcal{A}}'$ represent two elements of the Vortex-Heisenberg Lie algebra as in (8.57) :

$$\underline{\mathcal{A}} = \frac{1}{\sqrt{2}} \begin{pmatrix} 0 & 0 & 0 & 0 & 0 & 0 & \alpha_x i \\ 0 & 0 & 0 & 0 & 0 & 0 & \alpha_y j \\ 0 & 0 & 0 & 0 & 0 & 0 & \alpha_z k \\ 0 & -\alpha_z k & \alpha_y j & 0 & 0 & 0 & \gamma_x i \\ \alpha_z k & 0 & -\alpha_x i & 0 & 0 & 0 & \gamma_y j \\ -\alpha_y j & \alpha_x i & 0 & 0 & 0 & 0 & \gamma_z k \\ 0 & 0 & 0 & 0 & 0 & 0 & 0 \end{pmatrix} \tag{8.66}$$

and

$$\underline{\mathcal{A}}' = \frac{1}{\sqrt{2}} \begin{pmatrix} 0 & 0 & 0 & 0 & 0 & 0 & \alpha_x' i \\ 0 & 0 & 0 & 0 & 0 & 0 & \alpha_y' j \\ 0 & 0 & 0 & 0 & 0 & 0 & \alpha_z' k \\ 0 & -\alpha_z' k & \alpha_y j & 0 & 0 & 0 & \gamma_x' i \\ \alpha_z' k & 0 & -\alpha_x i & 0 & 0 & 0 & \gamma_y' j \\ -\alpha_y' j & \alpha_x i & 0 & 0 & 0 & 0 & \gamma_z' k \\ 0 & 0 & 0 & 0 & 0 & 0 & 0 \end{pmatrix}. \tag{8.67}$$

Since the Vortex-Heisenberg algebra is nilpotent we can apply the Baker-Campbell-Hausdorff-formula (6.66)

$$e^{\underline{\mathcal{A}}'} e^{\underline{\mathcal{A}}} = e^{\underline{\mathcal{A}}' + \underline{\mathcal{A}} + \frac{1}{2}[\underline{\mathcal{A}}', \underline{\mathcal{A}}]}. \tag{8.68}$$

Applying the matrix commutator (8.60) the exponent on the right hand side of (8.68) reads as:

$$\underline{\mathcal{A}}' + \underline{\mathcal{A}} + \frac{1}{2}[\underline{\mathcal{A}}', \underline{\mathcal{A}}] \tag{8.69}$$

Applying (8.67), (8.67) and the matrix commutator to (8.69) we obtain:

$$\underline{\mathcal{A}}' + \underline{\mathcal{A}} + \frac{1}{2}[\underline{\mathcal{A}}', \underline{\mathcal{A}}]$$

$$= \begin{pmatrix} 0 & 0 & 0 & 0 & 0 & 0 & (\hat{\alpha}_x' + \hat{\alpha}_x) i \\ 0 & 0 & 0 & 0 & 0 & 0 & (\hat{\alpha}_y' + \hat{\alpha}_y) j \\ 0 & 0 & 0 & 0 & 0 & 0 & (\hat{\alpha}_z' + \hat{\alpha}_z) k \\ 0 & (-\hat{\alpha}_z' - \hat{\alpha}_z) k & (\hat{\alpha}_y' + \hat{\alpha}_y) j & 0 & 0 & 0 & (\hat{\gamma}_x' + \hat{\gamma}_x + \frac{1}{2}(\hat{\alpha}_y' \cdot \hat{\alpha}_z - \hat{\alpha}_y \cdot \hat{\alpha}_z') i \\ (\hat{\alpha}_z' + \hat{\alpha}_z) k & 0 & (-\hat{\alpha}_x' - \hat{\alpha}_x) i & 0 & 0 & 0 & (\hat{\gamma}_y' + \hat{\gamma}_y + \frac{1}{2}(\hat{\alpha}_z' \cdot \hat{\alpha}_x - \hat{\alpha}_z \cdot \hat{\alpha}_i') j \\ (-\hat{\alpha}_y' - \hat{\alpha}_y) j & (\hat{\alpha}_x + \hat{\alpha}_x) i & 0 & 0 & 0 & 0 & (\hat{\gamma}_z' + \hat{\gamma}_z + \frac{1}{2}(\hat{\alpha}_x' \cdot \hat{\alpha}_y - \hat{\alpha}_x \cdot \hat{\alpha}_y') k \\ 0 & 0 & 0 & 0 & 0 & 0 & 0 \end{pmatrix}$$

with scaled $\hat{\alpha}_i = \frac{1}{\sqrt{2}}\alpha_i$ and $\hat{\gamma}_i = \frac{1}{\sqrt{2}}\gamma_i$, $i = x, y, z$. To obtain the vector representation of the group, we compare (8.66) with the above result of (8.69). We notice that the entries in the blue and red box add. For $k = x, y, z$ we obtain $\hat{\alpha}_k' + \hat{\alpha}_k$. In order to endow the group elements with a physical meaning, we set

$$\hat{\alpha}_k \longrightarrow a_k, \quad \text{and} \quad \hat{\alpha}_k' \longrightarrow r_k' \tag{8.70}$$

and define the vector $\mathbf{a}$ and $\mathbf{a}'$ as

$$\mathbf{a} = (a_x, a_y, a_z) \quad \text{and} \quad \mathbf{a}' = (a_x', a_y', a_z') \tag{8.71}$$

and summarize that the red and blue box reflect the sum $\mathbf{a}' + \mathbf{a}$. Now, we

regard the green box in (8.69) and set

$$\hat{\gamma}_k \longrightarrow A_k \quad \text{and} \quad \hat{\gamma}'_k \longrightarrow A'_k \tag{8.72}$$

Denoting

$$\mathbf{A} = (A_x, A_y, A_z) \quad \text{and} \quad \mathbf{A}' = (A'_x, A'_y, A'_z) \tag{8.73}$$

we can formulate the entries of the green boxed matrix as a vector composition:

$$\mathbf{A} + \mathbf{A}' + \frac{1}{2}\,\mathbf{a} \times \mathbf{a}'. \tag{8.74}$$

Thus, comparing 8.66 with 8.69 and using the notations and leads to the following Vortex-Heisenberg group operation:

$$\boxed{(\mathbf{a}, \mathbf{A}) * (\mathbf{a}', \mathbf{A}') = \left(\mathbf{a} + \mathbf{a}', \mathbf{A} + \mathbf{A}' + \frac{1}{2}\,\mathbf{a} \times \mathbf{a}'\right).} \tag{8.75}$$

We will discuss the physical meaning of the vectors $\mathbf{a}$ and $\mathbf{A}$ in section 8.5. We will interpret $\mathbf{a}$ as a displacement vector and $\mathbf{A}$ as an vector that is related to the area enclosed by a vortex. Finally, we have to prove that the set $M = \{(\mathbf{a}, \mathbf{A}) \mid \mathbf{a}, \mathbf{A} \in \mathbb{R}^3\}$ together with (8.75) is indeed group, the Vortex-Heisenberg group. Therefore, it needs to satisfy the group properties: we have to show the existence of the identity and the inverse element and that the associativity holds.

Claim 2. The identity element of the VH(3) is given by $e = (\mathbf{0}, \mathbf{0}) \in \mathbb{R}^6$ which corresponds to the unit matrix considering the matrix Lie group representation.

Proof. Let $g = (\mathbf{a}, \mathbf{A})$ an arbitrary element in VHG. Applying (8.75) it is:

$$\begin{aligned} e * g = (\mathbf{0}, \mathbf{0}) * (\mathbf{a}, \mathbf{A}) &= (\mathbf{0} + \mathbf{a}, \mathbf{0} + \mathbf{A} + \mathbf{a} \times \mathbf{0}) = (\mathbf{a}, \mathbf{A}) = g \\ &= (\mathbf{a}, \mathbf{A}) * (\mathbf{0}, \mathbf{0}) = g * e \end{aligned}$$

or, in terms of the above matrix representation $\underline{\mathcal{A}}((a_x, a_y, a_z, A_x A_y, A_z))$, it is:

$$\begin{aligned} \underline{\mathcal{A}}(a_x, a_y, a_z, A_x A_y, A_z)\underline{\mathcal{A}}(0,0,0,0,0,0) &= \underline{\mathcal{A}}((a_x, a_y, a_z, A_x A_y, A_z)) \\ &= \underline{\mathcal{A}}(0,0,0,0,0,0)\underline{\mathcal{A}}((a_x, a_y, a_z, A_x A_y, A_z)) \end{aligned} \tag{8.76}$$

$$\Longleftrightarrow \begin{pmatrix} 1 & 0 & 0 & 0 & 0 & 0 & a_x i \\ 0 & 1 & 0 & 0 & 0 & 0 & a_y j \\ 0 & 0 & 1 & 0 & 0 & 0 & a_z k \\ 0 & -a_z k & a_y j & 1 & 0 & 0 & A_x i \\ a_z k & 0 & -a_x i & 0 & 1 & 0 & A_y j \\ -a_y j & a_x i & 0 & 0 & 0 & 1 & A_z k \\ 0 & 0 & 0 & 0 & 0 & 0 & 1 \end{pmatrix} \begin{pmatrix} 1 & 0 & 0 & 0 & 0 & 0 & 0 \\ 0 & 1 & 0 & 0 & 0 & 0 & 0 \\ 0 & 0 & 1 & 0 & 0 & 0 & 0 \\ 0 & 0 & 0 & 1 & 0 & 0 & 0 \\ 0 & 0 & 0 & 0 & 1 & 0 & 0 \\ 0 & 0 & 0 & 0 & 0 & 1 & 0 \\ 0 & 0 & 0 & 0 & 0 & 0 & 1 \end{pmatrix}$$

$$= \begin{pmatrix} 1 & 0 & 0 & 0 & 0 & 0 & a_x i \\ 0 & 1 & 0 & 0 & 0 & 0 & a_y j \\ 0 & 0 & 1 & 0 & 0 & 0 & a_z k \\ 0 & -a_z k & a_y j & 1 & 0 & 0 & A_x i \\ a_z k & 0 & -a_x i & 0 & 1 & 0 & A_y j \\ -a_y j & a_x i & 0 & 0 & 0 & 1 & A_z k \\ 0 & 0 & 0 & 0 & 0 & 0 & 1 \end{pmatrix}$$

$$= \begin{pmatrix} 1 & 0 & 0 & 0 & 0 & 0 & 0 \\ 0 & 1 & 0 & 0 & 0 & 0 & 0 \\ 0 & 0 & 1 & 0 & 0 & 0 & 0 \\ 0 & 0 & 0 & 1 & 0 & 0 & 0 \\ 0 & 0 & 0 & 0 & 1 & 0 & 0 \\ 0 & 0 & 0 & 0 & 0 & 1 & 0 \\ 0 & 0 & 0 & 0 & 0 & 0 & 1 \end{pmatrix} \begin{pmatrix} 1 & 0 & 0 & 0 & 0 & 0 & a_x i \\ 0 & 1 & 0 & 0 & 0 & 0 & a_y j \\ 0 & 0 & 1 & 0 & 0 & 0 & a_z k \\ 0 & -a_z k & a_y j & 1 & 0 & 0 & A_x i \\ a_z k & 0 & -a_x i & 0 & 1 & 0 & A_y j \\ -a_y j & a_x i & 0 & 0 & 0 & 1 & A_z k \\ 0 & 0 & 0 & 0 & 0 & 0 & 1 \end{pmatrix}$$

□

Claim 3. Let now $g = (\mathbf{a}, \mathbf{A})$ an arbitrary element in VHG. Then, the inverse element $g^{-1} \in$VHG is given by:

$$g^{-1} = (-\mathbf{a}, -\mathbf{A}) \tag{8.77}$$

Furthermore, it is a left and a right inverse element. Moreover, the associative property holds.

Proof. Inserting the stated inverse element into the group operation, we obtain:

$$g * g^{-1} = (\mathbf{a} - \mathbf{a}, \mathbf{A} - \mathbf{A} - \mathbf{a} \times \mathbf{a}) = e = g^{-1} * g \tag{8.78}$$

Moreover, we now use the fact that we can assign each state to a matrix. The group operation is associative, because the matrix multiplication of a squared matrix is always associative. Therefore, we have shown that $(\mathrm{VH}(3), *)$ is a group. □

Claim 4. The map $\underline{\mathcal{A}} : \mathrm{VH} \longrightarrow GL$ is a group homomorphism, i.e.

$$\underline{\mathcal{A}}(g' * g) = \underline{\mathcal{A}}(g') \cdot \underline{\mathcal{A}}(g) \quad \forall g', g \in \mathrm{VH} \tag{8.79}$$

Proof. Let $g', g \in$VH(3) with $g' = (\mathbf{a}', \mathbf{A}')$ and $g := (\mathbf{a}, \mathbf{A})$. Applying (8.75) we obtain:

$$\underline{\mathcal{A}}(g' * g) = \begin{pmatrix} 1 & 0 & 0 & 0 & 0 & 0 & (a'_x + a_x)i \\ 0 & 1 & 0 & 0 & 0 & 0 & (a'_y + a_y)j \\ 0 & 0 & 1 & 0 & 0 & 0 & (a'_z + a_z)k \\ 0 & -(a'_z + a_z)k & (a'_y + a_y)j & 1 & 0 & 0 & (A'_x + A_x + \frac{1}{2}(a'_y a_z - a_y a'_z))i \\ (a'_z + a_z)k & 0 & -(a'_x + a_x)i & 0 & 1 & 0 & (A'_y + A_y + \frac{1}{2}(a'_z a_x - a_z a'_x))j \\ -(a'_y + a_y)j & (a'_x + a_x)i & 0 & 0 & 0 & 1 & (A'_z + A_z + \frac{1}{2}(a'_x a_y - a_x a'_y))k \\ 0 & 0 & 0 & 0 & 0 & 0 & 1 \end{pmatrix} \tag{8.80}$$

$$= \underline{\mathcal{A}}(g') \cdot \underline{\mathcal{A}}(g) \tag{8.81}$$

Furthermore it is

$$\underline{\mathcal{A}}(e) = \begin{pmatrix} 1 & & \\ & \ddots & \\ & & 1 \end{pmatrix}. \tag{8.82}$$

Because of (8.81) and (8.82) the map A is a group homomorphism and therefore a representation of the Vortex-Heisenberg-group VH(3). □

Proposition 1. Let M be a $(n \times n)$ matrix with $\lim_{k\to\infty}(\mathbb{I}_n - M)^k = 0$. Then, M is regular and the inverse Matrix of M is given by:

$$M^{-1} = \sum_{k=0}^{\infty} (\mathbb{I}_n - M)^k \tag{8.83}$$

Claim 5. Let A the above matrix representation of the VH(3). A satisfies:

$$\underline{\mathcal{A}}(g^{-1}) = \underline{\mathcal{A}}^{-1}(g) \tag{8.84}$$

Proof. (of the claim)
Applying proposition 1, since

$$(\mathbb{I}_7 - \underline{\mathcal{A}})^2 = 0 \tag{8.85}$$

The matrix $\underline{\mathcal{A}}$ is regular and its determinant is one. Let now $g \in$ VH(3). It is

$$\underline{\mathcal{A}}^{-1}(g) = \sum_{k=0}^{\infty} (\mathbb{I}_7 - \underline{\mathcal{A}})^k = (\mathbb{I}_7 - \underline{\mathcal{A}})^0 + (\mathbb{I}_7 - \underline{\mathcal{A}})^1 + 0 + 0 + \dots$$

$$= \begin{pmatrix} 1 & 0 & 0 & 0 & 0 & 0 & 0 \\ 0 & 1 & 0 & 0 & 0 & 0 & 0 \\ 0 & 0 & 1 & 0 & 0 & 0 & 0 \\ 0 & 0 & 0 & 1 & 0 & 0 & 0 \\ 0 & 0 & 0 & 0 & 1 & 0 & 0 \\ 0 & 0 & 0 & 0 & 0 & 1 & 0 \\ 0 & 0 & 0 & 0 & 0 & 0 & 1 \end{pmatrix} - \begin{pmatrix} 0 & 0 & 0 & 0 & 0 & 0 & a_x i \\ 0 & 0 & 0 & 0 & 0 & 0 & a_y j \\ 0 & 0 & 0 & 0 & 0 & 0 & a_z k \\ 0 & -a_z k & a_y j & 0 & 0 & 0 & A_x i \\ a_z k & 0 & -a_x i & 0 & 0 & 0 & A_y j \\ -a_y j & a_x i & 0 & 0 & 0 & 0 & A_z k \\ 0 & 0 & 0 & 0 & 0 & 0 & 0 \end{pmatrix} \tag{8.86}$$

$$= \begin{pmatrix} 1 & 0 & 0 & 0 & 0 & 0 & -a_x i \\ 0 & 1 & 0 & 0 & 0 & 0 & -a_y j \\ 0 & 0 & 1 & 0 & 0 & 0 & -a_z k \\ 0 & +a_z k & -a_y j & 1 & 0 & 0 & -A_x i \\ -a_z k & 0 & +a_x i & 0 & 1 & 0 & -A_y j \\ +a_y j & +a_x i & 0 & 0 & 0 & 1 & -A_z k \\ 0 & 0 & 0 & 0 & 0 & 0 & 1 \end{pmatrix} = \underline{\mathcal{A}}(g^{-1}) \tag{8.87}$$

□

Thus, we have derived a vector and a matrix representation of the Vortex-Heisenberg group VH(3) for three-dimensional incompressible, inviscid vortex dynamics. In the next section we will extend this group by rigid-body rotations SO(3).

8.4 The Helmholtz Vortex Lie group V(3)

In this section we will generalize the Vortex-Heisenberg Lie group VH(3) and include the angular momentum. Thus, the novel group will contain the circulation as a rotational part as well as rigid-body rotations about a given angle. In chapter 9, we will first apply the Vortex-Heisenberg group VH(3) to explain the mechanism of split of storms and at the end, we will show how the extended group can be applied to show the existence of further splits.

We will call the extension of the Vortex-Heisenberg Lie group Helmholtz Vortex group, because it is based on Helmholtz' vorticity equation. We can formulate the Helmholtz Vortex group that we will denote V(3) as semidirect product of the special orthogonal group SO(3) and the Vortex-Heisenberg group VH(3):

$$\mathrm{V}(3) = \mathrm{SO}(3) \ltimes \mathrm{VH}(3). \tag{8.88}$$

where, considering the definition of semidirect products (6.27), the corresponding homomorphism $\varphi : VH(3) \to V(3)$ is given by $x \mapsto \underline{\mathbf{R}}x$, where $\underline{\mathbf{R}}$ denotes a rotation matrix and is an element in SO(3). But, when we include the angular momentum, i.e. the Euclidean rotation represented by SO(3) (see (6.5)), we lose the nilpotency. Therefore, the Helmholtz Vortex group does not have the typical Heisenberg group structure. We will first introduce the novel group and then show that it satisfies the group properties.

The Helmholtz Vortex group is given by the set

$$V(3) = \{(\mathbf{a}, \mathbf{A}, \underline{\mathbf{R}}) \mid \mathbf{a}, \mathbf{A} \in \mathbb{R}^3,\ \underline{\mathbf{R}} \in SO(3)\} \tag{8.89}$$

together with the following group operation:

$$(\mathbf{a}, \mathbf{A}, \underline{\mathbf{R}}) * (\mathbf{a}', \mathbf{A}', \underline{\mathbf{R}}') = \left(\mathbf{a} + \underline{\mathbf{R}}\mathbf{a}', \pm\frac{1}{2}\mathbf{a} \times \underline{\mathbf{R}}'\mathbf{a} + \mathbf{A} + \underline{\mathbf{R}}\mathbf{A}', \underline{\mathbf{R}}\underline{\mathbf{R}}'\right) \tag{8.90}$$

for $\mathbf{a}, \mathbf{a}', \mathbf{A}, \mathbf{A}' \in \mathbb{R}^3$ and $\underline{\mathbf{R}}, \underline{\mathbf{R}}' \in SO(3)$. By extending the Vortex-Heisenberg group by the angular momentum, i.e. including rigid body rotations expressed by rotation matrices $\mathbf{R} \in$ SO(3), the Helmholtz Vortex group is a nine-dimensional group. Noting that we obtain two group operations with a non-trivial plus-minus sign in front of the cross product, we can distinguish between these operation by defining $V^+(3)$ and $V^-(3)$ with respect to

the different signs in (8.90).

$$
\begin{aligned}
V^{+}(3): \quad & (\mathbf{a}, \mathbf{A}, \underline{\mathbf{R}}) * (\mathbf{a}', \mathbf{A}', \underline{\mathbf{R}}') = \left(\mathbf{a} + \underline{\mathbf{R}}\mathbf{a}', +\frac{1}{2}\mathbf{a} \times \underline{\mathbf{R}}'\mathbf{a} + \mathbf{A} + \underline{\mathbf{R}}\mathbf{A}', \underline{\mathbf{R}}\underline{\mathbf{R}}' \right) \\
V^{-}(3): \quad & (\mathbf{a}, \mathbf{A}, \underline{\mathbf{R}}) * (\mathbf{a}', \mathbf{A}', \underline{\mathbf{R}}') = \left(\mathbf{a} + \underline{\mathbf{R}}\mathbf{a}', -\frac{1}{2}\mathbf{a} \times \underline{\mathbf{R}}'\mathbf{a} + \mathbf{A} + \underline{\mathbf{R}}\mathbf{A}', \underline{\mathbf{R}}\underline{\mathbf{R}}' \right)
\end{aligned}
\tag{8.91}
$$

The terms of the rigid body rotations in the Helmholtz Vortex group operation (8.91) are similar embedded as in the group operation of the three-dimensional Euclidean group that we have discussed in chapter 6, example 2. The Helmholtz Vortex group has an identity element, an inverse element and its group operation does satisfy the associative property.

Claim 6. The identity and inverse elements of $(\mathbf{a}, \mathbf{A}, \underline{\mathbf{R}})$ of $V^{+}(3)$ and $V^{-}(3)$ are given by

$$
\begin{aligned}
\text{Identity element:} \quad & (\mathbf{0}, \mathbf{0}, \mathbb{E}) \\
\text{Right and left inverse elements:} \quad & \left(-R^{-1}\mathbf{a}, -\underline{\mathbf{R}}^{-1}\mathbf{A}, \underline{\mathbf{R}}^{-1} \right)
\end{aligned}
\tag{8.92}
$$

where $\mathbb{E}$ denotes the unit matrix. Moreover, the associate property holds.

Proof. We show that there is an identity element $(0, 0, \mathbb{E})$:

$$
\begin{aligned}
& (\mathbf{a}, \mathbf{A}, \underline{\mathbf{R}}) * (0, 0, \mathbb{E}) = (\mathbf{a}, \mathbf{A}, \underline{\mathbf{R}}) \\
& (0, 0, \mathbb{E}) * (\mathbf{a}, \mathbf{A}, \underline{\mathbf{R}}) = (\mathbb{E}\,\mathbf{a}, \mathbb{E}\,\mathbf{A}, \underline{\mathbf{R}}) = (\mathbf{a}, \mathbf{A}, \underline{\mathbf{R}})
\end{aligned}
\tag{8.93}
$$

and the existence of the inverse elements $\left(-R^{-1}\mathbf{a}, -\underline{\mathbf{R}}^{-1}\mathbf{A}, \underline{\mathbf{R}}^{-1} \right)$:

$$
\begin{aligned}
& (\mathbf{a}, \mathbf{A}, \underline{\mathbf{R}}) * \left(-\underline{\mathbf{R}}^{-1}\mathbf{a}, -\underline{\mathbf{R}}^{-1}\mathbf{A}, \underline{\mathbf{R}}^{-1} \right) \\
& \qquad = (\mathbf{a} - \underline{\mathbf{R}}\underline{\mathbf{R}}^{-1}\mathbf{a}, \pm\frac{1}{2}\mathbf{a} \times (-\underline{\mathbf{R}}\underline{\mathbf{R}}^{-1}\mathbf{a}) + \mathbf{A} - \underline{\mathbf{R}}\underline{\mathbf{R}}^{-1}\mathbf{A}, \underline{\mathbf{R}}\underline{\mathbf{R}}^{-1}) \\
& \qquad = (0, 0, \mathbb{E})
\end{aligned}
\tag{8.94}
$$

and

$$\begin{aligned}
&\left(-\underline{\mathbf{R}}^{-1}\mathbf{a}, -\underline{\mathbf{R}}^{-1}\mathbf{A}, \underline{\mathbf{R}}^{-1}\right) * (\mathbf{a}, \mathbf{A}, \underline{\mathbf{R}}) \\
&= (-\underline{\mathbf{R}}^{-1}\mathbf{a} + \underline{\mathbf{R}}^{-1}\mathbf{a}, \pm\frac{1}{2}(-\underline{\mathbf{R}}^{-1}\mathbf{a}) \times \underline{\mathbf{R}}^{-1}\mathbf{a} - \underline{\mathbf{R}}^{-1}\mathbf{A} + \underline{\mathbf{R}}^{-1}A, \underline{\mathbf{R}}^{-1}\underline{\mathbf{R}}) \\
&= (0, 0, \mathbb{E})
\end{aligned} \tag{8.95}$$

Further, we need to prove the associative property of the group operation. Let $(\mathbf{a}, \mathbf{A}, \underline{\mathbf{R}})$, $(\mathbf{a}', \mathbf{A}', \underline{\mathbf{R}}')$ and $(\mathbf{a}'', \mathbf{A}'', \underline{\mathbf{R}}'')$ elements in Helmholtz Vortex group.

$$\begin{aligned}
&(\mathbf{a}'', \mathbf{A}'', \underline{\mathbf{R}}'') * [(\mathbf{a}', \mathbf{A}', \underline{\mathbf{R}}') * (\mathbf{a}, \mathbf{A}, \underline{\mathbf{R}})] \\
&= (\mathbf{a}'', \mathbf{A}'', \underline{\mathbf{R}}'') * \left(\mathbf{a} + \underline{\mathbf{R}}\mathbf{a}', \pm\frac{1}{2}\mathbf{a} \times \underline{\mathbf{R}}'\mathbf{a}' + \mathbf{A} + \underline{\mathbf{R}}\mathbf{A}', \underline{\mathbf{R}}\underline{\mathbf{R}}'\right) \\
&= (\underline{\mathbf{R}}\underline{\mathbf{R}}'\mathbf{a}'' + \underline{\mathbf{R}}\mathbf{a}' + \mathbf{a}, \pm\frac{1}{2}(\mathbf{a} + \underline{\mathbf{R}}\mathbf{a}') \times \mathbf{a}'') \pm \frac{1}{2}\mathbf{a} \times \underline{\mathbf{R}}\mathbf{a}' + \mathbf{A} + \underline{\mathbf{R}}\mathbf{A}' + \underline{\mathbf{R}}\underline{\mathbf{R}}'\mathbf{A}'', \\
&\quad \underline{\mathbf{R}}''\underline{\mathbf{R}}'\underline{\mathbf{R}}) \\
&= (\underline{\mathbf{R}}\underline{\mathbf{R}}'\mathbf{a}'' + \underline{\mathbf{R}}\mathbf{a}' + \mathbf{a}, \pm\frac{1}{2}(\mathbf{a} \times \underline{\mathbf{R}}\underline{\mathbf{R}}'\mathbf{a}'' + \underline{\mathbf{R}}\mathbf{a}' \times \underline{\mathbf{R}}'\underline{\mathbf{R}}\mathbf{a}'' + \mathbf{a} \times \underline{\mathbf{R}}\mathbf{a}') \\
&\quad + \mathbf{A} + \underline{\mathbf{R}}\mathbf{A}' + \underline{\mathbf{R}}\underline{\mathbf{R}}'\mathbf{A}'', \quad \underline{\mathbf{R}}''\underline{\mathbf{R}}'\underline{\mathbf{R}})
\end{aligned} \tag{8.96}$$

In the last step we applied $\underline{\mathbf{R}}\mathbf{a} \times \underline{\mathbf{R}}\mathbf{b} = \underline{\mathbf{R}}(\mathbf{a} \times \mathbf{b})$ which holds for $\mathbf{a}, \mathbf{b} \in \mathbb{R}^3$, $\underline{\mathbf{R}} \in SO(3)$. To satisfy the associate property last equation has to be equal to the following expression:

$$\begin{aligned}
&[(\mathbf{a}'', \mathbf{A}'', \underline{\mathbf{R}}'') * (\mathbf{a}', \mathbf{A}', \underline{\mathbf{R}}')] * (\mathbf{a}, \mathbf{A}, \underline{\mathbf{R}}) \\
&= (\underline{\mathbf{R}}\underline{\mathbf{R}}'\mathbf{a}'' + \underline{\mathbf{R}}\mathbf{a}' + \mathbf{a}, \pm\frac{1}{2}(\mathbf{a} \times \underline{\mathbf{R}}\underline{\mathbf{R}}'\mathbf{a}'' + \underline{\mathbf{R}}\mathbf{a}' \times \underline{\mathbf{R}}'\underline{\mathbf{R}}\mathbf{a}'' + \mathbf{a} \times \underline{\mathbf{R}}\mathbf{a}') \\
&\quad + \mathbf{A} + \underline{\mathbf{R}}\mathbf{A}' + \underline{\mathbf{R}}\underline{\mathbf{R}}'\mathbf{A}'', \quad \underline{\mathbf{R}}''\underline{\mathbf{R}}'\underline{\mathbf{R}})
\end{aligned} \tag{8.97}$$

The associative law is satisfied, because (8.97) = (8.96). Therefore, $V^+(3)$ as well as $V^-(3)$ with the operation defined in (8.90) satisfy all group properties. □

8.4.1 Embedding VH(3) in V(3)

The Vortex-Heisenberg group can be embedded in Helmholtz Vortex group, which can be seen by considering the neutral element of SO(3), i.e. the identity $\mathbb{E}$:

$$\boxed{(\mathbf{a}, \mathbf{A}) \cong (\mathbf{a}, \mathbf{A}, \mathbb{E}) \subset (\mathbf{a}, \mathbf{A}, \underline{\mathbf{R}})} \tag{8.98}$$

Thus, Helmholtz Vortex group can be seen as generalization of the previously discussed Vortex-Heisenberg group. And therefore, we see that the previously discussed VH(3) can also be extended by the group operation with the minus sign in front of the cross product:

$$VH(3): \quad (\mathbf{a}', \mathbf{A}') * (\mathbf{a}, \mathbf{A}) = \left(\mathbf{a}' + \mathbf{a}, \mathbf{A}' + \mathbf{A} + \frac{1}{2}\mathbf{a} \times \mathbf{a}'\right) \tag{8.99}$$

and

$$VH(3)^{-}: \quad (\mathbf{a}', \mathbf{A}') * (\mathbf{a}, \mathbf{A}) = \left(\mathbf{a}' + \mathbf{a}, \mathbf{A}' + \mathbf{A} - \frac{1}{2}\mathbf{a} \times \mathbf{a}'\right) \tag{8.100}$$

The group properties for $VH(2)^{-}$ are also satisfied since it is embedded in $V^{-}(3)$. Moreover, the groups for two-dimensional vortex dynamics VH(2) can analogously be extended by the planar rotations SO(2).

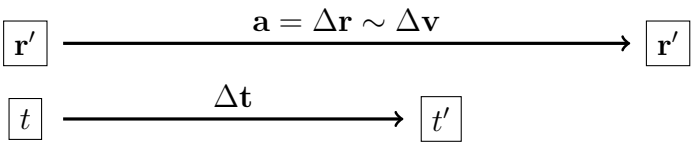

Figure 8.3: Consider the motion of an particle in a time frame Δt. During this time frame, the particle is locally displaced by $\mathbf{a} = \Delta\mathbf{r}$. If the velocity becomes larger, the displacement $\mathbf{a} = \Delta\mathbf{r}$ is larger, too.

8.5 Physical interpretation

So far, we considered the Vortex-Heisenberg group elements as pairs $(\mathbf{a}, A)$ with $\mathbf{a} = (a_x, a_y)$ and $A \in \mathbb{R}$ for 2D inviscid, incompressible vortex dynamics, respectively $(\mathbf{a}, \mathbf{A})$ with $\mathbf{a} = (a_x, a_y, a_z)$ and $\mathbf{A} = (A_x, A_y, A_z)$ for 3D inviscid, incompressible vortex dynamics. Moreover, we introduced the Helmholtz Vortex group, where the group elements are given by the triples $(\mathbf{a}, \mathbf{A}, \underline{\mathbf{R}})$, where $\mathbf{a} = (a_x, a_y, a_z)$, $\mathbf{A} = (A_1, A_2, A_3)$ and $\underline{\mathbf{R}} \in SO(3)$. The choice of these notations is based on the underlying physical interpretation of the group. The rotational matrix $\underline{\mathbf{R}} \in$ SO(3) describes rigid-body rotations about a given angle, but how can we interpret the tuple $(\mathbf{a},\ \mathbf{A})$?

8.5.1 Two dimensional vortex dynamics

In two dimensions, $\Delta\mathbf{v}$ and $\Delta\zeta$ describe small spatial local changes of the two-dimensional velocity vector $\mathbf{v}$ and the vorticity ζ. As corresponding group elements we consider the pair $(\mathbf{a}, A)$ with $\mathbf{a} = (a_x, a_y)$ and $A \in \mathbb{R}$. This notation is chosen analogously to the notation for classical mechanics discussed in Sudarshan and Mukunda (1974). We recall the zonal and meridional momentum with respect to the vorticity ζ:

$$P_x[\zeta] = \int_F df\ \zeta y, \quad P_y[\zeta] = -\int_F df\ \zeta x. \tag{8.101}$$

Now, assume infinitesimal area elements of the momentum (8.101). Similar to the approach of Sudarshan and Mukunda (1974), we propose the following notation of the group elements:

$$\begin{array}{ccccc} \text{algebra} & & & & \text{group} \\ \mathbf{v}_x & \longrightarrow & \exp((\zeta\ y \cdot a_x)^*) & \longrightarrow & a_x = x - x' \\ \mathbf{v}_y & \longrightarrow & \exp((-\zeta x \cdot a_y)^*) & \longrightarrow & a_y = y - y' \\ \zeta & \longrightarrow & \exp((\zeta \cdot A)^*) & \longrightarrow & A = F - F' \end{array} \tag{8.102}$$

where the asteriks denotes the scaling one over the action to obtain dimensionless exponents. Consider a state change. For example, let a state be characterized by a vortex that encloses a large area F. And consider a second state characterized by a vortex with a smaller enclosed area F'. The scalar quantity A denotes the change of the area element $\Delta F = F - F'$. And the vector $\mathbf{a} = (a_x, a_y)$ represents the displacement $a_x = \Delta x = x - x'$ and $a_y = \Delta y = y - y'$.

8.5.2 Three dimensional vortex dynamics

In three dimensional vortex dynamics, the elements of the Vortex-Heisenberg group are given by the tuple $(\mathbf{a}, \mathbf{A})$, where $\mathbf{a} = (a_x, a_y, a_z)$ and $\mathbf{A} = (A_x, A_y, A_z)$. As for two dimensional vortex dynamics, we interpret the physical meaning of the group elements analogously to classical mechanics suggested by Sudarshan and Mukunda (1974). For incompressible 3D vortex dynamics, the momentum is given by:

$$\mathbf{P} = \int_V d\tau \; \mathbf{v} = \frac{1}{2} \int_V d\tau \; (\mathbf{r} \times \boldsymbol{\xi}) \tag{8.103}$$

and the flux of vorticity reads as:

$$\mathbf{Z} = \int_V d\tau \; \boldsymbol{\xi}. \tag{8.104}$$

Now, we assume small volume elements of the momentum and the flux of vorticity leading to the following physical interpretations for the Vortex-Heisenberg algebra and for the Vortex-Heisenberg group:

$$\begin{array}{lcccl} \text{algebra} & & & & \text{group} \\ \mathbf{v} & \longrightarrow & \exp\left(\left(\frac{1}{2}(\mathbf{r} \times \boldsymbol{\xi}) \cdot \mathbf{a}\right)^*\right) & \longrightarrow & \mathbf{a} = \mathbf{r} - \mathbf{r}' \\ \boldsymbol{\xi} & \longrightarrow & \exp((\boldsymbol{\xi} \cdot \mathbf{A})^*) & \longrightarrow & \mathbf{A} = \mathbf{F} - \mathbf{F}', \end{array} \tag{8.105}$$

where the asteriks in the exponent denotes the scaling by one over the action to obtain dimensionless exponents.

Three idealized, infinitesimal vortex tubes are sketched in fig. 8.4. The vector $\mathbf{A} = |\Delta F| \cdot \mathbf{n}$ denotes the change of the area F with respect to the direction of the outer normal vector $\mathbf{n}$. The Pirouette effect is sketched, too. Consider a infinitesimal vortex tube (middle) enclosing a given area. For

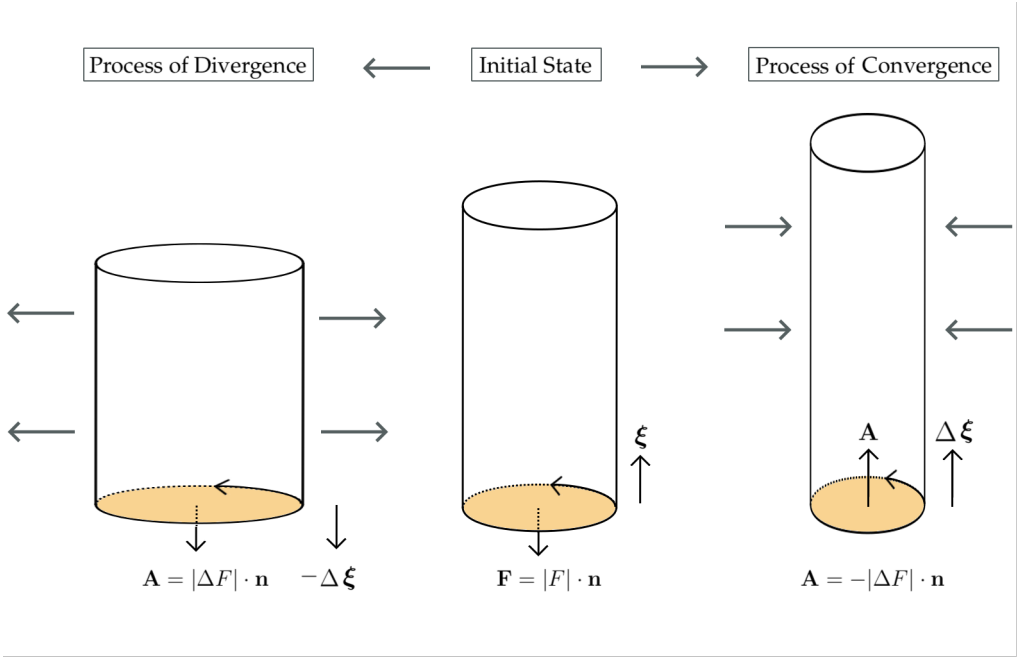

Figure 8.4: Infinitesimal vortex tubes are sketched. The 3D vorticity vector is parallel to the vortex tube and $\mathbf{A}$ denotes the change of the area marked in orange.

the processes of divergence, the radius of the vortex tube enlarges (l.h.s.). Thus, $\mathbf{A}$ points downwards. On the other hand, for the processes of convergence, the vortex tube becomes smaller such that $\mathbf{A}$ changes it sign (r.h.s.) and points into the inner of the vortex tube. The vector $\mathbf{A}$ is now parallel to $\Delta\boldsymbol{\xi}$. We recall that the vector $\mathbf{v}$ is the velocity tangent to the vortex tube and related to the momentum. Thus, $\mathbf{v}$ is associated with the vector $\mathbf{a}$, which denotes the displacement tangent to the vortex tube $\mathbf{a} = \Delta\mathbf{r}$, see fig. 8.3 and fig. 8.5. For a small vortex tube characterized by strong helical rotation, the vectors $\mathbf{v}$ and $\boldsymbol{\xi}$ (algebra), respectively $\mathbf{a}$ and $\mathbf{A}$ (group), become parallel such that their scalar product increases. It follows that the helicity density $h = \frac{1}{2}\mathbf{v} \cdot \boldsymbol{\xi}$ increases and is maximal if $\mathbf{v} \parallel \boldsymbol{\xi}$. This concept can be transferred to the group theoretical point of view:

$$h = \frac{1}{2}\mathbf{v} \cdot \boldsymbol{\xi} \rightarrow \frac{1}{2}\mathbf{a} \cdot \mathbf{A}. \tag{8.106}$$

The helicity changes its sign if the orientation of the rotation changes. Thus, the sign depends on the orientation of the system, whether it is a left-handed or a right-handed system, which is reflected in both representations of the helicity. The notation of the enstrophy can also be transferred to the

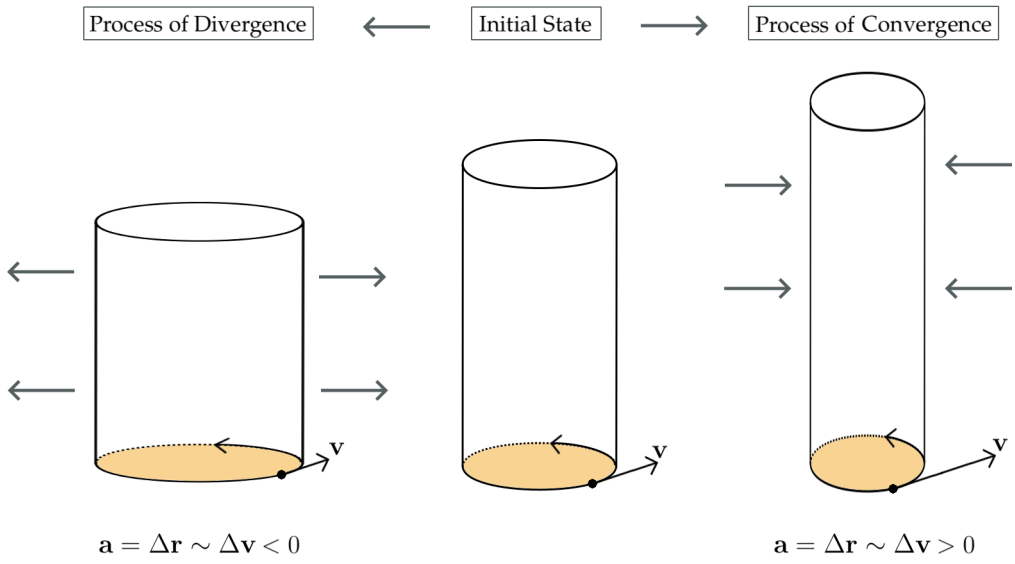

Figure 8.5: Infinitesimal vortex tubes are sketched. Consider the initial state (middle). If the velocity becomes larger, i.e. $\Delta\mathbf{v} > 0$, the displacement $\mathbf{a} = \Delta\mathbf{r}$ is larger than zero. If the velocity becomes slower, i.e. $\Delta\mathbf{v} < 0$ it is $\mathbf{a} = \Delta\mathbf{r} < 0$. Thus, the displacement is proportional to the change of the velocity.

group theoretical point of view:

$$\text{(algebra)} \quad \frac{1}{2}\mathbf{v}^2 \rightarrow \frac{1}{2}\mathbf{a}^2 \quad \text{(group)}. \tag{8.107}$$

The notations, the physical meaning, and the mathematical characterization of the basic quantities are summarized in table 8.1.

We consider group elements as local quantities describing the state of a subregion of a fluid - an infinitesimal vortex tube of finite lengths. In chapter 7, section 7.3.1, we have discussed the law of Biot-Savart, which can also be related to our group theoretical representation of vortex flows. While the Bio-Savart law provides the velocity induced at a given point, the group theoretical approach yields a description of the change of the velocity expressed by the displacement $\Delta\mathbf{r} = \mathbf{a}$. The group composition itself can be regarded as the change of a state. In the next chapter, we will use this concept and assign VH(3)-group elements to different meteorological wind fields such as shearing flows and tornados. By analyzing the corresponding group operation, we will discuss the conditions on the wind fields that lead to splitting storms. Moreover, we will also see the benefits of the additional rigid body rotation in the Helmholtz Vortex group and discuss one example of a splitting storm regarding this novel Helmholtz Vortex group.

Physical meaning	**Mathematical characterization**	**Lie algebra vh(3)**		**Lie group VH(3)**
Velocity	vector	$\mathbf{v}$	$\longrightarrow$	$\mathbf{a}$
Vorticity	pseudo-vector	$\boldsymbol{\xi}$	$\longrightarrow$	$\mathbf{A}$
Helicity density	pseudo-scalar	$\frac{1}{2}\mathbf{v}\cdot\boldsymbol{\xi}$	$\longrightarrow$	$\frac{1}{2}\mathbf{a}\cdot\mathbf{A}$
Enstrophy density	scalar	$\frac{1}{2}\boldsymbol{\xi}^2$	$\longrightarrow$	$\frac{1}{2}\mathbf{A}^2$
Kinetic energy density	scalar	$\frac{1}{2}\mathbf{v}^2$	$\longrightarrow$	$\frac{1}{2}\mathbf{a}^2$

Table 8.1: The physical meaning and the mathematical characterization as well as the notations of the algebra and group are summarized.

8.6 Summary

Starting with an introduction to continuous Nambu mechanics, we have shown a derivation of the Vortex-Heisenberg group for two- and three-dimensional fluid dynamics. Thereby, we introduced a matrix representation of the Vortex-Heisenberg Lie algebra which lead to a matrix as well as a vector representation of the Vortex-Heisenberg group. Moreover, we introduced the Helmholtz Vortex group, in which the Vortex-Heisenberg group is embedded. From the physical point of view we included the angular momentum to capture two different kinds of rotations: the flux of vorticity and the rigid body rotation about a given angle. We are now well prepared to apply this group to splitting storms.

Chapter 9

Splitting storms: An alternative explanation

In this chapter we will apply the Vortex-Heisenberg group VH(3) and the Helmholtz Vortex group V(3) that we have derived in the last chapter to give an alternative, novel explanation of vortex splits. We will transfer the abstract, mathematical concept of group elements and group operations to different, typical atmospheric wind fields and their interaction. Then, we will propose initial conditions for vortex splits and discuss our assumptions by analyzing the helicity density fields of five case studies.

This algebraic approach also leads to an alternative perspective on turbulence in terms of the understanding of the mechanism of vortex breakups. In two-dimensional fluid mechanics the quadratic quantities energy and enstrophy have two different cascades: the energy flows towards larger scales and the enstrophy towards small scales, see for example Kraichnan (1967), Kraichnan and Montgomery (1980), Boffetta and Ecke (2012), or Mininni and Pouquet (2013). In three dimensions, Kolmogorov's famous $k^{-5/3}-$ law states the energy flows towards smaller wave numbers (Kolmogorov, 1941). There are many works corroborating Kolmogorov's theory either numerically in terms of the Navier-Stokes equations or experimentally, see e.g. Kraichnan and Montgomery (1980), Chorin (1994) or Frisch (1995). By evaluating atmospheric measurements with airplanes Nastrom et al. (1984) were the first who could show that Kolmogorov's and Kraichnan's theories for 2D and 3D turbulence hold for atmospheric data sets. But, until know, flows are analyzed statistically considering the space of waves and not the space is regarded, where the flow actually evolves, as it was recently stated by (Cardesa et al., 2017).

In this chapter, we will consider 3D vortex dynamics. Our studies are based on the work of Névir and Blender (1993), who formulated the vorticity equation with respect to the energy *and* the helicity. We recall that the energy is a quadric quantity, whereas the helicity, given by the scalar product of the velocity and vorticity vectors, can have positive as well as negative values. The helicity is related to the rotation of vortex dynamics we think that it is an interesting and underestimated quantity concerning turbulence studies. First works on the helicity can be ascribed to Ertel and Rossby (1949), Betchov (1961), Moreau (1961), Moffatt (1969) and Kraichnan (1973). The sign-structure of the helicity might be a reason, why only few authors regard the helicity cascade, as for example Brissaud et al. (1973), Chen et al. (2003), Pouquet and Mininni (2010), Dallas and Tobias (2016). Why is the positive definite enstrophy cascade commonly examined, but not the helicity cascade?

Biferale et al. (2013) point out the importance of the helicity, its sign and its relation to the energy cascade. They show numerically that in all three-dimensional flows in nature one can find a subset of nonlinear evolution, which leads to a reverse energy transfer from small to large scales. The authors use setups with different sign of the helicity and show that the different cascades depend on the chosen sign of helicity. So far, energy cascades to larger scales were related to two-dimensional flows, but they show that it can also occur in three dimensions. The reversed energy cascade happens in cases, where the mirror symmetry is broken, underlining the importance of the quantity helicity itself, and in particular its sign. In these cases, the helicity cascades towards smaller scales and the energy cascades in opposite direction, to larger scales. Thus, the choice of a fixed sign of helicity influences the direction of the energy cascade. But in case the helicity field is zero, it does not influence the energy cascade.

Nambu-mechanics provides the possibility to analyze helicity fields independently of the energy. In this chapter we will use this advantage of Nambu mechanics and explore the helicity density field of vortex flows. We will propose initial conditions for vortex splits. Thereby, we define vortex splits with respect to the sign of the helicity density. A region with positive helicity density values can be related to a right rotating vortex and a helicity density region characterized by negative values can be assigned to a left rotating vortex. We will analyze the helicity field with respect to the Vortex-Heisenberg group VH(3) and the Helmholtz Vortex group V(3)

that we have derived in chapter 8. In order to transfer the group theoretical approach to splitting storms, we will first give a short introduction to tornadoes and splitting supercells. In the last part of this chapter we will shortly discuss the implications of this alternative, algebraic perspective on 3D vortex flows for (future) turbulence studies. To the best of our knowledge, an analysis of vortex splits based on a group theoretical approach is not yet known.

9.1 Tornadoes, supercells and splitting storms

Tornadoes are strongly rotating vortices with measured wind speeds ranging from 33 m/s up to 140 m/s. They are characterized by a violent rotating column of air that extends to the ground from the interior of a cumulonimbus cloud (Davies-Jones et al., 2001). Tornadoes can be classified into two types: Type I is associated with a larger-scale parent circulation. Such tornadoes form within a mesocyclone. Type II is generally a smaller and weaker vortex away from any mesocyclone. We will consider the large and violent tornadoes of Type I that occur usually in isolated supercell storms (Davies-Jones et al., 2001). Supercells are thunderstorms with a lifetime larger than one hour that have a high degree of spatial correlation between its mesocyclone and updraft. Thunderstorms may even produce more than one tornado, as it was, for instance, observed in Oklahoma, 18. June 1993 by Moller (1978). For details on the development and analysis of tornadoes see e.g. the classical works of Morton (1966), Davies-Jones et al. (1974), Klemp (1987), Snow (1984), or Davies-Jones (1995).

Klemp and Wilhelmson (1978) have studied the split of storms using three-dimensional cloud models. They state that splittings depend on the distribution and the intensity of low-level shear; and when storms split, two storms are generated, one cyclonically rotating updraft moving to the right of the initial wind and one anticyclonical storm, moving to the left. Neglecting the Coriolis effects, Klemp and Wilhelmson (1978) show numerically, how one idealized storm splits into two storms that are mirror images of each other. Moreover, by applying the kinematic vorticity number and analyzing the vorticity field Schielicke (2017) discusses case studies of splitting supercells numerically. We will shortly summarize the explanation of splitting storms due to the classical works of Klemp (1987) and Davies-Jones et al. (2001). We assume that the wind increases with height

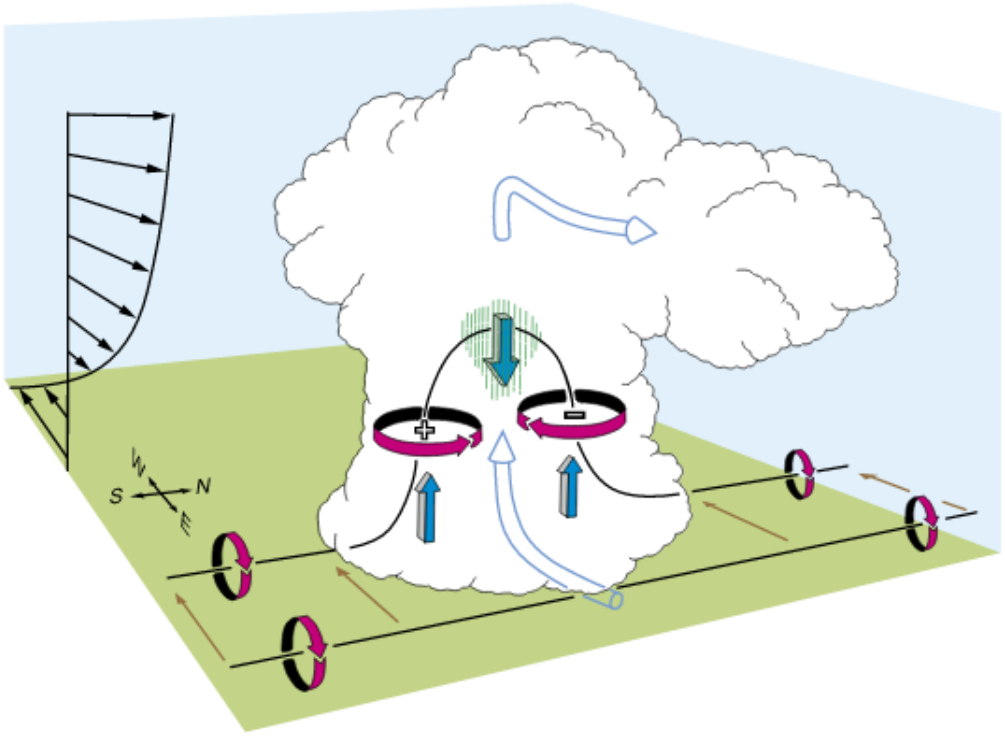

Figure 9.1: The onset of a splitting is shown. The tilting vortex lines produce a cyclonic vortex to the right of the peak and an anticyclonic vortex to the left of the peak. From Markowski and Richardson (2011), based on Klemp (1987)

and consider a flat surface as illustrated in fig. 9.1. Such a surface may be deformed by convection leading to a raising peak in the surface. The tilting vortex lines produce a cyclonic vortex to the right of the peak and an anticyclonic vortex to the left of the peak. The cylindrical arrows show the flow of the storm. It is shown how the updraft can cause a split into a cyclonic vortex on its right and an anticyclonic vortex on its left. Such strong rotating storms are characterized by large helicity.

9.2 Helicity, Beltrami fields and splitting storms

We cite Ertel and Rossby (1949) who already introduced the concept of the helicity in terms of a Lagrangian conserved quantity as follows: Let $\mathbf{v}$ be the absolute velocity and $\boldsymbol{\xi} = \nabla \times \mathbf{v}$ the absolute vorticity, further let ρ^{-1} the specific volume of a barotropic fluid and ΔW the gradient of the action W (=Hamilton's principal-function), then

$$\frac{d}{dt}\{\frac{1}{\rho}\boldsymbol{\xi} \cdot (\mathbf{v} - \nabla W)\} = 0 \tag{9.1}$$

where $\frac{d}{dt}$ denotes temporal differentiation following the motion of the fluid which provides the Lagrangian conservation.

Twelve years later, Betchov (1961) introduced the term helicity and its definition as it is known today; Moffatt (1969) was one of the first who considered the helicity as important quantity in terms of magnetohydrodynamics. Eight years later Lilly (1986) characterizes supercell thunderstorms by high helicity. He also proposes that the longevity of supercells is due to large helicity. Moreover, he shows that the structure and the motion of supercell storms can be modeled as purely helical flow. Purely helical flows are characterized by parallel velocity and vorticity vectors. Flows with this property are called *Beltramian* flows, which we will discuss more in detail in this chapter. Regarding observations as well as simulations Lilly (1986) comes to the result that long-lived isolated storms have nearly coincident updraft and vortex centers and therefore, it is reasonable to represent storms as Beltrami flows. Moreover, he proposes that helical Eddies have a longer lifetime, because they resist dissipation. In our simulations that are based on incompressible ideal fluid equations without dissipation. We will observe vortex splits in regions, where the storm 'collides' with its environment and show that most interaction takes place in these transitional or short-lived regions of low helicity. In our approach we will use the Vortex-Heisenberg groups and define splits as a decomposition of definite helicity fields into a helicity field with locally changing sign.

In the last chapter we have seen that using Nambu's formulation for three-dimensional fluid dynamics helicity is as important as kinetic energy. The helicity is given by

$$h_V = \frac{1}{2} \int_V d\tau \; \mathbf{v} \cdot \boldsymbol{\xi}, \tag{9.2}$$

and gives a measure of helical rotation. In our analysis, we will mainly consider the helicity density given by $h = \frac{1}{2}\mathbf{v} \cdot \boldsymbol{\xi}$. Webb et al. (2014) point out that the helicity is a pseudo-scalar that changes sign under 3D space reversal, i.e. $h \longrightarrow -h$, see table 8.1. Because of the parity transformations of the velocity and vorticity vectors $\mathbf{v}$ and $\boldsymbol{\xi}$:

$$\mathbf{v} \to -\mathbf{v} \quad \text{and} \quad \boldsymbol{\xi} \to \boldsymbol{\xi}, \tag{9.3}$$

the helicity density is a pseudo scalar:

$$\frac{1}{2}\mathbf{v}\cdot\boldsymbol{\xi} \rightarrow -\frac{1}{2}\mathbf{v}\cdot\boldsymbol{\xi}. \tag{9.4}$$

They state that *this is an important property of the helicity as it measures parity symmetry breaking. A parity invariant flow has zero helicity*. Therefore, flows with large positive helicity, as our example of the Beltrami flow (defined as solutions of (9.6)), are strongly symmetry breaking. We note the difference between the parity invariance of equations and solutions. The vortex equation is invariant under parity transformations, this property holds for classical physics in general, such as for the mass point equations. But solutions can break the symmetry, as for example the Beltrami flow field. One violent rotating vortex that represents a tornado can be represented idealized by such a symmetry breaking Beltrami field. If one vortex splits into two vortices as in supercells — that are mirror images of each other and thus have different sign of helicity — the helicity integrated over the whole fields will approach zero. Thus, the sum of the local helicity values is nearly zero and the total system conserves the symmetry. After a cascade of splits, a helicity-invariant field is obtained, where the symmetry is reestablished.

We shortly summarize the common explanation for splitting storms that is is based on the three-dimensional inviscid vorticity equation, where the source/sink term is included:

$$\frac{\partial\boldsymbol{\xi}}{\partial t} = \nabla\times(\mathbf{v}\times\boldsymbol{\xi}) + \nabla\times(b\mathbf{k}) \tag{9.5}$$

with buoyancy $b = g\theta'/\theta_0$, potential temperature $\theta = \theta_0 + \overline{\theta}(z) + \theta'(\mathbf{x},t)$, constant potential temperature θ_0, position vector $\mathbf{x}$ and time t (see e.g. Rotunno and Klemp, 1982). If the velocity vector $\mathbf{v}$ is parallel to the vorticity vector $\boldsymbol{\xi}$ pointing in the same or in the opposite direction, i.e.

$$\mathbf{v} = \lambda\boldsymbol{\xi}, \quad \lambda\in\mathbb{R}, \tag{9.6}$$

the flow is characterized by large helicity. Such flows with parallel vorticity and velocity fields are called Beltrami flows. Considering Beltrami flows, the so-called Lamb vector, given by the cross product $\mathbf{v}\times\boldsymbol{\xi}$ is zero. In this case, the first term on the right hand side in (9.5) vanishes leading to the reduced representation of the vorticity equation:

$$\frac{\partial\boldsymbol{\xi}}{\partial t} = \nabla\times(b\mathbf{k}). \tag{9.7}$$

Because the vanishing term is related to advection, stretching and tilting, the source, respectively sink, of vorticity is only given by the buoyancy production term which is related to the time rate of change of horizontal vorticity; the energy cascades is prevented by the vanishing non-linear term and the rotation can be preserved for a longer time. It is argued that in case the non-linear term $\mathbf{v} \times \boldsymbol{\xi} = 0$ in the vorticity equation (9.5) vanishes only a forcing driven by thermodynamics is possible. Only cases where $\mathbf{v} \times \boldsymbol{\xi} \neq 0$ can imply cascades. Since Beltrami flows are flows with large helicity, we will represent idealized storms as Beltrami-flows.

Definition 40. Beltrami vector field
A three-dimensional vector field $\mathbf{v}$ is called Beltrami if

$$(\nabla \times \mathbf{v}) \times \mathbf{v} = 0 \tag{9.8}$$

which means that the vector field and its curl are everywhere collinear. We can also write (9.8) as:

$$\nabla \times \mathbf{v} = \lambda(\mathbf{x})\mathbf{v} \tag{9.9}$$

where $\lambda(\mathbf{x})$ is a scalar function depending locally on $\mathbf{x}$. The solutions of (9.9) can be classified as different types of Beltrami fields (see, e.g., Amari et al., 2009):

1. Potential fields: $\lambda \equiv 0$, $\mathbf{v}$ is irrational and can be determined from a potential, i.e. $\mathbf{A} = \nabla\varphi$. This is the simplest case, but we want to describe tornados with the Beltrami field and therefore, the helicicity $\nabla \times \mathbf{v} = \lambda(\mathbf{x})\mathbf{v}$ must not vanish.

2. Non-linear Beltrami fields with a non-linear function $\lambda(\mathbf{x})$. So far, under assumptions the existence of non-linear Beltrami fields is proven (see, e.g., Boulmezaoud, 1999).

3. Linear Beltrami fields are characterized by constant $\lambda \in \mathbb{R}$.

All cases are described in detail in Bjørgum (1951) and Bjørgum (1952). For the latter case, several solutions exist and the helicity turns out to be extremal. For Beltrami flows, where $\nabla \times \mathbf{v} = \lambda\mathbf{v}$, the densities of the most

important quantities in vortex dynamics are given by:

$$\begin{aligned} \text{Kinetic Energy density:} \quad & H = \frac{1}{2}\mathbf{v}^2, \\ \text{Helicity density:} \quad & h = \frac{1}{2}\mathbf{v}\cdot\boldsymbol{\xi} = \frac{1}{2}\lambda\mathbf{v}^2, \\ \text{Enstrophy density:} \quad & \varepsilon = \frac{1}{2}\boldsymbol{\xi}^2 = \frac{1}{2}\lambda^2\mathbf{v}^2, \end{aligned} \tag{9.10}$$

leading, in case of linear Beltrami fields and $\mathbf{v}^2 > 0$, to the following relationship between these quantities, where the λ is endowed with the corresponding dimension:

a) $\lambda = 1$: energy = enstrophy = helicity

b) $0 < \lambda < 1$: $0 <$enstrophy $<$ helicity $<$ energy

c) $-1 < \lambda < 0$: helicity $< 0 <$ enstrophy $<$ energy

d) $\lambda > 1$: $0 <$ energy $<$ helicity $<$ enstrophy

e) $\lambda < -1$: helicity $< 0 <$ energy

Furthermore, the Cauchy-Schwarz inequality that is given by:

$$(\mathbf{v}\cdot\boldsymbol{\xi})^2 \leq (\mathbf{v}\cdot\boldsymbol{\xi})\cdot(\mathbf{v}\cdot\boldsymbol{\xi}) \tag{9.11}$$

is satisfied for Beltrami flows. We use the index B to mark the Beltramian property:

$$(\mathbf{v}_B\cdot\boldsymbol{\xi}_B)^2 = \mathbf{v}_B^2\cdot\boldsymbol{\xi}_B^2 \tag{9.12}$$

The latter equation holds, because inserting the Beltrami condition $\boldsymbol{\xi} = \lambda\mathbf{v}$ leads to:

$$(\mathbf{v}_B\cdot\boldsymbol{\xi}_B)^2 = (\mathbf{v}_B\cdot(\lambda\mathbf{v}_B))^2 = \mathbf{v}_B^2\cdot(\lambda\mathbf{v}))^2 = \mathbf{v}_B^2\cdot\boldsymbol{\xi}_B^2. \tag{9.13}$$

There are only few solutions of linear Beltrami vector fields satisfying (9.9) for a constant factor λ. The most popular solution was derived by Arnold (1965). These flows are called ABC-flows (to honor the three scientists V. Arnold, E. Beltrami and S. Childress) and as we will show in the following, for these solutions λ is equal to one. In this chapter we will explore helicity fields a the previously discussed equations will be used for their examination. Arnold (1965) and Childress (1970) conjectured the existence

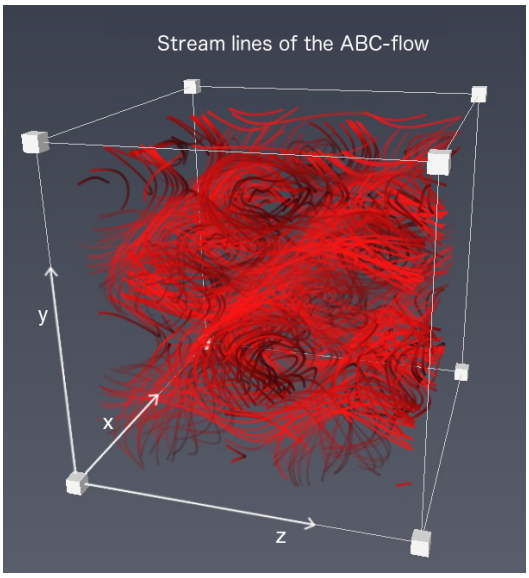

Figure 9.2: The stream lines of the ABC (9.14) flow with $A = 1$, $B = C = \frac{1}{2}$ are shown.

of chaotic paths for Beltrami flows. ABC flows are flows of the form:

$$\mathbf{v}_B = \mathbf{v}_B(x, y, z) = \begin{pmatrix} A\sin(z) + C\cos(y) \\ B\sin(x) + A\cos(z) \\ C\sin(y) + B\cos(x) \end{pmatrix}, \quad \text{with } 1 \geq A \geq B \geq C \geq 0 \tag{9.14}$$

see for example Dombre et al. (1986), Hénon (1966), Galloway (2012) or Arnold and Khesin (1992). In fig. 9.2 we illustrate the streams lines of an ABC-flow.

Linear Beltrami flows such as the ABC-flows (9.14) are characterized by local extrema of helicity. For $\lambda = \pm 1$ ($\lambda = 1$ for ABC-flows) and normed velocity fields, i.e. $|\mathbf{v}|^2 = 1$ it is:

$$h = \frac{1}{2}\,\mathbf{v} \cdot \boldsymbol{\xi} = \pm\frac{1}{2}\,\mathbf{v}^2 = \pm\frac{1}{2}. \tag{9.15}$$

Locally, the sign of the helicity field of a Beltrami flow does not change. It depends on the initial field and thus on the factor λ.

We summarize that the helicity density of Beltrami flows (9.15) is extremal, and for ABC-flow solutions, where $\lambda = 1$, the helicity density is maximal. On the other hand, tornadoes are strongly rotating vortices and characterized by high values of helicity (Davies-Jones et al., 1990). Combining both facts, it seems reasonable to regard tornadoes as ABC-flows.

Davies-Jones (2015) used a Beltrami flow as initial condition, because the Beltrami flow *resembles a mid-latitude mesocyclone*. Moreover, Raptis and Papageorgiou (2017) state that *Beltrami flows are of a characteristic topology akin to that of tornado flows [...]*.

So far, we have explored the helicity density $h = \frac{1}{2}\,\mathbf{v}\cdot\boldsymbol{\xi}$. Another possibilty to examine helicity fields is the so-called *relative helicity density*. It is defined as the cosine of the angle between the vorticity and the vorticity vector, i.e.:

$$h_{rel} = \cos(\mathbf{v}, \boldsymbol{\xi}) = \frac{\mathbf{v}\cdot\boldsymbol{\xi}}{|\mathbf{v}|\cdot|\boldsymbol{\xi}|}. \tag{9.16}$$

There are at least two advantages using this helicity-representation (9.16). (i) All values are dimensionless and $h_{rel} \in [-1, 1]$ which allows for a good comparison of the helicity of different states and (ii) we can quantify if the helicity field is locally a Beltrami field.

Davies-Jones et al. (1990) classified 28 tornadoes by its strength of rotation h_{srh} in $\frac{m^2}{s^2}$:

$$\begin{aligned} 150\ m^2s^{-2} < h_{srh} < 299\ m^2s^{-2} &\quad \text{weak tornadoes} \\ 300\ m^2s^{-2} < h_{srh} < 449\ m^2s^{-2} &\quad \text{strong tornadoes} \\ h_{srh} > 450\ m^2s^{-2} &\quad \text{violent tornadoes.} \end{aligned} \tag{9.17}$$

More precisely, h_{srh} is the so-called *storm-relative helicity* that can be derived under the assumption that there is no vertical wind. Here, it is integrated over the lowest 3 km:

$$h_{srh} = \int_0^{3km} dz\ (\mathbf{V} - \mathbf{C}) \cdot \left(\mathbf{k} \times \frac{\partial \mathbf{V}}{\partial z}\right), \tag{9.18}$$

where $\mathbf{V}$ denotes the environmental wind vector and $\mathbf{C}$ is the storm motion vector that can be approximately estimated by using the pressure-weighted mean wind in the lowest 5-6 km. The values of the storm-relative helicity range from approximately $150\ m^2s^{-2}$ to upwards of $1000\ m^2s^{-2}$.

In his recent work, Kurgansky (2017) also points out the significance of helicity by studying *intense atmospheric vortices* as tropical meso-scale vortices, tropical cyclones, and turbulence. In Chkhetiani (2005) further investigations of hurricanes, tornadoes and dust devils in terms of helicity can be found. Since violent tornadoes are related to large helicity, we think it is convenient to represent idealized, strong rotating storms by Beltrami flows.

9.3 Vortex splits induced by the Vortex-Heisenberg group

In the following we will use the Vortex-Heisenberg Lie group structure to explain vortex splits. For this approach, we will analyze the outcome of the group operation of two group elements with respect to helicity, energy and enstrophy densities. Each group element represents a certain flow, each characterized by its displacement $\mathbf{a}$ and the vector that is normal to the area enclosed by the circulation, denoted $\mathbf{A}$. We discussed the physical interpretation of the vectors $\mathbf{a}$ and $\mathbf{A}$ in chapter 8 section 8.5. We will examine the helicity density field of the state induced by the group operation as it is sketched below:

$$\begin{pmatrix} \textit{Initial State I} \\ \textit{helicity-free} \\ \textit{shear-flow} \end{pmatrix} \cdot \begin{pmatrix} \textit{Initial State II} \\ \textit{flow with} \\ \textit{max. helicity} \end{pmatrix} = \begin{pmatrix} \textit{Interaction} \\ \textit{Splitted flow field} \\ \pm\, \textit{helicity.} \end{pmatrix}$$

In chapter 6 section 6.1 we have compared this view with the group of rotations. Here, we will relate vortex splits to the sign of the helicity density because of the following reason: A helicity density field that shows locally positive as well as locally negative values gives rise to vortex splits, because different signs within the helicity density fields indicate different orientations of rotation. One should distinguish between vortex-circulations such as the vorticity and rigid body rotations about a given angle. Regarding the Vortex-Heisenberg group, we consider vortex-rotations related to the vorticity. The Helmholtz-Vortex group additionally contains the rigid body rotation. We will propose initial conditions for vortex splits and explore different examples for different flows. Thereby, we will consider a Beltrami field representing a supercell and different shear flows representing the atmospheric environment of the supercell. We will start with four case studies exploring helicity density fields with respect to the Vortex-Heisenberg group VH(3):

1. A Beltrami field and an atmospheric shear field with vanishing helicity

2. A Beltrami field and an atmospheric shear field with helicity

3. Two Beltrami fields

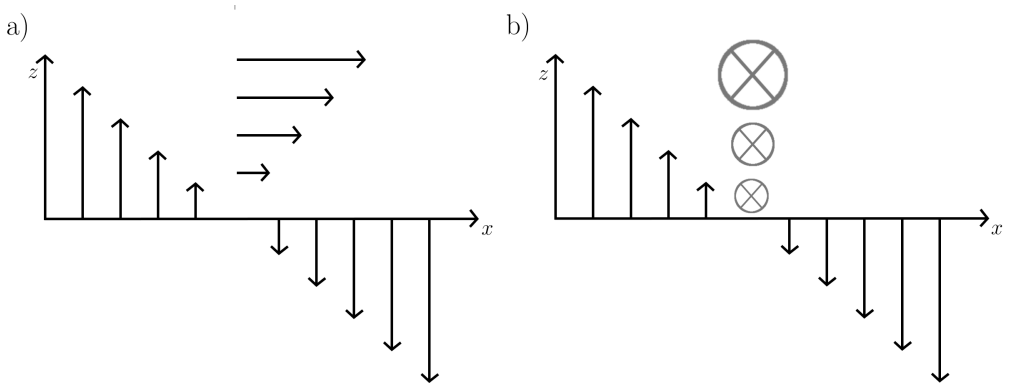

Figure 9.3: Two classical meteorological wind fields are sketched. Whereas the wind in a) is characterized by a planar rotation such that the helicity vanishes; the wind field sketched in (b) increases such that helicity can be measured.

4. The two shear fields of case 1 (with vanishing helicity field) and case 2 (with helicity), both wind fields are sketched in fig. 9.3.

And, as a fifth case, we examine the helicity field with respect to the Helmholtz Vortex group V(3), where the conservation of the angular momentum is additionally integrated:

5. A Beltrami field and an atmospheric shear field with vanishing helicity

The cases are summarized in table 9.1. In each example we will consider two initial flows, represented as group elements A and B and analyze the helicity density field of state C that results from the group composition of state A and B. Thus, state $C = A * B$ reflects the interaction of the atmospheric states A and B, or the change of the state.

One benefit of the group theoretical approach in general is the closure property. This means that a by group operation induced state is also an elements of the group. Thus, the group theoretical approach might be seen as a new conceptual structural integration method of Helmholtz 3D vorticity equation. Therefore, if the induced state can be related to a splitted helicity field we can state that storm splits yields a solution of Helmholtz' 3D vorticity equation. Furthermore, because of the existence of the inverse of each group element, the process is reversible and also the generation of the initial states can be explained by and related to the helicity density.

Group	Case Study	Initial State A	Initial State B	Induced state $C = A * B$
VH(3)	1	Beltrami $(\mathbf{v}_B, \boldsymbol{\xi}_B)$ h: extremal	Shear I (no tilting) $(\mathbf{v}_{s1}, \boldsymbol{\xi}_{s1})$ $h' = 0$	Split $(\mathbf{v}'', \boldsymbol{\xi}'')$ sign$(h'') : +/-$
	2	Beltrami $(\mathbf{v}_B, \boldsymbol{\xi}_B)$ h: extremal	Shear 2 (tilting) $(\mathbf{v}_{s2}, \boldsymbol{\xi}_{s2})$ sign$(h') : +/-$	Split $(\mathbf{v}'', \boldsymbol{\xi}'')$ sign$(h'') : +/-$
	3	Beltrami 1 $(\mathbf{v}_{B1}, \boldsymbol{\xi}_{B1})$ h: extremal	Beltrami 2 $(\mathbf{v}_{B2}, \boldsymbol{\xi}_{B2})$ h: extremal	No split $(\mathbf{v}'', \boldsymbol{\xi}'')$ sign(h'') =const
	4	Shear 1 (tilting) $(\mathbf{v}_{s2}, \boldsymbol{\xi}_{s2})$ sign$(h') : +/-$	Shear 2 (no tilting) $(\mathbf{v}_{s1}, \boldsymbol{\xi}_{s1})$ $h = 0$	No additional split $(\mathbf{v}'', \boldsymbol{\xi}'')$ sign$(h'') : +/-$
V(3)	5	Beltrami $(\mathbf{v}_B, \boldsymbol{\xi}_B, \underline{\mathbf{R}}_B)$ h: extremal	Shear I (tilting) $(\mathbf{v}_{s1}, \boldsymbol{\xi}_{s1}, \underline{\mathbf{R}}_{s1})$ $h' = 0$	Additional split $(\mathbf{v}'', \boldsymbol{\xi}'', \underline{\mathbf{R}}'')$ sign$(h'') : +/-$

Table 9.1: Five cases with initial fields characterized by different helicity fields are discussed.

We transfer the physical characterizations of the flow from the algebra to the group representatives as discussed in chapter 8 section 8.5 and use the notations from table 8.1, where $\mathbf{v}$ is the velocity vector and $\boldsymbol{\xi}$ the vorticity vector. Considering the associated Vortex-Heisenberg Lie group, we denote $\mathbf{a}$ the vector related to the velocity $\mathbf{v}$ and $\mathbf{A}$ the vector related to $\boldsymbol{\xi}$, i.e.

$$\begin{aligned} &\text{(algebra)} \quad \mathbf{v} \longrightarrow \mathbf{a} \quad \text{(group)}, \\ &\text{(algebra)} \quad \boldsymbol{\xi} \longrightarrow \mathbf{A} \quad \text{(group)}. \end{aligned}$$

Then, the Vortex-Heisenberg group $\mathrm{VH}(3)$ is given by the set $(\mathbf{a}, \mathbf{A}) \in \mathbb{R}^6$

together with the following group operation:

$$(\mathbf{a}'', \mathbf{A}'') = (\mathbf{a}', \mathbf{A}') * (\mathbf{a}, \mathbf{A}) = (\mathbf{a}' + \mathbf{a}, \mathbf{A}' + \mathbf{A}' + \frac{1}{2}\mathbf{a} \times \mathbf{a}'). \tag{9.19}$$

Now, we formulate the helicity, energy and enstrophy densities in terms of the Vortex-Heisenberg group. Using the VH(3)-group operation (9.19), we obtain the following expressions for the helicity density:

$$h'' = \frac{1}{2}\mathbf{a}'' \cdot \mathbf{A}'' = \frac{1}{2}(\mathbf{a}' + \mathbf{a}) \cdot (\mathbf{A}' + \mathbf{A} + \frac{1}{2}\mathbf{a} \times \mathbf{a}') = \frac{1}{2}(\mathbf{a}' + \mathbf{a}) \cdot (\mathbf{A}' + \mathbf{A}) \tag{9.20}$$

and the energy density reads

$$H'' = \frac{1}{2}\mathbf{a}''^2 = \frac{1}{2}(\mathbf{a}' + \mathbf{a})^2, \tag{9.21}$$

and the enstrophy density can be formulated as follows

$$\varepsilon'' = \frac{1}{2}\mathbf{A}''^2 = \frac{1}{2}\left(\mathbf{A}' + \mathbf{A} + \frac{1}{2}\mathbf{a}' \times \mathbf{a}\right) \cdot \left(\mathbf{A}' + \mathbf{A} + \frac{1}{2}\mathbf{a}' \times \mathbf{a}\right), \tag{9.22}$$

which can be written as

$$\begin{aligned} \varepsilon'' &= \frac{1}{2}\left[(\mathbf{A}' + \mathbf{A})^2 + (\mathbf{A}' + \mathbf{A}) \cdot (\mathbf{a}' \times \mathbf{a}) + \left(\frac{1}{2}\mathbf{a}' \times \mathbf{a}\right)^2\right] \\ &= \frac{1}{2}\left[(\mathbf{A}' + \mathbf{A})^2 + (\mathbf{A}' \cdot (\mathbf{a}' \times \mathbf{a}) + (\mathbf{A} \cdot (\mathbf{a}' \times \mathbf{a}) + \frac{1}{4}(\mathbf{a}' \times \mathbf{a})^2\right], \end{aligned} \tag{9.23}$$

where the two terms in the middle vanish if we consider Beltrami flows, because $\mathbf{a} = \lambda\mathbf{A}$, $\mathbf{a}' = \lambda'\mathbf{A}'$. But for non-Beltrami flows we see that the structure of the enstrophy (9.23) differs from the formulation of the helicity (9.20) and energy (9.21), because the helicity and energy density do not contain cross product terms. The cross product term reflects the nilpotent structure and therefore, the nilpotent structure should be reflected in the enstrophy density field, which will be explored in future studies. Here, we will discuss case studies, where the different structure of the enstrophy leads to a faster growth compared to the energy density fields, as it is observed in 3D turbulence studies.

To analyze the helicity field (9.20) in terms of the Vortex-Heisenberg group operation and examine five cases of different initial states we will shortly summarize the technical implementation.

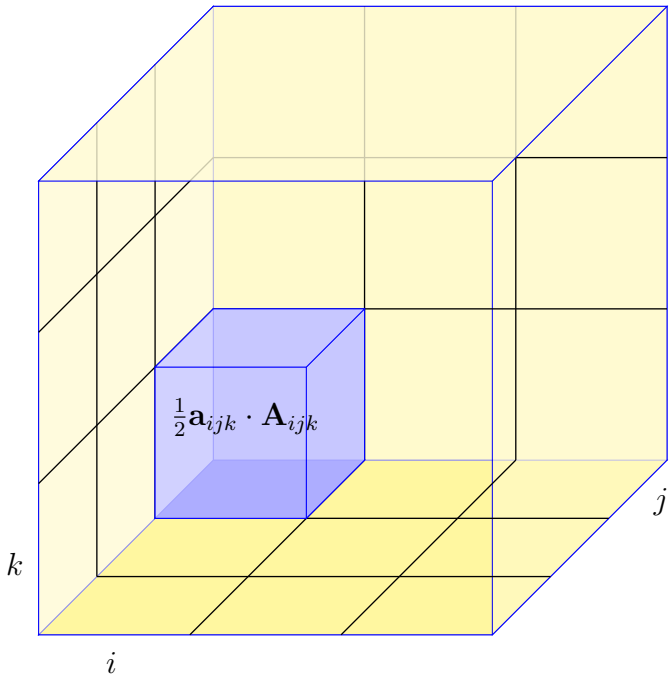

Figure 9.4: Calculation of the helicity density field in each three-dimensional grid box

9.3.1 Numerical implementation

The way atmospheric data sets are evaluated and numerically integrated depends on the research objectives. Today it is searched for suitable integration methods and models that take into account the consistency of 'local' and 'global' properties of prognostic partial and ordinary differential equations, as the local spatial or time derivative, conservation properties (conservation of energy, momentum, mass etc.), symplectic structures, volume of the phase space and symmetries (Sommer, 2010). Numerical weather prediction models are developed aiming for an exact solution locally, whereas climate prediction models pursue the aim to analyze global, characteristic, statistical features. In both cases, complex numerical schemes and approximations are needed to handle large data sets such as the DWD's ICON-model. For a detailed overview on the methods and equations of numerical weather prediction see e.g. Roulstone and Norbury (2013).

In this thesis, we show an alternative integration method. We consider analytical exact solutions of the Helmholtz vorticity equation. This allows for an illustration of these analytical solutions on a simple regular, Cartesian grid. Here, we focus on the representation of the previously discussed

helicity h_V. For this approach we use a simple discretization scheme considering the regular Cartesian grid:

$$h_V = \frac{1}{2}\int_V \mathbf{a}\cdot\mathbf{A}\, d\tau \approx \frac{1}{2}\sum_{i,j,k} V_{ijk}\, a_{ijk}\cdot A_{ijk}. \tag{9.24}$$

We assume a constant volume $V_{ijk} = V$, for all i, j, k in each threedimensional grid box leading to:

$$\hat{h}_V \approx V\frac{1}{2}\sum_{i,j,k} a_{ijk}\cdot A_{ijk} \tag{9.25}$$

as sketched in fig. 9.4. We will explore the *local* changes of the helicity density fields and shortly discuss the corresponding density fields of the energy and the enstrophy. In the following examples, we will calculate the **a**-and **A**-streamlines as well as the helicity, enstrophy and energy density fields for single grid boxes as sketched in fig. 9.4. To represent the results we show exemplarily two-dimensional hyperplanes.

We used Python to calculate the fields in three-dimensions, where the x, y- and z-axis range from -2π to 2π. The two-dimensional figures in this chapter are illustrated on a 1000×1000 horizontal grid. For the three-dimensional representations, as fig. 9.2, the software *Amira* was used, which has been designed and developed at the Zuse Institute Berlin (ZIB) for 3D visualization, geometry reconstruction, and data analysis. Here, we consider idealized flows in a scaled grid. The size of the flow field can be adapted to the larger, atmospheric scale. Now, we are prepared to discuss the five cases studies and explore our assumptions on the initial fields, when vortices split and when no split occurs. The different cases summarized in in table 9.1.

9.3.2 First case study: Simulating vortex splits

To visualize vortex splits, we analyze the helicity density field induced by the group operation of two group elements, where each group element represents a meteorological wind field. We interpret the group operation as state change caused by two wind fields and illustrate the resulting state change. The sign of the helicity density field gives rise to vortex splits. If the helicity density field has locally positive as well as negative values, we speak of a splitted vortex field. In this example, the first field represents a supercell given analytically by a strongly helical rotating Beltrami field. The

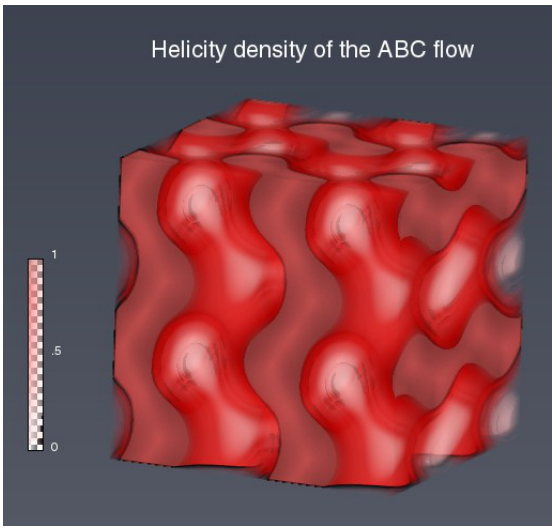

Figure 9.5: The helicity density field for an ABC-flow (9.26) with $A = 1,\ B = C = \frac{1}{2}$ is shown.

second field depicts its environment, a shear flow with vanishing helicity.

Both initial fields are characterized by helicity density values greater or equal to zero. We will show that they induce (by group operation) a helicity density field with positive *and* negative values. Such a helicity density field can be interpreted as a splitted vortex into a right rotating and a left rotating vortex.

Both fields are represented as elements of VH(3). We will denote the Beltrami field with $(\mathbf{a}_B, \mathbf{A}_B)$ and its environment with $(\mathbf{a}_{s1}, \mathbf{A}_{s1})$, where the subscript s denotes the shearing flow. As visualized in chapter 8, section 8.5, the vectors $\mathbf{a}$ and $\mathbf{A}$ are related to the velocity and the vorticity. Therefore, regarding the group, we transfer the physical characterizations of the flow from the algebra to the group representatives $\mathbf{v} \to \mathbf{a}$ and $\boldsymbol{\xi} \to \mathbf{A}$, see (8.105).

As Beltrami flow solution we consider the ABC-flow $\mathbf{a}_B$ of form (9.14) with $A = 1,\ B = C = \frac{1}{2}$:

$$\mathbf{a}_B = \lambda \cdot \boldsymbol{\nabla} \times \mathbf{a}_B = \mathbf{A}_B = \lambda \cdot \begin{pmatrix} \sin(z) + \frac{1}{2}\cos(y) \\ \frac{1}{2}\sin(x) + \cos(z) \\ \frac{1}{2}\sin(y) + \frac{1}{2}\cos(x). \end{pmatrix} \tag{9.26}$$

Here, the factor λ has the unit lengths $1m$; it will be omitted in the following. The streamlines of this ABC-flow are shown in fig. 9.2.

In fig. 9.5 the helicity density of the Beltrami flow is vizualized. We

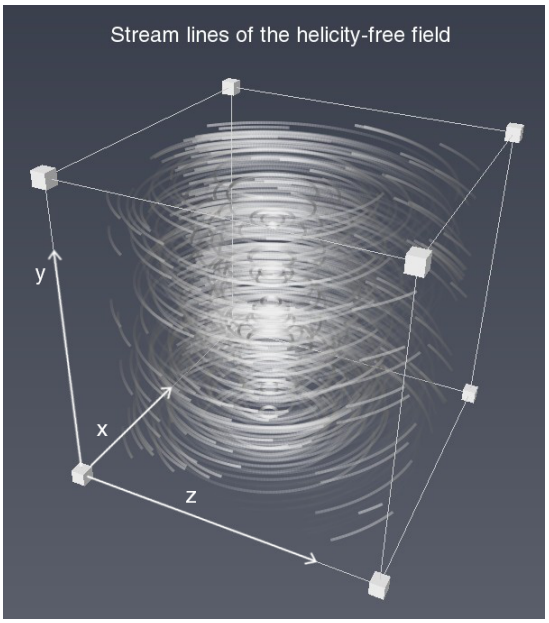

Figure 9.6: The stream lines of the **a**-field given in (9.27) are shown. The **a**-field is related to the wind field **v**, which is a shear field. The helicity of this field is zero because it is a rotation in the $x-z$-plane.

assume that the strong rotating supercell, represented by the Beltrami flow, is embedded in a typical meteorological shear flow. In our first case study, we consider a shear flow with non-zero vorticity vector but with a zero-valued helicity density field. This meteorological wind field is sketched in fig. 9.3 a). Mathematically, it is given by:

$$\mathbf{a}_{\text{s1}} = \mathbf{a}_{\text{s1}}(x,y,z) = \begin{pmatrix} z-z_0 \\ 0 \\ -x+x_0 \end{pmatrix}, \quad \text{with} \quad \nabla \cdot \mathbf{a}_{\text{s1}} = 0 \tag{9.27}$$

and its rotation, reads as:

$$\nabla \times \mathbf{a}_{\text{s1}}(x,y,z) = \begin{pmatrix} 0 \\ 2 \\ 0 \end{pmatrix} =: \mathbf{A}_{\text{s1}}. \tag{9.28}$$

The stream lines are illustrated in fig. 9.6. In case of planar rotations, as we find here in the $x-z$-plane, the three-dimensional vorticity field is orthogonal to the wind field. Thus, its scalar product and therefore the helicity

density vanishes everywhere:

$$h_{\mathrm{s1}} = \frac{1}{2}\mathbf{a}_{\mathrm{s1}} \cdot \mathbf{A}_{\mathrm{s1}} = 0. \tag{9.29}$$

Physically, we explore the interaction of two different flows in a conservative system meaning that we assume fluid flows in a system without friction.

Before we apply the Vortex-Heisenberg group operation to the ABC-flow and the shear flow, we will show that the shear flow yields a steady solutions of the Helmholtz vorticity equation. The Helmholtz vorticity equation for 3D dimensional incompressible, inviscid fluids is given by

$$\frac{\partial \boldsymbol{\xi}}{\partial t} = \boldsymbol{\xi} \cdot \nabla \mathbf{v} - \mathbf{v} \cdot \nabla \boldsymbol{\xi}. \tag{9.30}$$

Transferring the notations of the algebra to the notations of the group elements $\mathbf{v} \to \mathbf{a}$ and $\boldsymbol{\xi} \to \mathbf{A}$ we obtain a formulation for the shearing flow analogously to (9.30):

$$\frac{\partial \mathbf{A}_{s1}}{\partial t} = \mathbf{A}_{s1} \cdot \nabla \mathbf{a}_{s1} - \mathbf{a}_{s1} \cdot \nabla \mathbf{A}_{s1} = \begin{pmatrix} 0 & 0 & -1 \\ 0 & 0 & 0 \\ 1 & 0 & 0 \end{pmatrix} \cdot \begin{pmatrix} 0 \\ 2 \\ 0 \end{pmatrix} - \mathbf{0} = \mathbf{0}. \tag{9.31}$$

Thus, the shearing flow provides a steady solution of the Helmholtz vorticity equation. The same holds for the Beltrami flow. Using the Beltrami condition for linear Beltrami flows $\mathbf{A}_B = \lambda \mathbf{a}_B$, the Helmholtz vorticity equation reads as:

$$\frac{\partial \mathbf{A}_B}{\partial t} = \mathbf{A}_B \cdot \nabla \mathbf{a}_B - \mathbf{a}_B \cdot \nabla \mathbf{A}_B = \lambda\, \mathbf{a}_B \cdot \nabla \mathbf{a}_B - \lambda\, \mathbf{a}_B \cdot \nabla \mathbf{a}_B = \mathbf{0}. \tag{9.32}$$

Therefore, also the linear Beltrami flow is a steady solution of the Helmholtz equation.

In order to investigate the helicity density fields, we first recall the Vortex-Heisenberg group operation, using the notation for our two initial flows, the ABC-flow (9.26) and the shearing flow (9.27):

$$(\mathbf{a}'', \mathbf{A}'') = (\mathbf{a}_B, \mathbf{A}_B) * (\mathbf{a}_{\mathrm{s1}}, \mathbf{A}_{\mathrm{s1}}) = (\mathbf{a}_B + \mathbf{a}_{\mathrm{s1}}, \mathbf{A}_B + \mathbf{A}_{\mathrm{s1}} + \frac{1}{2}\mathbf{a}_B \times \mathbf{a}_{\mathrm{s1}}). \tag{9.33}$$

We first regard the components and insert the two initial fields (9.26) and the shearing flow (9.27). Then the $\mathbf{a}''$-field reads as:

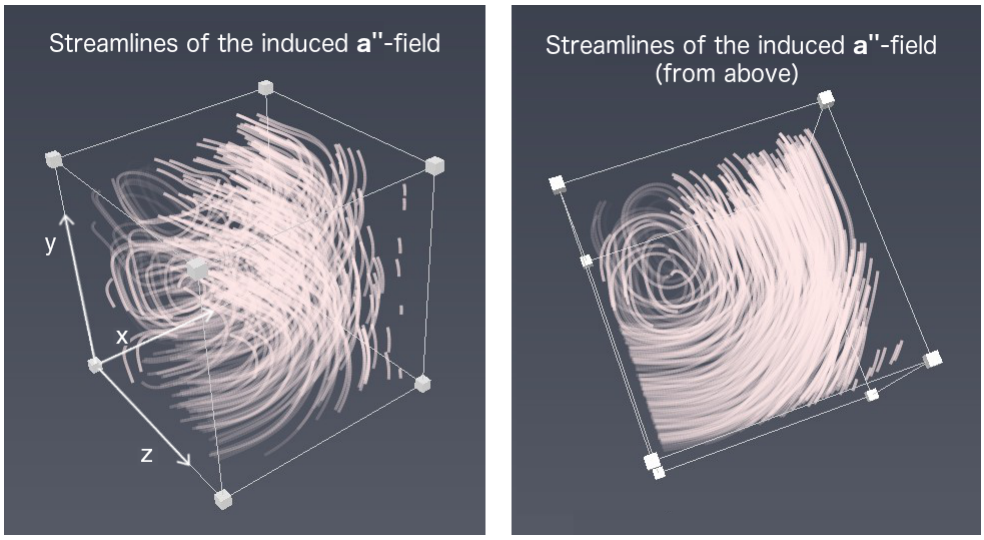

Figure 9.7: The $\mathbf{a}''$-streamlines are shown. They result from the application of the Vortex-Heisenberg group operation to a ABC flow and a shear field and can be related to velocity field. A similarity to the initial shear field shown in fig. 9.6 is apparent that is 'disturbed' by the ABC-fow in fig. 9.6.

$$\mathbf{a}'' = \mathbf{a}_B + \mathbf{a}_{s1} = \begin{pmatrix} \sin(z) + \frac{1}{2}\cos(x) + z - z_0 \\ \frac{1}{2}\sin(x) + \cos(z) \\ \frac{1}{2}\sin(y) + \frac{1}{2}\cos(x) - x + x_0 \end{pmatrix}. \tag{9.34}$$

The streamlines are illustrated from different perspectives in fig. 9.7, where we set $x_0 = z_0 = \pi$ for the shearing flow. As well the helical structure of the Beltrami flow $\mathbf{a}_B$ as the planar rotations of the shearing flow $\mathbf{a}_{s1}$ can be recognized. The stream lines of the induced $\mathbf{A}''$-field that are related to the vorticity are given by:

$$\begin{aligned} \mathbf{A}'' &= \mathbf{A}_B + \mathbf{A}_{s1} + \frac{1}{2}\mathbf{a}_B \times \mathbf{a}_{s1} \\ &= \begin{pmatrix} \sin(z) + \frac{1}{2}\cos(x) \\ \frac{1}{2}\sin(x) + \cos(z) + 2 \\ \frac{1}{2}\sin(y) + \frac{1}{2}\cos(x) \end{pmatrix} \\ &+ \frac{1}{2}\begin{pmatrix} (\frac{1}{2}\sin(x) + \cos(z))(-x + x_0) \\ \frac{1}{2}\sin(y) + \frac{1}{2}\cos(x)(z - z_0) - \sin(z) + \frac{1}{2}\cos(x)(-x + x_0) \\ (\frac{1}{2}\sin(x) + \cos(z))(-z + z_0) \end{pmatrix} \end{aligned} \tag{9.35}$$

They are shown in fig 9.8 indicating a more chaotic field than the two initial $\mathbf{A}$-streamlines. We interpret the generated group element $(\mathbf{a}'', \mathbf{A}'')$ as a state of the fluid that reflects the interaction of the ABC-flow with large helicity and the shearing flow with the vanishing helicity density field. Thus,

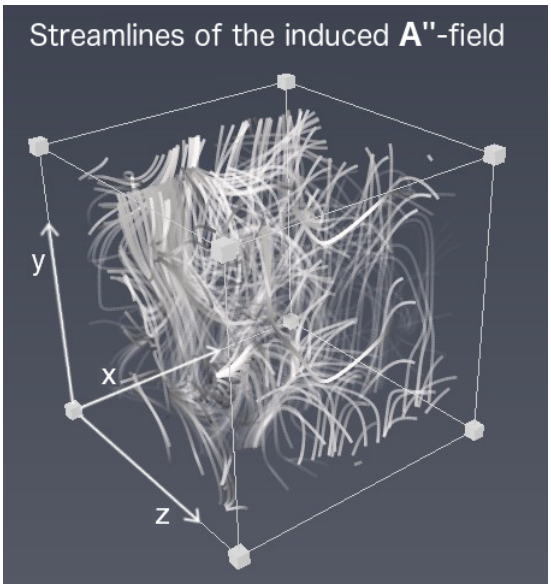

Figure 9.8: The $\mathbf{A}''$-streamlines are shown. It result from the application of the Vortex-Heisenberg group operation to a ABC flow and a shear field. A chaotic structure can be observed.

$(\mathbf{a}'', \mathbf{A}'')$ can also be seen as a the state change of a small, given region of a flow.

Now, we calculate the helicity density of the induced state $(\mathbf{a}'', \mathbf{A}'')$:

$$h'' = \frac{1}{2}\mathbf{a}'' \cdot \mathbf{A}'' = \frac{1}{2}(\mathbf{a}_B + \mathbf{a}_{\text{s1}}) \cdot (\mathbf{A}_B + \mathbf{A}_{\text{s1}} + \frac{1}{2}\mathbf{a}_B \times \mathbf{a}_{\text{s1}}) \tag{9.36}$$

which is equivalent to:

$$h'' = \frac{1}{2}\left(\mathbf{a}_B \cdot \mathbf{A}_B + \mathbf{a}_B \cdot \mathbf{A}_{\text{s1}} + \mathbf{a}_{\text{s1}} \cdot \mathbf{A}_B + \mathbf{a}_{\text{s1}} \cdot \mathbf{A}_{\text{s1}} + \frac{1}{2}(\mathbf{a}_B + \mathbf{a}_{\text{s1}}) \cdot (\mathbf{a}_B \times \mathbf{a}_{\text{s1}})\right) \tag{9.37}$$

The last summand vanishes, because a spat product of two equal vectors is zero. Inserting our wind field. The fourth summand is zero, because it is '2· helicity density' of the seharing wind field (9.27), which is zero. Applying the Beltrami condition with normalized proportionality factor, i.e. $\mathbf{a}_B = 1 \cdot \mathbf{A}_B$ last expression reduces to

$$h'' = \frac{1}{2}(\mathbf{a}_B \cdot \mathbf{a}_B + \mathbf{a}_B\mathbf{A}_{\text{s1}} + \mathbf{a}_{\text{s1}}\mathbf{a}_B) = \mathbf{a}_B \cdot (\mathbf{a}_B + \mathbf{A}_{\text{s1}} + \mathbf{a}_{\text{s1}}). \tag{9.38}$$

Last equation (9.38) is the general expression for a helicity field h'' that represents the interaction of a general shear flow and a general Beltrami flow. The relative helicity density of the two initial fields $h_{B,rel}$, $h_{\text{s1},rel}$ and

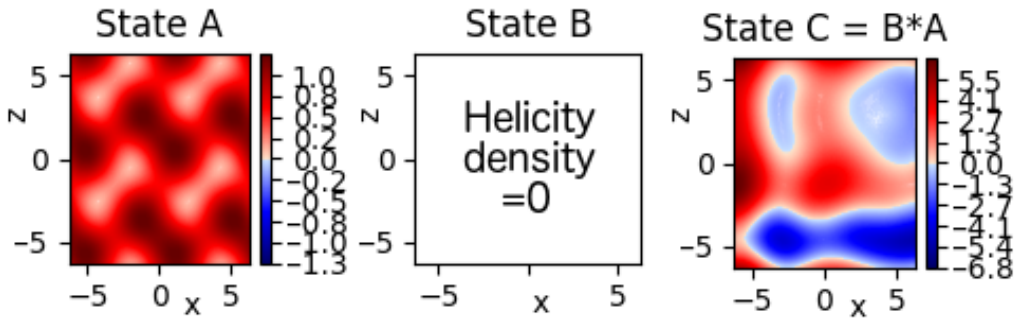

Figure 9.9: Relative helicity fields of the Beltrami flow (left), of $\mathbf{a}_S$ (middle) and of the induced third state (right) for $y = \pi/2$.

the relative helicity density of the induced state (9.33) are in fig. 9.9. For the helicity density field see appendix 12.1. Because we chose a Beltrami field with $\lambda = 1$, i.e. $\mathbf{a}_B = \mathbf{A}_B$, the helicity field of the Beltrami flow is everywhere positive. Moreover, the helicity (9.29) of the idealized shear flow field is zero. Therefore, neither initial field has negative helicity density values. However, combining these two non-negative helicity density fields by applying the group theoretical approach leads to the generation of a third field, which shows regions with positive as well as negative helicity densities. The relative helicity density field of the generated state is also shown in 3D in fig. 9.10. We recognize different signs of helicity that are marked in red (positive helicity density) and blue (negative helicity density). These different colored regions are related to different directions of rotation and can be interpreted as two different vortices, one vortex rotates clockwise and the other vortex rotates anti-clockwise.

We recognize that the colliding of different, contrarious characterized wind fields lead to vortex splits, which becomes apparent in regions, where the two different flows mostly interact. Thus, in the transitional regions of helicity free to large helicity the interaction is large which leads to vortex splits. This is in accordance with the argumentation of Lilly (1986) that most interaction appears in the transitional regions.

An interesting aspect is the closure property of groups. If the two initial group elements are solutions of the Helmholtz vorticity equation, and if we consider the transition from the Vortex-Heisenberg algebra vh(3) to the Vortex-Heisenberg group VH(3) as a structural integration, the generated group element $(\mathbf{a}'', \mathbf{A}'')$ can also be regarded as a solution of Helmholtz' vorticity equation. Moreover, because of the existence of identity elements in VH(3), we could *go backwards* and *generate* ABC-flows that we regard here as storms. Thus, the group theoretical approach shows, how we can

describe the generation of single storms, or the merging of storms as well as the split of storms. Next, we will show analytically that there exists at least one change of sign in the helicity field.

Claim 7. The helicity density field h'' given in (9.38) changes its sign locally at least in one point.

Proof. Let us assume again one wind field with positive helicity and one wind field with vanishing helicity representing a tornado and a shearing wind field. We determine the group operation and call the resulting field $(\mathbf{a}'', \mathbf{A}'')$ with helicity density field which depends on the local coordinates x, y and z:

$$h'' = h''(x, y, z) = \frac{1}{2}\, \mathbf{a}''(x, y, z) \cdot \mathbf{A}''(x, y, z). \tag{9.39}$$

We recall that different signs of the helicity can be related to different directions of rotation. Therefore, finding x-y-z-values, where the helicity changes its sign locally, would show the existence of a vortex split. In the first step we look for x-y-z-values with

$$h''(x, y, z) = \frac{1}{2}\, \mathbf{a}''(x, y, z) \cdot \mathbf{A}''(x, y, z) = 0 \iff \mathbf{a}''(x, y, z) \cdot \mathbf{A}''(x, y, z) = 0 \tag{9.40}$$

neglecting the constant $\frac{1}{2}$ in the following.

$$h''(x, y, z) = \begin{pmatrix} A\sin(z) + C\cos(y) \\ B\sin(x) + A\cos(z) \\ C\sin(y) + B\cos(x) \end{pmatrix} \cdot \begin{pmatrix} A\sin(z) + C\cos(y) + z - z_0 \\ B\sin(x) + A\cos(z) + 2 \\ B\cos(x) + C\sin(y) - x + x_0 \end{pmatrix} \tag{9.41}$$

$$\begin{aligned} h''(x, y, z) =& (A\sin(z))^2 + 2AC\sin(z)\cos(y) + (C\cos(y))^2 \\ &+ A\sin(z)(z - z_0) + C\cos(y)(z - z_0) + (B\sin(x))^2 + (A\cos(z))^2 \\ &+ 2AB\cos(z)\sin(x) + 2B\sin(x) \\ &+ 2A\cos(z) + (C\sin(y))^2 + (B\cos(x))^2 + 2\,(B\sin(y) + A\cos(x)) \\ &+ (-x + x_0)C\sin(y) + (-x + x_0)B\cos(x) \\ =& A^2 + B^2 + C^2 + 2AC\sin(z)\cos(y) + A\sin(z)(z - z_0) \\ &+ C\cos(y)(z - z_0) + 2AB\cos(z)\sin(x) + 2B\sin(x) \\ &+ 2A\cos(z) + 2\,(B\sin(y) + A\cos(x)) \\ &+ (-x + x_0)C\sin(y) + (-x + x_0)B\cos(x) \end{aligned} \tag{9.42}$$

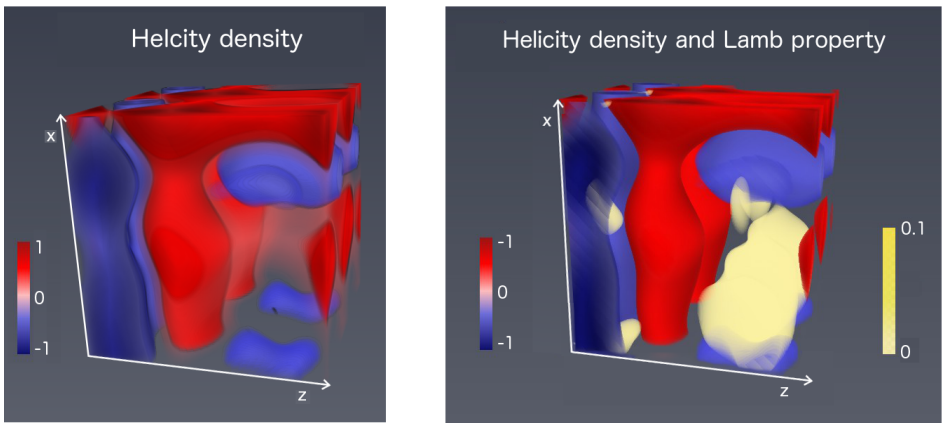

Figure 9.10: Applying the Vortex-Heisenberg Lie group operation to a ABC flow and a helicity-free field results in a third state. Here, the helicity field of the generated third state is shown where we see regions of positive and negative helicity which gives rise to splitted vortices. This is a three-dimensional illustration of the fig. on the r.h.s. in 9.9. The yellow regions in the figure on the r.h.s shows 'how Beltrami the flow is'.

Since our vortex rotates in the x-z plane we further simplify the solution and set $y = \frac{\pi}{2}$. We further assume $x_0 = z_0 = \pi$ for the wind field (9.42) leading to the following expression for the helicity:

$$\begin{aligned} h''(x, \frac{\pi}{2}, z) =& A^2 + B^2 + C^2 - 2AB\sin(x) + 2B\sin(x) - 2A + 2BC\cos(x) \\ &+ (x - x_0)C + (x - x_0)B\cos(x) \\ =& A^2 + B^2 + C^2 + \sin(x)(2B - 2AB) + \cos(x)(2BC + (x - x_0)B) \\ &+ (x - x_0)C - 2A \end{aligned} \tag{9.43}$$

Let now $A = 1$, $B = C = \frac{1}{2}$ and $x_0 = \pi$. We search for the roots with respect to the z-value π:

$$\begin{aligned} h''(x, \frac{\pi}{2}, \pi) &= -\frac{1}{2} + \cos(x)\left(\frac{1 + \pi - x}{2}\right) + \frac{x - \pi}{2} \\ &= (1 + \pi - x)(\cos(x) - 1) = 0 \quad \Longleftrightarrow \quad x = 2k\pi \quad \text{or} \quad x = \pi + 1 \end{aligned} \tag{9.44}$$

with $k \in \mathbb{Z}$. By simply inserting values near the roots, we see that the helicity density field changes its sign locally. □

The corresponding energy and enstrophy density fields (9.21) and (9.23) of the induced state are shown in appendix 12.1. These fields do not show

distinctive structures. This can be explained by the assumption of inviscid, incompressible flows.

Moreover, considering the by group operation induced state $(\mathbf{a}'', \mathbf{A}'')$, we would like to find out, where exactly the splits occur. In fig. 9.10 the yellow regions mark, where the field is nearly Beltrami. To determine these regions, we calculated the Lamb vector, i.e. the cross product $\mathbf{a}'' \times \mathbf{A}''$. The Lamb vector is zero where the Beltrami-condition holds, i.e. where $\mathbf{a}'' = \lambda \mathbf{A}''$. We call this condition *Lamb property*. It can be expressed in terms of the densities of the three conserved quantities:

$$|\mathbf{a}'' \times \mathbf{A}''|^2 = |\mathbf{a}''|^2 \cdot |\mathbf{A}''|^2 - (\mathbf{a}'' \cdot \mathbf{A}'')^2 = 0 \qquad \text{(Lamb property)}. \tag{9.45}$$

We can also formulate last equation in words:

$$\frac{\text{Energy density} \cdot \text{Enstrophy density}}{(\text{Helicity density})^2} - 1 = 0. \tag{9.46}$$

In the beginning of this chapter we have already discussed the Cauchy-Schwarz inequality (9.11) for Beltrami flows (9.12), which is equivalent to last expressions (9.45) and (9.46). In fig. 9.10 the yellow regions mark small values of the parameter $0.1 > \varepsilon > 0$ indicating small deviations of the Lamb property, i.e.

$$|\mathbf{a}'' \times \mathbf{A}''|^2 = \varepsilon. \tag{9.47}$$

Thus, the yellow regions mark the domains, where the flow is nearly Beltrami, because for Beltrami flows the velocity and vorticity vectors are parallel leading to a vanishing lamb vector. With respect to fig. 9.10, we observe that splits occur on the boundary of these yellow marked regions, i.e. where the helicity density field is not extremal. We can show exemplarily that in regions with smaller helicity values, i.e. where the vortex is not as strongly rotating (assuming non-planar rotations), the effect on disturbances (considering the shear flow as disturbance) of the *storm* is bigger, which allows for stronger interaction and thus for vortex splits. This is in accordance to the earlier mentioned work of Lilly (1986) who states strongly rotating supercells have a longer lifetime.

We summarize: First, we have used Nambu-mechanics to represent Helmholtz' 3D vorticity equation. Second, we have derived an algebra. Integrating this algebra led to a Lie group structure, which we have applied to a strong rotating supercell embedded in a typical atmospheric wind field.

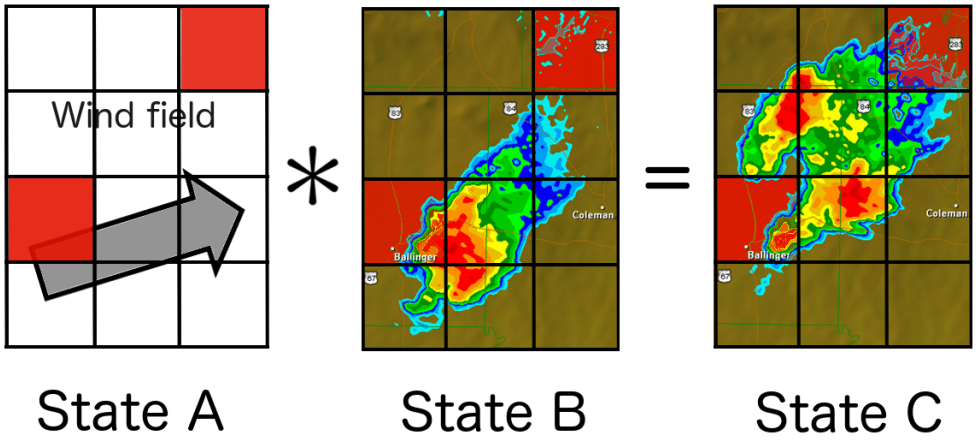

Figure 9.11: A sketch shows how the group operation can be transferred to describe the interaction of atmospheric fields. We examine the local interaction on a grid, where the two coupled states A and B can be seen as lying on each other as marked by the red boxes inducing state $C = A * B$. Courtesy of the National Weather Service for the composite reflectivity image.

Applying the group operation to these initial fields results in a field with positive and negative helicity density values, which can be interpreted as vortex split. It is sketched in fig. 9.11, where state A and state B interact such that they induce state $C = A * B$.

One can further combine the outcome with additional wind fields, but we assert that splits are best generated if two wind fields are combined that have different helicity density absolute values, such as one wind field with very large helicity and one wind field with vanishing helicity. Or, in other words: Two flows with different grade of Beltramization lead to vortex splits. Thus, by analyzing the helicity density fields with respect to its different signs, we have shown the existence and generation of vortex splits in a conservative system. Moreover, because of the closure property of groups, this splitted field is an element of the Vortex-Heisenberg Lie group and therefore, it yields a solution of Helmholtz' incompressible, inviscid 3D non-linear vorticity equation. Furthermore, because of the existence of the inverse of the group elements and the closure of the Vortex-Heisenberg group, we can think vice versa leading to the statement that strongly rotating fields such as Beltrami flows can also be generated. Thus, considering supercells as Beltrami-flows the existence of splitted vortices as well as the generation of strongly rotating vortices, e.g. supercells, can be explained analytically.

In appendix 12.1 (relative) helicity density, enstrophy density and energy density fields are shown for further iteratively generated fields. The group operation does not provide any information about the behavior of the flow at a specific time step. We analyze the state change of the fluid. However, applying iteratively the group operation we recognize a growth of the energy values, although we consider conservative systems. And increasing enstrophy densities. The enstrophy grows faster of the energy which can be explained by the non-conservation of the enstrophy for three dimensional fluids.

Most authors investigate storm splits numerically implementing the Navier-Stokes equation. Here, we introduced an algebraic approach starting with the 3D Helmholtz vorticity equation for incompressible, inviscid flows, we form an Lie algebra. And, because of its nilpotent structure, we find a map from the Lie algebra to the Lie group. Since we analyze the helicity fields regarding the group structure, one could speak of a structural integration of the Helmholtz equation. We come to the conclusion that splitting storms can be seen as a solution of Helmholtz' 3D vorticity equation, which in turn is given by the mathematical rotation ($\nabla\times$) of Euler's equations for incompressible, inviscid flows.

9.3.3 Second case study: A less distinctive split

In this case study we apply the Heisenberg-group operation to the ABC flow $\mathbf{a}_B$ from our last example, see (9.26) and a typical atmospheric wind field $\mathbf{a}_{s2}$ that *is* characterized by helicity. In the last case study we examined a Beltrami field and a shear field with vanishing helicity. We have already shown in (9.32) that the ABC-flow is a steady solution of Helmholtz vorticity equation. In our first case study we examined the interaction of two steady solutions. Here, we chose a different shearing field denoted with $\mathbf{a}_{s2}$ and sketched in fig. 9.3 b). Mathematically, the wind field and the corresponding rotational part are given by:

$$\mathbf{a}_{s2} = \mathbf{a}_{s2}(x,y,z) = \begin{pmatrix} 0 \\ z - z_0 \\ -x + x_0 \end{pmatrix}, \quad \nabla \cdot \mathbf{a}_{s2} = 0, \quad \mathbf{A}_{s2} = \nabla \times \mathbf{a}_{s2} = \begin{pmatrix} 1 \\ -1 \\ 0 \end{pmatrix}. \tag{9.48}$$

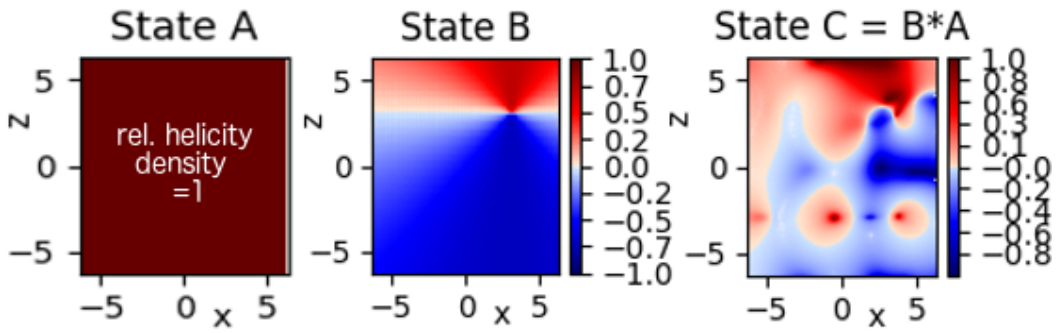

Figure 9.12: Relative helicity fields of the Beltrami flow (left), of $\mathbf{a}_{s2}$ (middle) and of the generated third state (right) for $y = \pi/2$.

Inserting this wind field in Helmholtz vorticity equation, we obtain:

$$\frac{\partial \mathbf{A}_{s2}}{\partial t} = \mathbf{A}_{s2} \cdot \nabla \mathbf{a}_{s2} - \mathbf{a}_{s2} \cdot \nabla \mathbf{A}_{s2} = \begin{pmatrix} 0 & 0 & 0 \\ 0 & 0 & -1 \\ 1 & 0 & 0 \end{pmatrix} \cdot \begin{pmatrix} 1 \\ -1 \\ 0 \end{pmatrix} - \mathbf{0} = \begin{pmatrix} 0 \\ 0 \\ 1 \end{pmatrix}. \tag{9.49}$$

Compared to the steady solution of the shearing flow in our first example, here the horizontal part of $\mathbf{A}$ does not change in time, but the vertical part of $\mathbf{A}$ increases in time. Thus, vorticity is produced, and this flow describes the tilting of an vortex. To summarize, in this case study we investigate the interaction of a tilting vortex, which is a non-steady solution of the Helmholtz vorticity equation, with a strong helical rotating vortex that is represented by a steady solution of Helmholtz vorticity equation.

In our first case study the helicity density of the initial shearing flow $(\mathbf{a}_{s1}, \mathbf{a}_{s1})$ was zero. Here, the helicity density of the state $(\mathbf{a}_{s2}, \mathbf{a}_{s2})$ does not vanish in general:

$$h_{s2} = \mathbf{a}_{s2} \cdot \mathbf{A}_{s2} = z_0 - z \neq 0. \tag{9.50}$$

The helicity is zero if and only if $z = z_0$. From a meteorological perspective, the wind field $\mathbf{a}_{s2}$ describes the tilting of a tornado, i.e. the process while a tornado can be developed. See the sketch in fig. 9.3 b). During this process, where the storm is not completely developed we do not expect a *perfect* split.

We apply the group operation for the shear field and the ABC flow (9.26) leading to the following helicity density field:

$$h'' = \frac{1}{2}\mathbf{a}'' \cdot \mathbf{A}'' = \frac{1}{2}(\mathbf{a}_B + \mathbf{a}_{s2}) \cdot (\mathbf{A}_B + \mathbf{A}_{s2} + \frac{1}{2}\mathbf{a}_B \times \mathbf{a}_{s2}). \tag{9.51}$$

The relative helicity field is shown in fig. 9.12 and the helicity density field is shown in the appendix 12.2. The positive-negative structure of helicity density field h_{s2} is due to the choice of z_0 that is here chosen to be π. Compared to the first case study, only slightly changes in the helicity field around $z = \pi$ can be observed, some positive and negative helicity structures are recognized but the split is not as distinctive as in the first case study. We think this is due to the shear field that does have non-zero helicity values. From meteorological point of view this chosen shear field represents the tilting of a tornado. During this process a split is not as distinctive compared to first case, where the helicity of the shear flow was zero.

In appendix 12.2 the energy, enstrophy and helicity density fields of the induced states are illustrated. We assume incompressible, inviscid flows. Therefore, for all five cases, we do not expect large changes in the structure of the energy and enstrophy fields. The value of the energy increases. This is due to the addition in the group operation. But the enstrophy increases much faster which is in accordance with the non-conservation of the enstrophy.

9.3.4 Third case study: Interaction of two Beltrami fields

As a third case study we consider the group operation of two Beltrami flows, say $(\mathbf{a}_{B1}, \mathbf{A}_{B1})$ and $(\mathbf{a}_{B2}, \mathbf{A}_{B2})$. We recall from (9.32) that linear Beltrami fields are steady solutions of the Helmholtz vorticity equation. We consider two general linear Beltrami flows with $\lambda_{B1}\mathbf{a}_{B1} = \mathbf{A}_{B1}$ and $\lambda_{B2}\mathbf{a}_{B2} = \mathbf{A}_{B2}$ and $\lambda_{B1}, \lambda_{B2} \in \mathbb{R}$. In order to investigate their interaction in terms of the helicity density fields, we first calculate the group operation of the initial states

$$\begin{aligned}(\mathbf{a}'' \cdot \mathbf{A}'') &= (\mathbf{a}_{B2}, \mathbf{A}_{B2}) * (\mathbf{a}_{B1}, \mathbf{A}_{B1}) \\ &= \frac{1}{2}\left(\mathbf{a}_{B2} + \mathbf{a}_{B1}, \mathbf{A}_{B2} + \mathbf{A}_{B1} + \frac{1}{2}\mathbf{a}_{B1} \times \mathbf{a}_{B2}\right).\end{aligned} \tag{9.52}$$

Determining the helicity density field of this induced state leads to:

$$\begin{aligned}h'' &= \frac{1}{2}\mathbf{a}'' \cdot \mathbf{A}'' = \frac{1}{2}\left(\mathbf{a}_{B2} + \mathbf{a}_{B1}) \cdot (\mathbf{A}_{B2} + \mathbf{A}_{B1} + \frac{1}{2}\mathbf{a}_{B1} \times \mathbf{a}_{B2}\right) \\ &= \frac{1}{2}(\mathbf{a}_{B2} + \mathbf{a}_{B1}) \cdot (\lambda_{B2}\mathbf{a}_{B2} + \lambda_{B1}\mathbf{A}_{B1}) \\ &= \frac{1}{2}(\lambda_{B1}^2\mathbf{a}_{B1}^2 + \lambda_{B2}^2\mathbf{a}_{B2}^2 + (\lambda_{B1} + \lambda_{B2})\mathbf{a}_{B1}\mathbf{a}_{B2}).\end{aligned} \tag{9.53}$$

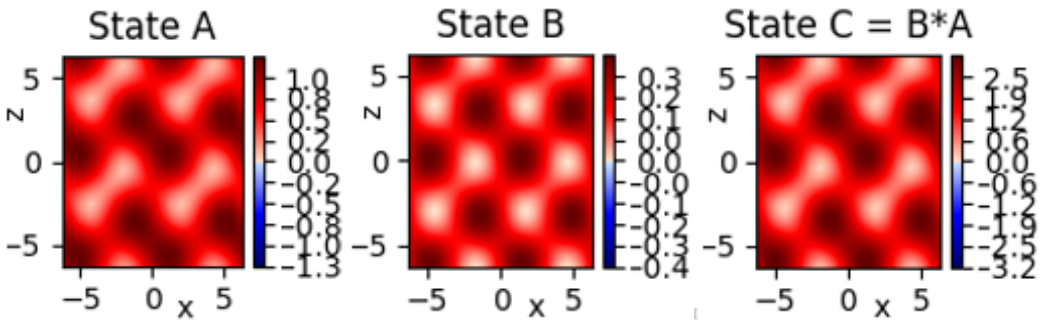

Figure 9.13: Helicity fields of two ABC-flows with parameters $A_1 = 1, B_1 = 0.9$ and $C_1 = 0.5$ for (l.h.s), $A_2 = 0.5, B_2 = 0.4$ and $C_2 = 0.1$ (middle), the helicity field of the by group operation induced state which is also a ABC-flow has the parameters $A_3 = (A_1 + A_2)$, $B_3 = (B_1 + B_2)$ and $C_3 = (C_1 + C_2)$ set the parameters (r.h.s), z-x-plane for $y = \pi/2$.

Therefore, different signs of λ may lead to different sign-structures in the helicity density fields. For $\lambda_{B1} = \lambda_{B2} := \lambda$ the helicity density is positive definite:

$$h'' = \frac{1}{2}(\lambda^2 \mathbf{a}_{B1}^2 + \lambda^2 \mathbf{a}_{B2}^2 + 2\lambda \mathbf{a}_{B1}\mathbf{a}_{B2}) = (\lambda \mathbf{a}_{B1} + \lambda \mathbf{a}_{B2})^2 \geq 0 \tag{9.54}$$

For ABC-flow solutions (9.14) the proportionality factor is λ is equal to one for all parameters A, B and C. Thus, a vortex split can not be caused by two ABC-flows.

Let now $\mathbf{a}_{B1}$ and $\mathbf{a}_{B2}$ be two arbitrary but fixed ABC-flows (9.14). Independent of the exact choice of the parameters A, B and C, these flows satisfy the relationship: $\mathbf{a}_{B1} = \mathbf{A}_{B1}$ and $\mathbf{a}_{B2} = \mathbf{A}_{B2}$ which can be directly shown using the trigonometric properties. Considering both ABC-flows as elements in VH(3) and denoting the induced state as in (9.52) $(\mathbf{a}'', \mathbf{A}'')$, we can analyze the helicity density field of the induced state (see (9.54)):

$$\begin{aligned} h'' = (\mathbf{a}_{B2} + \mathbf{a}_{B1})^2 &= \left(\begin{pmatrix} A_2 \sin(z) + C_2 \cos(y) \\ B_2 \sin(x) + A_2 \cos(z) \\ C_2 \sin(y) + B_2 \cos(x) \end{pmatrix} + \begin{pmatrix} A_1 \sin(z) + C_1 \cos(y) \\ B_1 \sin(x) + A_1 \cos(z) \\ C_1 \sin(y) + B_1 \cos(x) \end{pmatrix} \right)^2 \\ &= \left(\begin{pmatrix} A_3 \sin(z) + C_3 \cos(y) \\ B_3 \sin(x) + A_3 \cos(z) \\ C_3 \sin(y) + B_3 \cos(x) \end{pmatrix} \right)^2 \end{aligned} \tag{9.55}$$

with $A_3 = (A_1 + A_2)$, $B_3 = (B_1 + B_2)$ and $C_3 = (C_1 + C_2)$. Thus, the result is a squared ABC-flow. The helicity field of state $(\mathbf{a}_{B1}, \mathbf{A}_{B1}) := A$, state

$(\mathbf{a}_{B2}, \mathbf{A}_{B2}) := B$ and the helicity field of the by group operation induced state $(\mathbf{A} * \mathbf{B}) = (\mathbf{a}'', \mathbf{A}'') := C$ are shown in fig. 9.13, where we set the parameters $A_1 = 1, B_1 = 0.5$ and $C_1 = 0.5$ for $\mathbf{a}_{B1}$, and $A_2 = 0.5, B_2 = 0.4$ and $C_2 = 0.1$ to define $\mathbf{a}_{B2}$.

$$\mathbf{a}_{B1} = \begin{pmatrix} \sin(z) + 0.5\cos(y) \\ 0.5\sin(x) + \cos(z) \\ 0.5\sin(y) + 0.5\cos(x) \end{pmatrix}, \quad \mathbf{a}_{B2} = \begin{pmatrix} 0.5\sin(z) + 0.1\cos(y) \\ 0.4\sin(x) + 0.5\cos(z) \\ 0.1\sin(y) + 0.4\cos(x) \end{pmatrix}, \tag{9.56}$$

In fig. 9.13 the helicity fields of the three ABC-flows are illustrated. All three fields have a similar positive helicity structure such that no split can occur.

As we have seen in the beginning of this chapter (9.46), for these kind of Beltrami-flows with $\lambda = 1$ it is:

$$\text{Energy = Helicity = Enstrophy} \tag{9.57}$$

up to dimensional constants equal to one. Since the energy always is positive definite, the helicity field must be positive definite, too. The helicity density fields of nine iteratively induced states are shown in appendix 12.3. All by group operation induced states hold the same structure as the initial fields in fig. 9.13. This structure can also be recognized in the enstrophy and energy density fields, also shown in appendix 12.3.

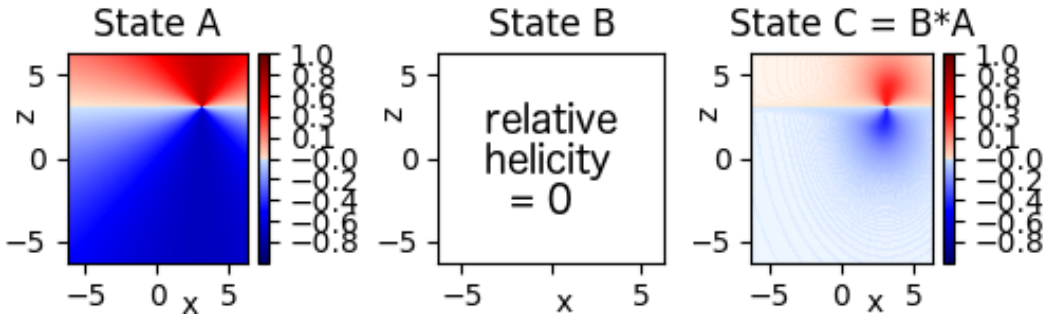

Figure 9.14: Helicity fields of shearing wind field (l.h.s.), of the wind field with helicity (middle) and of the induced helicity field (r.h.s.), $y = \pi/2$.

9.3.5 Fourth case study: Interaction of two shearing flows

Now, we couple the two atmospheric shear fields from the first and second examples. The wind fields are illustrated in fig. 9.3. Mathematically, they are given by:

$$\mathbf{a}_{\text{s2}} = \mathbf{a}_{\text{s2}}(x, y, z) = \begin{pmatrix} 0 \\ z - z_0 \\ -x + x_0 \end{pmatrix}, \quad \mathbf{a}_{\text{s1}} = \mathbf{a}_{\text{s1}}(x, y, z) = \begin{pmatrix} z - z_0 \\ 0 \\ -x + x_0 \end{pmatrix}. \tag{9.58}$$

We expect that these two fields do not generate a split, because we propose that a perfect split is induced by two fields with contrary absolute helicity values, as we have shown in the first example. But in this fourth case study, we regard two flows with similar structure, both represent a shear field. We recall the helicity densities h_{s1} and h_{s1} of the first and second case studies

$$h_{\text{s2}} = z_0 - z, \quad h_{\text{s1}} = 0. \tag{9.59}$$

And the helicity of the induced state is given by:

$$h'' = (\mathbf{a}_{s2} + \mathbf{a}_{s1}) \cdot (\mathbf{A}_{s2} + \mathbf{A}_{s1} + \frac{1}{2}\mathbf{a}_{s2} \times \mathbf{a}_{s1}). \tag{9.60}$$

Inserting the fields (9.58) into the last equation we obtain:

$$\begin{aligned} h'' &= \left(\begin{pmatrix} 0 \\ z - z_0 \\ -x + x_0 \end{pmatrix} + \begin{pmatrix} z - z_0 \\ 0 \\ -x + x_0 \end{pmatrix} \right) \cdot \left(\begin{pmatrix} 1 \\ -1 \\ 0 \end{pmatrix} + \begin{pmatrix} 0 \\ 0 \\ 0 \end{pmatrix} + \begin{pmatrix} (z - z_0)(x - x_0) \\ (z - z_0)(x - x_0) \\ -(z - z_0)^2 \end{pmatrix} \right) \\ &= (z - z_0)^2(-x + x_0)[(z - z_0)^2 + 2] \end{aligned} \tag{9.61}$$

The zero-valued regions of the induced helicity field (9.61) depend on the choice of x_0 and z_0. Therefore, the helicity field of the induced state provides the same plus-minus structure as the initial field given by the group element $(\mathbf{a}_{s2}, \mathbf{A}_{s2})$ and no further vortex split occurs. The helicity fields for $x_0 = \pi$ of the initial fields as well as the induces third state are illustrated in fig. 9.14. In appendix 12.3 additional results of the induced enstrophy density field (9.23) and energy density field (9.21) are shown in appendix 12.1, where we do not recognize large changes in the enstrophy and energy fields.

9.4 Vortex splits induced by Helmholtz Vortex Lie group V(3)

In the last chapter we have introduced Helmholtz' Vortex Lie group V(3) which we derived by extending the Vortex-Heisenberg group by the angular momentum. The group operation of the Vortex-Heisenberg group:

$$(\mathbf{a}, \mathbf{A}, \underline{\mathbf{R}}) * (\mathbf{a}', \mathbf{A}', \underline{\mathbf{R}}') = \left(\mathbf{a} + \underline{\mathbf{R}}\mathbf{a}', \mathbf{A} + \underline{\mathbf{R}}\mathbf{A}' \pm \frac{1}{2}\mathbf{a} \times \underline{\mathbf{R}}\mathbf{a}' \right), \tag{9.62}$$

where $\mathbf{a}, \mathbf{a}', \mathbf{A}, \mathbf{A}' \in \mathbb{R}^3$ and $\underline{\mathbf{R}} \in SO(3)$. In order to examine the helicity density fields and, thus, vortex splits, in terms of Helmholtz' Vortex group, we will shortly discuss the parity transformation and the helicity density field for V(3). In the previous case studies we have seen the importance of the sign of the helicity fields. Thus, we ask if the parity transformation is reflected in the Helmholtz vortex group operation. The vector $\mathbf{A}$ corresponds to the vorticity vector that does not change its sign under parity transformation, whereas the local coordinate vector $\mathbf{a}$ does change its sign under parity transformation:

$$\mathbf{a} \longrightarrow -\mathbf{a}, \quad \mathbf{A} \longrightarrow \mathbf{A}, \quad \text{and} \quad \underline{\mathbf{R}} \longrightarrow \underline{\mathbf{R}} \tag{9.63}$$

And for two elements in V(3) we obtain:

$$\begin{aligned}(-\mathbf{a}, \mathbf{A}, \underline{\mathbf{R}}) * (-\mathbf{a}', \mathbf{A}', \underline{\mathbf{R}}') &= \left(-\mathbf{a} - \underline{\mathbf{R}}\mathbf{a}', \pm\frac{1}{2}\mathbf{a} \times \underline{\mathbf{R}}\mathbf{a}' + \mathbf{A} + \underline{\mathbf{R}}\mathbf{A}', \underline{\mathbf{R}}\underline{\mathbf{R}}' \right) \\ &= (-\mathbf{a}'', \mathbf{A}'', \underline{\mathbf{R}}'').\end{aligned} \tag{9.64}$$

Especially the fact that the discplacement vector $\mathbf{a}$ (which is related to the velocity) changes its sign, but not $\mathbf{A}$ might be related to the existence of left- and right moving storms. In order to explore vortex splits with respect to the Helmholtz Vortex group, we will now calculate the helicity density h'' of the state $(\mathbf{a}'', \mathbf{A}'', \underline{\mathbf{R}}'')$ induced by the by the Helmholtz Vortex group operation:

$$(\mathbf{a}'', \mathbf{A}'', \underline{\mathbf{R}}'') = (\mathbf{a}', \mathbf{A}', \underline{\mathbf{R}}') * (\mathbf{a}, \mathbf{A}, \underline{\mathbf{R}}) \tag{9.65}$$

Then, the helicity density is given by:

$$\begin{aligned}
h'' &= \mathbf{a}'' \cdot \mathbf{A}'' \\
&= (\mathbf{a} + \underline{\mathbf{R}}\mathbf{a}') \cdot \pm \left(\frac{1}{2}\mathbf{a} \times \underline{\mathbf{R}}\mathbf{a}' + \mathbf{A} + \underline{\mathbf{R}}\mathbf{A}' \right) \\
&= \underbrace{\mathbf{a} \cdot (\mathbf{a} \times \underline{\mathbf{R}}\mathbf{a}')}_{=0} + \mathbf{a} \cdot \mathbf{A} + \mathbf{a} \cdot (\underline{\mathbf{R}}\mathbf{A}') + \underbrace{(\underline{\mathbf{R}}\mathbf{a}') \cdot \left(\pm \frac{1}{2}\mathbf{a} \times \underline{\mathbf{R}}\mathbf{a}' \right)}_{=0} \\
&\quad + (\underline{\mathbf{R}}\mathbf{a}') \cdot \mathbf{A} + \underbrace{(\underline{\mathbf{R}}\mathbf{a}') \cdot (\underline{\mathbf{R}}\mathbf{A}')}_{\mathbf{a}' \cdot \mathbf{A}' \text{ for } \underline{\mathbf{R}} \in SO(3)} \\
&= \underbrace{\mathbf{a} \cdot \mathbf{A}}_{h} + \underbrace{\mathbf{a}' \cdot \mathbf{A}'}_{h'} + \underbrace{\mathbf{a} \cdot (\underline{\mathbf{R}}\mathbf{A}') + (\underline{\mathbf{R}}\mathbf{a}') \cdot \mathbf{A}}_{\text{interaction-term}}
\end{aligned} \tag{9.66}$$

Analogously to the calculation of the helicity density regarding VH(3), the cross product term vanishes. Therefore, the helicity density does not depend on the sign in front of the cross product. Thus, the helicity density field of V(3)$^+$ and V(3)$^-$ does not differ. The same holds for the energy density field. The sign in front of the cross product only affects the calculation of the enstrophy density field. The enstrophy and energy densities can be derived analogously to (9.21) and (9.23). We obtain:

$$\begin{aligned}
H'' &= \frac{1}{2}(\mathbf{a} + \underline{\mathbf{R}}\mathbf{a}')^2 \\
\varepsilon'' &= \frac{1}{2}\left[(\mathbf{A} + \underline{\mathbf{R}}\mathbf{A}')^2 \pm (\underline{\mathbf{R}}\mathbf{A}' \cdot (\underline{\mathbf{R}}\mathbf{a}' \times \mathbf{a}) \pm (\mathbf{A} \cdot (\underline{\mathbf{R}}\mathbf{a}' \times \mathbf{a}) \pm \frac{1}{4}(\underline{\mathbf{R}}\mathbf{a}' \times \mathbf{a})^2 \right] \\
\underline{\mathbf{R}}'' &= \underline{\mathbf{R}}\underline{\mathbf{R}}',
\end{aligned} \tag{9.67}$$

where the last line represents the solid rotational part of the flow, i.e. the angular momentum, represented by rotational matrices in SO(3). We note that for $\underline{\mathbf{R}} = \underline{\mathbf{R}}' = \mathbb{E}$ we obtain $\underline{\mathbf{R}}'' = \mathbb{E}$. In this case, the energy, helicity and enstrophy density correspond to the energy, helicity and enstrophy

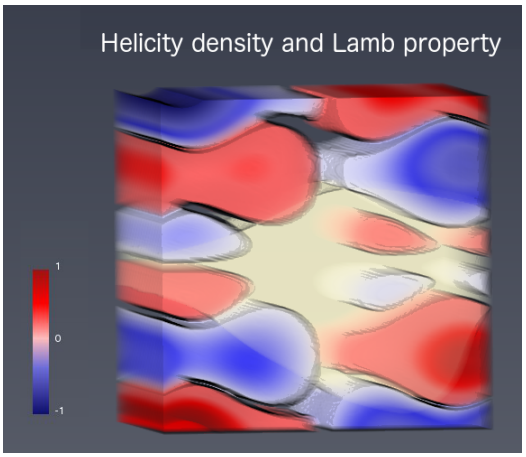

Figure 9.15: Helicity density of a fourth state generated by Helmholtz' Vortex group. The yellow region illustrates the areas that are (approximately) Beltrami. The split occurs on the boundary of this region.

densities of the Vortex-Heisenberg group.

9.4.1 Fifth case study: Splitting storms and the Helmholtz Vortex group

Now, we will couple the state $(\mathbf{a}'', \mathbf{A}'')$ of the first case study with the shear field with vanishing helicity, where we extend the shear field by a rigid body rotation. In order to apply the Helmholtz Vortex group operation, we consider as first field initial field the outcome (9.33) of the Vortex-Heisenberg group operation of our first case study $(\mathbf{a}'', \mathbf{A}'')$. We notice that $VH(3)$ is embedded in $V(H)$ and thus, we can extend $(\mathbf{a}'', \mathbf{A}'')$ by a rotational matrix $\underline{\mathbf{R}}'' \in SO(3)$:

$$(\mathbf{a}'', \mathbf{A}'') \mapsto (\mathbf{a}'', \mathbf{A}'', \underline{\mathbf{R}}''). \tag{9.68}$$

Here, we consider $\underline{\mathbf{R}}''$ as rotation around the y-axis about $\pi/2$. As second initial state we consider the shear flow without helicity from our first case study (9.27) and extend it by the unity matrix to obtain an element in V(3):

$$(\mathbf{a}_{s1}, \mathbf{A}_{s1}) \mapsto (\mathbf{a}_{s1}, \mathbf{A}_{s1}, \mathbb{E}) \tag{9.69}$$

Now, we apply the Helmholtz Vortex group operation (8.89) to these two initial states and obtain the state $(\mathbf{a}''', \mathbf{A}''', \underline{\mathbf{R}}''')$

$$(\mathbf{a}''', \mathbf{A}''', \underline{\mathbf{R}}''') = (\mathbf{a}'', \mathbf{A}'', \underline{\mathbf{R}}'') * (\mathbf{a}_{s1}, \mathbf{A}_{s1}, \mathbb{E}), \tag{9.70}$$

which is a further element of the Helmholtz' Vortex group, because of the closure property of groups. The helicity density of this group element

$$h''' = (\mathbf{a}''' \cdot \mathbf{A}''') \tag{9.71}$$

is shown in 3D in fig. 9.15. The helicity density fields of all states we consider in this example are summarized in fig. 9.16. We see that a further split is generated, which was not possible by applying the Vortex-Heisenberg group operation again. But, extending the Vortex-Heisenberg group to the Helmholtz Vortex group allows for further vortex breakups.

Regarding fig. 9.15, the yellow region shows the area, where the squared absolute value of the Lamb vector approaches zero, i.e. $|\mathbf{a} \times \mathbf{A}|^2 \approx 0$. As we have discussed in the first case study, the Lamb vector is zero if either the the vectors $\mathbf{a}$ and $\mathbf{A}$ are zero or if they are parallel. The last case characterizes a strongly helical rotating Beltrami field. Similar to our first example of a vortex split regarding the Vortex-Heisenberg group (see fig. 9.10) we recognize that the positive-negative structures are located at the boundary of the Beltrami-like region.

To summarize, by integrating the angular momentum into the Vortex-Heisenberg group, we could induce further splits, as summarized in fig. 9.16. We think that even more splits can be caused such that a *helicity cascade* can be generated even in conservative systems, which has not be shown so far. We will discuss possible implications for turbulence in the next section.

9.5 Implications for turbulence theory

Classical turbulence studies regard the famous law of Kolmogorov $E(k) \sim \epsilon^{2/3} k^{-5/3}$ for the energy cascade in three dimensions and Kraichnan's law for the enstrophy cascade in two dimensions $E(k) \sim \eta^{2/3} k^{-3}$. Both are classically analyzed in the space of wave numbers k Here, ϵ denotes the energy dissipation and η the enstrophy dissipation. It was found that the energy in three dimensions as well as the enstrophy in two dimensions cascade from larger to smaller scale. Furthermore, in two dimensions an anti-cascade of the energy was found. The first investigations of the different cascades can be ascribed to Kolmogorov (1941), Onsager (1949), Weizsäcker (1948), Heisenberg (1948), Obukhov (1941) and Kraichnan (1967). There are many works corroborating Kolmogorov's and Kraichnan's theories either

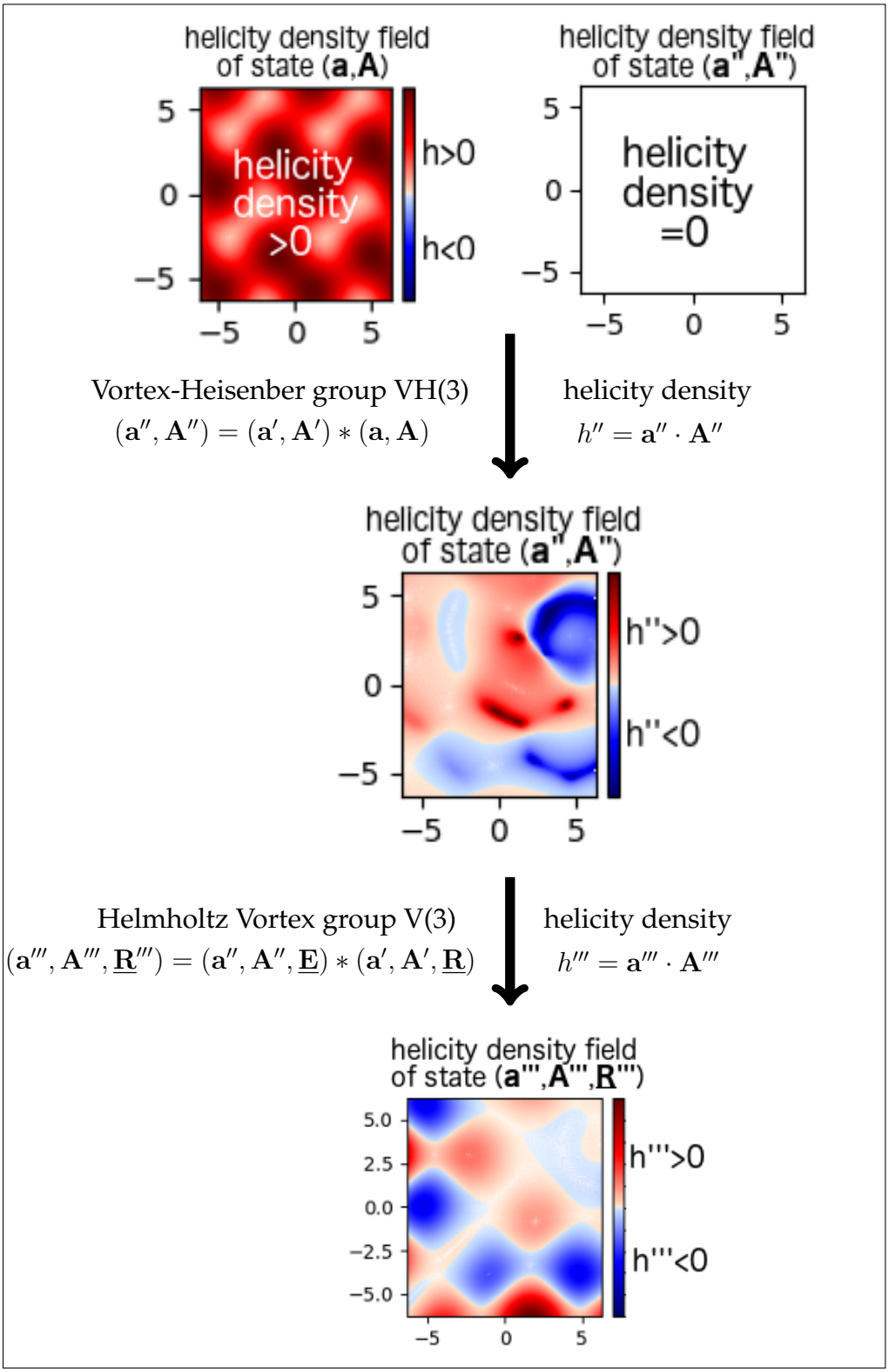

Figure 9.16: Starting with two initial fields, each indicating a state of a meteorological flow, the induced helicity field is characterized by a plus-minus structure. Coupling this field again with the initial shear field, further vortex breakups can be provoked.

numerically, in terms of the Navier-Stokes equations, or experimentally, see e.g. the works of Kraichnan and Montgomery (1980), Chorin (1994), Frisch (1995), Boffetta and Ecke (2012) or Mininni and Pouquet (2013). Nastrom et al. (1984) were the first, who showed that Kolmogorov's and Kraichnans theories holds for atmospheric data sets.

Comparing 2D and 3D flows with respect to their constitutive conservation laws, we recognize that in two dimensions the energy as well as the enstrophy are both positive definite. In three dimensions, the energy is positive definite, whereas the helicity can have positive as well as negative sign, depending on the direction of the vortex rotation and the velocity. This sign structure seems to be a reason, why the helicity has only rarely discussed (Kurgansky, 2017). First works concerning the helicity can be ascribed to Ertel and Rossby (1949), Betchov (1961), Moreau (1961), Moffatt (1969) and Kraichnan (1973). Concerning turbulence studies, and especially the breakup of vortices, we think that it is an interesting and underestimated quantity. On the one hand, the helicity is a constitutive quantity of the Nambu representation for three-dimensional incompressible fluids. On the other hand, in contrast to mass points that move on straight lines, vortices naturally rotate, and the helicity is related to such vortex rotations.

We notice some of the few works that did consider the helicity as an important quantity besides the energy. Brissaud et al. (1973) discuss the cascades of energy and helicity as well as a pure helicity cascades with no energy cascades. By dimensional analysis they obtained a $E(k) \sim k^{-7/3}$-law for a anti-cascade of the helicity. Today, it is known that there is a joint cascade of helicity and energy (see, e.g., Kurgansky, 2017). Chen et al. (2003) discussed the cascades of energy and helicity, regarding both signs of the helicity, see also the works of Pouquet and Mininni (2010) and Dallas and Tobias (2016). In their recent work, Biferale et al. (2013) show numerically that, in nature, in all three-dimensional flows one can find a subset of nonlinear evolution, which leads to a reverse energy transfer from small to large scales. The authors use setups with fixed sign of the helicity and show that the cascade depends on the chosen sign of helicity. In this way, the authors show that there exist energy cascades to larger scale in three dimensions, too. So far, energy cascades to larger scales were related to two-dimensional flows. The reversed energy cascade happens in cases, where the mirror symmetry is broken, underlining the importance of the quantity helicity itself, and in particular its sign. In these cases, the helicity cascades

towards smaller scales and the energy cascades in opposite direction, to larger scales. Thus, the choice of a fixed sign of helicity influences the direction of the energy cascade. In case the helicity field is zero, the energy cascades to smaller scales.

So far, systems with friction are used to study the different cascades. Mostly, flows are analyzed statistically considering the space of wave numbers leading to a global perspective. In this approach not the physical configuration space is regarded, where the flow actually evolves (Cardesa et al., 2017). Considering the physical space allows for a local view on vortex dynamics. Using direct numerical simulation, Cardesa et al. (2017) follow individual eddy structures in the physical space. They time-track vortices by using a technique for the tracking of coherent structures and observed that vortices often merge with or split from other vortices during its life. The authors observe the split and merge of vortices.

Considering the technical setup of turbulence studies, we cite Brissaud et al. (1973) that *it is difficult to fed helicity in a fluid without at the same time injecting no energy*. We think that the application of the Nambu formulation can help to tackle this problem. To examine vortex dynamics, the Nambu bracket is determined with respect to the helicity. Thus, the helicity and the energy can be regarded separately. And we think that the Nambu representation provides a direct approach to study vortex breakups, or vortex dynamics in general, because this formulation of the vorticity equation it is based on *vortex*-related quantities.

In fig. 9.17 we sketch how our group theoretical approach could be unified with Kolmogorov's concept. Kolmogorov did not derive his famous $k^{-5/3}$-law from a set of equations, such as the Navier-Stokes equations. It is derived by dimensional analysis of the energy dissipation. In this thesis, we consider an algebraic approach, derived from the Helmholtz vorticity equation, to explain the mechanism of vortex breakups with respect to the sign structure of the helicity. There are also at least two advantages of the group theoretical approach for further investigations on turbulence theory. As we have discussed in chapter 8, a group is a set of elements satisfying some properties such that the group is closed under the group operation. Physically, each group element of the Vortex-Heisenberg group VH(3) is related to a wind and a vorticity field. Starting with two Vortex-Heisenberg group elements and applying the corresponding group operation results in a further element which can also be related to a wind and a vorticity field.

Because of the closure property of groups and recalling that the Vortex-Heisenberg group is derived from Helmholtz' vorticity equation, all wind and vorticity fields that result from the Vortex-Heisenberg group operation can be seen as solutions of Helmholtz' vorticity equation. Furthermore, because of the closure property of groups and the existence of inverse group elements we can consider a helicity field with a plus-minus-sign structure and generate a Beltrami flow field characterized by a helicity density field with one sign, as indicated as *Beltramization* in fig. 9.17.

In contrast to Kolmogorov, we consider conservative systems. We think that it seems reasonable that friction is only related to the direction of the cascade and not to the mechanism of vortex split, as indicated in fig. 9.17. Such assumptions can only be explored in conservative systems. But to compare frictional and inviscid processes a future goal is the derivation of a Nambu bracket for dissipative systems. Our algebraical concept can be seen complementary to Kolmogorov's classical point of view that is sketched in fig. 9.17. He was the first who proposed the vortex breakups. A unifying concept might be helpful for a better understanding of turbulent vortex flows.

9.6 Summary

In the previous chapters we applied Nambu-mechanics to formulate fluid mechanics from an algebraic point of view. Based on the works of Névir and Blender (1993) and Névir (1998) we have introduced a novel matrix representation of the Vortex-Heisenberg algebra vh(3) and derived a vector and a matrix representation of the Vortex-Heisenberg group VH(3), where the group operation itself was communicated with Peter Névir in private communication with Anton Schober in 2010. In this chapter we have applied the Vortex-Heisenberg group to explain the mechanism of vortex splits.

There are some advantages of the group theoretical approach. A group is a set together with a group operation. And the elements of the set need to satisfy some properties such that the group is closed under the group operation. One important property is the closure-property of groups. Because of the closure property, we can apply the group operation to generate further group elements. Consider two initial group elements characterizing two wind and vorticity fields, combine them by the VH(3)-operation. Then, we obtain a third group element. And this induced group element can be seen as solution of the Helmholtz vorticity equation, because VH(3) is derived from Helmholtz vorticity equation.

We considered the group elements as atmospheric states and interpreted the outcome of the Vortex-Heisenberg group operation as interaction of two states. Then, we examined the helicity density fields of the initial states and the induced state. We represented a supercell by a ABC-flow and chose this ABC-flow as one initial field and a shear field with vanishing helicity density as second initial field. We define a vortex split in terms of the sign of the helicity density field. If the helicity density field of the induced state contains different signs of helicity density that differs from the helicity density structure of the initial fields, we speak of vortex splits. In this way we showed the existence of vortex splits as well as the generation of supercells in conservative settings. We have discussed four case studies with respect to the Vortex-Heisenberg group considering different initial flows. We could corroborate our assumption that vortex splits occur for two initial fields with contrary absolute values of the helicity density. As a fifth case, we have applied the novel Helmholtz Vortex Lie group V(3) to show that further vortex splits can be generated.

Moreover, we can transfer the mathematical group property of the existence of inverse elements to atmospheric flows. Starting with a helicity field

with a small-scale plus-minus structure we can apply the VH(3)-group operation and obtain a helicity density field with larger-scale sign structures up to a helicity density field without a change of sign.

Furthermore, the Nambu bracket is based on the vorticity equation. We determined the Nambu bracket with respect to the helicity. In this way, we express the vorticity equation in terms of a vortex-related conserved quantity. In our algebraic approach to understand the initial conditions that cause vortex splits we have considered conservative systems leading to the assumption that the direction of the cascade is determined by the dissipation. But the mechanism of the vortex breakup might not depend on friction.

Kolmogorov proposed the decay of vortices independent of the sign structure of the helicity. Here we related the split of vortices to the helicity density field regarding conservative systems, i.e. no friction. Thus, our result can be seen as an extension to Kolmogorov's theory and the unification of both concepts might deepen the understanding of turbulent flows.

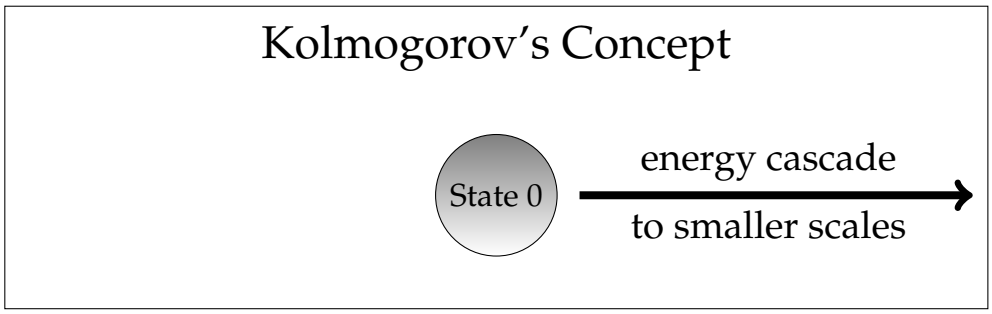

Dissipation, System with broken time reversal

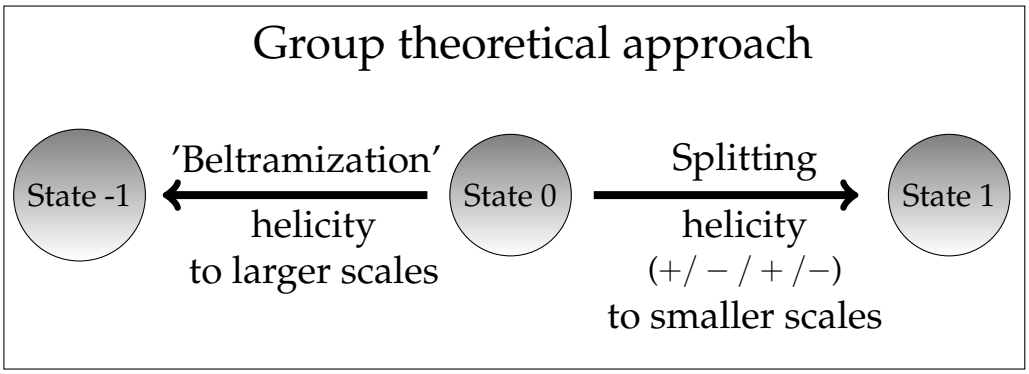

Conservative System with time reversal

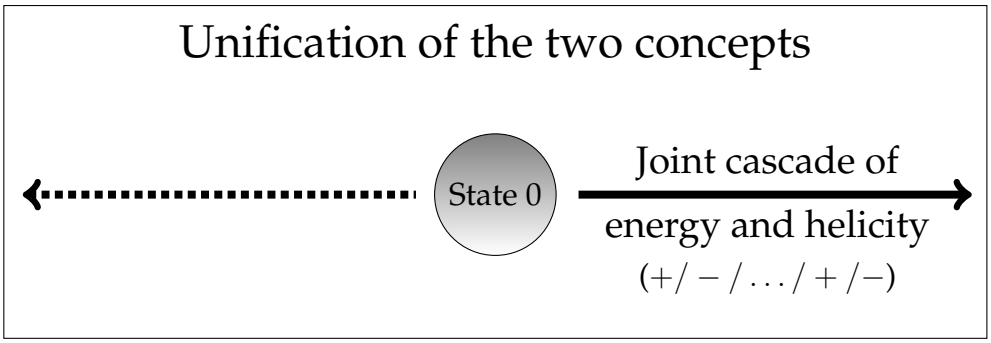

Dissipation

Figure 9.17: Comparison of Kolmogorov's concept of the energy cascade with the here introduced group theoretical approach based on Helmholtz' vorticity equation

Chapter 10

Sub-Riemannian Geometry applied to VH(2) and VH(3)

In this chapter we will apply sub-Riemannian geometry to derive shortest paths of vortices in two-and three dimensions. Shortest paths between two points are commonly called geodesics. But what are geodesics in terms of vortex dynamics? For two dimensional dynamics, we will consider the idealized point vortex model we explored in the first part of this thesis. Then, we can define vortex geodesics by shortest paths of single point vortices. In three dimensions, we will outline the concept, how sub-Riemannian geometry can be applied to find shortest motions, too, but we will not find *one* answer, what 3D-vortex geodesics are.

Applying sub-Riemannian geometry to vortex dynamics we will first regard pure mathematics of the fields differential geometry and algebra. Then, we will apply this theoretical concept to fluid dynamics, which further can be transferred to atmospheric phenomena. In order to find vortex geodesics, we first have to find the right spaces, where we can measure distances. Mathematically, there are many different metric spaces, each defined by a set with a metric. Let us start start with the well-known Euclidean geometry in three dimensions. The Euclidean distance between two points is given by a straight line segment, which is the shortest path between two points and therefore the geodesic.

This concept can be generalized to find shortest paths on arbitrary smooth manifolds, as we have sketched in fig. 10.1. Let us consider a smooth curved surface M, for example the sphere $M = S^2$ embedded in a three dimensional space, and denote with A a starting point on this curved surface M. We look for the shortest path from A to another point B on M. In

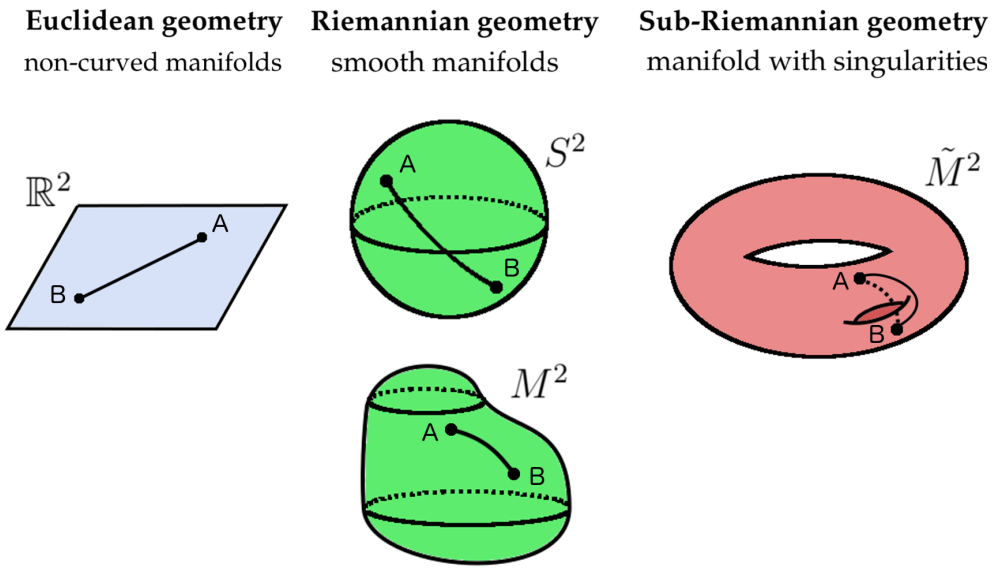

Figure 10.1: The differences between Euclidean, Riemannian and sub-Riemannian geometry are shown. All spaces can be endowed with a suitable metric to connect two points A and B on a manifold. In case of a non-smooth manifold, we have to move on so-called horizontal bundles, because the motion is restricted by singularities. Sub-Riemannian geometry is also called singular Riemannian geometry.

this case, Euclidean geometry is not an appropriate choice to measure the distance between A and B, because it would be the secant line; the shortest path from A to B on the manifold is curved, too, and can not be a segment of a straight line. We would like to move *on* the surface, as for example on the sphere, and we assume that we are not allowed to cross the sphere. As a first guess, we would use Riemannian geometry, where the so-called Riemannian metric is defined with respect to the manifold such that the Riemannian metric can be used to measures lengths of paths on *any smooth* manifold. On a sphere it turns out that the shortest path between two points lies on a great circle, see fig. 10.1, and the geodesics is given by a formula of the arccosine.

Sometimes the constraints restrict the motion such that the manifold is not smooth anymore. In this case, we have to measure distances using tangent spaces. At each point on a Riemannian manifold the tangent space is endowed with the Euclidean structure. This structure smoothly depends on the point where the tangent space is attached. Let us assume, we have a walk on a Riemannian manifold M and we stop at a point p in M. Then, the tangent vectors in this point give us the directions where to move. We can move in all directions on the tangent plane. And we can measure lengths

of vectors and angles between vectors that are attached at the same point. These measurements are done using the Euclidean rules.

Let us now assume that we stand on a sub-Riemannian manifold. But we are not allowed to move in all directions. There are constraints, for example a physical law, that restrict our motion. A sub-Riemannian space is a smooth manifold with a fixed admissible subspace in any tangent space where the admissible subspaces are equipped with Euclidean structures (Barilari et al., 2016; Agrachev et al., 2016). The distance between two points in a sub-Riemannian space is the infimum of the length of admissible paths connecting the points. As we will discuss more in detail later in this chapter, sub-Riemannian geodesics are measured by moving along curves that are tangent to so-called horizontal subspaces. For example, we would use sub-Riemannian geometry if we aim for finding the shortest orbits of satellites in space, or if we park a car. In the last example our constraint is given by the fact that we can not drive a car sidewards. Thus, to describe the position of a car we consider its location ($\mathbb{R}^2$) and an angle (S^1), i.e. a point on the manifold $\mathbb{R}^2 \times S^1$. Its shortest path can be determined by the infimum of a sub-Riemannian path, we call this shortest path sub-Riemannian goedesics. For further readings see, e.g., Montgomery (2006), Calin and Chang (2009) or Barilari et al. (2016).

From mathematical perspective, nilpotent groups allow for the application of sub-Riemannian geometry. Therefore, the classical Heisenberg group is an example for the derivation of sub-Riemannian geodesics. Physically, the group representation for electric charged particles in static inhomogeneous magnetic fields is given by a Heisenberg group (Monroy-Pérez and Anzaldo-Meneses, 1999; Montgomery, 2006). Classical mass points move on straight lines, therefore, we can find their shortest paths without applying sub-Riemannian geometry. But charged particles behave similar to vortices. In chapter 8 we have shown that VH(2) holds the classical Heisenberg group structure, even though it is derived from the vorticity equation. We have shown that VH(2) as VH(3) are nilpotent groups providing a natural structure to apply sub-Riemannian geometry. Physically, vortex motion is constrained by conservation laws: the conservation of the linear momentum $\mathbf{P}$, the angular momentum $\mathbf{L}$ and the energy can all be expressed by the vorticity. There are also scale-dependent conservation laws for incompressible, inviscid fluids such as the enstrophy and circulation in two dimensions and the helicity and the flux of vorticity in three

dimensions, as we have discussed in chapter 7; Therefore, the motion of vortices is constrained by vortical rotations. We think that the constraints on the vortex motions are mathematically reflected in the nilpotent structure of the Vortex-Heisenberg group that we have derived and explored in the previous chapters. This nilpotent structure provides a natural sub-Riemannian applicability.

But, so far, sub-Riemannian geometry has not been considered for the study of vortex dynamics. Instead, the Riemannian view has been used for the investigation of extremal principles for hydrodynamic systems, see e.g. Arnold and Khesin (1992) or Holm et al. (1998). where mostly the energy is considered to derive extremal principles for fluid dynamical systems. But, to the best of our knowledge, there are no investigations of the derivation of vortex geodesics regarding additional vortex-related quantities. The major difference is the set of equation that provides the underlying structure. The Euler equation is commonly used as basis for the geometrical as well as for the algebraical view. In contrast, in this thesis, the algebraic and geometric views on vortex dynamics are based on the Helmholtz equation. This means that most authors consider wind field as basis variable and analyze the kinetic energy and the vortex quantities based on the Euler equations. The Helmholtz equation results from the rotation of the Euler equations, i.e. $\nabla\times$ Euler equations, leading to the description of the time evolution of the vorticity. But, some authors do consider the vorticity equation as basis, but they still deal with the Hamiltonian structure, which takes only the energy into account and not the vortex-related conservation laws.

Thus, the use of the Nambu representation to form a Lie algebra for vortex dynamics that is directly based on the vorticity equation can be seen as an advantage. Moreover, the conservation of mass is implicitly included in the Nambu formulation, whereas, concerning the Euler equations of motion and the corresponding Hamiltonian view, the incompressibility condition, i.e. the conservation of mass, is expressed by an additional equation. In other words: using the vortex equation, we are already on the appropriate hierarchical level to build a Lie algebra that can be used for the derivation of shortest paths of vortices.

We will show that the vortex geodesics for two-dimensional vortex dynamics is comparable to the sub-Riemannian application of charged particles in a magnetic field (Monroy-Pérez and Anzaldo-Meneses, 1999). The vortex geodesics for two-and three-dimensional vortex flows will be de-

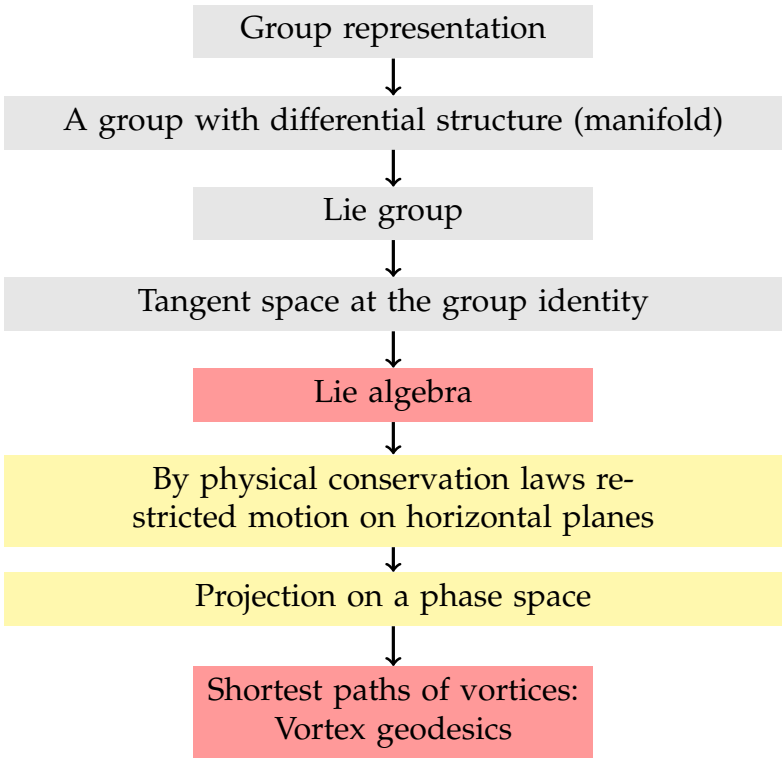

Figure 10.2: How to derive vortex geodesics via sub-Riemannian geometry.

rived after the generalized algorithm of Monroy-Pérez and Anzaldo-Meneses (2006). The steps for the derivations regarding sub-Riemannian geometry are summarized in fig. 10.2. Starting with Lie group, which is a group with an underlying manifold, we can consider a Lie algebra, which can be regarded as the tangent space at the group identity. The tangent space, denoted by TM, is the space that contains all velocity vectors of all possible curves lying on the manifold M. Further, we denote with $T_{\mathrm{x}}M$ the tangent space of M in a point $\mathrm{x} \in M$. As discussed in the previous paragraph, regarding the sub-Riemannian structure, standing on the tangent space gives us the direction where to move, but we have some restriction, where we are allowed to move. Now, we have to split the tangent space of the tangent space (short: TTM) into vertical and horizontal subboundles and use the isomorphism $TTM \cong TM$, see (10.18) and (10.14), because we are only allowed to walk on horizontal planes. From the fluid dynamical perspective, it is natural that vortices do not move on straight lines, they are restricted by the rotational part of the motion leading to constraints with respect to the vortex-related conserved quantities.

A classical example of sub-Riemannian geometry is Dido's problem (see,

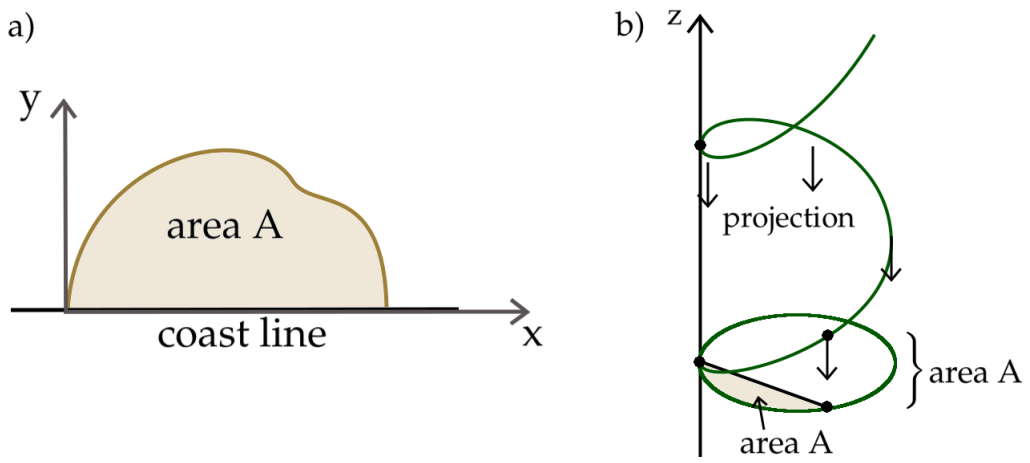

Figure 10.3: a) Dido's problem was to enclose a maximal area with a leather string of fixed length. b) To solve her problem, she had to extend the space by a z-coordinate, and the projection of the 3D curves leads to a solution. Based on Montgomery (2006).

e.g. Montgomery, 2006). It goes back to the time of the beginning of Rome. Queen Dido had to flee, arriving at Africa she was allowed to get as much land as she could enclose with a leather string of fixed lengths. She got a piece of land at he coast. Approximating the coast line by a straight line, she had to tackle the question: What is the shape of the curve that encloses a maximal area? This problem is called Dido's problem, illustrated in fig. 10.3, and the solution – a half circle – can be derived by the use of sub-Riemannnian geometry.

To find shortest paths on a land surface with the constrained of the enclosure of a maximal area seems like a two-dimensional problem. Consider the coordinates x, y and the differential 1-form (see def. 43)

$$\omega = \frac{1}{2}(xdy - ydx), \tag{10.1}$$

which satisfies $d\omega = dy \wedge dy$. Denote with A the area enclosed by a planar curve c (the leather string of fixed lengths) and a straight line segment (the coast line), where the straight line segment and the curve intersect at the origin. The area A is given by:

$$A(c) = \int_c \omega \tag{10.2}$$

the curve c is a function $c = (x(t), y(t))$ with length

$$l(c) = \int_c ds, \tag{10.3}$$

where $ds = \sqrt{dx^2 + dy^2} = \|\dot{c}\|dt$.

To solve Dido's problem we construct a three-dimensional geometry and add a third direction z such that we can find three dimensional curves of the form $(x(t), y(t), z(t))$. Therefore, we consider the 1-form

$$\dot{z} = \frac{1}{2}(-y(t)\dot{x}(t) + x(t)\dot{y}(t)). \tag{10.4}$$

such that the single planar curve $c(t) = (x(t), y(t))$ is linked to a family of three-dimensional curves that we denote with $\gamma(t) = (x(t), y(t), z(t))$. We define the length of this paths γ to be equal to the Euclidean length l of the two-dimensional curve (10.3). Such three-dimensional paths γ are called horizontal path. We will give a precise mathematical definition later in this chapter. Then, each planar curve $(x(t), y(t))$ has a lift to $(x(t), y(t), z(t))$ in $\mathbb{R}^3$, where $z(t)$ is given by the integral:

$$z(t) = z(t) - z(0) = \frac{1}{2}\int_0^t (x(t)dy(t) - y(t)dx(t)). \tag{10.5}$$

Or in other words, $c(t)$ is the projection of $\gamma(t)$ to the plane. We apply Stoke's theorem, assume the following initial conditions $z(0) = 0$, $x(0) = y(0) = 0$ such that c joins the origin and it also joins (x_1, y_1). Then, for the endpoints of the 3D curve γ we obtain ($x_1, y_1, A(c)$.) Thus, this example yields the solution of Dido's problem: Finding a shortest curve between two points, where the curve together with the straight line between the points enclose a certain – in this case a maximal – area (see, e.g. Montgomery, 2006). The algebra is hidden in the part, where we considered the three-dimensional curves as horizontal paths. These paths γ are on tangent spaces, and Lie algebras can be regarded as tangent spaces at the group identity. Our motivation of the first example was to illustrate the applicability of sub-Riemannian geometry to a simple problem.

We will begin with an introduction to the basic differential geometric definitions in section 10.1. The basics are needed for the general algorithm to find sub-Riemannian geodesics for a 2-step nilpotent Lie algebra that we will introduce in section 10.2. Thereby, we will consider a tangent boundle

$\Delta \subset TM$ that is spanned by vector fields $\mathbf{X}_1, \dots \mathbf{X}_n$. These vector fields are associated with Hamiltonian functions that generate the Lie algebra. We will regard the Vortex-Heisenberg Lie algebras vh(2) and vh(3). For each Lie algebra we will obtain a pair $(\mathbf{h}, \underline{\mathbf{H}})$ that is composed of a vector $\mathbf{h}$ and a matrix $\mathbf{H}$:

i) For vh(2) we will obtain a vector $\mathbf{h} \in \mathbb{R}^2$ and $\mathbf{H} \in$Mat(2×2)

ii) And for vh(3) we will obtain a vector $\mathbf{h} \in \mathbb{R}^3$ and $\mathbf{H} \in$Mat(3×3).

Determining the corresponding hauptspace leads to the phase space of the geodesics. We remark that the Hamiltonian here is not related to the energy. In this chapter, we are looking for geodesics and therefore, we apply optimal control theory where the notion Hamiltonian is commonly used for the function which solution provides extremal trajectories, especially under constraints. The Russian mathematician Lev Pontryagin introduced this terminology in 1965.

In section 10.3 we will consider the Vortex-Heisenberg Lie algebra vh(2) which was derived in chapter 6. The Vortex-Heisenberg Lie algebra vh(2) provides the structure of a (2,3)-sub-Riemannian geometry. In general, a $(n, n(n+1)/2)$- sub-Riemannian geometry can be applied to a $(n(n+1)/2)$-dimensional Lie algebra with a rank n distribution. A distribution Δ of rank n is a subspace of the tangent space of a manifold, where there exist n linearly independent vector fields that form a basis for the distribution Δ. For vh(2), we have seen that the corresponding Nambu brackets of the momenta P_x and P_y and the circulation Γ result in the circulation:

$$\{P_x, \mathcal{E}, P_y\} = \Gamma, \quad \{P_x, \mathcal{E}, \Gamma\} = \{P_y, \mathcal{E}, \Gamma\} = 0 \tag{10.6}$$

Thus, the rank of the Lie algebra is three (P_x, P_y, Γ) with rank of distribution 2, which is the number of elements P_x, P_z. We will show, how the from the Vortex-Heisenberg algebra resulting two-dimensional sub-Riemannian vortex geodesics can be related to a special point vortex system that we have discussed in chapters 3 and 4.

Finally, in section 10.5, we will search for geodesics for three-dimensional vortex flows. The sub-Riemannian geodesics are based on he Vortex-Heisenberg Lie algebra vh(3) that we have derived in chapter 6. We recall the bracket relations of the components of the 3D momentum P_x, P_y and P_z

and the flux of vorticity $\mathbf{Z} = (Z_x, Z_y, Z_z)$ with respect to the helicity h_V:

$$\{P_i, h_V, P_j\} = \epsilon_{ijk} Z_k, \quad \{Z_i, h_V, P_j\} = \{Z_i, h_V, Z_j\} = 0. \tag{10.7}$$

The dimension of the Vortex-Heisenberg Lie algebra is 6 (6 elements: P_x, P_y, P_z, Z_x, Z_y, Z_z) with rank 3 distribution. Therefore, vh(3) yields an example of a (3,6)-sub-Riemannian geometry. But this application should be seen as an outlook, which will be more examined in future studies. In two dimensions, we can compare the (2,3)-sub-Riemannian geodesics with a discrete point vortex model. Such an idealized discrete model does not exist for three dimensions.

10.1 Basics of differential geometry

We will start with an introduction to the basics of differential geometry. For more detailed proofs or explanations, see e.g. Kühnel (1999), Berger and Gostiaux (2012) or Do Carmo et al. (2017).

Definition 41. Tangent space
The tangent space, denoted by TM, is the space that contains all velocity vectors of all possible curves lying on the manifold M. With $T_{\mathbf{x}}M$ we denote the tangent space of M in a point $\mathbf{x} \in M$.

Definition 42. Linear form and dual space
Let V be a vector space over a field K. Then, a linear functional or linear form (which is also called one-form or covector) is a map from V to K that is linear and satisfies the following conditions:

$$\begin{aligned} \varphi(\mathbf{v} + \mathbf{w}) &= \varphi(\mathbf{v}) + \varphi(\mathbf{w}) && \text{for all } \mathbf{v}, \mathbf{w} \in V \\ \varphi(a\mathbf{v}) &= a\varphi(\mathbf{v}) && \text{for all } \mathbf{v} \in V, a \in K. \end{aligned} \tag{10.8}$$

All linear functionals from V to K form a vector space $\mathrm{Hom}(V, K)$ over the field K. This space

$$V^* := \mathrm{Hom}(V, K) = \{\phi : V \longrightarrow K | \ \phi \text{ linear } \} \tag{10.9}$$

is called the dual space of V.

We notice that dealing with Lie algebras means dealing with linear spaces. Therefore, to find vortex geodesics based on the Vortex-Heisenberg algebra,

we need to introduce the following definitions.

Definition 43. Pfaffsche Form
A Pfaffsche Form ω on M (also called 1-Form or differential form) assigns a linear form $\omega_p \colon \mathrm{T}_{\mathbf{x}}M \to \mathbb{R}$ to each point $\mathbf{x} \in M$.

Such linear forms are called cotangent vectors which are elements of the so-called dual space (or cotangent space) $\mathrm{T}^*_{\mathbf{x}}M$ with respect to the tangent space T_pM. Therefore, a Pfaffsche Form ω is a map

$$\omega \colon M \to \bigcup_{\mathbf{x}\in M} \mathrm{T}^*_{\mathbf{x}}M, \quad \mathbf{x} \mapsto \omega_{\mathbf{x}} \in \mathrm{T}^*_{\mathbf{x}}M. \tag{10.10}$$

Example 8. A 1-form ϕ on $\mathbb{R}^3$ is a function on the set of all tangent vectors to $\mathbb{R}^3$ such that ϕ_p is is linear using the notation $\phi_p := \phi(p)$. This means, for $\alpha, \beta \in \mathbb{R}$ and tangent vectors $\mathbf{v}, \mathbf{w} \in \mathbb{R}^3$ it is:

$$\phi_p(\alpha\mathbf{v} + b\mathbf{w}) = \alpha\phi_p(\mathbf{v}) + \beta\phi_p(\mathbf{w}) \tag{10.11}$$

We follow for example O'Neill (2006) and emphasize that for every tangent vector $\mathbf{v}$, ϕ_p maps to a real number. Moreover, for each point $\mathbf{x} \in \mathbb{R}^3$, the resulting function $\phi_{\mathbf{x}} : T_{\mathbf{x}}\mathbb{R}^3 \to \mathbb{R}$ is linear. That means that at each point $\mathbf{x}$, $\phi_{\mathbf{x}}$ is an element of the dual space of $T_{\mathbf{x}}\mathbb{R}^3$

Definition 44. Parallel vector field
A vector field $\mathbf{V}(t)$ along a regular parametrized curve γ of constant length is called parallel if the derivative $\mathbf{V}'(t)$ is normal to the tangent plane $T_{\mathbf{x}}M$ at each point $\mathbf{x} = \gamma(t)$ of the curve.

If for all t the parallel field $\mathbf{V}'(t)$ is normal to the tangent plane, the length of the vectors $\mathbf{V}(t)$ is constant, which follows immediately from:

$$\frac{d}{dt}|\mathbf{V}|^2 = \frac{d}{dt}(\mathbf{V}\cdot\mathbf{V}) = 2\mathbf{V}'\cdot\mathbf{V} = 0. \tag{10.12}$$

Definition 45. Geodesics
A unit speed curve γ on a surface M is a geodesic if and only if its tangent vectors $\gamma'(t)$ form a parallel field.

Example 9. Let us consider the great circle on a 2-sphere. If we move along the geodesic, i.e. along the great circle parametrized as regular curve, we recognize that the angle of the tangent vector is constant. Therefore, the tangent vectors of the great circle form a parallel field. Thus, the great circle is a geodesic curve on the 2-sphere.

The concept of the covariant derivative can be used to determine directional derivatives of vector fields, i.e. the infinitesimal transport of a vector field in a given direction.

Definition 46. Covariant derivative and parallel transport
Let $\mathbf{V}$ be a smooth vector field along a curve $c : I \to M$ on a manifold. Then the covariant derivative of $\mathbf{V}$ along c at the point $p = c(t)$ is given by

$$\frac{D_c\mathbf{V}}{dt}(p) = \frac{D_c\mathbf{V}}{dt}(c(t)) = \lim_{s\to t} \frac{P_{c(t),c(s)}\mathbf{V}_{c(s)} - \mathbf{V}_{c(t)}}{s-t} \in T_pM \tag{10.13}$$

with parallel transport $P_{c(t),c(s)}$ of the tangent vector $\mathbf{V}_{c(s)}$ to the tangent vector at the point $c(t)$.

We can picture the covariant derivative $\frac{D_c\mathbf{V}}{dt}(c(t))$ as the projection of $\frac{d\mathbf{V}}{dt}$ into the tangent plane to the surface. Physically, the covariant derivative $\frac{D_c\mathbf{V}}{dt}(c(t))$ of a particle trajectory $c(t)$ along the surface with velocity field represents the acceleration component of the particle along the surface.

Let now TM denote the tangent bundle, $T_{\mathbf{x}}M$ the tangent space at the point $\mathbf{x}$ and TTM ($T_{\mathbf{x}}TM$) the tangent space of the tangent space (at the point $\mathbf{x}$). Consider the maps θ and $d\theta$:

$$\theta : TM \to T \quad \text{and} \quad d\theta : TTM \to TM \tag{10.14}$$

Using the notation $d\theta(\mathbf{x}) := d_{\mathbf{x}}\theta$ the kernel and the image of $d\theta$ of $d_{\mathbf{x}}\theta$ are given by:

$$\begin{aligned} \mathrm{Ker}(d_{\mathbf{x}}\theta) &= \{\mathbf{N} \in T_{\mathbf{x}}TM \mid d\theta(\mathbf{N}) = \mathbb{1}_{T_{\theta(\mathbf{x})}}M \in T_{\theta(\mathbf{x})}M\} \\ \mathrm{Im}(d_{\mathbf{x}}\theta) &= \{d_{\mathbf{x}}\theta(\mathbf{N}) \mid \mathbf{N} \in T_{\mathbf{x}}M)\} \end{aligned} \tag{10.15}$$

We remark that $\ker(d_{\mathbf{x}}\theta) \subseteq TTM$ and $\mathrm{im}(d_{\mathbf{x}}\theta) \subseteq TM$ such that there exists an isomorphisms $\varphi : TTM \to TM$ such that $TTM \cong TM$, $T_{\mathbf{x}}TM \cong T_{\theta(\mathbf{x})}M$ respectively, as illustrated in the following diagram:

$$\begin{array}{ccc} TTM & \xrightarrow{d_{\mathbf{x}}\theta} & TM \\ \varphi \big\downarrow & & \\ TM & \xrightarrow{\varphi^{-1}} & TTM \end{array}$$

Now, we can identify:

$$\varphi(\ker(d_{\mathbf{x}}\theta)) \cong \ker(d_{\mathbf{x}}\theta) \quad \text{and} \quad \varphi^{-1}(\mathrm{im}(d_{\mathbf{x}}\theta)) \cong \mathrm{im}(d_{\mathbf{x}}\theta) \tag{10.16}$$

and set

$$V_{\mathbf{x}} := \ker(d_{\mathbf{x}}\theta) \quad \text{and} \quad H_{\mathbf{x}} = V_{\mathbf{x}}^{\perp}. \tag{10.17}$$

Then, we can write:

$$\boxed{T_{\mathbf{x}}TM = H_{\mathbf{x}} \oplus V_{\mathbf{x}}} \tag{10.18}$$

Further, denote $\mathbf{c}\|_0^t \in T_{c(t)}M$ the vector that we obtain by shifting the tangent vector $\mathbf{x}$ parallel along $\gamma|_{[0,t]}$, where γ is a geodesic. Then we get an isomorphism

$$h_{\gamma,\mathbf{x}}^{-1} : TM \to T_{\mathbf{x}}TM, \quad \mathbf{v} \mapsto \frac{\partial}{\partial t}\Big|_{t=0} \left(\mathbf{c}_{\mathbf{x}}\|_0^t\right). \tag{10.19}$$

And the image of the isomorphism $h_{\gamma,\mathbf{x}}^{-1}$ can be identified with $H_{\mathbf{x}}$, i.e.

$$\mathrm{Im}(h_{\gamma,\mathbf{x}}^{-1}) \cong H_{\mathbf{x}} \tag{10.20}$$

leading to the following definition of $H_{\mathbf{x}}$:

$$\begin{aligned} H_{\mathbf{x}} := \{\dot{\mathbf{c}}(0) \mid \mathbf{c} : I \to \text{TM parallel along a geodesic } \gamma, \\ \gamma : I \mapsto M \text{ with } \gamma(0) = \theta(\mathbf{x}) \text{ und } \mathbf{X}(0) = \mathbf{x}\}. \end{aligned} \tag{10.21}$$

which corroborates the above representation of $T_{\mathbf{x}}TM$ as direct sum of $H_{\mathbf{x}}$ and $V_{\mathbf{x}}$.

10.2 Sub-Riemannian geometry of a step-2 nilpotent Lie algebra

In part 2 we have explored the Vortex-Heisenberg Lie algebra and the corresponding Vortex-Heisenberg Lie group for two- und three-dimensional vortex flows. In chapter 9 we have shown how this group theoretical point of view can be applied to atmospheric phenomena such as splitting storms.

Here, we will use this algebraic analysis to derive vortex geodesics. In general, sub-Riemannian geometry can be used to study constrained physical systems. Regarding hydrodynamical systems, the conservation of the vortex quantities restrict the motion on the tangent space. Furthermore, as we have shown in chapter 8, vh(2) and vh(3) are nilpotent algebras. Both together lead to a natural sub-Riemannian structure for vortex dynamics. In this section we will summarize, how sub-Riemannian geodesics can be determined for general step-2 nilpotent algebras. In sections 10.3 and 10.5

we will apply this proceeding to the two- and three-dimensional Vortex-Heiseberg algebras vh(2) and vh(3).

Denote $\mathfrak{g}$ a arbitrary step-2 nilpotent Lie-Algebra with respect to the step-2 nilpotent Lie group G and denote $\{\mathbf{X}_i, \mathbf{X}_{jk} \mid i = 1, \dots, n,\ 1 \leq j < k \leq n\}$ the basis of the $n(n+1)/2$-dimensional Lie Algebra $\mathfrak{g}$ with multiplication table:

$$[\mathbf{X}_i, \mathbf{X}_j] = \mathbf{X}_{ij},\ [\mathbf{X}_i, \mathbf{X}_{jk}] = 0,\ [\mathbf{X}_{ij}, \mathbf{X}_{kl}] = 0. \tag{10.22}$$

In order to derive the $(n, n(n+1)/2)$-sub-Rimannian geodesics with respect to the Lie algebra, we consider $\mathfrak{g}$ as a family of left-invariant vector fields on the Lie group G. Then $\Delta = \text{span}(\mathbf{X}_1, \dots, \mathbf{X}_n)$ is a left invariant bracket generating distribution on the Lie group G and of rank n. Further, we assume that the vectors $\mathbf{X}_i(g),\ \ i = 1, \dots, n$ are orthogonal such that we can define an inner product on the plane $\Delta(g) = \text{span}(\mathbf{X}_1(g), \dots, \mathbf{X}_n(g))$ that varies smoothly with respect to g.

Definition 47. sub-Riemannian distance, sub-Riemannian length
Let $g : [0, T] \longrightarrow G$ be a horizontal curve, then $\dot{g} \in \Delta(g)$ almost everywhere. Let $\mathbf{x}, \mathbf{x}_T \in G$. Then the sub-Riemannian distance is defined as

$$d(\mathbf{x}, \mathbf{x}_T) = \inf\{\, l(g) \mid g : [0, T] \longrightarrow G \text{ is horizontal, } g(0) = \mathbf{x},\ g(T) = \mathbf{x}_T\} \tag{10.23}$$

with the sub-Riemann length l of the curve g:

$$l(g) = \int_0^T \|\dot{g}(t)\| dt. \tag{10.24}$$

with respect to the inner product defined by $X_i(g)$ as explained before the definition.

We are looking for the Sub-Riemannian geodesics on the group G, i.e. for the minimization of the functional in the class of horizontal curves. For this approach we combine our differential geometry definitions we introduced in the last section with the Lie group and Lie algebra definitions from chapter 6. We recall the definitions from section 6.1 that a Lie group is a group with a manifold structure and a Lie algebra corresponds to the tangent space at the identity group element.

The following paragraph is summarized after Percacci (2017). Let us call the Lie group G and let the multiplication $* : G \times G \to G$ and the

inverse $I : G \to G$ are smooth maps. We consider the diffeomorphisms $L_g : G \to G$ defined by $L_g(g') = gg'$ satisfying the composition property of the Lie group. Then, a vector field $\mathbf{v} \in \mathbf{X}(G)$ is called left-invariant if $TL_g(\mathbf{v}) = \mathbf{v}$ for all $g \in G$. We note that (i) the Lie bracket of two left-invariant vector fields is a left-invariant vector field, and (ii) right-invariant vector fields can be defined analogously. As we have discussed before with respect to the Lie bracket, the left-invariant vector fields form a Lie algebra $L(G)$ of the Lie group G. Denote the identity element of the group with e and with $\bar{\mathbf{v}} \in T_eG$ the vector tangent to the group G at the identity such that can define a unique left-invariant vector field $\mathbf{v}$ that coincides with $\bar{\mathbf{v}}$ in the identity:

$$\mathbf{v}(g) = TL_g(\bar{\mathbf{v}}) \tag{10.25}$$

(see chapter 6 section 6.1.) Therefore, there is a one-to-one correspondence between elements of T_eG and left-invariant vector fields such that the dimension of the Lie algebra $L(G)$ is equal to dim(G). We recall that a Lie bracket of two vector fields $\mathbf{X}$ and $\mathbf{Y}$ is left-translation invariant if $\mathbf{X}$ and $\mathbf{Y}$ are left-invariant.

We denote with $g \mapsto L_g$ the left-action on the group G that defines tangent and cotangent bundle trivializations. Then we can write:

$$G \times \mathfrak{g} \simeq TG, \qquad G \times \mathfrak{g}^* \simeq T^*G, \tag{10.26}$$

with respect to the mappings

$$(\mathbf{g}, \mathbf{X}) \mapsto d_eL_g\mathbf{X}, \qquad (\mathbf{g}, \mathbf{x})) \mapsto d_eL_{g^{-1}}(g)^*\mathbf{x}. \tag{10.27}$$

We remind that the space of left-invariant vector fields can be identified with the tangent space of the group identity such that we can relate this notation to the Lie bracket we have discussed in the previous chapters. Using the isomorphism $\varphi : TTM \to TM$ explained in section 10.1, i.e. $TTM \cong TM$, we obtain the double bundle

$$TT^*G \simeq (G \times \mathfrak{g}^*) \times (\mathfrak{g} \times \mathfrak{g}^*). \tag{10.28}$$

Now, we can represent any tangent vector as pair $((g, p), (\mathbf{X}, \mathbf{Y}^*))$ and the symplectic form $\omega_{(g,\mathbf{x})}$ is given by:

$$\omega_{(g,\mathbf{x})}((\mathbf{X}_1, \mathbf{Y}_1^*), (\mathbf{X}_2, \mathbf{Y}_2^*))) = \mathbf{Y}_1^*(\mathbf{X}_2) - \mathbf{Y}_2^*(\mathbf{X}_1) - \mathbf{x}[\mathbf{X}_1, \mathbf{X}_2] \tag{10.29}$$

See Monroy-Pérez and Anzaldo-Meneses (2006) for further details.

Let now $H : T^*G \longrightarrow \mathbb{R}$ be a Hamiltonian function. As we have noticed in the beginning of this chapter, in this context the Hamiltonian does not represent the energy. It is a vector field which solution provides the geodesics. The flow of the Hamiltonian vector field H is given by the system:

$$\begin{aligned} \frac{d\mathbf{g}}{dt} &= (dL_g)(dH) \\ \frac{d\mathbf{x}}{dt} &= -(\mathrm{ad}^* dH)(\mathbf{x}), \end{aligned} \tag{10.30}$$

Let now H_i be the Hamiltonian function with respect to the vector field $\mathbf{X}_i$ and denote H_{ij} the Hamilton function corresponding to $\mathbf{X}_{ij}$, that means $H_{ij} = \mathcal{H}_{\mathbf{X}_{ij}}$. The Lie Poisson bracket is given by

$$[H_i, H_j] = H_{ij}, \tag{10.31}$$

where H_{ij} are central elements of the Lie algebra $T^*\mathfrak{g}$ generated by the bracket relation (10.31). These Hamiltonians depend only on the second variable $\mathbf{x}$, because of the left invariance of the vector fields.

Further, denote $\{\mathbf{X}_i^*, \mathbf{X}_j^*\}$ the dual basis of the basis $\{\mathbf{X}_i, \mathbf{X}_j\}$. Applying (10.30) the dual variable $\mathbf{x}$ can be identified with the vector

$$\mathbf{x} \simeq \sum_{i=1}^{n} \mathbf{x}(\mathbf{X}_i)\mathbf{X}_i^* + \sum_{i<j}^{n} \mathbf{x}(\mathbf{X}_{ij})\mathbf{X}_{ij}^* = \sum_{i=1}^{n} H_i \mathbf{X}_i^* + \sum_{i<j}^{n} H_{ij}\mathbf{X}_{ij}^*. \tag{10.32}$$

Moreover, because of the commutator (10.31), $\mathbf{x}$ can be identified with the pair

$$\mathbf{x} \simeq (\mathbf{h}, \underline{\mathbf{H}}) \in \mathbb{R}^n \times \mathfrak{so}(n) \tag{10.33}$$

with

$$\mathbf{h} = \begin{pmatrix} H_1 \\ H_2 \\ \vdots \\ H_n \end{pmatrix} \quad \text{and} \quad \underline{\mathbf{H}} = \begin{pmatrix} H_{11} & H_{12} & \dots & H_{1n} \\ H_{21} & H_{22} & \dots & H_{2n} \\ \vdots & & \ddots & \vdots \\ H_{n1} & \dots & \dots & H_{nn} \end{pmatrix} \tag{10.34}$$

Using the above identification and (10.30) the geodesics are completely described by the second equation of the following system (Monroy-Pérez

and Anzaldo-Meneses, 2006):

$$\frac{d\mathbf{g}}{dt} = H_1\mathbf{X}_1(\mathbf{g}) + \cdots + H_n\mathbf{X}_n(\mathbf{g})$$

$$\boxed{\frac{d\mathbf{x}}{dt} = (\dot{\mathbf{h}}, \dot{\underline{\mathbf{H}}}) = (\underline{\mathbf{H}}\mathbf{h}, \mathbf{0})} \tag{10.35}$$

Because $\mathbf{x}$ can be identified with the pair $(\mathbf{h}, \underline{\mathbf{H}})$, we can take the exponential ansatz to solve (10.35). Taking the initial condition $\mathbf{h}_0 = \mathbf{h}(0)$ the integral curves are given by

$$t \mapsto (\mathbf{h}(t), \underline{\mathbf{H}}(t)) = \exp(t\underline{\mathbf{H}}\mathbf{h}_0, \underline{\mathbf{H}}(0)). \tag{10.36}$$

The calculation of the exponential function leads to the geodesic equation. To solve the exponential function we apply Lagrange's and Sylvester's formula that represents an analytic function $f(A)$ of a diagonalizable $n \times n$-matrix $\underline{\mathbf{A}}$ in terms of the eigenvalues λ_i and eigenvectors of $\underline{\mathbf{A}}$:

$$f(\underline{\mathbf{A}}) = \sum_{i=1}^{n} f(\lambda_i)A_i \tag{10.37}$$

The solution depends on the dimension. We need to distinguish between even and odd dimensions:

1. Even n: $\underline{\mathbf{H}} \in \text{Mat}(n \times n)$, non-singular, skew-symmetric with $n/2$ different eigenvalues.

2. Odd n: $\underline{\mathbf{H}}$ has one zero-valued eigenvalue and the other eigenvalues are all different. The nonzero eigenvalues appear in $\pm$-pairs and are imaginary.

For the eigenvalue zero, the projector is real and symmetric. We denote it $\underline{\boldsymbol{\pi}}_0$. For all other eigenvalues μ, the spectral projectors $\underline{\boldsymbol{\pi}}_\mu$ are hermitian matrices. Denote σ the set of eigenvalues. Now, we apply Lagrange-Sylvester-formula and obtain

$$\exp(t\mathbf{H}) = \sum_{\mu\in\sigma} e^{t\mu}\ \underline{\boldsymbol{\pi}}_\mu \tag{10.38}$$

which is the spectral formula for $\exp(t\underline{\mathbf{H}})$ in terms of the spectral projectors. We notice that spectral projectors are orthogonal projections.

Determining the $(n, n(n+1)/2)$-sub-Riemannian geodesics

Now, we are prepared to calculate the sub-Riemannian geodesics for the general case of an n-dimensional Lie algebra following the work of Monroy-Pérez and Anzaldo-Meneses (2006). The notations $(n, n(n+1)/2)$-sub-Riemannian geometry is composed by a $(n(n+1)/2)$-dimensional Lie algebra with a rank n distribution. A distribution Δ of rank n is a subspace of the tangent space of a manifold, where there exist n linearly independent vector fields that form a basis for the distribution Δ. Thus, this general case could be adapted to the n-dimensional Vortex-Heisenberg group VH(n). In this thesis, we explore VH(2) and VH(3). The rank of the Lie algebra vh(2) is three (P_x, P_y, Γ) with rank of distribution $n = 2$ leading to a (2,3)-sub-Riemannnian structure for two-dimensional incompressible, inviscid flows. The Lie algebra vh(3) of three dimensional vortex flows has six dimensions (6 elements: $P_x, P_y, P_z, Z_x, Z_y, Z_z$) with a rank $n = 3$ distribution. Thus, here (3,6)-sub-Riemannnian geometry can be applied. In order to apply their algorithm to two- and three-dimensional atmospheric vortex motions, we will first summarize the algorithm of Monroy-Pérez and Anzaldo-Meneses (2006) to find geodesics for n-dimensional algebras.

In the end of the last section, we suggested to apply the Lagrange-Sylvester formula (10.38) to obtain a solution of the following differential equation for geodesics $\mathbf{x}_g$ (see (10.35)):

$$\frac{d\mathbf{x}_g}{dt} = (\dot{\mathbf{h}}, \dot{\underline{\mathbf{H}}}). \tag{10.39}$$

To apply the Lagrange-Sylvester formula, we first calculate the eigenspaces of the corresponding systems. We will use the following notations for the eigenvectors, eigenvalues and projectors:

$$\begin{aligned} \{\mathbf{v}_1, \mathbf{v}_{-1}, \ldots, \mathbf{v}_{\lfloor n/2 \rfloor}, \mathbf{v}_{-\lfloor n/2 \rfloor}\} \subset \mathbb{C} \quad & \text{(Eigenvectors)} \\ \{i\lambda_1, -i\lambda_1, \ldots, i\lambda_{\lfloor n/2 \rfloor}, -i\lambda_{-\lfloor n/2 \rfloor}\} \quad & \text{(Eigenvalues)} \\ \{\underline{\boldsymbol{\pi}}_1, \underline{\boldsymbol{\pi}}_{-1}, \ldots, \underline{\boldsymbol{\pi}}_{\lfloor n/2 \rfloor}, \underline{\boldsymbol{\pi}}_{-\lfloor n/2 \rfloor}\} \quad & \text{(Projectors)} \end{aligned} \tag{10.40}$$

with $\mathbf{v}_{-k} = \overline{\mathbf{v}}_k$ and $\lambda_i \in \mathbb{R}$. Monroy-Pérez and Anzaldo-Meneses (2006) show that all $\mathbf{v}_i$ are orthogonal, i.e. $\mathbf{v}_i \cdot \mathbf{v}_j = \delta_{ij}$.

We note that for odd n we obtain an additional (real) eigenvector $\mathbf{v}_0$, an additional eigenwert $\lambda_0 = 0$ and its projector $\underline{\boldsymbol{\pi}}_0$ ($\mathbf{v}_0 \in \mathrm{Ker}(H)$). The orthogonality implies: $\mathrm{Re}(\mathbf{v}_i) \cdot \mathrm{Re}(\mathbf{v}_j) = \delta_{ij}\mathrm{Im}(\mathbf{v}) \cdot \mathrm{Im}(\mathbf{v}_j)$ and $\mathrm{Re}(\mathbf{v}_j) \cdot \mathrm{Im}(\mathbf{v}_j) = 0$.

Therefore,

$$\{\mathrm{Re}(\mathbf{v}_1), \mathrm{Im}(\mathbf{v}_1), \ldots, \mathrm{Re}(\mathbf{v}_{\lfloor n/2 \rfloor}), \mathrm{Im}(\mathbf{v}_{\lfloor n/2 \rfloor})\} \tag{10.41}$$

is an orthogonal basis of $\mathbb{R}^n$ for even n. And

$$\{\mathrm{Re}(\mathbf{v}_1), \mathrm{Im}(\mathbf{v}_1), \ldots, \mathrm{Re}(\mathbf{v}_{\lfloor n/2 \rfloor}), \mathrm{Im}(\mathbf{v}_{\lfloor n/2 \rfloor}), \mathbf{v}_0\} \tag{10.42}$$

yields an orthogonal basis of $\mathbb{R}^n$ for odd n. Because $\mathbf{h}_0$ is a real constant vector it is:

$$\mathrm{span}(\mathrm{Re}((\mathbf{h}_0 \cdot \mathbf{v}_k)\mathbf{v}_k), \mathrm{Im}((\mathbf{h}_0 \cdot \mathbf{v}_k)\mathbf{v}_k)) = \mathrm{span}(\mathrm{Re}(\mathbf{v}_k), \mathrm{Im}(\mathbf{v}_k)). \tag{10.43}$$

for $k = 1, 2, \ldots \lfloor n/2 \rfloor$. We obtain a basis $\{\boldsymbol{\alpha}_k, \boldsymbol{\beta}_k\}$ with

$$\boxed{\boldsymbol{\alpha}_k = 2\,\mathrm{Im}((\mathbf{h}_0 \cdot \mathbf{v}_k)\mathbf{v}_k),\ \boldsymbol{\beta}_k = 2\,\mathrm{Re}((\mathbf{h}_0 \cdot \mathbf{v}_k)\mathbf{v}_k),\ \boldsymbol{\gamma}_0 = (\mathbf{h}_0 \cdot \mathbf{v}_0)\mathbf{v}_0.} \tag{10.44}$$

for $k = 1, 2, \ldots \lfloor n/2 \rfloor$.

We search for the solution for the pair $(\mathbf{x}_g, \underline{\mathbf{z}}_g) \in \mathbb{R}^n \times \mathfrak{so}(n)$, i.e. the geodesic arc. Let this geodesic arc be defined in a certain interval with the following initial condition

$$(\mathbf{x}_g(0), \underline{\mathbf{z}}_g(0)) = (\mathbf{0}, \underline{\mathbf{0}}). \tag{10.45}$$

Assuming that $(\mathbf{x}_g, \underline{\mathbf{z}}_g)$ is a projection of a normal extremal and all eigenvalues of $\underline{\mathbf{H}}$ are non-zero, we can apply (10.38) leading to the following geodesic equations:

$$\mathbf{x}_g = \begin{cases} \sum_{\mu \in (\sigma)} \frac{1}{\mu}(e^{\mu t} - 1)\ \underline{\boldsymbol{\pi}}_\mu \mathbf{v}_0 & \text{for n even} \\ \sum_{\mu \in (\sigma - \{0\})} \frac{1}{\mu}(e^{\mu t} - 1)\ \underline{\boldsymbol{\pi}}_\mu \mathbf{v}_0 + t\underline{\boldsymbol{\pi}}_0 \mathbf{v}_0 & \text{for n odd} \end{cases} \tag{10.46}$$

Now, we can formulate the geodesic arc $(\mathbf{x}_g, \mathbf{z}_g)$ with respect to the above basis (10.44) given by $\{\boldsymbol{\alpha}_k, \boldsymbol{\beta}_k\}$ for n even, and by $\{\boldsymbol{\alpha}_k, \boldsymbol{\beta}_k, \boldsymbol{\gamma}_0\}$ for n odd. We obtain the trajectories:

$$\boxed{\begin{aligned} \mathbf{x}_g &= \sum_{i=1}^{\lfloor n/2 \rfloor} \frac{1}{\lambda_i}(\cos(\lambda_i t) - 1)\boldsymbol{\alpha}_i + \frac{1}{\lambda_i}\sin(\lambda_i t)\boldsymbol{\beta}_i && \text{(for } n \text{ even)} \\ \underline{\mathbf{z}}_g &= \sum_{i=1}^{\lfloor n/2 \rfloor} A_{ij}\boldsymbol{\alpha} \wedge \boldsymbol{\alpha}_j + B_{ij}\boldsymbol{\alpha} \wedge \boldsymbol{\beta}_j + C_{ij}\boldsymbol{\beta} \wedge \boldsymbol{\beta}_j && \text{(for } n \text{ even)} \end{aligned}} \tag{10.47}$$

with

$$
\begin{aligned}
A_{ij} &= \frac{1-\cos(\lambda_i-\lambda_j)t}{2\lambda_i(\lambda_i-\lambda_j)} + \frac{\cos(\lambda_i+\lambda_j)t-1)}{2\lambda_i(\lambda_i-\lambda_j)} - \frac{\cos(\lambda_j t)-1}{\lambda_i\lambda_j} \\
B_{ij} &= \frac{(\lambda_j-\lambda_i)\sin(\lambda_i+\lambda_j)t}{2\lambda_i\lambda_j(\lambda_i+\lambda_j)} + \frac{(\lambda_j+\lambda_i)\sin(\lambda_i-\lambda_j)t}{2\lambda_i\lambda_j(\lambda_i-\lambda_j)} - \frac{\sin(\lambda_j t)}{\lambda_i\lambda_j},\ i\neq i,
\end{aligned}
\tag{10.48}
$$

$$
\begin{aligned}
B_{ii} &= \frac{t}{\lambda_i} - \frac{\sin(\lambda t)}{\lambda_i^2} \\
C_{ij} &= \frac{1-\cos(\lambda_i-\lambda_j)t}{2\lambda_i(\lambda_i-\lambda_j)} - \frac{\cos(\lambda_i+\lambda_j)t-1}{2\lambda(\lambda_i+\lambda_j)}.
\end{aligned}
\tag{10.49}
$$

For n odd the same equations (10.47) hold but with the additional $t\boldsymbol{\gamma}_0$ and with the additional two terms:

$$
\begin{aligned}
&\sum_{i=1}^{\lfloor n/2\rfloor}\left(\frac{-t}{\lambda_i}(\cos(\lambda_i t)+1) + \frac{1}{\lambda_i^2}2\sin(\lambda_i t)\boldsymbol{\alpha_i}\wedge\boldsymbol{\gamma}_0\right) \\
&\quad + \sum_{i=1}^{\lfloor n/2\rfloor}\left(\frac{1}{\lambda_i^2}(2(1-\cos(\lambda_i t)) - \lambda_i t\sin(\lambda_i t))\right)\boldsymbol{\beta_i}\wedge\boldsymbol{\gamma}_0
\end{aligned}
\tag{10.50}
$$

We cite Monroy-Pérez and Anzaldo-Meneses (2006) and summarize that in even dimensions the projections of the components of $\mathbf{x}_g$ to the planes $\{\mathrm{Re}(\mathbf{v}_k), \mathrm{Im}(\mathbf{v}_k)\}$, for $k = 1, 2, \ldots \lfloor n/2\rfloor$, are circles passing through the origin with radii $1/\lambda_k$, and centered at span$(\boldsymbol{\alpha}_k)$. Furthermore, in odd dimensions, since $\mathbf{x}_g$ varies linearly in the direction of the vector $\boldsymbol{\gamma}_0$, the projections of the component $\mathbf{x}_g$ to the three-dimensional subspaces span$(\boldsymbol{\alpha}_k, \boldsymbol{\beta}_k, \boldsymbol{\gamma}_0)$ (identical to span$(\mathrm{Re}(\mathbf{v}_k), \mathrm{Im}(\mathbf{v}_k))$) are helices. In this case we can write explicitly the parameter $t = (\mathbf{h}_0 \cdot (\underline{\boldsymbol{\pi}}_0\mathbf{x}_g))/\|\underline{\boldsymbol{\pi}}_0\mathbf{h}_0\|^2$

10.3 (2,3)-sub-Riemannian geometry

In the last section we have summarized the algorithm the general $(n, n(n+1)/2))$-sub-Riemannian geodesics for a $n(n+1)/2$-dimensional Lie group with a rank n distribution. This algorithm could be applied to the n-dimensional Vortex-Heisenberg group, which might be explored in future studies. Here, we regard the special case of (2,3)-sub-Riemannian geometry, which was introduced by Brockett (1982), to find geodesics for the two-dimensional vortex flows. A classical example is given by charged mass points, (see, e.g., Monroy-Pérez and Anzaldo-Meneses, 1999). Its algebraic

structure is isomorphic to the two-dimensional Vortex-Heisenberg algebra.

Here, we will first outline the derivation of the general (2,3)-sub-Riemannian geodesic after Monroy-Pérez and Anzaldo-Meneses (2006) in order to apply this algorithm to find geodesics for the idealized point vortex model that we have discussed in the first part of this thesis. Physically, the point vortex motion is restricted by the conservation laws, and all of them can be expressed with respect to the circulation. Mathematically, the conservation laws imply a nilpotent Lie algebra such that sub-Riemannian geometry is a suitable choice to find vortex geodesics.

Consider the following nonzero bracket of the three-dimensional, second-step nilpotent Lie Algebra:

$$[\mathbf{X}_1, \mathbf{X}_2] = \mathbf{X}_{12}. \tag{10.51}$$

We use the same notations as in the last section for arbitrary $n \in \mathbb{N}$ and denote with H_i the Hamiltonian functions corresponding to the vector field $\mathbf{X}_i$, $i = 1, 2$, respectively H_{ij} to $\mathbf{X}_{ij}$, $i, j = 1, 2$. Then, we obtain the pair $(\mathbf{h}, \underline{\mathbf{H}}) \in \mathbb{R}^2 \times \mathfrak{so}(2)$ (see (10.33)). Now, we consider the following initial values

$$\mathbf{h}_0 = (H_1, H_2)^T. \tag{10.52}$$

and solve the equation

$$\frac{d\mathbf{x}_g}{dt} = (\dot{\mathbf{h}}, \dot{\underline{\mathbf{H}}}) \tag{10.53}$$

to derive the vortex geodesics $\mathbf{x}_g$.

In order to solve (10.53), we apply Lagrange-Sylvester formula (10.37) leading to two eigenvalues

$$\{-i\lambda_1, i\lambda_1\} \tag{10.54}$$

with $\underline{\mathbf{H}}^2 + \lambda_1^2 \mathbf{E} = 0$, where $\underline{\mathbf{E}}$ denotes the 2×2 identity matrix. The spectral projector is given by

$$\underline{\boldsymbol{\pi}}_1 = \frac{1}{2i\lambda_1}(\underline{\mathbf{H}} + i\lambda_1 \underline{\mathbf{E}}). \tag{10.55}$$

And, using (10.44), the basis of the projection plane reads as

$$\boldsymbol{\beta}_1 = (H_1, H_2)^T, \ \boldsymbol{\alpha}_1 = (-H_2, H_1)^T. \tag{10.56}$$

Finally, the geodesic equation is given by:

$$\boxed{\mathbf{x}_g = \frac{1}{\lambda_1}(\cos(\lambda_1 t) - 1)\boldsymbol{\alpha}_1 + \frac{1}{\lambda_1}\sin(\lambda_1 t)\boldsymbol{\beta}_1} \tag{10.57}$$

and

$$\underline{\mathbf{z}}_g = \left(\frac{t}{\lambda_1} - \frac{\sin(\lambda_1 t)}{\lambda_1^2}\right)\boldsymbol{\alpha}_1 \wedge \boldsymbol{\beta}_1, \tag{10.58}$$

where $\wedge$ denotes the wedge-product.

10.4 Deriving geodesics for point vortex systems

Now, we will apply the Vortex-Heisenberg Lie algebra to the previous general algorithm to derive geodesics for two-dimensional incompressible, inviscid flows. We first recall the discretized vortex model resulting in the point vortex equations that we have explored in chapters 3 and 4. The zonal and meridional momenta and the total circulation for a N-point vortex system are given by:

$$P_x = \sum_{i=1}^{N} \Gamma_i y_i, \quad P_y = -\sum_{i=1}^{N} \Gamma_i x_i \quad \text{and} \quad \Gamma = \sum_{i=1}^{N} \Gamma_i \tag{10.59}$$

Névir (1998) shows that the bracket relations of discrete, two-dimensional point vortex systems are comparable to the Nambu bracket relations of continuous, two dimensional, incompressible, inviscid flows with respect to the enstrophy.

$$[P_x, P_y] = \Gamma, \quad \text{and} \quad [P_x, \Gamma] = [P_y, \Gamma] = 0, \tag{10.60}$$

see also chapter 3. We notice that we do not regard the energy, but the direct vortex-related quantities.

We obtain a nilpotent algebra which allows for a direct transformation from the algebra to the group as we have summarized in chapter 8. Moreover, the nilpotent property leads to the choice of the sub-Riemannian space to represent 2D vortex dynamics. The motion in sub-Riemannian spaces is always restricted by constrains. Here, the vortex motion is restricted by conservation laws such as the momentum, the energy, the circulation, the center of circulation, the relative angular momentum or the angular momentum. All conservation laws can be expressed by the circulation, as we

have shown in chapter 3. Because of these restrictions, we can not use Euclidean or Riemannian goemetry to determine vortex paths. This setting together with the nilpotent structure provides a natural sub-Riemannian space for the search for vortex geodesics.

We consider the single trajectories of the i-th point vortex of an N-point vortex system and show examples of two and three point vortex systems. First, we scale the momentum of the i-th point vortex $\mathbf{P}^{(i)} = (P_x^{(i)}, P_y^{(i)})$ by the area F:

$$P_x^{(i)} = \frac{\Gamma}{F} y, \qquad P_y^{(i)} = -\frac{\Gamma}{F} x \tag{10.61}$$

such that the unit of P_x and P_y is m/s, a velocity. We recall that Γ denotes the circulation. W.o.l.g. we assume that $\left(\frac{\Gamma}{F}\right)^2 = 1$. The (2×2)-matrix $\underline{\mathbf{H}}$ and the vector $\mathbf{h} \in \mathbb{R}^2$ form the pair $(\mathbf{h}, \underline{\mathbf{H}})$ which is given by:

$$\underline{\mathbf{H}} = \begin{pmatrix} \{P_x^{(i)}, P_x^{(i)}\} & \{P_x^{(i)}, P_y^{(i)}\} \\ \{P_y^{(i)}, P_x^{(i)}\} & \{P_y^{(i)}, P_y^{(i)}\} \end{pmatrix} = \begin{pmatrix} 0 & \frac{\Gamma}{F} \\ -\frac{\Gamma}{F} & 0 \end{pmatrix}, \quad \mathbf{h} = \begin{pmatrix} H_1 \\ H_2 \end{pmatrix} = \begin{pmatrix} P_x^{(i)} \\ P_y^{(i)} \end{pmatrix} \tag{10.62}$$

with respect to the Nambu-bracket $\{\cdot, \cdot\}$, see also (8.23) in chapter 8.

We recall that the geodesics are the solution of the following differential equation that was derived in (10.35)

$$\frac{d\mathbf{x}_g}{dt} = (\dot{\mathbf{h}}, \dot{\underline{\mathbf{H}}}) = (\underline{\mathbf{H}}\mathbf{h}, \mathbf{0}). \tag{10.63}$$

Here, the components of $\mathbf{h}$ are the linear momenta of the single vortices that form together a N-point vortex system. In contrast to classical mechanical systems, where the momentum is given by the velocity, here, the linear momenta depend on the local coordinates – one hierarchical level lower than the mass point momenta. The components of $\mathbf{h}$ are given by the linear momenta, and thus, $\mathbf{h}$ depends on the local coordinates $\mathbf{h} = \mathbf{h}(x, y)$. Therefore, for the general case, where we do not consider the origin, we can assume $\dot{\mathbf{h}} \neq 0$. On the other hand, $\underline{\mathbf{H}}$ is formed by the circulations that are constant, therefore, it is $\dot{\underline{\mathbf{H}}} = 0$.

In order to solve (10.63), we apply Lagrange-Sylvester-formula, i.e. the spectral formula in terms of spectral projectors. To derive the eigenvalues, eigenvectors and projectors, we first calculate the characteristic polynomial

of the rotational matrix $\underline{\mathbf{H}}$:

$$\begin{aligned}\det(\underline{\mathbf{H}} - \kappa\underline{\mathbf{E}}) = \det\left(\begin{pmatrix} -\kappa & \frac{\Gamma}{F} \\ -\frac{\Gamma}{F} & -\kappa \end{pmatrix}\right) &= \kappa^2 + \left(\frac{\Gamma}{F}\right)^2 \\ = \left(\kappa + i\frac{\Gamma}{F}\right)\ \left(\kappa - i\frac{\Gamma}{F}\right) &= 0.\end{aligned} \tag{10.64}$$

Thus, the solutions κ_1 and κ_2 of last equation are the eigenvalues:

$$\kappa_1 = i\frac{\Gamma}{F}, \quad \kappa_2 = -i\frac{\Gamma}{F} \quad \Rightarrow \quad \lambda = \frac{\Gamma}{F} \tag{10.65}$$

We will use the following notation:

$$\{\kappa_1, \kappa_2\} = \{i\lambda, -i\lambda\} = \left\{i\frac{\Gamma}{F}, -i\frac{\Gamma}{F}\right\} \tag{10.66}$$

The algebraic multiplicity m_k of both eigenvalues is one. Further, consider the hauptspace

$$\mathrm{Haupt}(\kappa_k, \underline{\mathbf{H}}) = \mathrm{Kern}(\underline{\mathbf{H}} - \kappa_k\underline{\mathbf{E}})^{m_k} \tag{10.67}$$

of the eigenvalue κ_k. Denote $\underline{\mathbf{B}}$ the block matrix of eigenvectors. Thus, $\underline{\mathbf{B}}$ is invertible and given by

$$\underbrace{\underline{\mathbf{B}}}_{n\times n} := \left(\underbrace{\mathbf{v}_1}_{n\times m_1} | \ldots | \underbrace{\mathbf{v}_k}_{n\times m_n}\right). \tag{10.68}$$

In our example it is $n = 2$ and the algebraic multiplicity of both eigenvalues is one, i.e., $m_1 = m_2 = 1$, we summarize:

$$\kappa_1 = +i\,\frac{\Gamma}{F}, \kappa_2 = -i\,\frac{\Gamma}{F}, \Rightarrow \lambda = \frac{\Gamma}{F},\ \mathbf{v}_1 = \begin{pmatrix} i \\ 1 \end{pmatrix},\ \mathbf{v}_2 = \begin{pmatrix} -i \\ 1 \end{pmatrix}, \tag{10.69}$$

where $\mathbf{v}_1$ and $\mathbf{v}_2$ are the eigenvectors. The geometric mulplicity here must be equal to the algebraic multiplicity, because the algebraic multiplicity is one and the geometric mulplicity is smaller than (or equal to) the algebraic mulplicity and larger than (or equal to) one. Therefore, the hauptspace is equals to the eigenspace and thus the basis of the hauptspace can be represented by the above introduced matrix $\underline{\mathbf{B}}$ given by

$$\underline{\mathbf{B}} = (\mathbf{v}_1|\mathbf{v}_2) = \begin{pmatrix} i & -i \\ 1 & 1 \end{pmatrix} \quad \text{and} \quad \underline{\mathbf{B}}^{-1} = \frac{1}{2i}\begin{pmatrix} 1 & i \\ -1 & i \end{pmatrix} =: \begin{pmatrix} \mathbf{C}_1 \\ \mathbf{C}_2 \end{pmatrix}. \tag{10.70}$$

Now, we can determine the spectral projectors:

$$\begin{aligned}\underline{\boldsymbol{\pi}}_1 &= \mathbf{v}_1\,\mathbf{C}_1 = \frac{1}{2i}\begin{pmatrix} i \\ 1 \end{pmatrix}\begin{pmatrix} 1 & i \end{pmatrix} = \frac{1}{2i}\begin{pmatrix} i & -1 \\ 1 & i \end{pmatrix} \\ \underline{\boldsymbol{\pi}}_2 &= \mathbf{v}_2\,\mathbf{C}_2 = \frac{1}{2i}\begin{pmatrix} -i \\ 1 \end{pmatrix}\begin{pmatrix} -1 & i \end{pmatrix} = \frac{1}{2i}\begin{pmatrix} i & 1 \\ -1 & i \end{pmatrix}\end{aligned} \tag{10.71}$$

and show that:

$$\underline{\mathbf{H}}^2 + \kappa^2\underline{\mathbf{E}} = \underline{\mathbf{H}}^2 + \left(\frac{\Gamma}{F}\right)^2\underline{\mathbf{E}} = \begin{pmatrix} 0 & \frac{\Gamma}{F} \\ -\frac{\Gamma}{F} & 0 \end{pmatrix}^2 + \begin{pmatrix} \frac{\Gamma}{F} & 0 \\ 0 & \frac{\Gamma}{F} \end{pmatrix} = \begin{pmatrix} 0 & 0 \\ 0 & 0 \end{pmatrix}. \tag{10.72}$$

Then, with (10.44) the basis vectors are given by

$$\boldsymbol{\alpha}^{(i)} = \begin{pmatrix} -H_2 \\ H_1 \end{pmatrix} = \begin{pmatrix} -P_y^{(i)} \\ P_x^{(i)} \end{pmatrix},\ \boldsymbol{\beta}^{(i)} = \begin{pmatrix} H_1 \\ H_2 \end{pmatrix} = \begin{pmatrix} P_x^{(i)} \\ P_y^{(i)} \end{pmatrix}. \tag{10.73}$$

Inserting $\boldsymbol{\alpha}, \boldsymbol{\beta}$ and λ into the following geodesic equation (see (10.47)):

$$\mathbf{x}_g^{(i)} = \frac{1}{\lambda}\left(\cos(\lambda t) - 1\right)\boldsymbol{\alpha}^{(i)} + \frac{1}{\lambda}\sin(\lambda t)\boldsymbol{\beta}^{(i)} \tag{10.74}$$

leads to the sub-Riemannian geodesics for the i-th point vortex of an N-point vortex system:

$$\boxed{\mathbf{x}_g^{(i)} = \frac{F}{\Gamma}\left(\cos\left(\frac{\Gamma}{F}t\right) - 1\right)\begin{pmatrix} -P_y^{(i)} \\ P_x^{(i)} \end{pmatrix} + \frac{F}{\Gamma}\sin\left(\frac{\Gamma}{F}t\right)\begin{pmatrix} P_x^{(i)} \\ P_y^{(i)} \end{pmatrix}} \tag{10.75}$$

with respect to the phase space with total circulation Γ, linear momenta $P_x^{(i)}$ and $P_y^{(i)}$ and a vortex-surface-parameter F. Here we considered N-point vortex systems. We hypothesize that sub-Riemannian geodesics in N-point vortex systems can be regarded as relative equilibria solutions of the point vortex equations of motions. In this thesis, we will focus on $N = 2$- and $N = 3$-point vortex systems, because point vortex systems formed by one, two or three point vortices are integrable. Vortex constellations of more than three point vortices will be investigated in future studies.

10.4.1 Comparing the sub-Riemannian-geodesics to point vortex trajectories for $N = 2$ and $N = 3$

To compare the (2,3)-sub-Riemannian geodesics (10.75) to point vortex dynamics that we have explored in the beginning of this theses, see chapters 3 and 4, we reformulate last expression (10.75) for the geodesic $\mathbf{x}_g^{(i)}$:

$$\begin{aligned}
\mathbf{x}_g^{(i)} &= \frac{F}{\Gamma}\left(\cos\left(\frac{\Gamma}{F}t\right)-1\right)\begin{pmatrix}-P_y^{(i)}\\ P_x^{(i)}\end{pmatrix}+\frac{F}{\Gamma}\sin\left(\frac{\Gamma}{F}t\right)\begin{pmatrix}P_x^{(i)}\\ P_y^{(i)}\end{pmatrix}\\
&= \frac{F}{\Gamma}\left(\cos\left(\frac{\Gamma}{F}t\right)-1\right)\begin{pmatrix}\frac{\Gamma}{F}x\\ \frac{\Gamma}{F}y\end{pmatrix}+\frac{F}{\Gamma}\sin\left(\frac{\Gamma}{F}t\right)\begin{pmatrix}\frac{\Gamma}{F}y\\ -\frac{\Gamma}{F}ix\end{pmatrix}\\
&= \frac{F}{\Gamma}\begin{pmatrix}\cos\left(\frac{\Gamma}{F}t\right)\frac{\Gamma}{F}x-\frac{\Gamma}{F}x+\sin\left(\frac{\Gamma}{F}t\right)\frac{\Gamma}{F}y\\ \\ \cos\left(\frac{\Gamma}{F}t\right)\frac{\Gamma}{F}y-\frac{\Gamma}{F}y-\sin\left(\frac{\Gamma}{F}t\right)\frac{\Gamma}{F}x\end{pmatrix}\\
&= \frac{\Gamma}{F}\frac{F}{\Gamma}\begin{pmatrix}\cos\left(\frac{\Gamma}{F}t\right)x+\sin\left(\frac{\Gamma}{F}t\right)y\\ \\ -\sin\left(\frac{\Gamma}{F}t\right)x+\cos\left(\frac{\Gamma}{F}t\right)y\end{pmatrix}-\frac{\Gamma}{F}\frac{F}{\Gamma}\begin{pmatrix}x\\ y\end{pmatrix}\\
&= \begin{pmatrix}\cos\left(\frac{\Gamma}{F}t\right) & \sin\left(\frac{\Gamma}{F}t\right)\\ \\ -\sin\left(\frac{\Gamma}{F}t\right) & \cos\left(\frac{\Gamma}{F}t\right)\end{pmatrix}\begin{pmatrix}x\\ y\end{pmatrix}-\begin{pmatrix}x\\ y\end{pmatrix}.
\end{aligned} \tag{10.76}$$

Now, we set

$$\underline{\mathbf{R}}\left(\frac{\Gamma}{F}t\right) := \begin{pmatrix}\cos(\frac{\Gamma}{F}t) & \sin(\frac{\Gamma}{F}t)\\ \\ -\sin(\frac{\Gamma}{F}t) & \cos(\frac{\Gamma}{F}t)\end{pmatrix}. \tag{10.77}$$

Thus, we can express the geodesic equation:

$$\boxed{\mathbf{x}_g^{(i)} = \underline{\mathbf{R}}\left(\frac{\Gamma}{F}t\right)\,\mathbf{x}-\mathbf{x}} \tag{10.78}$$

Therefore, vortex geodesics in the phase space spanned by $\boldsymbol{\alpha}$ and $\boldsymbol{\beta}$ are rotations around the initial coordinates that are reflected. The geodesics pass the origin as shown by the solid lines in fig. 10.4.

Let us now compare this result with a point vortex system that we have discussed in the first part of this thesis. One point vortex systems always remains in calm, because they are located in its center of circulation. Thus, we first consider the simplest non-trivial dynamical system of two point vortices. Unless their total circulation is equal to zero, two vortices rotate

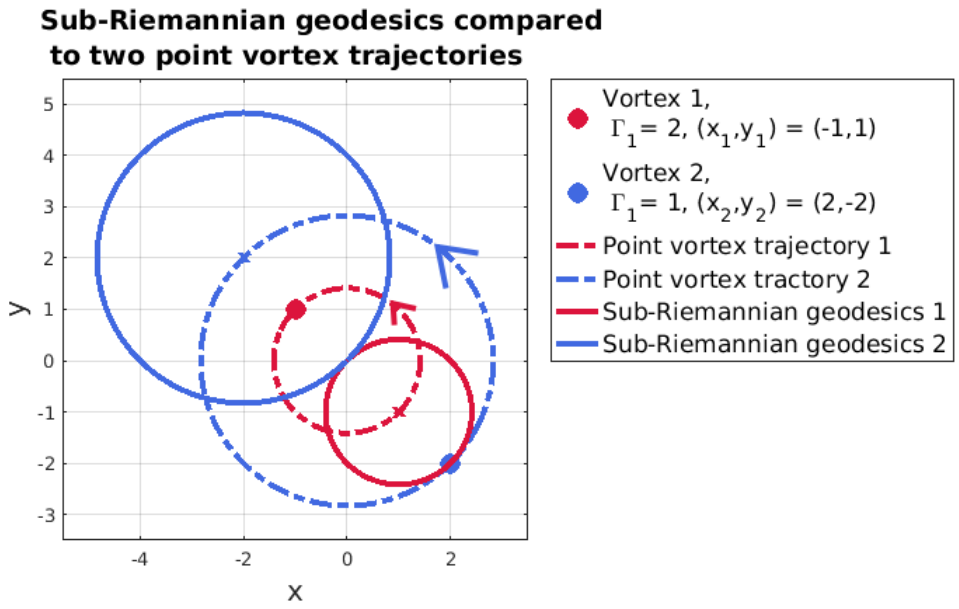

Figure 10.4: The solid line are the trajectories of the sub-Riemannian geodesics of two vortices, whereas the dashed line are the point vortex trajectories. The circulations of the systems where chosen to be equal but the trajectories are calculated with different models. Their trajectories are congruent.

uniformly around the center of circulation (3.11). See e.g. fig. 10.4, where the center of circulation is in the origin and the red and blue point vortex trajectories are shown by the dashed lines. The dots show the initial coordinates of the two point vortices and the arrows indicate the direction of the rotation. Here, the total circulation (the sum of the circulations of the single vortices) is three. For systems with total circulation equal zero the center of circulation would approach infinity and the whole point vortex system would translate. To illustrate the point vortex trajectories the point vortex equations (3.3) were calculated using MATLAB's ode45 solver that is based on an explicit Runge-Kutta formula. The colored solid lines in fig. 10.5 indicate the corresponding sub-Riemannian geodesics with respect to the basis α and β. Their projection would lead to a representation in the space of local coordinates. Regarding (10.77) and (10.78), the center of the sub-Riemannian geodesics are always given by the coordinate that results from the point reflection of the initial coordinate of the point vortices. This is due to the initial conditions given by the starting point $(0, 0)$, because the Vortex-Heisenberg group identity is in $(0, 0)$ and the Vortex-Heisenberg Lie algebra is the tangent space at the group identity. The centers of the sub-Riemannian geodesics are indicated by the crosses in fig. 10.4 and fig. 10.5. The rotational centers of the sub-Riemannian geodesics lie on the point vor-

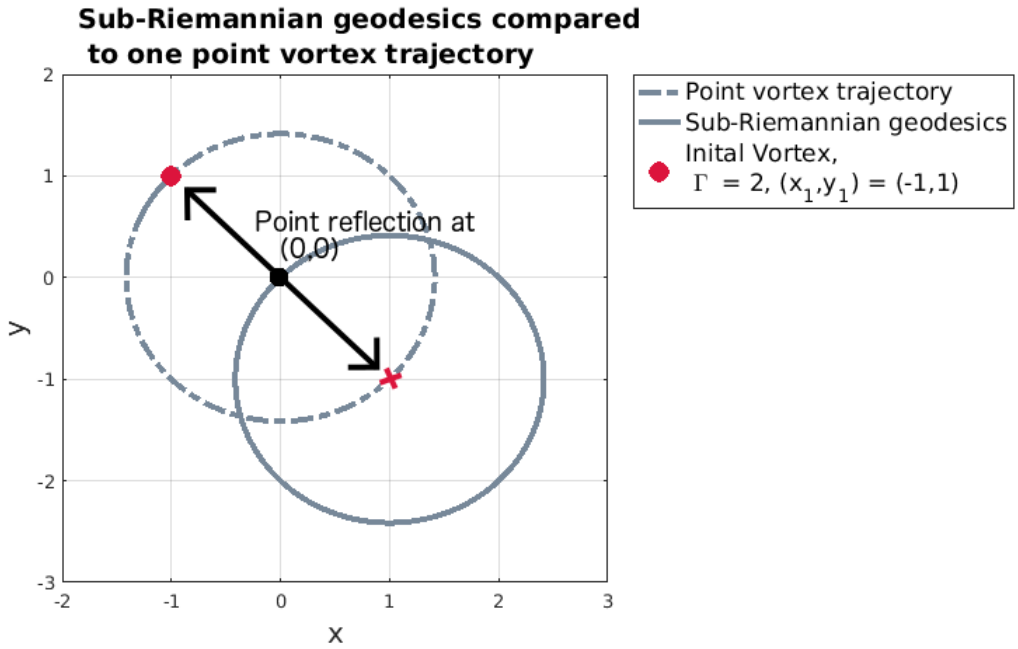

Figure 10.5: The colored trajectories show the sub-Riemannian geodesic of three vortices based on the Vortex-Heisenberg Lie algebra. The black line illustrates the point vortex motion. Even though both trajectories are determined with different models, we see that both trajectories are congruent.

tex trajectory. Thus, the point vortex trajectory and the sub-Riemannian geodesics have the same radius!

We can transfer the idea of two point vortices moving along shortest paths to weather situations. One example is a weather situation formed by a central low pressure system and a high pressure system that rotates around the low. The motion of the low can be seen as a sub-Riemannian geodesics.

As second example we consider a three point vortex system. It is called relative equilibrium if the three vortices forms an equilateral triangle. One example of a three point vortex equilibrium is shown in fig. 10.6, where the initial locations of the vortices are marked by the colored dots. In this example, the total circulation is unequal to zero, $\Gamma_1+\Gamma_2+\Gamma_1 = 3 \neq 0$. See chapters 3 and 4 for further examples of three point vortex systems. Three point vortex equilibria rotate uniformly around the center of circulation (3.11). If the total circulation is zero, the center of circulation would approach infinity and the whole point vortex system would translate. In fig. 10.6 the center of circulation lies at the origin and the point vortex motion in the x-y-plane is indicated by the black circle. Here, the equations of motion (3.3) were solved to illustrate the point vortex equilibrium motion using MATLAB's

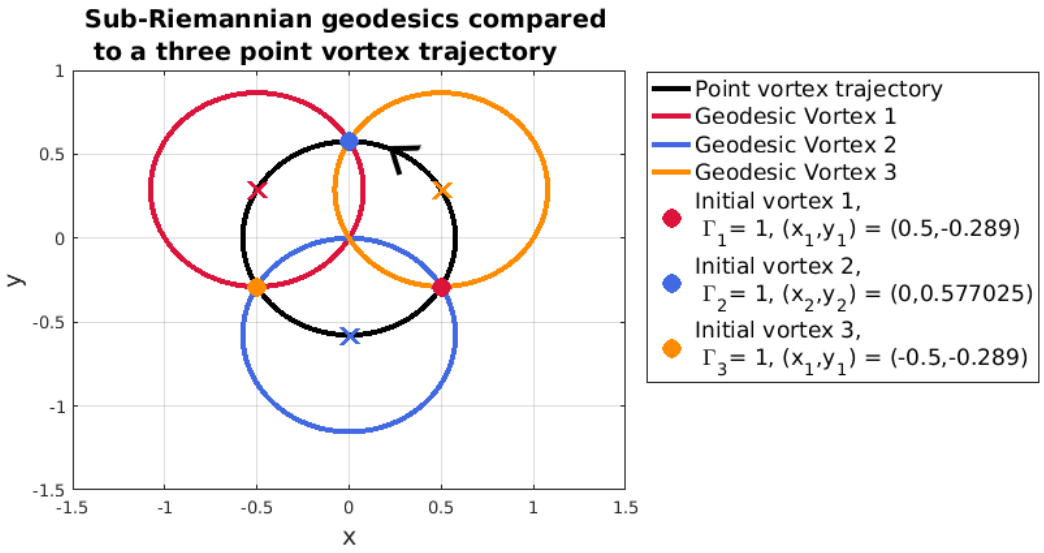

Figure 10.6: The colored trajectories show the sub-Riemannian geodesics of three vortices based on the Vortex-Heisenberg Lie algebra. The black line illustrates the motion of the three-point vortex system forming an relative equilibrium. The black point vortex trajectory was determined by solving the the point vortex equations given in chapter 3. Even though the trajectories are determined with different approaches, we see that the sub-Riemann geodesics and the point vortex trajectories are congruent.

ode45 solver that is based on an explicit Runge-Kutta (4,5) formula.

The colored solid lines in fig. 10.6 show the sub-Riemannian geodesics (10.75) with respect to the basis α and β, where each sub-Riemannian vortex trajectory is regarded separately with the common total circulation Γ. All trajectories pass the Vortex-Heisenberg group identity element $(0, 0)$ which were chosen as initial condition for the general sub-Riemannian geodesics (see (10.45)), because the Lie algebra is the tangent space at the identity element. Therefore, compared to the point vortex trajectory, each sub-Riemannian trajectory is shifted to pass the origin. The black line shows the point vortex motion of the equilibrium. As we found for the two-vortex systems, the sub-Riemannian geodesics are rotations, where the center is given by the point reflection of the initial coordinates, see fig. 10.6, where the centers are marked by the colored crosses. They lie on the point vortex trajectory. We can conclude that also for the three-vortex equilibrium the single point vortex trajectories and the sub-Riemannian geodesics have the same radius!

We have shown examples of two-and three-point vortex systems, where the sub-Riemannian geodesics and the point vortex trajectories are congru-

ent. In both examples, the center of circulation of the point vortex systems lies at the origin. If one choses different center of circulation, the trajectories become scaled, and a scaling factor need to be respected. If the total sum of circulation is equal to zero – as we have e.g. discussed for three point vortices with respect to atmospheric blockings in chapter 4 – the point vortex system equilibrium would translate. This also coincides with sub-Riemannian geodesics, because in this case, we obtain an abnormal extremal which, independent of the applied physical realization, leads to a straight line as geodesics (see, e.g. Monroy-Pérez and Anzaldo-Meneses, 2006). In part I, chapters 3 and 4, but also in part II of this thesis, we have seen that a vortex is characterized by its vortical rotation. All physical conserved quantities contain the circulation. Therefore, it is natural that – in contrast to mass point dynamics – point vortices usually do not move on straight lines.

Why are point vortex geodesics congruent with point vortex equilibria trajectories? Let us regard one point vortex of a two-or three point vortex system, assuming that the vortex system does not form an equilibrium. We also assume that the vortex does not expand or collapse. In this case, the vortex interacts with other point vortices and rotates several times around the center of circulation until it arrives its starting point again. See e.g. fig. 3.2 in chapter 3. Sometimes, a strong interaction between the vortices leads to additional rotations around another point vortex. Now, we measure and compare the lengths of the paths of the vortex that rotates several times around the center of circulation and interacts with other vortices of the point vortex system. We find that a point vortex that is part of an equilibrium takes the shortest path back to its starting point. Therefore, it is reasonable that the sub-Riemannian vortex geodesics derived by the algebraic approach coincides with the point vortex equilibrium.

10.5 How can 3D vortex geodesics be derived?

In this section we will outline the concept to apply (3,6)-sub-Riemannnian geometry to the Vortex-Heisenberg algebra vh(3). The question arises what *are* geodesics in three-dimensional flows physically? The idealized two-dimensional point vortex systems can be seen as the intersection of a plane with (straight) vortex lines. Therefore, regarding three-dimensional vortex flows, we suggest to relate vortex geodesics to the motion of vortex lines. A

vortex line is a material line that is composed of many Lagrangian particles with infinitesimal rotation.

The Vortex-Heisenberg Lie algebra vh(3) representing the dynamics of three dimensional vortex flows has six dimensions, because it is generated by three components of the momentum $\mathbf{P} = (P_x, P_y, P_z)$ and three components of the total flux of vorticity $\mathbf{Z} = (Z_x, Z_y, Z_z)$. The bracket relations with respect to the helicity h_V read as

$$\{P_i, h_V, P_j\} = \epsilon_{ijk} Z_k. \tag{10.79}$$

See chapter 7 for the definition of the bracket. Thus, the Lie algebra is endowed with a rank $n = 3$ distribution. Therefore, we can apply (3,6)-sub-Riemannnian geometry to vh(3) aiming for the derivation of 3D vortex geodesics. The fist investigations of (3,6)-sub-Riemannian geometry can be ascribed to Myasnichenko (2002). Here, we will proceed analogously to the previously discussed (2,3)-vortex geodesics in section 10.3 after Monroy-Pérez and Anzaldo-Meneses (2006).

Mathematically, the Lie algebra vh(3) is nilpotent and therefore, it yields a natural sub-Riemannian structure. We have discussed that sub-Riemannian geometry is used to find geodesics for systems, where the motion is restricted. Regarding vortex dynamics, the motion is restricted by physical conservation laws such as the conservation of the flux of vorticity. Moreover, the conservation of the linear momenta, energy and helicity play a crucial role restrict the motion of the vortices. We have summarized the conserved quantities for 3D flows in chapter 7, (7.52). But as in the previous chapters, we do not take the conservation of energy into account, but the vortex-related conserved quantities to determine the geodesics.

The geodesics are given by the following differential equation (see (10.35))

$$\frac{d\mathbf{x}_g}{dt} = (\dot{\mathbf{h}}, \dot{\underline{\mathbf{H}}}) = (\underline{\mathbf{H}}\mathbf{h}, \mathbf{0}). \tag{10.80}$$

Thus, we first have to determine thepair $(\mathbf{h}, \underline{\mathbf{H}})$ (see (10.33)). The tensor $\underline{\mathbf{H}}$ is given by the Nambu bracket of the linear momenta $\mathbf{P} = (P_x, P_y, P_z)$:

$$\underline{\mathbf{H}} = \begin{pmatrix} \{P_x, h_V, P_x\} & \{P_x, h_V, P_y\} & \{P_x, h_V, P_z\} \\ \{P_y, h_V, P_x\} & \{P_y, h_V, P_y\} & \{P_y, h_V, P_z\} \\ \{P_z, h_V, P_x\} & \{P_z, h_V, P_y\} & \{P_z, h_V, P_z\} \end{pmatrix}, \tag{10.81}$$

where the Nambu bracket of the linear momenta with respect to the helicity results in the total flux of vorticity (10.79).

The Vortex-Heisenberg algebra is derived for continuous vortex dynamics, but we aim for discrete 3D vortex geodesics. Therefore, we discretize the global fields of the momentum $\mathbf{P} = (P_x, P_y, P_z)$ that is given by the integral over the velocity $\mathbf{v}$ and the total flux of vorticity $\mathbf{Z} = (Z_x, Z_y, Z_z)$ that is defined by the integral over the vorticity vector $\boldsymbol{\xi}$. Approximating the integrals by n summands

$$\mathbf{Z} = \int_V d\tau \; \boldsymbol{\xi} \approx \sum_{i=m}^{n} \Delta V_m \; \boldsymbol{\xi}_m \tag{10.82}$$

and

$$\mathbf{P} = \frac{1}{2} \int_V d\tau \; (\mathbf{r} \times \boldsymbol{\xi}) = \int_V d\tau \; \mathbf{v} \approx \sum_{i=m}^{n} \Delta V_m \; \mathbf{v}_m, \tag{10.83}$$

we divide the flow field into n pieces, each with unit volume ΔV_i: Then, the discretized pair $(\mathbf{h}, \underline{\mathbf{H}})$ is given by the anti-symmetric rotational tensor and the vector of the relative momenta

$$\underline{\mathbf{H}} = \begin{pmatrix} 0 & Z_z & -Z_y \\ -Z_z & 0 & Z_x \\ Z_y & -Z_x & 0 \end{pmatrix}, \quad \mathbf{h} = \begin{pmatrix} P_x \\ P_y \\ P_z \end{pmatrix}. \tag{10.84}$$

In two-dimensions, we considered the momenta of each point vortex separately, and the common total circulation of the whole point vortex system. Here, we regard each vortex line separately and use the index (i) to mark the i-the vortex line. To solve (10.80) for this system we apply Lagrange-Sylvester formula that is the spectral formula for $\exp(t\underline{\mathbf{H}})$ (10.38). Thus, we first need to calculate the eigenspaces and projectors. Therefore, we apply the eigenwert equation and obtain for the i-th vortex line:

$$\begin{aligned} \det(\underline{\mathbf{H}}^{(i)} - \kappa \underline{\mathbf{E}}) &= \det \begin{pmatrix} -\kappa & Z_z^{(i)} & -Z_y^{(i)} \\ -Z_z^{(i)} & -\kappa & Z_x^{(i)} \\ Z_y^{(i)} & -Z_x^{(i)} & -\kappa \end{pmatrix} \\ &= -\kappa^3 + Z_z^{(i)} Z_x^{(i)} Z_y^{(i)} - Z_y^{(i)}(-Z_z^{(i)})(-Z_x^{(i)}) - Z_y^{(i)}(-\kappa)(-Z_y^{(i)}) \\ &\quad - (Z_x^{(i)}) Z_x^{(i)}(-\kappa) + \kappa(-Z_z^{(i)}) Z_z^{(i)} = -\kappa^3 - \kappa({Z_y^{(i)}}^2 + {Z_x^{(i)}}^2 + {Z_z^{(i)}}^2) \\ &= -\kappa(\kappa^2 + ({Z_y^{(i)}}^2 + {Z_x^{(i)}}^2 + {Z_z^{(i)}}^2) = -\kappa(\kappa^2 + |\mathbf{Z}^{(i)^2}|^2). \end{aligned} \tag{10.85}$$

Thus,

$$\det(\underline{\mathbf{H}}^{(i)} - \kappa\underline{\mathbf{E}}) = 0 \iff \kappa = 0 \quad \text{or} \quad \kappa = i|\mathbf{Z}^{(i)}|. \tag{10.86}$$

We summarize the set of eigenvalues

$$\{\kappa_1, \kappa_2, \kappa_3\} = \{i\lambda, -i\lambda, 0\} = \{i|\mathbf{Z}^{(i)}|, -i|\mathbf{Z}^{(i)}|, 0\}, \quad \Rightarrow \lambda = |\mathbf{Z}^{(i)}|, \tag{10.87}$$

where $\underline{\mathbf{H}}^{(i)}$ and λ satisfy the condition $\underline{\mathbf{H}}^{(i)}(\underline{\mathbf{H}}^{(i)^2} + \lambda^2\underline{\mathbf{E}}) = 0$ as proposed in Monroy-Pérez and Anzaldo-Meneses (2006). We now determine the projectors $\underline{\boldsymbol{\pi}}_0^{(i)}$ and $\underline{\boldsymbol{\pi}}_1^{(i)}$:

$$\underline{\boldsymbol{\pi}}_0^{(i)} = \frac{1}{\lambda^2}(\underline{\mathbf{H}}^{(i)^2} + \lambda^2\underline{\mathbf{E}}) = \frac{1}{|\mathbf{Z}^{(i)}|^2}\cdot$$
$$\begin{pmatrix} -Z_z^{(i)^2} - Z_y^{(i)^2} - |\mathbf{Z}^{(i)}|^2 & Z_x^{(i)}Z_y^{(i)} & Z_y^{(i)}Z_z^{(i)} \\ Z_x^{(i)}Z_y^{(i)} & -Z_z^{(i)^2} - Z_x^{(i)^2} - |\mathbf{Z}^{(i)}|^2 & Z_y^{(i)}Z_z^{(i)} \\ Z_x^{(i)}Z_z^{(i)} & Z_y^{(i)}Z_z^{(i)} & -Z_y^{(i)^2} - Z_x^{(i)^2} - |\mathbf{Z}^{(i)}|^2 \end{pmatrix} \tag{10.88}$$

and

$$\underline{\boldsymbol{\pi}}_1^{(i)} = \frac{1}{2\lambda^2}\underline{\mathbf{H}}^{(i)}(\underline{\mathbf{H}}^{(i)} + i\lambda\underline{\mathbf{E}}) = \frac{1}{2|\mathbf{Z}^{(i)}|^2}\cdot$$
$$\begin{pmatrix} -Z_z^{(i)^2} - Z_y^{(i)^2} - i|\mathbf{Z}^{(i)}| & Z_x^{(i)}Z_y^{(i)} & Z_y^{(i)}Z_z^{(i)} \\ Z_x^{(i)}Z_y^{(i)} & -Z_z^{(i)^2} - Z_x^{(i)^2} - i|\mathbf{Z}| & Z_y^{(i)}Z_z^{(i)} \\ Z_x^{(i)}Z_z^{(i)} & Z_y^{(i)}Z_z^{(i)} & -Z_y^{(i)^2} - Z_x^{(i)^2} - i|\mathbf{Z}^{(i)}| \end{pmatrix} \tag{10.89}$$

The eigenvector for the zero eigenvalue reads as

$$\mathbf{v}_0^{(i)} = \frac{1}{|\lambda|}\cdot\begin{pmatrix} H_{23}^{(i)} \\ -H_{13}^{(i)} \\ H_{12}^{(i)} \end{pmatrix} = \frac{1}{|\mathbf{Z}^{(i)}|}\cdot\begin{pmatrix} Z_z^{(i)} \\ Z_x^{(i)} \\ Z_y^{(i)} \end{pmatrix}. \tag{10.90}$$

Thus, the basis vector $\boldsymbol{\gamma}_0^{(i)}$ for the i-th vortex line is given by:

$$\begin{aligned}\boldsymbol{\gamma}_0^{(i)} &= \frac{1}{\lambda}(H_1^{(i)}H_{23}^{(i)} - H_2^{(i)}H_{13}^{(i)} + H_3^{(i)}H_{12}^{(i)})\mathbf{v}_0^{(i)} \\ &= \frac{1}{|\mathbf{Z}^{(i)}|^2}(P_x^{(i)}Z_x^{(i)} + P_y^{(i)}Z_y^{(i)} + P_z^{(i)}Z_y^{(i)}) \begin{pmatrix} Z_x^{(i)} \\ Z_y^{(i)} \\ Z_z^{(i)} \end{pmatrix} \\ &= \frac{1}{|\mathbf{Z}^{(i)}|^2}(\mathbf{P}^{(i)} \cdot \mathbf{Z}^{(i)})\mathbf{Z}^{(i)}\end{aligned} \tag{10.91}$$

and the basis vectors $\boldsymbol{\beta}^{(i)}$ and $\boldsymbol{\alpha}^{(i)}$ read as:

$$\boldsymbol{\beta}^{(i)} = \frac{1}{2}\left(\mathbf{P}^{(i)} - \boldsymbol{\gamma}_0\right) = \frac{1}{2}\left(\mathbf{P}^{(i)} - \frac{1}{|\mathbf{Z}^{(i)}|^2}(\mathbf{P}^{(i)} \cdot \mathbf{Z}^{(i)})\mathbf{Z}^{(i)}\right) \tag{10.92}$$

and

$$\begin{aligned}\boldsymbol{\alpha}^{(i)} &= -\frac{1}{\lambda}\underline{\mathbf{H}}^{(i)}\boldsymbol{\beta}^{(i)} \\ &= \frac{1}{-|\mathbf{Z}^{(i)}|}\begin{pmatrix} 0 & Z_z^{(i)} & -Z_y^{(i)} \\ -Z_z^{(i)} & 0 & Z_x^{(i)} \\ Z_y^{(i)} & Z_x^{(i)} & 0 \end{pmatrix} \cdot \frac{1}{2}\left(\mathbf{P}^{(i)} - \frac{1}{i|\mathbf{Z}^{(i)}|^2}(\mathbf{P}^{(i)} \cdot \mathbf{Z}^{(i)})\mathbf{Z}^{(i)}\right). \\ &= \frac{1}{2|\mathbf{Z}^{(i)}|}\mathbf{P}^{(i)} \times \mathbf{Z}^{(i)} + \frac{1}{2|\mathbf{Z}^{(i)}|^3}(\mathbf{P}^{(i)} \cdot \mathbf{Z}^{(i)})\,(\mathbf{Z}^{(i)} \times \mathbf{Z}^{(i)}) \\ &= \frac{1}{2|\mathbf{Z}^{(i)}|}\mathbf{P}^{(i)} \times \mathbf{Z}^{(i)}\end{aligned} \tag{10.93}$$

Now, we have derived a basis $\{\boldsymbol{\alpha}^{(i)}, \boldsymbol{\beta}^{(i)}, \boldsymbol{\gamma}_0^{(i)}\}$ for each discrete vortex line. And we can formulate the geodesics equation (10.47) with respect to the basis leading to an equation for geodesics for three-dimensional incompressible, inviscid flows.

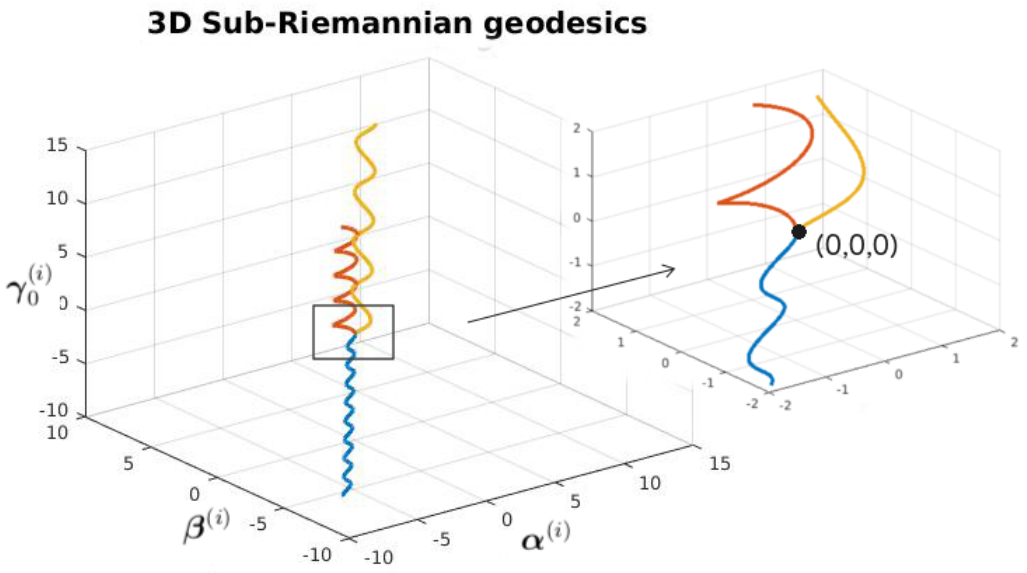

Figure 10.7: Three examples of 3D vortex geodesics derived by (3,6)-Sub-Riemannian geodesics are shown. Because of the initial condition, all three vortex lines intersect in the origin.

Then, the 3D geodesics are given by:

$$\begin{aligned}\mathbf{x}_g^{(i)} &= \frac{1}{2|\mathbf{Z}^{(i)}|^2}\left[\cos(|\mathbf{Z}^{(i)}|t-1)\right](\mathbf{P}\times\mathbf{Z}^{(i)}) \\ &+ \frac{1}{2|\mathbf{Z}^{(i)}|}\sin(|\mathbf{Z}^{(i)}|t)\left(\mathbf{P}^{(i)} - \frac{1}{|\mathbf{Z}^{(i)}|^2}(\mathbf{P}^{(i)}\cdot\mathbf{Z}^{(i)})\mathbf{Z}^{(i)}\right) \\ &+ t\,\frac{1}{|\mathbf{Z}^{(i)}|^2}(\mathbf{P}^{(i)}\cdot\mathbf{Z}^{(i)})\mathbf{Z}^{(i)}\end{aligned} \tag{10.94}$$

One example is shown in fig. 10.7. Here we chose the following local coordinates and vorticity vectors $\mathbf{x}_1 = (1,0,1)$, $\boldsymbol{\xi}_1 = (2,1,5)$, $\mathbf{x}_2 = (1,-1,0)$, $\boldsymbol{\xi}_2 = (1,3,1)$ and $\mathbf{x}_3 = (0,4,0)$, $\boldsymbol{\xi}_3 = (2,1,5)$. We see that all lines are helices that start from the origin, which is due to the initial condition. The helical structure is discussed by Monroy-Pérez and Anzaldo-Meneses (2006) for general nilpotent algebras.

In the last section we explored two-dimensional flows, where vortex geodesics can be interpreted as motion of Lagrangian particles. Here, we derived geodesics for three-dimensional vortex flows, where we could think of *frozen vortex lines* as three-dimensional discrete vortices indicated by the colored lines in fig. 10.7. Analogously to the 2D-vortex geodesics, we might interpret these helical curves as discrete, 3D *equilibrium* solutions of vortex flows. From meteorological perspective, examples of vortex lines are the

centerlines of tropical cyclones.

We conclude that 3D vortex geodesics for incompressible, inviscid flows can be derived from the nilpotent algebra for vortex dynamics. They are geometrically given by helices. In three dimensions it is hard to compare this helical motion with previous studies, since we could not find an idealized, analogous concept for three dimensions, as we did in two dimensions, where we could compare the geodesics with point vortex equilibria. But, we recall that the Vortex-Heisenberg algebra is based on the conservation laws of the helicity, the total flux of vorticity and the 3D linear momentum. All of them contain the vorticity as non-rigid rotational vortex-quantity. Therefore, the helical paths of the vortices seem to be natural, but we will investigate 3D vortex geodesics more in detail in future studies. In this thesis, we only outline a concept to derive 3D vortex geodesics starting from the Vortex-Heisenberg algebra.

10.6 Summary

The physical conservation laws that restrict the motion of fluid flows as well as the mathematical, nilpotent structure of the Vortex-Heisenberg algebras vh(2) and vh(3) that we have derived in the previous chapters motivated us to apply sub-Riemannian geometry to find point vortex geodesics. We have also introduced a concept to derive of vortex geodesics for three-dimensional flows. The question arose, what are vortex geodesics in three dimensions? The answer could be: frozen vortex lines.

However, by applying sub-Riemannian geometry to the Vortex-Heisenberg algebras that are based on the Nambu formulation for incompressible fluids we explore vortex dynamics from a reference system, where we *sit on the vortex* and move with the vortex. In two spatial dimensions, we can imagine to move with a point vortex, whereas in three dimensions we consider vortex tubes, or vortex lines that are vortex tubes with infinitesimal radii, as we have sketched in chapter 8, section 8.5.

So far, the Riemannian view has been used for the investigation of extremal principles for hydrodynamic systems, where mostly the energy is considered to derive variational principles for fluid dynamics. This is due to the system of equations, where the extremal principles are derived from. For incompressible hydrodynamical systems, most authors consider the Euler equations which describe the time evolution of the velocity. Then,

it is an obvious choice to explore further problems in terms of the Hamiltonian structure determined by the kinetic energy. Some authors also regard the enstrophy, but the helicity rarely is taken into account. In this thesis, our studies are based on the Helmholtz equation that is obtained by the rotation of the Euler equations and describes the evolution of the vorticity. The Nambu bracket is directly based on the Helmholtz vorticity equation, which leads to Lie algebras that are based on vortex-related conservation laws. These conservation laws determine and at the same time restrict the vortex motions. Thus, in this chapter we applied sub-Riemannnian geometry to vortex dynamcs. To the best of our knowledge, there have been no investigations of the derivation of vortex geodesics in terms of sub-Riemannian geometry before.

In this chapter we started with an introduction to basic differential geometric definitions which we have used for an examination of the Vortex-Heisenberg Lie algebra we have derived in chapter 8 and applied to the atmospheric phenomena of splitting storms in chapter 9. We then calculated sub-Riemannian geodesics for two and three-dimensional vortex dynamics. For this purpose we applied the algorithm of Monroy-Pérez and Anzaldo-Meneses (2006) to the two- and three-dimensional Vortex-Heisenberg algebras vh(2) and vh(3).

For 2D as well as for 3D the phase space is constructed such that the sub-Riemannian trajectories pass the origin. But in 2D, a simple translation of the trajectories shows the congruence of the derived vortex geodesics and a planar point vortex motion, where the point vortices form an equilibrium. We have discussed point vortex systems forming a relative equilibria in chapters 3 and 4. Why are point vortex equilibria and sub-Riemannian geodesics congruent? To answer this question, we consider initial local coordinates of one point vortex which is part of a two-or three point vortex system. This vortex starts moving and wants to arrive its initial position as soon as possible again. Its motion is restricted by fluid dynamical conservation laws that contain the rotational aspect, i.e. the circulation. In chapter 3 we discussed three kinds of idealized point vortex motion: (i) Collapse and expanding motion. In this case, the vortices do not arrive at their initial points again. (i) Arbitrary periodic motion: Here, the vortices rotate around the center of circulation several times until they reach their initial position again. But if the three vortices form (iii) an equilibrium with non-vanishing total circulation, they only rotate once around the center of circulation until

they reach the initial coordinates again. Therefore, we think that a vortex takes the shortest path if and only if it is part of a equilibrium constellation. This explains why the trajectories of a point vortex equilibrium and sub-Riemannnian vortex geodesics are congruent.

If the total sum of circulation is equal to zero, a case we have discussed with respect to atmospheric blockings in chapter 4, the point vortex system equilibrium will translate. This vortex motion also coincides with the sub-Riemannian view, because in this case, we obtain an abnormal extremal which mathematically leads to a straight line as geodesic. It would be interesting to investigate sub-Riemannian geometry for N-point vortex constellations, where $N \geq 4$. We hypothesize that such geodesics would also be congruent to relative equilibria.

In three dimensions, we find that the vortex geodesics are geometrically given by helices. Regarding the conserved quantities for three dimensional vortex flows, the helicity, the total flux of vorticity and the linear momentum, the helical paths seem to be natural, because all conservation laws contain the vorticity as rotational part. The geodesics could be thought of as *frozen vortex lines* as three-dimensional discrete vortex structures. Analogously to the 2D-vortex geodesics, we might interpret these helical curves as discrete, 3D *equilibrium* solutions of vortex flows. We will examine three-dimensional vortex geodesics more in detail in future studies.

With this approach for the derivation of vortex dynamics we have shown that the algebraic view on vortex dynamics provides the possibilities for alternative descriptions and point of views on vortex dynamics.

Chapter 11

SUMMARY

In this thesis we have investigated 2D and 3D atmospheric vortex dynamics in terms of discrete as well as continuous Nambu mechanics. The discrete Nambu formulation allows for a geometric view on vortex dynamics such as the classification of planar point vortex motions. Continuous Nambu mechanics allows for algebraic studies of hydrodynamical systems. Using this algebraic approach, we could explain vortex splits and derive shortest paths of vortices. To investigate discrete as well as continuous Nambu mechanics and their atmospheric applications this thesis was structured into two parts. In the first part, we investigated discrete Nambu mechanics and the idealized point vortex model and in the second part we developed an algebraic view to analyze vortex dynamics based on continuous Nambu mechanics.

In the first part, we started with an introduction to discrete Nambu mechanics in chapter 2. An advantage of the discrete Nambu formulation is that we do not have to solve explicitly the differential equations of motion, we can find solutions geometrically. In chapter 3, we used this geometric approach to classify point vortex motions by illustrating the surfaces of two conserved quantities. These results were also published in Müller and Névir (2014). In case of three point vortices, the phase space is spanned by their intervortical distances. We could find two conserved quantities that depend on the phase space coordinates. They are given by the energy and the relative angular momentum . Using the Nambu formulation, the intersection curves of these two surfaces give rise to the kind of motion. We found that an ellipse represents periodic motion, and pairs of nearly straight lines classify the collapse and expanding of a three point vortex system; it depends on the initial conditions, which line represents the col-

lapse and which line represents the expanding motion. Furthermore, the point vortex system forms a relative equilibrium if the two surfaces only intersect in one point.

In chapter 4 we regarded such a relative equilibrium of three point vortices and applied the idealized point vortex model to explain atmospheric blockings. Theoretically, the three point vortex constellation translates westwards with constant velocity. Then, stationarity can be explained if the translation velocity wetwards is equal to the velocity of the mean flow eastwards denoted as westerlies in the meteorological context. To corroborate our novel concept, we analyzed two case studies where we showed that the stationarity of the high and low pressure areas can indeed be explained by the vanishing sum of the wind speed from NCEP-reanalysis data and the point vortex translation velocity. These results are represented in Müller et al. (2015). Recently, we could corroborate this concept to explain atmospheric blockings statistically for 347 cases in the Euro-Atlantic region in the period 1990–2012 (Hirt et al., 2018). Comparing our conceptional result with the well-known theories based on Rossby-waves we think that our discrete view yields an alternative explanation that could further be used as a concept for an alternative view on atmospheric phenomena. Therefore, in our working group further atmospheric phenomena were investigated transferring the point vortex concept to the (rotating) sphere on synoptic scale (Pueltz, 2014; Braun, 2016), and to the planetary scale investigating the stability of the QBO confirming and the observed Holton-Tan effect during winter period (Hirt, 2016; Müller et al., 2015)

In the second part of the thesis we have shown how continuous Nambu mechanics allows for an algebraic approach to explore atmospheric phenomena such as vortex splits. This algebraic approach is based on the works of Névir and Blender (1993) and Névir (1998), who introduced the continuous Nambu bracket for incompressible fluids. These works provided the basis to derive a group for vortex dynamics. After an introduction to Lie groups and Lie algebras in chapter 6, chapter 8 we started from the Nambu bracket for two- and three-dimensional vortex flows and introduced a novel matrix representations for two- as well as for three-dimensional vortex flows. In the second step, we further used these representations to derive novel matrix representation for the Vortex-Heisenberg groups VH(2) and VH(3). We also derived a vector representation for VH(2) and VH(3) corroborating the results communicated with Peter Névir in

private communication with Anton Schober in 2010. The name Vortex-Heisenberg group was chosen, because the Vortex-Heisenberg group for two-dimensional vortex dynamics is isomorphic to the Standard-Heisenberg group for mass point mechanics, even though it is based on different sets of equations. In the last section of chapter 8, we introduced a further group that we named Helmholtz Vortex group. Our goal was to find a group that captures vortex rotations as well as rigid body rotations about a given angle. Therefore, we extended the Vortex-Heisenberg group by rigid body rotations and obtained the Helmholtz Vortex group, which can be expressed as semi-direct product of the Vortex-Heisenberg group and SO(3).

In chapter 9, we showed an atmospheric application of the algebraic approach to vortex dynamics. Based on the three-dimensional Vortex-Heisenberg group, we could give an alternative explanation of the generation of vortex splits by examining the sign structure of helicity density fields. There are some advantages of the group theoretical approach: A group is a set together with a group operation. And the elements of the set satisfy some properties such that the group is closed under the group operation. This seemingly harmless property has major consequences. The Nambu formulation represents the vorticity equation, and the Nambu bracket generates the Vortex-Heisenberg Lie algebra. This Lie algebra is the tangent space at the group identity and thus, the Vortex-Heisenberg Lie group can be seen as structural integration of the Helmholtz vorticity equation. Then, calculating the Vortex-Heisenberg group operation of two elements leads to a third element, where all three elements can be seen as solution of the Helmholtz vorticity equation, because of the closure property.

We discussed five case studies, where we transferred this concept to typical atmospheric wind and vorticity fields to investigate their interaction and to analyze the conditions of vortex splits. For this approach, we gave the group elements suitable, physically and mathematically reasonable meanings: Each group element is given by a pair of three-dimensional vector fields that are related to a wind field and the associated vorticity field. We proposed initial states with positive and vanishing helicity that induce a third state. The induced state reflects the interaction of the initial state, and if its helicity density field is divided into positive and negative regions, it gives rise to vortex splits.

In the first case study, we chose as first initial field an ABC-flow to represent a supercell, because such flows are solutions of Beltrami flows that

have extremal helicity fields (Arnold, 1965). As second initial field we considered an atmospheric shear field representing the environment of the supercell. Each initial field defines a Vortex-Heisenberg group element and we determined the helicity density fields of the initial states as well as the helicity density field of the state that results from the group operation, which reflects the interaction of the two initial fields. In the first case, both initial fields have only positive helicity density values. However, the helicity density field of the induced state shows a plus-minus structure which can be related to cyclonic and anticyclonic rotating vortices – and thus to splitted vortices. As a result, the interaction of a Beltrami flow and a pure shear flow leads to splitting vortex cells. This is in accordance to published literature (see, e.g. Klemp, 1987), but it is here approached from a novel, mathematical way of applying group theory.

In our second case study we showed an example of a less distinctive split, because the helicity density fields of initial flows have similar structures. In the third case study we regarded two Beltrami flows and in the fourth case study we examined the interaction of two shear flows. The third and fourth case studies are examples, where we found no split. All four example corroborated our assumption that vortex splits are induced by initial fields with contrary helicity structures. In our last case study we applied the Helmholtz Vortex Lie group V(3) and showed that further splits can be generated. In future studies, we will aim for a statistical analysis of vortex splits to extend and corroborate the here presented conceptual ideas based on the algebraic approach. We recognize a further advantage of the group theoretical approach: the existence of inverse group elements. We considered strongly helical rotating wind fields, such as Beltrami flows, as initial fields to induce the vortex split. But applying the property of the existence of inverse elements a helicity transfer to larger scales is also possible.

The analysis of vortex breakups has implications for turbulence studies. Compared to Kolmogorov's work on the energy dissipation caused by friction, we have explored helicity density fields in conservative systems. Both together might lead to a unifying concept for a better understanding of turbulent vortex flows.

Finally, in chapter 10 we have shown how the Vortex-Heisenberg Lie algebra based on the Nambu-brackets allows for the derivation of 2D point vortex geodesics. The Vortex-Heisenberg algebra is nilpotent, which leads

to a natural structure to apply sub-Riemannian geometry for the search for geodesics. We found that these vortex geodesics are congruent with point vortex equilibria that we have discussed mathematically in chapter 3 and applied to explain atmospheric blockings in chapter 4. We also showed the concept how 3D vortex geodesics can be derived. We have interpreted the outcome as frozen vortex lines. But this should be more explored in future studies.

To summarize, in this thesis we have investigated discrete as well as continuous Nambu mechanics for two- and three-dimensional incompressible, inviscid fluids and applied the geometric as well as algebraic views of vortex dynamics to different atmospheric phenomena. We think that this work will inspire a new way of analyzing 2D- and 3D vortex dynamics and might help deepening the understanding of vortex interactions.

Chapter 12

Storm splitting – Case studies

In chapter 9 we have applied the Vortex-Heisenberg group operation (denoted with $*$) to group elements that are related to different atmospheric wind and vorticity fields. We have discussed four cases, where we considered two initial flows as group elements $A = (\mathbf{a}, \mathbf{A})$ and $B = (\mathbf{a}', \mathbf{A}')$, and a third field C that we obtained by applying the group operation $C = B * A = (\mathbf{a}, \mathbf{A}) * (\mathbf{a}', \mathbf{A}') = (\mathbf{a}'', \mathbf{A}'')$. We chose the different flow fields:

1. A Beltrami and an atmospheric shear field with vanishing helicity
2. A Beltrami field and an atmospheric shear field with non-vanishing helicity
3. Two Beltrami fields
4. The two shear fields from case 1 and case 2

In chapter 9 we mainly discussed the helicity density and the relative helicity fields, here we will also show the enstrophy and energy density fields. Moreover, we will illustrate how these examples develop if we apply the Vortex-Heisenberg group operation iteratively to obtain further states. More precisely, in chapter 9 we considered only the outcome $C = A * B$, here we generate more fields in the following way:

$$\begin{aligned} &A, B: \text{ initial fields} \\ &C = B * A, \quad D = C * B, \quad E = D * C, \quad F = E * D \\ &G = F * E \quad H = G * F \quad I = H * G, \end{aligned} \tag{12.1}$$

The fields of the relative helicity density, helicity density, enstrophy density and energy density of each of the four cases are shown. The notations we use for the four cases are summarized in table 9.1.

12.1 Case study 1 - Vortex splits

In section 9.3.2 we have explored the helicity fields of the following ABC-flow

$$\mathbf{a}_B = \mathbf{A}_B = \lambda \cdot \begin{pmatrix} \sin(z) + \frac{1}{2}\cos(y) \\ \frac{1}{2}\sin(x) + \cos(z) \\ \frac{1}{2}\sin(y) + \frac{1}{2}\cos(x). \end{pmatrix} \tag{12.2}$$

with $\lambda = 1$ providing an extremal helicity density field that is positive definite everywhere. As second initial fields we considered the following shear flow:

$$\mathbf{a}_{\text{s1}} = \mathbf{a}_{\text{s1}}(x, y, z) = \begin{pmatrix} z - z_0 \\ 0 \\ -x + x_0 \end{pmatrix}. \tag{12.3}$$

The helicity density of the shear flow is zero everywhere. The helicity density field, the relative helicity density field, the enstrophy density field and the energy density fields are shown in figures 12.1, 12.2, 12.3, and 12.4. The changing sign structure of the helicity density can be interpreted as the split of vortices into right an left moving parts. In this example we consider supercells as ABC-flows, which are solutions Beltrami flows. This helicity field indicates the existence vortex splits. Moreover, the generation of supercells can be explained. But the structure of the induced helicity density only changes slightly by applying further group operations. But if we extend the Vortex-Heisenberg group by including the angular momentum, we obtain the Helmholtz Vortex group. Applying this group, we can achieve further splits of the helicity field into regions of negative and positive helicity. Thus, we state that one can induce a cascade of helicity to smaller scales, as we have discussed in chapter 9, subsection 9.4.1, see also fig. 9.15.

Applying the Vortex-Heisenberg group operation (9.62), we can also analyze the energy (9.21). As shown in fig. 12.4, the energy decreases if we apply the group operation iteratively. This can be explained by the definition of the energy density given by the sum of states. But compared to the values of the enstrophy density field in fig. 12.3 the energy does not grow as fast, which is in accordance with the non-conservation of the enstrophy in three dimensions. Moreover, the energy field as well in the enstrophy field do no show significant structural changes.

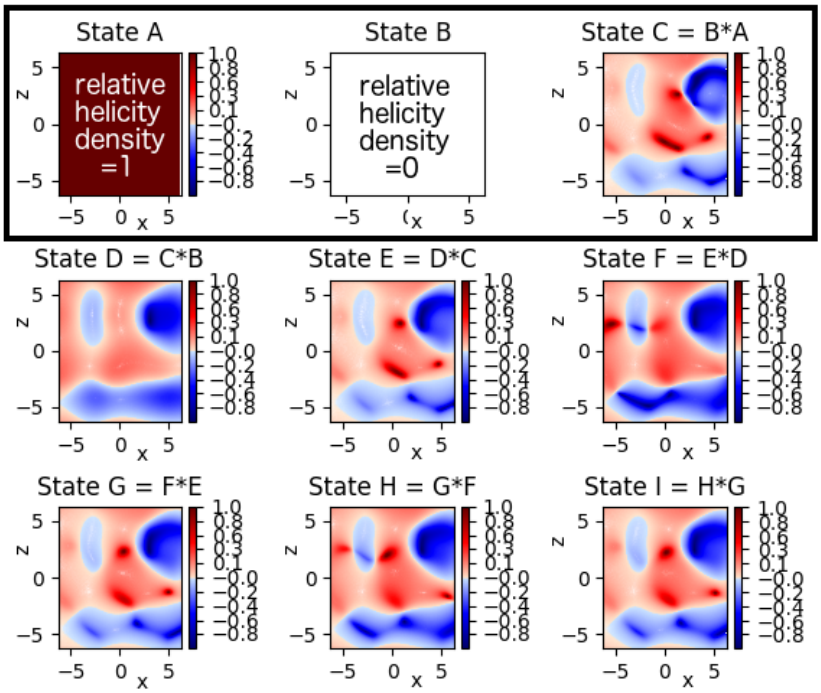

Figure 12.1: Relative helicity density fields of the first case study are shown. Two initial fields: ABC-flow (State A), a flow field with vanishing helicity (State B), and by group operation induced states C-I of the first case study

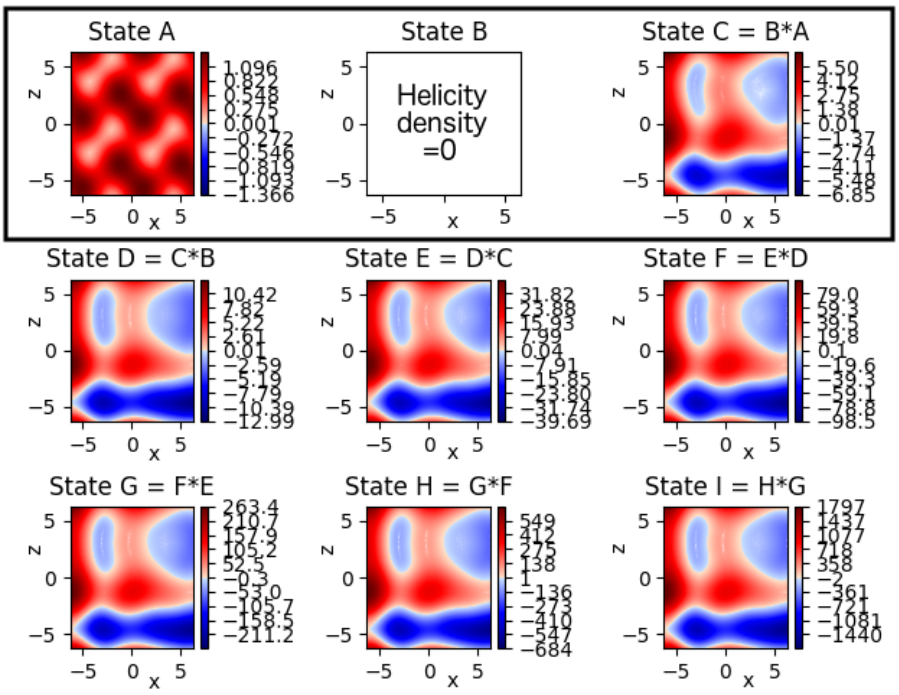

Figure 12.2: Helicity density fields of the first case study are shown. Two initial fields: ABC-flow (State A), a flow field with vanishing helicity (State B), and by group operation induced states C to I. The group operation leads to a helicity field that is splitted into positive and negative regions.

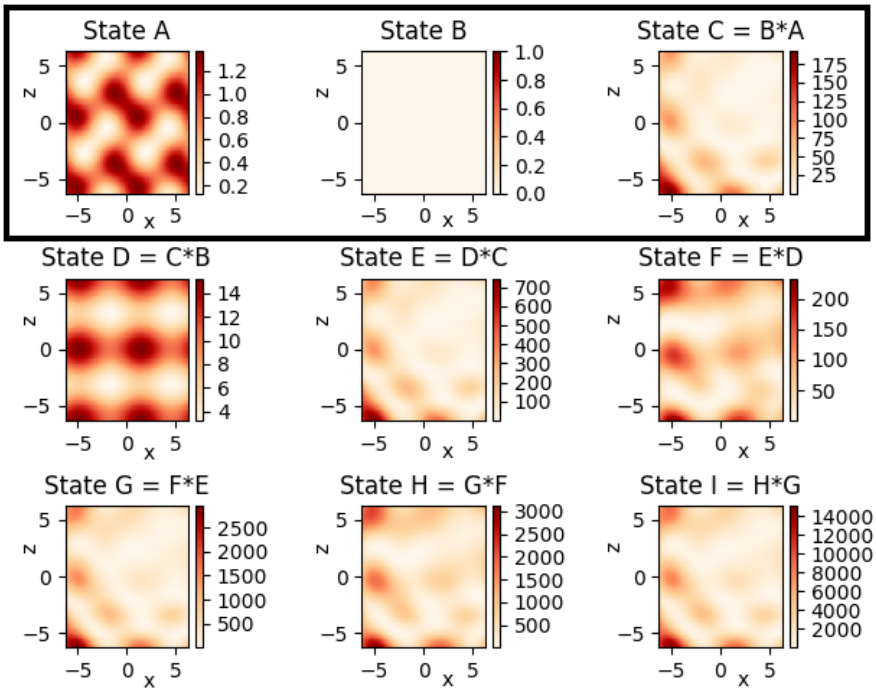

Figure 12.3: Enstrophy fields of the first case study are shown. Two initial fields: ABC-flow (State A), a flow field with vanishing helicity (State B), and by group operation induced states C-I.

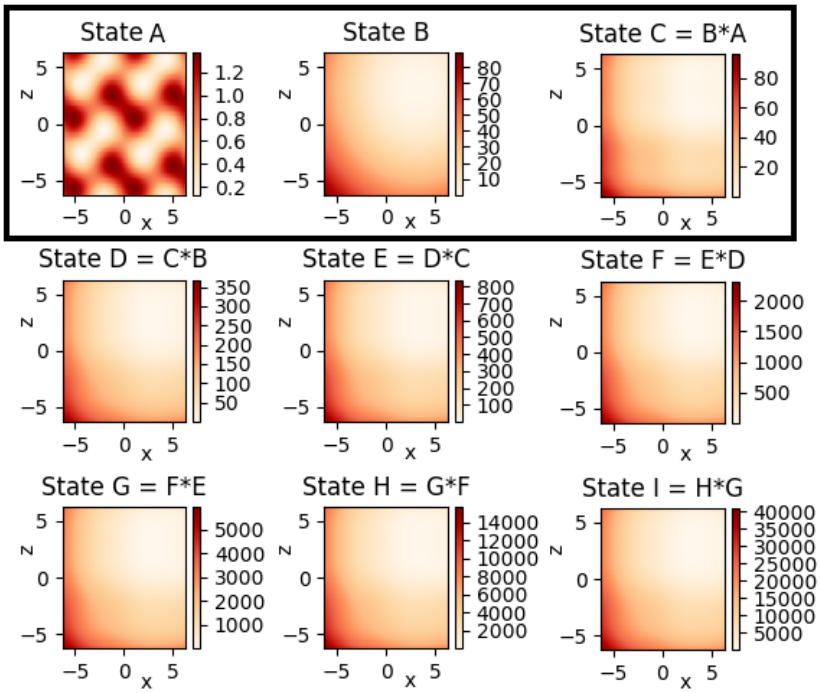

Figure 12.4: Energy fields of the first case study are shown. Two initial fields: ABC-flow (State A), a flow field with vanishing helicity (State B), and by group operation induced states C-I.

12.2 Case study 2 - A less distinctive split

In the second case study, explored in chapter 9, subsection 9.3.3, the ABC-flow (12.2) was chosen as initial state A and a shear field given by

$$\mathbf{a}_h = \mathbf{a}_h(x, y, z) = \begin{pmatrix} 0 \\ z - z_0 \\ -x + x_0 \end{pmatrix}, \tag{12.4}$$

with non-vanishing helicity is here considered as state B. The helicity density and the relative helicity density fields are shown in fig. 12.5 an fig. 12.6. Already the initial field B is divided into a region with negative helicity density values and a region with positive helicity density values. In the helicity field of state C we recognize further local changes of the signs. The initial shear field B describes a tilting vortex. Therefore, it is reasonable that the split is not as distinctive as in the first case.

Applying the group operation iteratively, the energy density in fig. 12.7 does not show a change in its structure. And, compared to the enstrophy density in fig. 12.8 the values do not grow as much as the enstrophy density values. This is in accordance with the assumption of a conservative system that does not allow changes in the energy field, but the enstrophy is an increasing quantity.

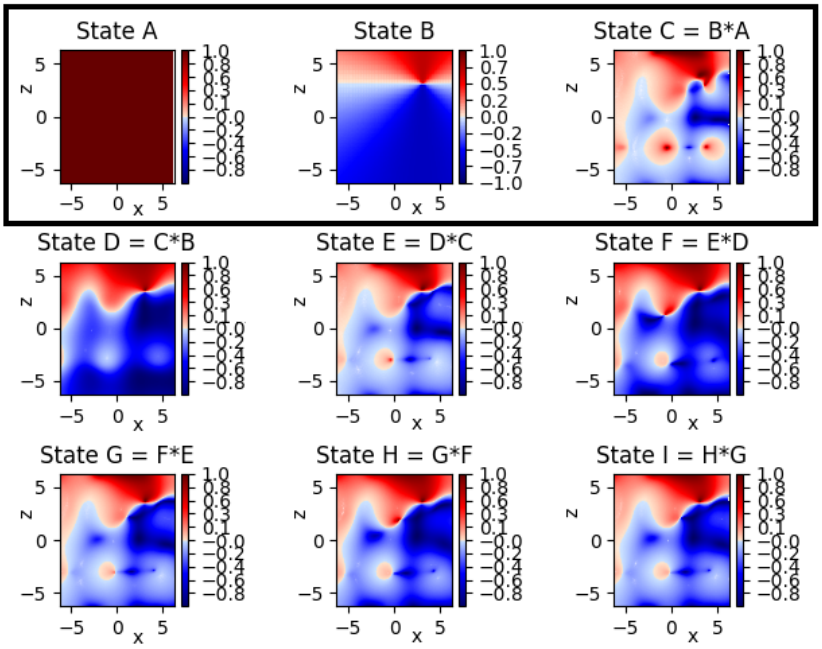

Figure 12.5: The relative helicity density fields of the second case study are shown. Initial field A is a Betrami flow and the initial shear field B describes a tilting vortex. Applying the group operation leads to a vortex split that is not as distinctive as in the first case.

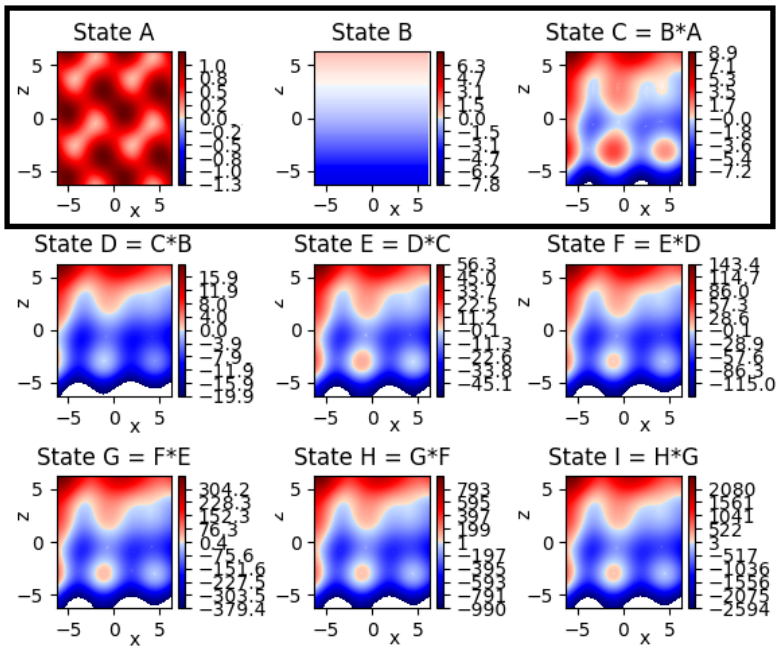

Figure 12.6: Helicity density fields of the second case study are shown. In state C we recognize only small regions with sign changes in the helicity field.

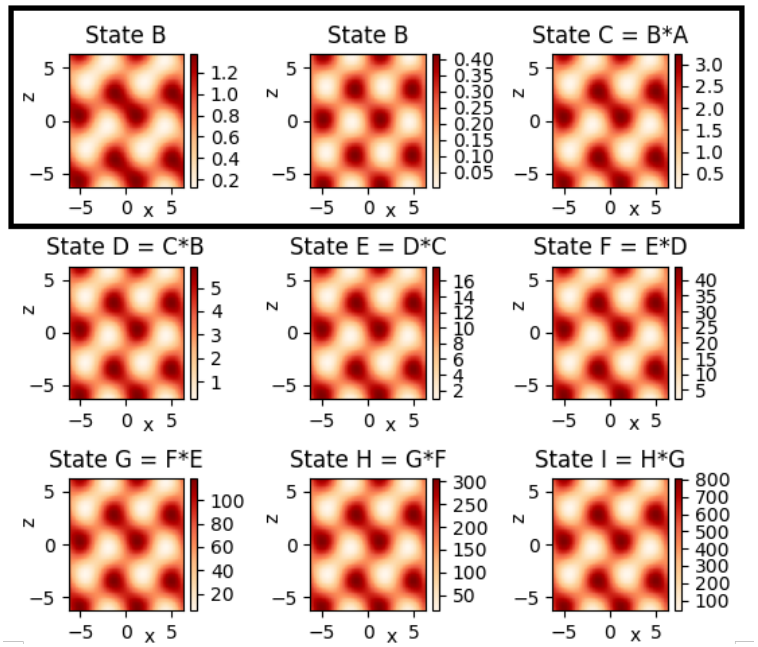

Figure 12.7: Energy density fields of the second case study. The structure of the fields does not change and the values do not increase as much as the enstrophy values.

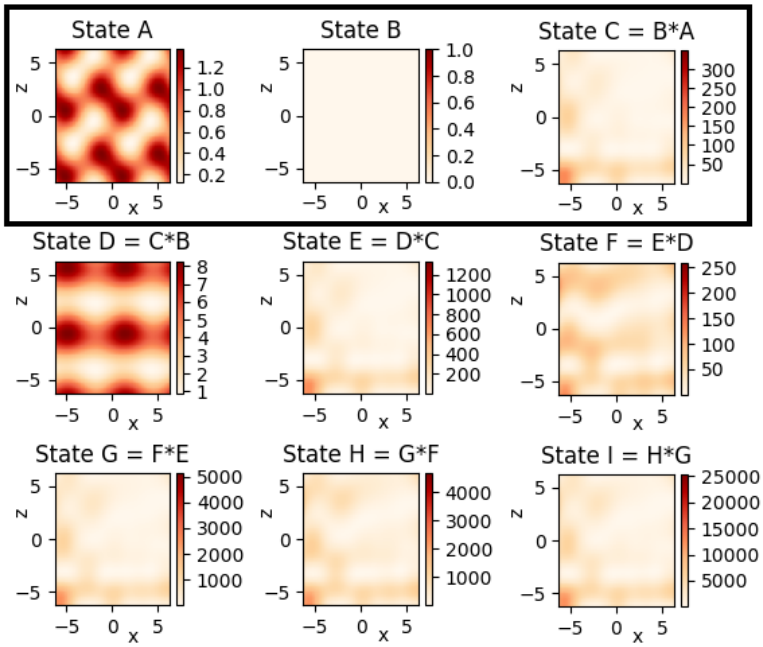

Figure 12.8: The results of the enstrophy density fields of the second case study. A growth of the enstrophy can be observed which is due to the non-conservation of the enstrophy for three dimensional flows.

12.3 Case study 3 - Two Beltrami fields

Here, we show the results of the VH(3)-group operation of the third case study, where we chose as initial flows two different, linear ABC-flows $\mathbf{a}_{B1}$

and $\mathbf{a}_{B1}$ given by:

$$\mathbf{a}_{B1} = \mathbf{A}_{B1} = \begin{pmatrix} \sin(z) + 0.5\cos(y) \\ 0.5\sin(x) + \cos(z) \\ 0.5\sin(y) + 0.5\cos(x) \end{pmatrix}, \mathbf{a}_{B2} = \mathbf{A}_{B2} = \begin{pmatrix} 0.5\sin(z) + 0.1\cos(y) \\ 0.4\sin(x) + 0.5\cos(z) \\ 0.1\sin(y) + 0.4\cos(x). \end{pmatrix} \tag{12.5}$$

As we have discussed in chapter 9 subsection 9.3.4, see also (9.46) for these kind of Beltrami-flows it is

$$\text{Energy = Helicity = Enstrophy} \tag{12.6}$$

up to dimensional unit constants. This relation is reflected in figures 12.9, 12.10 and 12.11, where the density fields of the helicity, energy and enstrophy are shown.

The energy is always positive definite, therefore, the helicity and enstrophy fields are positive definite, too. As we have shown in subsection 9.3.4 analytically, all by group operation induced states hold the same structure as the initial fields. And, concerning the sign of the helicity density fields, we recall (9.54), where we have shown that the helicity density of the initial states as well as the helicity density of their group operation is positive definite. Moreover, in (9.55) we have shown that the helicity field of the induced state is a squared ABC-flow, and thus all induced states have positive helicity density fields. Furthermore, because of the equality of the energy, enstrophy and helicity densities, all three fields provide the same structure as the helicity density field. The relative helicity is one everywhere. Therefore, this field is not represented for this case.

12.4 Case study 4 - Two shearing flows

In the fourth example we discussed the two different shear flows from case study one and case study two, given by:

$$\mathbf{a}_h = \mathbf{a}_h(x, y, z) = \begin{pmatrix} 0 \\ z - z_0 \\ -x + x_0 \end{pmatrix}, \tag{12.7}$$

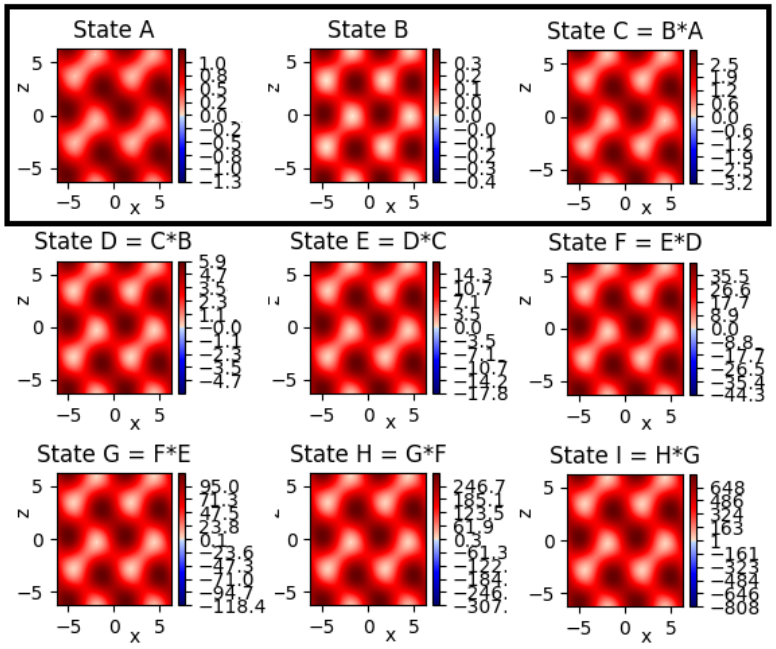

Figure 12.9: The Helicity fields the third case study are shown. Two ABC-flows with parameters $A_1 = 1, B_1 = 0.9$ and $C_1 = 0.5$ for (State A), $A_2 = 0.5, B_2 = 0.4$ and $C_2 = 0.1$ (State B), and the helicity field of the by group operation induced states C to I. All states have the same structure.

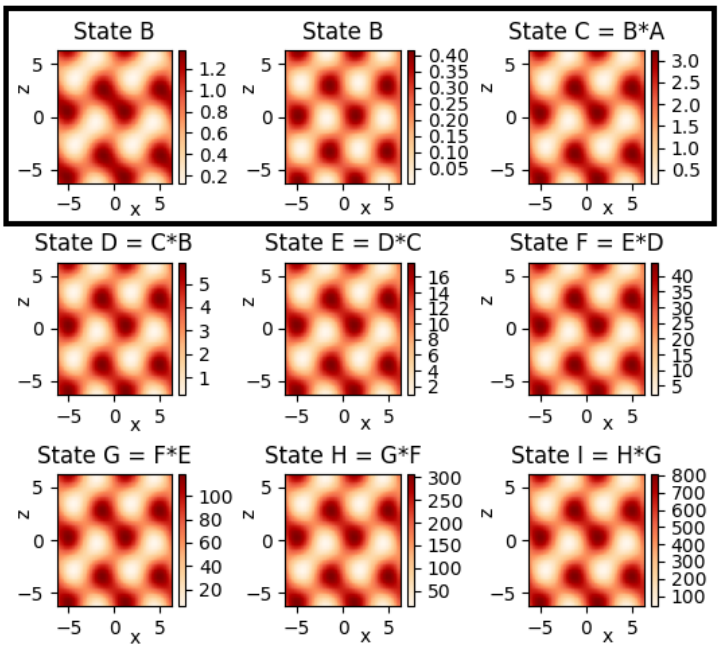

Figure 12.10: The energy density fields of the third case study is shown; They show the same structure as the helicity density fields.

with non-vanishing helicity field and

$$\mathbf{a}_{s1} = \mathbf{a}_{s1}(x, y, z) = \begin{pmatrix} z - z_0 \\ 0 \\ -x + x_0 \end{pmatrix}, \tag{12.8}$$

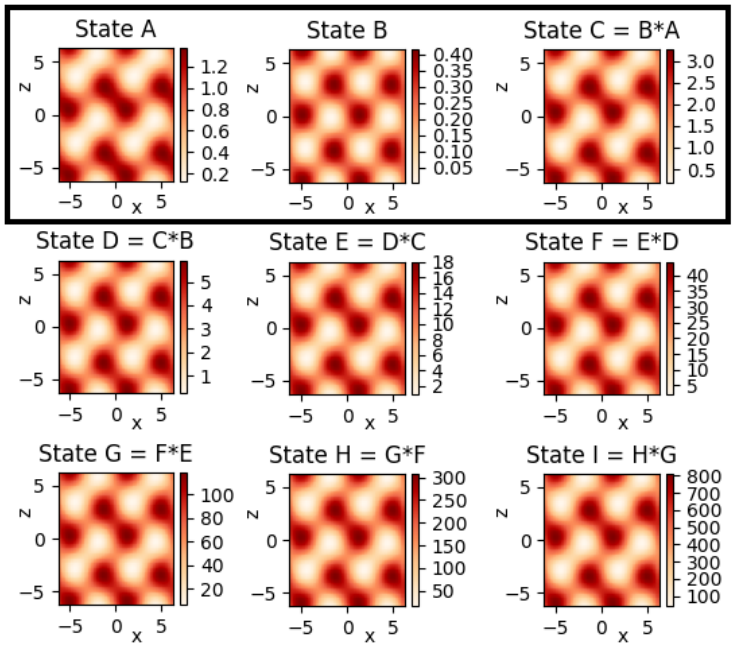

Figure 12.11: The Enstrophy density fields of the third case study are illustrated.

with helicity field equal to zero.

The Vortex-Heisenberg group operation of these initial states does not induce a field that can be interpreted as a vortex split. States C to state I hold the same structure as the initial field, see figures 12.12 and 12.13. Comparing the enstrophy density field in fig. 12.14 and the energy density field in fig. 12.15 we notice a faster increasing of the enstrophy density compared to the growth of the energy density. We have observed the same relation in the cases one and two. This effect can be explained by the non-conservation of the enstrophy leading to a faster growth than the energy. A disadvantage of the algebraic approach is the non-conservation of the energy density field, but we think that our algebraic approach can be used for further examinations of the helicity density structure, for example in terms of turbulence studies.

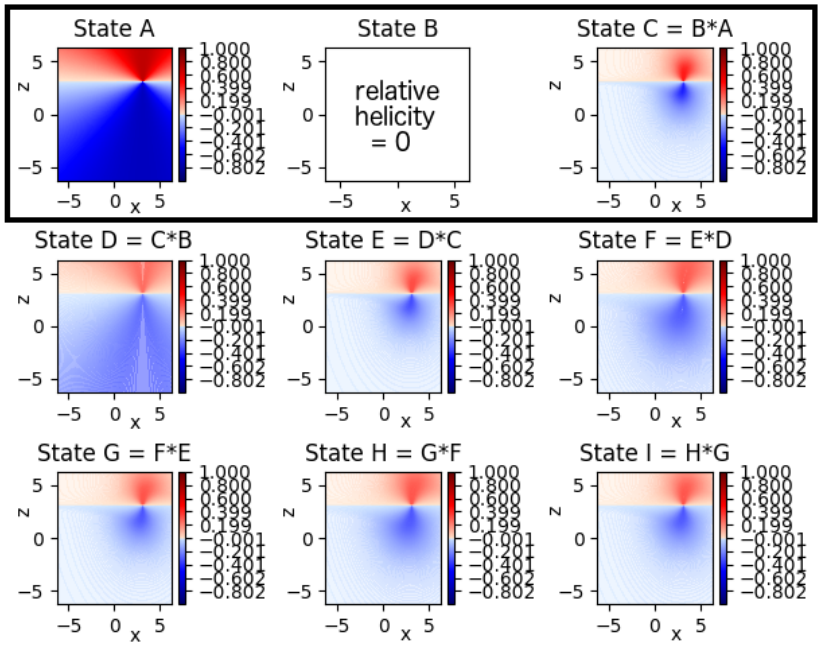

Figure 12.12: The results of the fourth case study is shown. The relative helicity density fields of a wind field with helicity (State A), of the wind field with vanishing helicity (State B) and of the induced helicity fields are illustrated. We do not observe a split in this example.

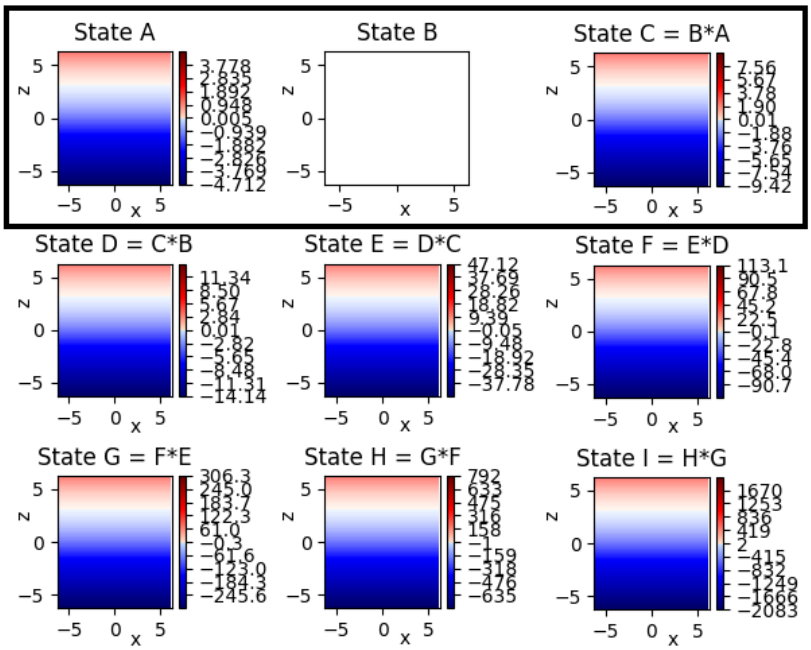

Figure 12.13: The helicity density fields of the fourth case study are shown. Because of the addition-terms in the group operation, we only recognize a growth of the values of the helicity density, but not a structural change.

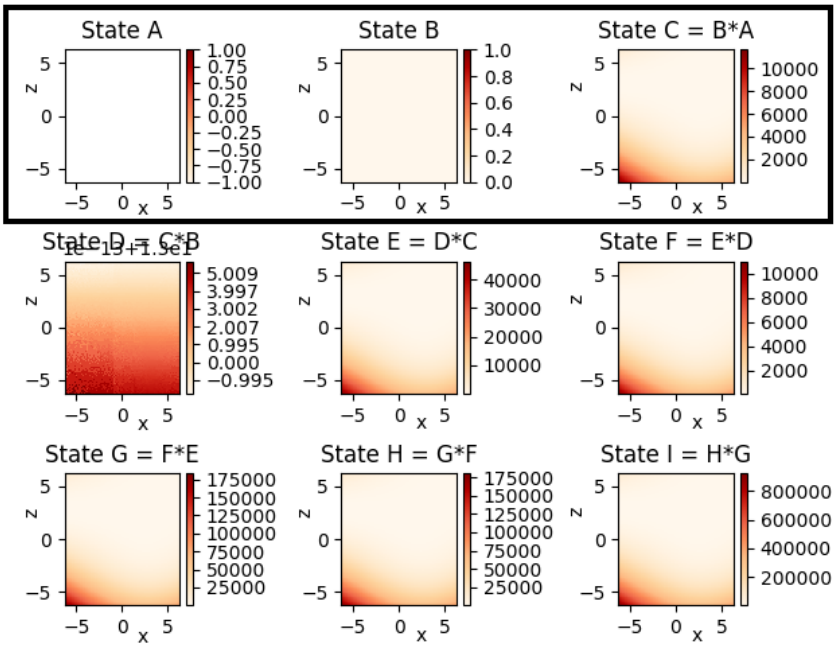

Figure 12.14: The enstrophy density fields are shown. No structural changes can be observed.

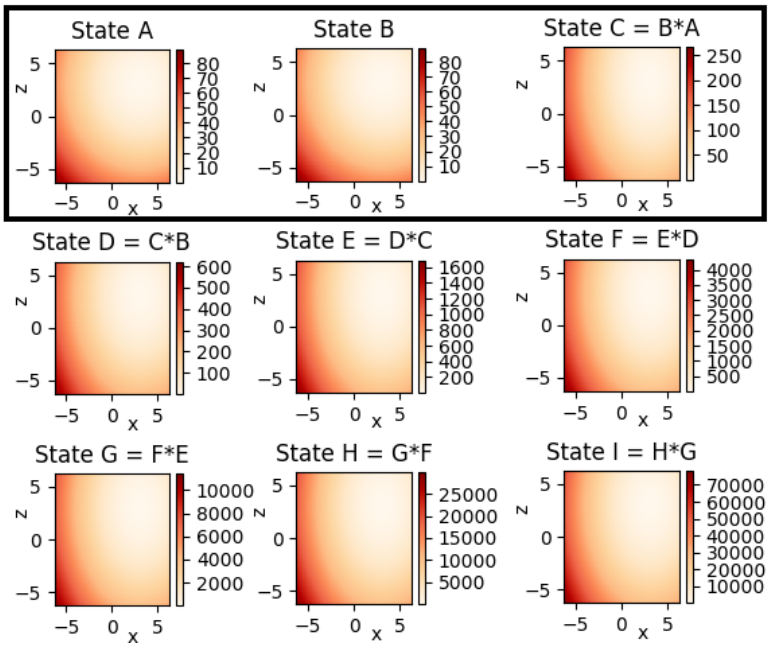

Figure 12.15: The energy density fields of the fourth case study are shown. A structural change of the energy density field can not be observed. The energy value grows not as fast as the values of the enstrophy density, see fig. 12.14.

Bibliography

Adams, N. A. (2015). *Fluidmechanik II: Einfuehrung in die Dynamik der Fluide*. Technische Universität München. Accessed: 2017-12-18.

Agrachev, A. A., Barilari, D., and Boscain, U. (2016). Introduction to riemannian and sub-riemannian geometry. Accessed: 2018-02-25.

Akcoglu, M. A., Bartha, P. F., and Ha, D. M. (2011). *Analysis in vector spaces*. John Wiley & Sons.

Altenhoff, A. M., Martius, O., Croci-Maspoli, M., Schwierz, C., and Davies, H. C. (2008). Linkage of atmospheric blocks and synoptic-scale rossby waves: a climatological analysis. *Tellus A*, 60(5):1053–1063.

Amari, T., Boulbe, C., and Boulmezaoud, T. Z. (2009). Computing beltrami fields. *SIAM Journal on Scientific Computing*, 31(5):3217–3254.

Aref, H. (1979). Motion of three vortices. *Physics of Fluids (1958-1988)*, 22(3):393–400.

Aref, H. (2007). Point vortex dynamics: A classical mathematics playground. *Journal of mathematical Physics*, 48(6):065401.

Aref, H. (2009). Stability of relative equilibria of three vortices. *Physics of Fluids*, 21(9):094101.

Aref, H. (2010). Self-similar motion of three point vortices. *Physics of Fluids (1994-present)*, 22(5):057104.

Aref, H., Beelen, P., and Brøns, M. (2012). Bilinear relative equilibria of identical point vortices. *Journal of nonlinear science*, 22(5):849–885.

Arnold, V. (1965). *Sur la topologie des écoulements stationnaires des fluides parfaits*, volume 261, pages 17–20. C. R. Acad. Sci. Paris.

Arnold, V. I. (1966). Sur la géométrie différentielle des groupes de lie de dimension infinie et ses applicationsa l'hydrodynamique des fluides parfaits. *Ann. Inst. Fourier*, 16(1):319–361.

Arnold, V. I. (1969a). Hamiltonian nature of the Euler equations in the dynamics of a rigid body and of an ideal fluid. In *Vladimir I. Arnold-Collected Works*, pages 175–178. Springer.

Arnold, V. I. (1969b). On one-dimensional cohomology of the Lie algebra of divergence-free vector fields and on rotation numbers of dynamic systems. In *Vladimir I. Arnold-Collected Works*, pages 179–182. Springer.

Arnold, V. I. and Khesin, B. A. (1992). Topological methods in hydrodynamics. *Annual review of fluid mechanics*, 24(1):145–166.

Baker, A. (2012). *Matrix groups: An introduction to Lie group theory*. Springer Science & Business Media.

Barilari, D., Boscain, U., and Sigalotti, M. (2016). *Geometry, analysis and dynamics on sub-Riemannian manifolds. Volume II*. Zürich: European Mathematical Society (EMS).

Bateman, H. (1929). Proceedings of the royal society.

Berger, M. and Gostiaux, B. (2012). *Differential Geometry: Manifolds, Curves, and Surfaces*, volume 115. Springer Science & Business Media.

Betchov, R. (1961). Semi-isotropic turbulence and helicoidal flows. *Physics of Fluids (1958-1988)*, 4(7):925–926.

Biferale, L., Musacchio, S., and Toschi, F. (2013). Split energy–helicity cascades in three-dimensional homogeneous and isotropic turbulence. *Journal of Fluid Mechanics*, 730:309–327.

Bihlo, A. (2008). Rayleigh–Bénard convection as a Nambu-metriplectic problem. *Journal of Physics A: Mathematical and Theoretical*, 41(29):292001.

Bjørgum, O. (1951). *On Beltrami vector fields and flows, Part I: A comparative study of some basic types of vector fields*. Universitetet Bergen.

Bjørgum, O. (1952). *On Beltrami vector fields and flows, Part II: The case when Ω is constant in space*. Universitetet Bergen.

Blackmore, D., Ting, L., and Knio, O. (2007). Studies of perturbed three vortex dynamics. *Journal of mathematical Physics*, 48(6):065402.

Blender, R. and Badin, G. (2015). Hydrodynamic nambu brackets derived by geometric constraints. *Journal of Physics A: Mathematical and Theoretical*, 48(10):105501.

Blender, R. and Lucarini, V. (2013). Nambu representation of an extended Lorenz model with viscous heating. *Physica D: Nonlinear Phenomena*, 243(1):86–91.

Bluestein, H. B. (1992). *Synoptic-dynamic Meteorology in Midlatitudes: Observations and theory of weather systems*, volume 2. Taylor & Francis.

Boer, G. J. and Shepherd, T. (1983). Large-scale two-dimensional turbulence in the atmosphere. *J. Atmos. Sci.*, 40(1):164–184.

Boffetta, G. and Ecke, R. E. (2012). Two-dimensional turbulence. *Annual Review of Fluid Mechanics*, 44:427–451.

Bott, A. (2012). *Synoptische Meteorologie: Methoden der Wetteranalyse und-prognose*. Springer Verlag.

Boulmezaoud, T. Z. (1999). On the existence of non-linear beltrami fields. *Comptes Rendus de l'Académie des Sciences-Series I-Mathematics*, 328(5):437–442.

Braun, G. (2016). Der Einfluss der Kugelgestalt der Erde auf die Stabilität atmosphärischer Wirbelkonfigurationen mit einem idealisierten Punktwirbelmodell.

Brissaud, A., Frisch, U., Leorat, J., Lesieur, M., and Mazure, A. (1973). Helicity cascades in fully developed isotropic turbulence. *Physics of Fluids (1958-1988)*, 16(8):1366–1367.

Brockett, R. W. (1982). *Control theory and singular Riemannian geometry*, pages 11–27. Springer.

Brunt, D. (1939). *Physical and dynamical meteorology*. Cambridge University press.

Calin, O. and Chang, D.-C. (2009). Sub-riemannian geometry. *Cambridge University Press*, 24:134.

Cardesa, J. I., Vela-Martín, A., and Jiménez, J. (2017). The turbulent cascade in five dimensions. *Science*, page eaan7933.

Chapman, D. M. (1978). Ideal vortex motion in two dimensions: symmetries and conservation laws. *Journal of Mathematical Physics*, 19(9):1988–1992.

Charney, J. G. (1963). Numerical experiments in atmospheric hydrodynamics. In *Experimental Arithmetic, High Speed Computing and Mathematics. Proc. Symp. Appl. Math*, volume 15, pages 289–310.

Chen, Q., Chen, S., Eyink, G. L., and Holm, D. D. (2003). Intermittency in the joint cascade of energy and helicity. *Physical review letters*, 90(21):214503.

Childress, S. (1970). New solutions of the kinematic dynamo problem. *Journal of Mathematical Physics*, 11(10):3063–3076.

Chkhetiani, O. G. (2005). Vorticity intensification in turbulent flows with helicity. *Izvestiya Atmospheric and Oceanic Physics*, 41(2):145–149.

Chorin, A. J. (1994). *Vorticity and turbulence*, volume 103. Springer Science & Business Media.

Clebsch, A. (1859). Ueber die Integration der hydrodynamischen Gleichungen. *Journal für die reine und angewandte Mathematik*, 56:1–10.

Cohen, A. M., Cuypers, H., and Sterk, H. (1999). *Algebra Interactive!: learning algebra in an exciting way*. Springer Science & Business Media.

Dallas, V. and Tobias, S. M. (2016). Forcing-dependent dynamics and emergence of helicity in rotating turbulence. *Journal of Fluid Mechanics*, 798:682–695.

Davies-Jones, R. (1995). Tornadoes. *Scientific American*, 273:48–57.

Davies-Jones, R. (2015). A review of supercell and tornado dynamics. *Atmospheric Research*, 158:274–291.

Davies-Jones, R., Burgess, D., and Foster, M. (1990). Helicity as tornado forecast parameter. *Preprints, 16th Conf. on Severe Local Storms*.

Davies-Jones, R., Trapp, R. J., and Bluestein, H. B. (2001). *Tornadoes and tornadic storms*, pages 167–221. Springer.

Davies-Jones, R. P., Kessler, E., and Hess, W. N. (1974). Tornados. In *Weather and Climate Modification*, pages 552–595. John Wiley, New York.

Do Carmo, M. P., Fischer, G., Pinkall, U., and Reckziegel, H. (2017). Differential geometry. In *Mathematical Models*, pages 155–180. Springer.

Dombre, T., Frisch, U., Greene, J. M., Hénon, M., Mehr, A., and Soward, A. M. (1986). Chaotic streamlines in the abc flows. *Journal of Fluid Mechanics*, 167:353–391.

Dritschel, D. G. (1985). The stability and energetics of corotating uniform vortices. *Journal of Fluid Mechanics*, 157:95–134.

Egger, J. (1992). Point vortices in a low-order model of barotropic flow on the sphere. *Quarterly Journal of the Royal Meteorological Society*, 118(505):533–552.

Elliott, R. D. and Smith, T. B. (1949). A study of the effects of large blocking highs on the general circulation in the northern-hemisphere westerlies. *Journal of Meteorology*, 6(2):67–85.

Ertel, H. and Rossby, C.-G. (1949). A new conservation-theorem of hydrodynamics. *Geofisica pura e applicata*, 14(3-4):189–193.

Fortak, H. (1965). *Vorlesungen über Hydrodnamik*, volume 1. Berlin: Institut für theoretische Meteorologie der Freien Universität Berlin.

Friedlander, S. (1975). Interaction of vortices in a fluid on the surface of a rotating sphere. *Tellus*, 27(1):15–24.

Friedrich, K. and Bissolli, P. (2011). Die Hitzewelle in Osteuropa 2011. *Promet*, 37(1,2):44–52.

Frisch, U. (1995). *Turbulence: the legacy of AN Kolmogorov*. Cambridge university press.

Gage, K. (1979). Evidence far a $k^{-5/3}$ law inertial range in mesoscale two-dimensional turbulence. *JJ. Atmos. Sci.*, 36(10):1950–1954.

Galloway, D. (2012). Abc flows then and now. *Geophysical & Astrophysical Fluid Dynamics*, 106(4-5):450–467.

Garriott, E. B. (1904). Long range forecasts. *US Weather Bureau Bulletin*, 35.

Gobet, T. (2017). Lie algebras, part ii. Accessed: 2017-11-12.

Gröbli, W. (1877). *Specielle Probleme über die Bewegung geradliniger paralleler Wirbelfäden*. Zürcher und Furrer.

Guha, P. (2001). Volume preserving multidimensional integrable systems and Nambu–Poisson geometry. *Journal of Nonlinear Mathematical Physics*, 8(3):325–341.

Guha, P. (2004). Applications of nambu mechanics to systems of hydrodynamical type ii. *Journal of Nonlinear Mathematical Physics*, 11(2):223–232.

Hall, B. C. (2003). *Lie groups, Lie algebras, and representations: an elementary introduction*, volume 222. Springer.

Hantel, M. (2013). *Einführung Theoretische Meteorologie*. Springer-Verlag.

Heisenberg, W. (1948). Zur statistischen Theorie der Turbulenz. *Zeitschrift für Physik*, 124(7-12):628–657.

Helmholtz, H. (1858). Über hydrodynamischer Gleichungen welche den Wirbelbewegungen entsprechen. *J. Reine Angew. Math*, 5:25–55.

Hénon, M. (1966). *Sur la topologie des lignes de courant dans un cas particulier*, volume 262. C. R. Acad. Sci. Paris.

Hirt, M. (2016). Statistical and dynamical analyses of atmospheric blockings with the idealized point vortex model.

Hirt, M., Schielicke, L., Müller, A., and Névir, P. (2018). Statistics and dynamics of blockings with a point vortex model. *Tellus A*, 70(1):1458565.

Holm, D. D. and Kupershmidt, B. A. (1983). Noncanonical Hamiltonian formulation of ideal magnetohydrodynamics. *Physica D: Nonlinear Phenomena*, 7(1-3):330–333.

Holm, D. D., Marsden, J. E., and Ratiu, T. S. (1998). The euler–poincaré equations and semidirect products with applications to continuum theories. *Advances in Mathematics*, 137(1):1–81.

Isernhagen, C. (2015). Blockierende Wetterlagen aus Sicht der atmosphärischen Wirbeldy- namik: Theorie und Anwendung.

Jacobi, C. G. J. (1866). *Vorlesungen über dynamik*. G. Reimer.

Kanamitsu, M., Ebisuzaki, W., Woollen, J., Yang, S.-K., Hnilo, J. J., Fiorino, M., and Potter, G. L. (2002). Ncep-doe amip-ii reanalysis (r-2). *Bulletin of the American Meteorological Society*, 83(11):1631–1643.

Karpfinger, C. and Meyberg, K. (2017). Grundbegriffe der Ringtheorie. In *Algebra*, pages 169–185. Springer.

Kirchhoff, G. (1876). *Vorlesungen über mathematische Physik I*, volume 1. Teubner.

Kisil, V. V. (2012). Hypercomplex representations of the heisenberg group and mechanics. *International Journal of Theoretical Physics*, 51(3):964–984.

Klein, R. (2010). Scale-dependent models for atmospheric flows. *Annual review of fluid mechanics*, 42:249–274.

Klemp, J. B. (1987). Dynamics of tornadic thunderstorms. *Annual review of fluid mechanics*, 19(1):369–402.

Klemp, J. B. and Wilhelmson, R. B. (1978). Simulations of right-and left-moving storms produced through storm splitting. *Journal of the Atmospheric Sciences*, 35(6):1097–1110.

Knapp, A. W. (2006). *Basic algebra*. Springer Science & Business Media.

Knapp, A. W. (2013). *Lie groups beyond an introduction*. Springer Science & Business Media.

Kolmogorov, A. N. (1941). The local structure of turbulence in incompressible viscous fluid for very large reynolds numbers.

Kraichnan, R. H. (1967). Inertial ranges in two-dimensional turbulence. *The Physics of Fluids*, 10(7):1417–1423.

Kraichnan, R. H. (1973). Helical turbulence and absolute equilibrium. *Journal of Fluid Mechanics*, 59(04):745–752.

Kraichnan, R. H. and Montgomery, D. (1980). Two-dimensional turbulence. *Reports on Progress in Physics*, 43(5):547.

Kuhlbrodt, T. and Névir, P. (2000). Low-order point vortex models of atmospheric blocking. *Meteorology and Atmospheric Physics*, 73(3-4):127–138.

Kühnel, W. (1999). *Differentialgeometrie*, volume 2003. Springer.

Kühnel, W. (2011). *Matrizen und Lie-Gruppen, Eine geometrische Einführung*. Wiesbaden: Vieweg and Teubner, Spinger.

Kuo, H.-l. (1949). Dynamic instability of two-dimensional nondivergent flow in a barotropic atmosphere. *Journal of Meteorology*, 6(2):105–122.

Kurgansky, M. V. (2017). Helicity in dynamic atmospheric processes. *Atmospheric and Oceanic Physics*, 53(2):127–141.

Lagrange, L. (1788). Mécanique analytique, paris. *MJ Bertrand. Mallet-Bachelier.)[aPJHS]*.

Lange, H.-J. (2002). *Die Physik des Wetters und des Klimas*. Dietrich Reimer-Verlag, Berlin.

Lévy-Leblond, J.-M. (1971). Galilei group and Galilean invariance. In *Group Theory and its Applications, Volume II*, pages 221–299. Elsevier.

Lilly, D. K. (1986). The structure, energetics and propagation of rotating convective storms. part ii: Helicity and storm stabilization. *Journal of the atmospheric sciences*, 43(2):126–140.

Lorenz, E. N. (1963). Deterministic nonperiodic flow. *J. Atmos. Sci.*, 20(2):130–141.

Lorenz, M. (2018). *A Tour of Representation Theory*. American Mathematical Society.

Majda, A. J. and Bertozzi, A. L. (2002). *Vorticity and incompressible flow*, volume 27. Cambridge University Press.

Makhaldiani, N. (1998). The system of three vortexes of two dimensional ideal hydrodynamics as a new example of the (integrable) Nambu-Poisson mechanics. *arXiv preprint solv-int/9804002*.

Markowski, P. and Richardson, Y. (2011). *Mesoscale meteorology in midlatitudes*, volume 2. John Wiley & Sons.

Marsden, J. and Weinstein, A. (1983). Coadjoint orbits, vortices, and Clebsch variables for incompressible fluids. *Physica D: Nonlinear Phenomena*, 7(1):305–323.

Marsden, J. E. and Ratiu, T. (2013). *Introduction to mechanics and symmetry: a basic exposition of classical mechanical systems*, volume 17. Springer Science & Business Media.

Mayer, A. M. (1878). Floating magnets. *Nature*, 18:258–260.

Mininni, P. D. and Pouquet, A. (2013). Inverse cascade behavior in freely decaying two-dimensional fluid turbulence. *Physical Review E*, 87(3):033002.

Moffatt, H. K. (1969). The degree of knottedness of tangled vortex lines. *Journal of Fluid Mechanics*, 35(1):117–129.

Moller, A. R. (1978). The improved nws storm spotters? training program at ft. worth, tex. *Bulletin of the American Meteorological Society*, 59(12):1574–1582.

Monroy-Pérez, F. and Anzaldo-Meneses, A. (1999). Optimal control on the Heisenberg group. *Journal of dynamical and control systems*, 5(4):473–499.

Monroy-Pérez, F. and Anzaldo-Meneses, A. (2006). The step-2 nilpotent (n,n(n+1)/2) sub-riemannian geometry. *Journal of dynamical and control systems*, 12(2):185–216.

Montgomery, R. (2006). *A tour of subriemannian geometries, their geodesics and applications*. Number 91. American Mathematical Soc.

Moreau, J.-J. (1961). Constantes dun ilot tourbillonnaire en fluide parfait barotrope. *Comptes Rendus hebdomadaires des seances de l academie des sciences*, 252(19):2810.

Morikawa, G. K. and Swenson, E. V. (1971). Interacting motion of rectilinear geostrophic vortices. *Physics of Fluids (1958-1988)*, 14(6):1058–1073.

Morton, B. R. (1966). Geophysical vortices. *Progress in Aerospace Sciences*, 7:145–194.

Müller, A. and Névir, P. (2014). A geometric application of Nambu mechanics: the motion of three point vortices in the plane. *Journal of Physics A: Mathematical and Theoretical*, 47(10):105201.

Müller, A., Névir, P., and Klein, R. (2018). Scale dependent analytical investigation of the dynamic state index concerning the quasi-geostrophic theory. *Math. Clim. Weather Forecast.*, 4(1):1–22.

Müller, A., Névir, P., Schielicke, L., Hirt, M., Pueltz, J., and Sonntag, I. (2015). Applications of point vortex equilibria: blocking events and the stability of the polar vortex. *TellusA*, 67.

Myasnichenko, O. (2002). Nilpotent (3,6)-sub-riemannian problem. *Journal of dynamical and control systems*, 8(4):573–597.

Nambu, Y. (1973). Generalized Hamiltonian dynamics. *Physical Review D*, 7(8):2405.

Namias, J. (1947). *Extended forecasting by mean circulation methods*. US Department Commerce, Weather Bureeau.

Nastrom, G., Gage, K., and Jasperson, W. (1984). Kinetic energy spectrum of large-and mesoscale atmospheric processes. *Nature*, 310(5972):36.

NCEP (2000). National centers for environmental prediction/national weather service/noaa/u.s. department of commerce, ncep/doe reanalysis 2 (r2). research data archive at the national center for atmospheric research, computational and information systems laboratory. Technical report. Accessed: 2015-8-05.

Névir, P. (1998). *Die Nambu-Felddarstellungen der Hydro-Thermodynamik und ihre Bedeutung für die dynamische Meteorologie*. Habilitation dissertation, Freie Universität Berlin.

Névir, P. and Blender, R. (1993). A Nambu representation of incompressible hydrodynamics using helicity and enstrophy. *Journal of Physics A: Mathematical and General*, 26(22):L1189.

Névir, P. and Blender, R. (1994). Hamiltonian and Nambu representation of the non-dissipative Lorenz equations. *Contributions to atmospheric physics*, 67(2):133–140.

Newton, P. K. (2001). *The N-vortex problem: analytical techniques*, volume 145. Springer Science & Business Media.

NMI (2014). Norsk riksringkasting. Technical report. Accessed: 2015-12-01.

Novikov, E. A. (1975). Dynamics and statistics of a system of vortices. *Zh. Eksp. Teor. Fiz*, 68:1868–1882.

Obukhov, A. (1941). On the distribution of energy in the spectrum of turbulent flow. *Bull. Acad. Sci. USSR, Geog. Geophys.*, 5:453–466.

Obukhov, A. M., Kurgansky, M. V., and Tatarskaya, M. S. (1984). Dynamic conditions for the origin of drought and other large-scale weather anomalies (russian). *Meteorologiia i Gidrologiia*, pages 5–13.

O'Neill, B. (2006). *Elementary differential geometry*. Academic press.

Onsager, L. (1949). Statistical hydrodynamics. *Il Nuovo Cimento (1943-1954)*, 6(2):279–287.

Pedlosky, J. (2013). *Geophysical fluid dynamics*. Springer Science & Business Media.

Pelly, J. L. and Hoskins, B. J. (2003). A new perspective on blocking. *Journal of the atmospheric sciences*, 60(5):743–755.

Percacci, R. (2017). Lecture notes on lie groups. Accessed: 2017-12-27.

Poincaré, H. (1901). Sur une forme nouvelle des équations de la mécanique. *CR Acad. Sci*, 132:369–371.

Polvani, L. M. and Dritschel, D. G. (1993). Wave and vortex dynamics on the surface of a sphere. *Journal of Fluid Mechanics*, 255:35–64.

Pouquet, A. and Mininni, P. D. (2010). The interplay between helicity and rotation in turbulence: implications for scaling laws and small-scale dynamics. *Philosophical Transactions of the Royal Society of London A: Mathematical, Physical and Engineering Sciences*, 368(1916):1635–1662.

Pueltz, J. (2014). Blockierende Wetterlagen und ihre Beschreibung mit der Punktwirbeldynamik in der Ebene und auf der Kugel.

Raptis, T. E. and Papageorgiou, C. D. (2017). Beltrami flows, non-diffracting waves and the axion beltrami-maxwell postulates. *arXiv preprint arXiv:1801.02945*.

Ratiu, T. (1982). Euler-Poisson equations on Lie algebras and the N-dimensional heavy rigid body. *American journal of mathematics*, pages 409–448.

Rex, D. F. (1950a). Blocking action in the middle troposphere and its effect upon regional climate i. *Tellus*, 2(3):196–211.

Rex, D. F. (1950b). Blocking action in the middle troposphere and its effect upon regional climate ii. *Tellus*, 2(4):275–301.

Rex, D. F. (1951). The effect of atlantic blocking action upon european climate. *Tellus A*, 3(2):100–112.

Richling, A., Kadow, C., Illing, S., and Kunst, O. (2015). Blocking. Accessed: 2017-06-05.

Rotunno, R. and Klemp, J. B. (1982). The influence of the shear-induced pressure gradient on thunderstorm motion. *Monthly Weather Review*, 110(2):136–151.

Roulstone, I. and Norbury, J. (2013). *Invisible in the Storm: the role of mathematics in understanding weather*. Princeton University Press.

Salazar, R. and Kurgansky, M. V. (2010). Nambu brackets in fluid mechanics and magnetohydrodynamics. *Journal of Physics A: Mathematical and Theoretical*, 43(30):305501.

Salmon, R. (1982). Hamilton's principle and Ertel's theorem. *AIP Conference Proceedings*, 88(1):127–135.

Salmon, R. (1988). Hamiltonian fluid mechanics. *Annual review of fluid mechanics*, 20(1):225–256.

Schielicke, L. (2017). *Scale-dependent identification and statistical analysis of atmospheric vortex structures in theory, model and observation*. PhD thesis, Freie Universiät Berlin.

Schielicke, L., Névir, P., and Ulbrich, U. (2016). Kinematic vorticity number–a tool for estimating vortex sizes and circulations. *Tellus A*, 68.

Shepherd, T. G. (1990). *Symmetries, conservation laws, and Hamiltonian structure in geophysical fluid dynamics*, volume 32, pages 287–338. Elsevier.

Snow, J. T. (1984). The tornado. *Scientific American*, 250(4):86–105.

Sommer, M. (2010). *Numerische und geometrische Aspekte der Energie-Wirbel-Theorie*. PhD thesis, Freie Universität Berlin.

Sommer, M., Brazda, K., and Hantel, M. (2011). Algebraic construction of a nambu bracket for the two-dimensional vorticity equation. *Physics Letters A*, 375(37):3310–3313.

Stillwell, J. (2008). *Naive lie theory*. Springer Science & Business Media.

Sudarshan, E. C. G. and Mukunda, N. (1974). *Classical dynamics: a modern perspective*. World Scientific.

Synge, J. L. (1949). On the motion of three vortices. *Can. J. Math*, 1(3):257–270.

Tabor, M. (1989). *Chaos and integrability in nonlinear dynamics: an introduction*. Wiley.

Takhtajan, L. (1994). On foundation of the generalized nambu mechanics. *Communications in Mathematical Physics*, 160(2):295–315.

Tibaldi, S. and Molteni, F. (1990). On the operational predictability of blocking. *TellusA*, 42(3):343–365.

Truesdell, C. (1954). *The Kinematics of Vorticity*. Indiana University Press, Bloomington.

Vinogradov, A. M. and Kupershmidt, B. A. (1977). The structures of Hamiltonian mechanics. *Russian Mathematical Surveys*, 32(4):177.

Webb, G. M., Dasgupta, B., McKenzie, J. F., Hu, Q., and Zank, G. P. (2014). Local and nonlocal advected invariants and helicites in magnetohydrodynamics and gas dynamics i: Lie dragging approach. *Journal of Physics A: Mathematical and Theoretical*, 47(9):095501.

Weizsäcker, C. v. (1948). Das Spektrum der Turbulenz bei großen Reynoldsschen Zahlen. *Zeitschrift für Physik*, 124(7-12):614–627.

Weyl, H. (1950). *The theory of groups and quantum mechanics*. Courier Corporation.

Wipf, A. (2016). *Symmetrien in der Physik*. Vorlesungsskript Friedrich-Schiller-Universität. Accessed: 2017-09-12.

Wu, J.-Z., Ma, H.-Y., and Zhou, M.-D. (2007). *Vorticity and vortex dynamics*. Springer Science & Business Media.

Yeh, T.-C. (1949). On energy dispersion in the atmosphere. *Journal of Meteorology*, 6(1):1–16.

List of Figures

List of Tables

Acknowledgments

I would like to thank PD Dr. Peter Névir and Prof. Dr. Rupert Klein for giving me the opportunity to explore novel ideas in the framework of the Helmholtz graduate research school GEOSIM. I am thankful to the Helmholtz association and the Helmholtz graduate research school GEOSIM and I also thank Deutsche Forschungsgemeinschaft for their support within the framework of CRC 1114 'Scaling Cascades in Complex Systems', project A01.

I thank my supervisor PD Dr. Peter Névir for the inspiring years with numerous discussions, for his help for a better understanding of meteorology and physics to combine the different disciplines of mathematics, physics and meteorology.

I am thankful to Prof. Dr. Rupert Klein who supported me during the last years giving me the opportunities to make experience to work with and talk to mathematicians on (moist) atmospheric fluid dynamics.

I also thank Prof. Dr. Henning Rust for taking his time to review my thesis and for his support during the last years in A01.

I would like to thank Lisa Schielicke, Tobias Mestekemper and Alistair Cloete for their helpful discussions and comments and for reading carefully through different parts of my thesis. I am also grateful to Linda Michalk, Katrin Grigalat, Andreas Litzba, the Ultrateam, and my family for their enormous support during the years.

Selbstständigkeitserklärung

Hiermit erkläre ich, daß ich die vorliegende Arbeit selbstständig angefertigt, nicht anderweitig zu Prüfungszwecken vorgelegt und keine anderen als die angegebenen Hilfsmittel verwendet habe. Sämtliche wissentlich verwendete Textausschnitte, Zitate oder Inhalte anderer Verfasser wurden ausdrücklich als solche gekennzeichnet.

Berlin, den 20. März 2018